STRUCTURAL BEHAVIOUR OF THICK CONCRETE PLATES

EMAD RAOUF M. RIZK


CENTRE FOR NFLD. STUDIES
MEMORIAL UNIVERSITY
OF NEWFOUNDLAND

Structural Behaviour of Thick Concrete Plates

by

Emad Raouf M. Rizk, B.Sc., M.Sc.

A thesis submitted to the School of Graduate Studies in conformity with the requirements for the Degree of Doctor of Philosophy

Faculty of Engineering and Applied Science
Memorial University of Newfoundland
July 2010

St. John's Newfoundland Canada

Abstract

Most concrete codes have empirical equations to estimate the minimum steel reinforcement requirements for flexural members. High-strength thick concrete plates are used as structural component in offshore and containment structures for nuclear power generation. An accurate estimate of the minimum steel flexural reinforcement ratio can result in saving millions of dollars for a single project. The recommended concept utilizes the fracture mechanics principles to modify the sandwich panel model and to account for slab thickness. In summary, the two new main contributions in this research includes consideration of the size effect through fracture mechanics and consideration of the torsional moment for thick plates in calculating the minimum reinforcement of thick plates.

Different design codes have different formulae to calculate crack spacing and crack width developed in flexural members. Most of these formulae are based on the analysis of results on beams or one-way slabs. Crack control equations for beams underestimate the crack width developed in plates and two-way slabs due to loading and constraint effects. It seems that little attention has been paid in determining the crack spacing and width in reinforced concrete plates. The behavior of reinforced concrete plates is different from beams or one-way slabs; therefore, the methods developed for beams cannot be directly applied to plates and two-way slabs. In this research investigation, a two-way numerical model is proposed for calculating the crack spacing for plates. A special focus is given to thick concrete plates used for offshore and nuclear containment structures. The proposed equation takes into account the effect of steel reinforcement in the transverse direction through the splitting bond stress. The equation provides good estimates for crack spacing and crack width in plates and two-way slabs with different concrete covers.

Concrete slabs without shear reinforcement usually exhibit brittle shear failure under a concentric force transferred between the column and the slab. Conventional design methods consider potential shear failures of a slab as a wide beam as well as punching failures in the vicinity of concentrated loads. Most of design codes try to avoid minimum shear reinforcement requirements for slabs by limiting nominal shear stresses at well-defined critical sections to guard against such failure modes. With the extensive use of thick plates of more than 250 mm thick, made of high strength concrete (HSC) for offshore structures, different guidelines must be used to provide minimum shear reinforcement requirements for thick concrete plates. The current research provides procedure for dimensioning of the plate shear core that is the main interest of this work. The proposed models to calculate minimum shear reinforcement for thick plates account for member size effect through fracture mechanics concepts.

The experimental phase of this research work includes testing of two groups of specimens. The first group (Group A) is designed to investigate the effect of small reinforcement ratios and slab thickness on the behaviour of two-way slabs. The second group (Group B) is designed to investigate the effect of slab thickness, reinforcement ratio and shear reinforcement on the structural behavior of thick concrete plates.

The strut-and-tie method is a rational approach to structural concrete design that results in a uniform and consistent design philosophy. A strut-and-tie model is developed to model the punching shear behaviour of thick concrete plates. This model provides a quick and simple approach to evaluate the punching shear capacity of concrete slabs.

Acknowledgements

Many thanks to my mother for her prayer, love, and support. Without her, this work would never have come into existence. Thanks to my father with whom I wish I could share these moments. I am sure that his spirit is always with me. Also thanks to my wife for her continuous support. I am also grateful to my sister and my brothers for their love and support.

Many thanks are due to my supervisor Dr. H. Marzouk Chair and Professor, Department of Civil Engineering, Faculty of Engineering, Architecture and Science, Ryerson University, for his continuous support, guidance, and patience during the course of the program. I appreciate his commitment to help me doing this work in this shape.

I would like to thank Dr. A. Hussein for his advices and his effective guidance regarding the Experimental work presented in the thesis. His valuable comments and revisions improved writing of the final thesis.

The author would also like to thank Dr. S. Bruneau for his continuous encouragement and his valuable comments; it was great pleasure to work as a teaching assistance with him.

The author would also like to thank Mr. N. Dawood Ph.D. for his assistance during preparation of the specimens and during testing.

The author would also like to thank Mr. M. Hossin M. Eng. for providing his test data.

Sincere thanks are due to Mr. Matthew Curtis, Mr. Shawn Organ, Mr. Darryl Pike and the Technical Staff of the Structural Engineering Laboratory of Memorial University of Newfoundland for their assistance during the preparation of the specimens and during testing.

Sincere thanks are extended to Capital Ready Mix Ltd., Newfoundland, for providing the concrete for this project.

I appreciate and thank the School of Graduate Studies at Memorial University of Newfoundland for the financial support of this doctoral study.

The author is grateful to the Natural Sciences and Engineering Research Council of Canada (NSERC) for providing the funds for the project.

St. John's, Newfoundland Emad Rizk
April 30, 2010

Table of Contents

Abstract i

Acknowledgments ii

Table of Contents iii

List of Figures viii

List of Tables xi

Notation and list of abbreviations xii

1. Introduction 1
1.1 General 1
1.2 Scope of Research 3
1.3 Research Objectives 5
1.4 Thesis Outline 7

2. Literature Review 9
2.1 Introduction 9
2.2 Minimum Flexural Reinforcement 9
2.2.1 Historical development of North American Codes 10
2.3 Effect of Member Size on Minimum Reinforcement Ratio 14
2.3.1 Slab Size Effect 14
2.4 Minimum Flexure Reinforcement for HSC Plates 16
2.5 Minimum Shear Reinforcement 17
2.5.1 Minimum Shear Reinforcement for Plates and Two-Way Slabs 18
2.6 Shear Strength of Two-Way Slabs 22
2.7 Shear Design of Two-Way Slabs 23
2.7.1 Canadian standard 2004 (CSA-A23.3-04) requirements 24
2.7.2 ACI 318-08 24
2.7.3 European codes 25
2.8 Cracking in Reinforced Concrete Structures 26
2.9 Crack Spacing 27
2.9.1 ACI 318-99 Approach 29
2.9.2 ACI 318-05 Major Changes 30
2.9.3 Eurocode EC2 Provisions 30
2.10 Research on Cracking in Beams and One-Way Slabs 32
2.11 Research on cracking in Plates and Two-Way Slabs 32
2.12 Crack Width 34
2.13 Factors Affecting Crack Width 34
2.13.1 Effect of Concrete Cover 35
2.13.2 Effect of Reinforcement Ratio and Bar Diameter 36
2.14 Crack Width and Crack Spacing Based on Fracture Mechanics 36
2.15 Tension Chord Method 37

2.16 Codes Provisions for Crack width Calculations....38
2.16.1 Norwegian Code....38
2.16.2 CEB-FIP (1990) Code....39
2.17 Summary....39

3. The Experimental Program....41
3.1 General....41
3.2 Test Parameters....41
3.3 Test Specimens....46
3.4 Properties of Material....48
3.4.1 Normal Strength Concrete Mixture....48
3.4.2 High Strength Concrete Mix Design....48
3.5 Curing....49
3.6 Compressive Strength of the Test Slabs....49
3.7 Slab Formwork and Fabrication....50
3.8 Test Set-up....53
3.9 Instrumentation and Measurements....57
3.9.1 Deflections....57
3.9.2 Steel Strains....58
3.9.3 Concrete Strains....59
3.9.4 Crack Measurements....60
3.9.5 Data Acquisition System....61
3.10 Test Procedure....62

4. Structural Behaviour of Thick Two-Way Slabs Reinforced with Minimum Reinforcement Ratios....64
4.1 Introduction....64
4.2 Test Results....65
4.2.1 Load-Deflection Characteristics....66
4.2.2 Deflection Profiles....69
4.2.3 Ductility and Energy Absorption Characteristics....73
4.2.4 Concrete Strains....75
4.2.5 Steel Strains....79
4.3 Cracking and Failure Characteristics....84
4.3.1 Crack Spacing....84
4.3.2 Crack Width....89
4.3.2.1 Crack Width Measurements....90
4.4 Modes of Failure....94
4.5 Summary....94

5. Structural Behaviour of Thick Plates....96
5.1 Introduction....96
5.2 Test Specimens....97
5.3 Test Setup....98
5.4 Test Procedure....99
5.5 Test Results....100

5.5.1 Load-Deflection Characteristics....101
5.5.2 Deflection Profiles....103
5.5.3 Ductility and Energy Absorption Characteristics....106
5.5.4 Concrete Strains....108
5.5.5 Steel Strains....111
5.6 Cracking and Failure Characteristics....115
5.6.1 Crack Spacing....116
5.6.2 Crack Width....119
5.7 Modes of Failure....123
5.8 Effectiveness of Shear Reinforcement....123
5.9 Summary....124

6. Minimum Flexural Reinforcement for Thick HSC Plates....127
6.1 Introduction....127
6.2 Slab size effect....127
6.3 Analytical Investigation....128
6.3.1 Effect of Torsional Moment on Minimum Reinforcement of Thick Plates..129
6.3.2 Marti's Shear Sandwich Model (1990)....134
6.3.2.1 Uncracked Core....135
6.3.2.2 Cracked Core....135
6.3.3 Modified Sandwich Model....137
6.4 Comparison of Proposed Model with Different Code Predictions....140
6.4.1 Comparison between the Values of Proposed Model with Experimental Results....141
6.4.2 Proposed Model versus Different Codes Formulae....143
6.5 Minimum Shear Reinforcement for Thick Plates and Two-Way Slabs....146
6.6 Development of Minimum Shear Reinforcement Ratio for Two-Way Slabs....146
6.6.1 North American Codes Requirements....146
6.6.2 European Codes Requirements....147
6.7 Shear Transfer in the Interior of a Slab....148
6.8 Dimensioning of Sandwich Model Core....150
6.8.1 Slabs without Shear Reinforcement....150
6.8.2 Slabs with Shear Reinforcement....151
6.9 Punching Shear Distribution....152
6.10 Minimum Shear Reinforcement Based on Truss Model....152
6.10.1 Evaluation of Minimum Shear Reinforcement....153
6.11 Minimum Shear Reinforcement Ratio Based on the Diagonal Cracking Load..156
6.12 Minimum Shear Reinforcement Ratio Based on Compression Field Theory....158
6.13 Comparison of Proposed Formula with Different Design Codes formulae....160
6.14 Discussion....163
6.15 Summary....165

7. Estimate of Crack Spacing and Crack Width for Thick Concrete Plates and Two-Way Slabs....166
7.1 Introduction....166
7.2 Crack Spacing....167

7.3 Mechanism of Bond Transfer....167
7.4 Analytical Model....169
7.4.1 Bond Stress Distribution....169
7.4.2 Longitudinal Steel Reinforcement (Loading Direction)....169
7.4.3 Transverse Steel Reinforcement and Splitting Bond Stress....171
7.5 Crack Spacing for Beams and One-Way Slabs....174
7.6 Discussion....175
7.6.1 Verification of Proposed Model....175
7.6.2 Comparison of Experimental and Theoretical Estimates of Crack Spacing 183
7.7 Crack Width....184
7.8 Characteristic Crack Width....184
7.8.1 Maximum Crack Width....184
7.8.2 Crack Width for Beams and One-Way Slabs....186
7.9 Comparison of Calculated Crack Width Values with Different Code Predictions....186
7.10 Summary....190

8. Minimum Shear Reinforcement for Thick Concrete Plates Based on a Strut-and-Tie Model....192
8.1 Introduction....192
8.2 Bottle-Shaped Strut....193
8.2.1 Strut Failure by Longitudinal Cracking....194
8.3 Minimum Shear Reinforcement Based on Strut-and-Tie Model....196
8.3.1 Evaluation of Transverse Tensile Forces acting on a Bottle-Shaped Strut...196
8.4 Proposed Strut-and-Tie Model for Punching Shear of Concrete Slabs....199
8.4.1 Symmetric Punching Shear of Concrete Slabs....199
8.4.2 Stress Fields, Strut-and-Tie Model....200
8.4.3 Shear Cracking, the Crack Zone....201
8.4.4 Punching Failure Mechanism, Ultimate Failure Zone....203
8.4.5 High Radial Compression Stress Failure Mechanism....203
8.5 Strut-and-Tie Model for Symmetric Loaded Concrete Slabs with Punching Shear Reinforcement....205
8.6 Comparison of Available Test Results versus the Proposed STM Model....209
8.7 Experimental Test Results versus Codes Predictions and STM Model....212
8.8 Outline of Design Procedure using STM Model....215
8.9 Summary....215

9. Summary and Conclusions....217
9.1 Summary....217
9.2 Conclusions....218
9.2.1 Minimum Flexural Reinforcement for Thick HSC Plates....218
9.2.2 Minimum Shear Reinforcement for Thick HSC Plates....219
9.2.3 Crack Spacing and Crack Width for Thick Concrete Plates....221
9.2.4 Punching Shear of Thick Concrete Plates....222

References **224**

Appendix A **233**

List of Figures

Figure 2.1: Effective embedment thickness (effective tension area) 28
Figure 2.2: Effective area, $A_{c,ef}$ for use in equations (2.6): (*a*) beam; (*b*) slab; (*c*) member in tension (reference CEB FIB Model code 1990) 31
Figure 3.1: Details of typical test specimen HS2 (h = 300 mm) 44
Figure 3.2: Details of typical test specimen HS7 (h = 400 mm) 44
Figure 3.3: Dimensions and reinforcement details of slab HS5 with T-headed shear reinforcement (h = 300 mm) 45
Figure 3.4: Arrangement of T-headed shear reinforcement in slab HS5 (h = 300 mm) 45
Figure 3.5: The concrete compression testing machine 51
Figure 3.6: A reinforcement cage in the formwork for a typical slab (group A) 52
Figure 3.7: A reinforcement cage in the formwork for a typical slab (group B) 52
Figure 3.8: A reinforcement cage in the formwork for slab HS5 with T-headed shear stud reinforcement (h = 300 mm) 53
Figure 3.9: The test set-up for Group A 55
Figure 3.10: Test setup for group B: (*a*) Isometric view; (*b*) Front view 56
Figure 3.11: Test set-up for group B: (*a*) A Specimen during testing; (*b*) Typical specimen indicates size effect challenge 57
Figure 3.12: A typical arrangement of LVDT's 58
Figure 3.13: A typical arrangement of the steel strain gauges 59
Figure 3.14: Concrete Strain gauge locations (The strain gauges were located at 100 mm apart) 60
Figure 3.15: Crack Displacement Transducer (KG-A) 61
Figure 3.16: Marking the cracks on a typical slab 63
Figure 4.1: Typical load-deflection characteristics at center span of tested slabs: (*a*) Series A1; (*b*) Series A2; (*c*) Series A3 69
Figure 4.2: Deflection profile for tested slabs: (*a*) NS1 and (*b*) NS2 71
Figure 4.3: Deflection profile for tested slabs: (*a*) NS3 and (*b*) HS1 72
Figure 4.4: Deflection profile for tested slabs: (*a*) NS4 and (*b*) HS2 73
Figure 4.5: Load versus concrete strain for NS1 76
Figure 4.6: Load versus concrete strain for NS2 76
Figure 4.7: Load versus concrete strain for NS3 77
Figure 4.8: Load versus concrete strain for HS1 77
Figure 4.9: Load versus concrete strain for NS4 78
Figure 4.10: Load versus concrete strain for HS2 78
Figure 4.11: Load versus concrete strain for HS3 79
Figure 4.12: Typical load-tension steel strain behavior at the column periphery for Series A1: (*a*) NS1; (*b*) NS2 81
Figure 4.13: Typical load-tension steel strain behavior at the column periphery for Series A2: (*a*) NS3; (*b*) HS1 82
Figure 4.14: Typical load-tension steel strain behavior at the column periphery for Series A3: (*a*) NS4; (*b*) HS2; (*c*) HS3 83
Figure 4.15: Crack patterns of Series A1: (*a*) NS1; (*b*) NS2 86
Figure 4.16: Crack patterns of Series A2: (*a*) NS3; (*b*) HS1 87

Figure 4.17: Crack patterns of Series A3: (*a*) NS4; (*b*) HS2; (*c*) HS3 89
Figure 4.18: Crack width expansion versus steel strain for NS3 (h = 250 mm).....91
Figure 4.19: Crack width expansion versus steel strain for HS1 (h = 250 mm).....92
Figure 4.20: Crack width expansion versus steel strain for NS4 (h = 300 mm).....92
Figure 4.21: Crack width expansion versus steel strain for HS2 (h = 300 mm).....93
Figure 4.22: Crack width expansion versus steel strain for HS3 (h = 300 mm).....93
Figure 5.1: Typical load-deflection characteristics at center span of test slabs: (*a*) Series B1; (*b*) Series B2 102
Figure 5.2: Deflection profile for slabs: (*a*) HS4; (*b*) HS5; (*c*) HS6.....105
Figure 5.3: Deflection profile for slabs: (*a*) NS5; (*b*) HS7 106
Figure 5.4: Load versus concrete strain for HS4.....109
Figure 5.5: Load versus concrete strain for HS5.....109
Figure 5.6: Load versus concrete strain for HS6.....110
Figure 5.7: Load versus concrete strain for HS7.....110
Figure 5.8: Typical load-tension steel strain behavior at the column periphery for Series B1: (*a*) HS4; (*b*) HS5; (*c*) HS6.....113
Figure 5.9: Typical load-tension steel strain behavior at the column periphery for Series B2: (*a*) NS5; (*b*) HS7 114
Figure 5.10: Load-shear stud steel strain behavior for slab HS5 114
Figure 5.11: Crack patterns of Series B1: (*a*) HS4; (*b*) HS5; (*c*) HS6.....118
Figure 5.12: Crack patterns of Series B2: (*a*) NS5; (*b*) HS7 119
Figure 5.13: Crack width expansion versus steel strain for HS4 (h = 350 mm).....121
Figure 5.14: Crack width expansion versus steel strain for HS5 (h = 300 mm).....121
Figure 5.15: Crack width expansion versus steel strain for HS6 (h = 350 mm).....122
Figure 5.16: Crack width expansion versus steel strain for NS5 (h = 400 mm).....122
Figure 5.17: Crack width expansion versus steel strain for HS7 (h = 400 mm).....123
Figure 6.1: Resolution of moments.....133
Figure 6.2: Normalized torsional moment vs. aspect ratio ($(M_{xy}+ M_x)/M_{x,\max+ve}$ vs. a/b) for clamped rectangular plates 133
Figure 6.3: Statics of slab elements: (*a*) Stress resultants; (*b*) Sandwich model; (*c*) Pure shear in uncracked core; (*d*) Diagonal compression field in cracked core 136
Figure 6.4: Schematic of reinforced concrete section in bending.....140
Figure 6.5: Modified sandwich model 140
Figure 6.6: Comparison of minimum reinforcement ratios calculated by different codes $f_c^{'} = 35$ MPa 144
Figure 6.7: Comparison of minimum reinforcement ratios calculated by different codes $f_c^{'} = 70$ MPa 145
Figure 6.8: Comparison of minimum reinforcement ratios calculated by different codes $f_c^{'} = 90$ MPa 145
Figure 6.9: Slab element internal forces V_{xz} and V_{yz} 149
Figure 6.10: Maximum transverse shear force.....149
Figure 6.11: Effective width of truss model idealization for slab column connection 155
Figure 6.12: Equivalent plastic truss model idealization and equilibrium of bottom chord joints.....155

Figure 6.13: Shear stress distribution in a slab cross section just before the formation of shear cracks 159
Figure 6.14: Stress fields in the core of reinforced concrete slab 159
Figure 6.15: Comparison of minimum shear reinforcement requirements for beams by various design codes as a function of concrete compressive strength $f_c^{'}$ 161
Figure 6.16: Comparison of minimum shear reinforcement requirements for two-way slabs by EC2 and proposed formula as a function of concrete compressive strength $f_c^{'}$: (*a*) h = 250 mm; (*b*) h = 500 mm; (*c*) h = 1000 mm 162
Figure 7.1: Bond transfer mechanism 168
Figure 7.2: Distribution of bond stress, splitting stress and tensile stress over a section: (*a*) A Plan of a Two-way Plate; (*b*) Cross section of two-way plate 171
Figure 7.3: Stresses in a circular concrete prism subjected to bond stresses: (*a*) parabolic stress distribution; (*b*) triangular stress distribution; (*c*) diameter of the effective embedment zone 175
Figure 7.4: Comparison of crack spacing equations at 150 mm bar spacing 182
Figure 7.5: Comparison of crack spacing equations at 250 mm bar spacing 182
Figure 8.1: Strut-and-tie model for bottle-shaped strut; (*a*) Transverse stress distribution; (*b*) Compression isostatics; (*c*) Elastic distribution; (*d*) equivalent strut and tie model 194
Figure 8.2: Stress fields generated in a slab column connections after cracking 198
Figure 8.3: Strut and tie model for a slab column connection reinforced with minimum shear reinforcement 199
Figure 8.4: Refined strut and tie model for symmetric punching of concrete slab 201
Figure 8.5: High radial compression stress failure mechanism 201
Figure 8.6: Strut and tie Model for a thick plate with shear reinforcement; (*a*) Equivalent plastic truss; (*b*) Force carried by concrete; (*c*) Force carried by shear reinforcement 209

List of Tables

Table 3.1 Mix proportions 43
Table 3.2 Details of test specimens 43
Table 3.3 Minimum reinforcement ratios required by different codes for tested slabs 43
Table 4.1 Details of Group A test specimens 65
Table 4.2 Deflection characteristics of test slabs 67
Table 4.3 Observed ductility and energy absorbtion 75
Table 4.4 Experimental measured crack spacing and crack width for tested slabs 85
Table 5.1 Details of Group B test specimens 100
Table 5.2 Deflection characteristics of test slabs 101
Table 5.3 Observed ductility and energy absorbtion 108
Table 5.4 Measured crack spacing and crack width 120
Table 6.1 Details of test specimens by Battista (1992) 142
Table 6.2 Minimum reinforcement ratios required by proposed equation and different codes formulae for tested slabs by Battista (1992) 143
Table 6.3 Minimum shear reinforcement requirements in different design codes 163
Table 7.1 Details of test specimens by Gilbert and Nejadi (2004) 179
Table 7.2 Details of test specimens by Frosch et al. (2003) 179
Table 7.3 Details of test specimens by Hossin and Marzouk (2008) 180
Table 7.4 Comparison between the calculated crack spacing values using code formulae with the measured experimental values for test specimens by Gilbert and Nejadi (2004) 180
Table 7.5 Comparison between the calculated crack spacing values using code formulae with the measured experimental values for test specimens by Frosch et al. (2003) 181
Table 7.6 Comparison between the calculated crack spacing values using code formulae with the measured experimental values for test specimens by Hossin and Marzouk (2008) 181
Table 7.7 Comparison between the calculated crack spacing values using code formulae with the measured experimental values 183
Table 7.8 Comparison between the calculated crack width values using code formulae with the measured experimental values for test specimens by Gilbert and Nejadi (2004) 188
Table 7.9 Comparison between the calculated crack spacing values using code formulae with the measured experimental values for test specimens by Frosch et al. (2003) 188
Table 7.10 Comparison between the calculated crack spacing values using code formulae with the measured experimental values for test specimens by Hossin and Marzouk (2008) 189
Table 7.11 Comparison between the calculated crack width values using code formulae with the measured experimental values 189
Table 8.1 Comparison between ultimate calculated loads with test results 211
Table 8.2 Comparison between ultimate calculated loads with test results 211
Table 8.3 Comparison between ultimate calculated loads with test results 211
Table 8.4 Comparison between ultimate calculated loads with test results 212
Table 8.5 Comparison of code predictions with test results 214

Notation and List of Abbreviations

A_c = area of concrete cross section

$A_{c,ef}$ = area of concrete symmetric with reinforcing steel divided by number of bars

A_g = the gross area of the cross section

A_s = area of reinforcement within the effective embedment thickness

$A_{s,\min}$ = the minimum flexure reinforcement area

$A_{v,\min}$ = minimum web reinforcement area

$A_{z,\min}$ = area of minimum shear reinforcement

a_x, a_y = the cross-sectional areas of the orthogonal bottom reinforcements per unit width of the slab

b = width of the section (also plate span)

b_o = perimeter of critical section for shear in slabs and footings

b_t = width of tension side

b_w = minimum effective web width

C = side length of square column

c = concrete cover; thickness of cover element (sandwich model)

C_c = clear cover from the nearest surface in tension to the flexural tension reinforcement

c_s = the diameter of the effective embedment zone where the reinforcing bar can influence the concrete bond

d = effective depth to the centroid of the tensile reinforcement

d_b = reinforcing bar diameter

d'_{be} = equivalent bar diameter of the outer layer of the bars

d_c = thickness of cover from the extreme tension fiber to the closest bar

d_v = the effective shear depth of the core, is given by $d_v = h - c$

D = bending rigidity of the plate

D = diameter of column

E_s = steel modulus of elasticity

E_c = the tangent modulus of elasticity of concrete

f_b = bond strength

f_{bo} = maximum bond strength

f'_c = uniaxial compressive strength of concrete (cylinder strength)

$f_{c2,\max}$ = the crushing strength of cracked concrete

f_{ck} = the characteristic compressive strength of the concrete in MPa

f_{cm} = the cylindrical compressive strength of concrete

f_{ct} = the direct tensile strength of concrete

$f_{ct,eff}$ = tensile strength of the concrete effective at the formation of the first crack

f_{ctm} = the mean value of the concrete tensile strength at the time that the crack forms

f_r = the rupture strength of concrete

f_{sk} = the characteristic reinforcement strength defined as yield stress or as the 0.2 % proof stress in MPa

$f_{sp,t}$ = splitting bond stress

f_{tk} = the expected lower characteristic tensile strength of the concrete in MPa

f_s = stress in reinforcement due to applied load

f_y = yield stress of steel

$f_{ywd,ef}$ = the effective design strength of the punching shear reinforcement

G_f = the fracture energy

h = section height

h_{ef} = effective embedment thickness

k = fracture coefficient depending on the type of loading and boundary conditions.

k_1 = coefficient that characterizes bond properties of bars

k_2 = coefficient to account for strain gradient

k_b = a constant to account for the surface characteristics of the bar and the distribution of bond stress

kd = the distance from extreme compression fiber to the neutral axis calculated using first moment equation of area

K_{Ic} = the critical stress intensity factor calculated as $(G_f E_c)^{0.5}$

k_t = tensile stress factor

k_w = size effect factor (NS 3473 E 1989)

l_{ch} = characteristic length

$l_{s,max}$ = the length over which slip between steel and concrete occurs; steel and concrete strains, which occur within this length, contribute to the width of the crack

M_c = magnified factored moment to be used for design of compression member.

M_{cr} = cracking bending moment

M_u = ultimate bending moment

M_x = bending moment per unit length

M_y = bending moment per unit length

M_{xy} = torsional moment per unit length

M_u = ultimate bending moment

N_p = brittleness number

N_{PC} = the critical value of the brittleness number, which distinguishes two failure modes (brittle and ductile)

N_x = in plane axial applied force per unit length

N_y = in plane axial applied force per unit length

N_{xy} = in plane shearing force per unit length

P_{ult} = the corresponding ultimate punching shear capacity failure mechanism

S = center-to-center spacing of flexural tension reinforcement nearest to the surface of the extreme tension face

s = maximum spacing of shear reinforcement

S_m = the average crack spacing of cracks normal to the reinforcement

S_{mx} = the crack spacing for cracks normal to x reinforcement

S_{my} = the crack spacing for cracks normal to y reinforcement

$S_{m\theta}$ = the average crack spacing for cracks inclined to the reinforcement

S_r = the spacing of shear links in the radial direction

S_{rm} = average stabilized crack spacing

S_t = the spacing of shear links in the tangential direction

U = ductility, is defined as the ratio of the Post ultimate deflection Δ_U to deflection at first yield Δ_y

u_1 = for both circular and square loaded areas being the length of a square perimeter 1.5 d from the loaded area

V_c = nominal shear strength provided by concrete

V_x = shearing force per unit length

V_y = shearing force per unit length

v_u = the shear strength of slab as defined by the Canadian code CSA-23.3-04[14]

w = the fluid pressure on the face, MPa

w = the plate's deflection

w_k = the characteristic crack width

w_m = average crack width

y = the depth of flexural compression zone in slab (depth of neutral plane)

y_1 = the distance from the neutral axis to the center of the lower tensile force

α = sensitivity number

α = the angle between stirrups and longitudinal axis of the beam

α_s = constant used to compute V_c in slabs and footings

β = member size effect factor

β = coefficient relating the average crack width to the design value

ν = Poisson's ratio

τ_{bk} = lower fractile value of the average bond stress

λ = modification factor of lightweight concrete

$\rho_{z,\min}$ = the minimum shear reinforcement ratio

σ_{cp} = the average stress in concrete section due to normal force

σ_s = stress in the tension reinforcement computed on the basis of a cracked section

σ_{sr} = stress in the tension reinforcement computed on the basis of a cracked section under loading conditions that cause the first crack

σ_{s2} = reinforcement stress at the crack location

σ_{sE} = steel stress at point of zero slip

$\rho_{s,ef}$ = effective reinforcement ratio; and equals the area of the steel considered divided by the area of effective zone where the concrete can influence the crack widths

Δ_U = Post ultimate deflection

Δ_y = deflection at first yield

λ = modification factor reflecting the reduced mechanical properties of lightweight concrete

θ = the angle of inclination of normal to crack to x reinforcement

α_s = constant used to compute V_c in slabs and footings

Δ_U = Post ultimate deflection

Δ_y = deflection at first yield

ε_1 = the largest tensile strain in the effective embedment zones

ε_2 = the smallest tensile strain in the effective embedment zones

ε_{cr} = strain in concrete at cracking

ε_{ct} = tensile strain in concrete

ε_{cm} = average concrete strain within segment length, $l_{s,max}$

ε_{cs} = strain of concrete due to shrinkage

$\rho_{s,ef}$ = effective reinforcement ratio; and equals the area of the steel considered divided by the area of effective zone where the concrete can influence the crack widths

θ = the angle of inclination of normal to crack to x reinforcement

ϕ_s = reinforcing bar diameter or equivalent diameter of bundled bars

ACI = American Concrete Institute

CEB = Comite' Euro-Internationale de Beton

CSA = Canadian Standard Associations

EC2 = Euro-code

FIP = Federation Internationale de la Procontrainte

STM = Strut and tie model

NS = Norwegian Council for Building Standardization

Chapter 1

Introduction

1.1 General

Concrete structures codes have minimum steel reinforcement requirements for flexural members. Steel reinforcement requirements are intended to prevent excessive cracking at service loads for aesthetic and durability reasons, tie the structure together, ensure adequate deflection, provide a ductile response and ensure adequate warning of an impending failure at extreme overloads. While the minimum reinforcement requirements are empirical, there is a definite need to change it for thick concrete structures.

High-strength thick concrete plates are desirable structural elements for offshore and containment structures for nuclear power generation construction. For this application, current empirical building design codes formulae for minimum flexural reinforcement ratios seem to provide excessive reinforcement. The minimum required amount of reinforcement that is enough for crack control is not easily determined. Since the analysis of crack formation is complex, the present minimum reinforcement guidelines are empirical and have not normally considered the effect of member size (size effect). An accurate estimate of the minimum flexure reinforcement ratio can result in saving millions of dollars for a single project (Hibernia oil platform).

One of the objectives of good structural design is to limit the crack that forms in concrete members to an acceptable width. The definition of what is acceptable depends on the intended use of the structure, the anticipated loading, and the environment to which it is exposed. In general, for a water-retaining concrete vessel or a foundation wall protecting a dry basement space, 0.5 mm cracks that allow water to seep through are not acceptable.

However, the same cracks in a non-exposed beam within a building envelope may be permissible. Engineering judgment, durability requirements and experience should lead to a decision on the level of crack control that is necessary. Some guidelines are also given by codes of practice.

The expression for crack spacing and crack width is based on the beam theory in several design codes, such as the Canadian offshore code CSA-S474-04, Norwegian Code 3473E (1989) and European CEB-FIP (1990) model code. The extensive use of thick concrete plates with thick clear concrete covers for offshore and nuclear containment structures requires the development of new rational formulae to accurately predict crack spacing and width.

Punching shear failures of concrete flat plate structures are undesirable modes of failure since they give little warning and have catastrophic consequences. However, although extensive research has been done on the punching shear strength of slabs, to date there is still no generally applicable, rational theory. The current building codes design procedures are based on empirical-based formulae that are based on the results of experimental tests performed mostly on thin slabs, and questions have been raised about their reliability to accurately predict the punching shear strength, especially for thick concrete plates. Moreover, there is a great discrepancy between different design codes (i.e. North American and European codes). ACI 318-08 design code does not even account for some basic and proven factors affecting the shear capacity of concrete members such as the effect of member size on the shear capacity of slab elements "size effect."

Thick concrete plates (250-500 mm) without shear reinforcement usually exhibit brittle shear failure under a central force that is transferred between the column and the plate. Conventional design methods consider potential punching failures in the vicinity of concentrated loads. Nominal shear stresses at well-defined critical sections are limited to guard against such failure modes. With the extensive use of thick plates of more than 250 mm thick made of high strength concrete for offshore structures and nuclear containment structures, different design codes must provide shear reinforcement requirements for such thick concrete plates. There have been several research investigations to study the effectiveness of different types of shear reinforcement used in two-way slabs. Different tests proved that the use of shear reinforcement in the form of stirrups, bent-up bars, or structural shear studs prevented brittle failure of test specimens.

1.2 Scope of Research

Research results suggest that the minimum flexure reinforcement ratio is member size dependent. However, the exact tendency of performance criterion is not very clear. The present minimum reinforcement guidelines are empirical and do not normally consider the effect of member depth (size effect). The main reason for the disregard of the size effect is the lack of conclusive experimental tests especially for thick high strength concrete slabs. The current research presents the need for an experimental work required in order to better understand the structural behaviour of thick HSC plates. The current research has a main objective to investigate the current design codes formulae for minimum flexural reinforcement requirements and with application to thick concrete plates used in offshore structures and to control cracking of high strength offshore concrete structures.

Providing a minimum amount of steel reinforcement is the conventional method of crack control. The idea is to use enough reinforcement to prevent a single, wide crack from forming. Instead, it is preferable that cracking is distributed so that many cracks of small widths form. Distributed, small cracks provide much better resistance to the flow of water through the concrete. Use of thick concrete covers in offshore and nuclear containment applications is increasing because it is a durability issue. Most crack width models indicate that increasing concrete covers results in increased crack spacing and hence increased crack width; this means that thick concrete covers are detrimental to crack control. The current research is focused on evaluating the effect of using thick concrete covers on crack widths and crack properties of thick plates used for offshore and nuclear containment structures. This study will address the two main issues that control crack width and concrete cover and their influence on each other. The objective is to achieve the benefit of both for the proper design of durable concrete in aggressive environments.

The purpose of this investigation is to study the mechanism by which cracks form in flexural thick specimens, and to develop formulae that will enable the design engineer to predict the spacing and width of cracks.

Design formulae for punching shear, or two-way shear, are based on the results of experimental tests performed mostly on thin slabs. Design codes, however, are generally applied to design thick plates and footings. The few available tests performed on thick slabs exhibit a notable size effect. As a consequence, there is a need for a rational model correctly describing punching shear and accounting for size effect (defined as decreasing nominal shear strength with increasing size of the member). The work done presents an experimental investigation required to study the structural behaviour of thick concrete

plates. Twelve thick concrete specimens with total thickness of 150-400 mm had been tested to examine the accuracy of available design equations. Eleven specimens had no shear reinforcement, whereas the remaining one included T-headed shear reinforcement consisting of vertical bars mechanically anchored at top and bottom by welded anchor plates.

The scope of this work is extended to include theoretical investigation of minimum flexure and shear reinforcement of plates. The theoretical investigation includes developing new formulae to calculate minimum flexure and minimum shear reinforcement requirements for thick plates. The research is also extended to investigate crack spacing and crack width for plates and two-way slabs. The investigation includes developing formula to calculate crack spacing based on the action of two-way slabs. Such a model is needed for researchers and engineers to predict the spacing and width of cracks. In addition, a strut-and-tie model is to be developed to investigate the behaviour of thick plates with and without shear reinforcement.

1.3 Research Objectives

The objectives of the current research program are to investigate the structural behavior of offshore thick concrete plates. The specific objectives of both experimental and theoretical investigations can be summarized as follows:

- To establish experimental data for high strength concrete plate sections up to 400 mm thickness with 60-70 mm clear concrete cover under punching and flexure loading, these experimental data are required to better understand the size effect phenomena and to investigate the effect of plate's thickness on the structural behavior of thick HSC plates (size effect).

- To investigate the suitability of current minimum flexure reinforcement formula recommended in CSA-S474-04 Standard against other existing formulae, to develop formula to calculate minimum flexure reinforcement for thick plates and two-way slabs considering the torsional moment effect and member size effect, to check the validity of the new minimum flexure reinforcement criteria against experimental data, to develop formula to calculate minimum shear reinforcement required to prevent brittle shear failure of thick plates in the vicinity of concentrated loads and to recommend minimum shear reinforcement requirements for thick HSC plates.
- To develop formula to calculate crack spacing and crack width for plates and two-way slabs, based on action of two-way slabs to help researchers and engineers to determine the suitable bar spacing to control crack.
- To analyze the punching shear behaviour of thick concrete plates, using a strut-and-tie model. This model provides a quick rational and simple approach to punching shear behavior, and to investigate the size effect in high strength concrete plates in order to better understand the punching mechanism of thick plates.

Assessment of the proposed models will be achieved through comparing prediction given by each model against collected test results. Twelve full-scale, normal and high-strength concrete specimens with different thick concrete covers and reinforcement ratios tested under flexural loading were selected for the experimental investigation. All specimens were instrumented to enable their various behavioral aspects to be studied as each test

carried out. A new test setup was built to handle thicker full scale specimens under higher flexural loads.

1.4 Thesis Outline

Chapter 2 is divided into three phases intended to survey relevant research work. The first phase surveys research work related to the design and code requirements of minimum flexure and shear reinforcement for beams, one- and two-way slabs. The second phase surveys research work related to the design and code requirements of crack spacing and crack width of beams, one- and two-way slabs. The third phase surveys experimental research work related to the punching shear behaviour of slabs using different types of concrete or shear reinforcement.

In Chapter 3, details of the test set up, the loading frame, instrumentation and preparation of high strength concrete specimens are given. In addition, the cracking behavior of high strength reinforced concrete plates is examined experimentally, with emphasis on the effect of concrete cover, bar spacing and plate thickness. Finally, a description of the instrumentation and the data acquisition system is provided.

Chapter 4, reports the observed test results in terms of load-deflection relationship, strains in concrete and steel bars, crack width, and crack patterns for first slabs group (group A). The load carrying capacity as well as the deformational characteristics of the tested specimens is discussed.

Chapter 5, reports the observed test results in terms of load-deflection relationship, strains in concrete and steel bars, crack width, and crack patterns for second slabs group (group B); this group has thicker specimens compared to specimens from the first group (group

A). The load carrying capacity as well as the deformational characteristics of the tested specimens is discussed.

Chapter 6 introduces a model developed to calculate minimum flexure reinforcement for plates and two-way slabs. The model presents two new main contributions, the first contribution considers the size effect through fracture mechanics concepts and the second contribution considers the torsional moment effect for thick plates in calculating minimum flexure reinforcement of clamped or continuous plates. This chapter also introduces different models developed to calculate minimum shear reinforcement for thick plates.

Chapter 7 introduces developed model for calculating crack spacing for plates and two-way slabs. The proposed model takes into account the effect of steel reinforcement in the transverse direction through the splitting bond stress. The new equation provides good estimates for crack spacing in plates and two-way slabs with different concrete covers.

Chapter 8 introduces a method to calculate minimum shear reinforcement required to prevent brittle shear failure of thick concrete plates in the vicinity of concentrated loads based on a strut-and-tie model. This chapter presents a strut-and-tie model also developed to model the punching shear behaviour of a concrete plate. This model provides a quick and simple approach to calculate punching shear capacity of concrete plates. It is applicable for both normal and high strength concrete plates under symmetric and unsymmetric loading with and without shear reinforcement.

The last chapter, Chapter 9, summarizes and concludes the findings of the experimental work presented in Chapters 4 and 5, and of the theoretical work presented in Chapters 6, 7 and 8.

Chapter 2

Literature Review

2.1 Introduction

Design codes specify minimum flexure reinforcement for reinforced concrete beams and slabs. With the extensive use of thick concrete plates, the empirical expressions used in the past for minimum flexure reinforcement that usually ignored the effect of concrete member thickness, have to be revised. Research results suggest that the minimum reinforcement ratio is member size dependent. However, with the lack of experimental data, the effect of member size is not clear. Slabs may be subdivided into thick slabs with a thickness greater than about one-tenth of the span, thin slabs with a thickness less than about one-fortieth of the span, and medium-thick slabs. Thick slabs transmit a portion of the loads as a flat arch and have significant in-plane compressive forces, with the result that the internal resisting compressive force is larger than the internal tensile force. Thin slabs transmit a portion of the loads acting as a tension membrane. A medium-thick slab does not exhibit either arch action or membrane action.

2.2 Minimum Flexural Reinforcement

Research results suggest that the minimum reinforcement ratio is member size dependent. However, the exact tendency performance criterion is not very clear. The main criterion for evaluating the minimum flexural reinforcement requirements is to have an ultimate moment, M_u greater than the cracking moment, M_{cr}. Although all researchers agree that the ultimate moment should be greater than the cracking moment, there is no agreement on the ratio. Most design codes deal with the minimum steel reinforcement ratio independent of member size. Only a few codes, such as the Norwegian Code 3473 E

(1989) and some recent numerical studies (Bosco and Carpinteri 1992), suggest that the minimum reinforcement ratio is a size dependent factor. Recent analytical advances make it possible to use fracture mechanics concepts to rationally define the minimum reinforcement requirements necessary to avoid a brittle failure.

Tests that determine the amount of reinforcement required to prevent brittle failure in high-strength concrete slabs was conducted by Battista (1992). The researcher found that the Canadian building code requirement of CSA-A23.3-94 Clause 7.8.1, which specifies $A_{smin} = 0.002\ A_g$, can be sufficient in producing a ductile failure for slabs with strengths up to 85 MPa. Battista (1992) found that thicker slabs cracked at a lower calculated stress than thinner slabs, implying that the minimum reinforcement ratio for thicker members can be less than that required for thinner members. The fact that larger members crack at lower values of flexural tensile stresses is recognized in the CEB-FIP (1990) model Code, where the flexural cracking stress is assumed to be inversely proportional to the fourth root of the depth, up to depths of one meter.

2.2.1 Historical Development of North American Codes

The minimum flexural reinforcement requirements given in the old Canadian building standard (CSA-A23.3-84) is the same as the ACI 318-89 code, which are briefly summarized in the following paragraph. The SI units are used for all the expressions. The CSA-A23.3-84 and ACI 318-89 expression is as follows:

$$\rho_{min} = \left(\frac{A_s}{b_w d}\right)_{min} = \frac{1.4}{f_y} \tag{2.1}$$

The expression in the Canadian standard (CSA-A23.3-84) for minimum flexural reinforcement was revised in 1994 to include the concrete strength. The expression is very similar to the one given in ACI 318-95.

$$\rho_{\min} = \left(\frac{A_s}{b_t h}\right)_{\min} \cong 0.2\frac{\sqrt{f_c'}}{f_y} \tag{2.2}$$

The limit of validity for concrete strength is given as 20 MPa < f_c' < 80 MPa.

North American design codes such as ACI 318-08 and CSA-A23.3-04 Codes do not account for the member size effect. The ACI 318-08 code states that at every section of a flexural member where tensile reinforcement is required by analysis, it should not be less than that given by:

$$A_{s\min} = \frac{0.25\sqrt{f_c'}}{f_y} b_w h \quad (\text{mm}^2) \tag{2.3}$$

where b_w is the minimum effective web width, h is the height of the member, f_c' is the specified compressive strength of concrete and f_y is the specified yield strength. $A_{s\min}$ shall not be taken less than 1.4 $b_w d / f_y$. For statically determinate members with a flange in tension, $A_{s,\min}$ shall not be less than the value given by Equation (2.3), except where b_w is replaced by either $2b_w$ or the width of the flange, whichever is smaller.

The 2004 Canadian Offshore Code CSA-S474-04 states that the area of reinforcement near each face and in each of the two orthogonal reinforcement directions shall not be less than 0.003 times the area of the concrete section for all exterior elements. The area of primary reinforcement near the concrete face of an element exposed to fluid pressure shall not be less than the area calculated using the following equation:

$$A_s = \left[\frac{f_{cr} + w}{f_y}\right] b\, h_{ef} \ (\text{mm}^2) \tag{2.4}$$

where w is the fluid pressure on the face, MPa, the centre-to-centre spacing of the reinforcing bars near each concrete face and in each direction should not exceed 300 mm.

This equation gives high values for minimum reinforcement, especially for structures subjected to high fluid pressures.

The Norwegian code (NS 3473 1989) accounts for the effect of the member size. The code determines that transverse to the main reinforcement and directly on this, a continuous minimum reinforcement shall be placed. The reinforcement shall have a total cross-sectional area equal to:

$$A_s \geq 0.25\, k_w\, A_c\, f_{tk} / f_{sk} \tag{2.5}$$

where $k_w = 1.5 - h/h_1 \geq 1.0$ (size effect factor), h is the thickness of the cross section and $h_1 = 1000$ mm, f_{tk} is the expected lower characteristic tensile strength of the concrete in MPa and f_{sk} is the characteristic steel reinforcement strength defined as the yield stress or the 0.2 % proof stress in MPa. In concrete structures where special requirements to limiting crack widths apply, the minimum reinforcement should be at least twice the value given above.

Eurocode 2 (2004) states that, if crack control is required, a minimum amount of bonded reinforcement is required to control cracking in areas where tension is expected. The amount may be estimated from equilibrium between the tensile force in concrete just before cracking and the tensile force in reinforcement at steel reinforcement yielding stress or at a lower stress if necessary to limit the crack width.

Unless a more rigorous calculation shows lesser areas to be adequate, the required minimum areas of reinforcement may be calculated as follows. In profiled cross sections like T-beams and box girders, minimum reinforcement should be determined for the individual parts of the section (webs, flanges).

$$A_{s,\min} = K_c\, K\, f_{ct,eff}\, A_{ct} / \sigma_s \tag{2.6}$$

where $A_{s,\min}$ is the minimum area of reinforcing steel within the tensile zone, A_{ct} is the area of concrete within tensile zone. The tensile zone is that part of the section to be in tension just before formation of the first crack, σ_s is the absolute value of the maximum stress permitted in the reinforcement immediately after formation of the crack. This may be taken as the yield strength of the reinforcement, f_{yk}. A lower value may, however, be needed to satisfy the crack width limits according to the maximum bar size or the maximum bar spacing, $f_{ct,eff}$ is the mean value of the tensile strength of the concrete effective at the time when the cracks may first be expected to occur, $f_{ct,eff} = f_{ctm}$ or lower, ($f_{ctm(t)}$), if cracking is expected earlier than 28 days, k is the coefficient that allows for the effect of non-uniform self-equilibrating stresses that lead to a reduction of restraint forces, $k = 1.0$ for webs with $h \leq 300$ mm or flanges with widths less than 300 mm, and $k = 0.65$ for webs with $h \geq 800$ mm or flanges with widths greater than 800 mm intermediate values may be interpolated, k_c is a coefficient that takes account of the nature of the stress distribution within the section immediately prior to cracking and of the change of the lever arm, for pure tension, $k_c = 1$.

Ghali et al. (1986) recommended that if the reinforcement in a cross-section of a member is below a minimum ratio, $\rho_{\min,y}$, to ensure that yielding of the reinforcement occurs at the formation of the first crack. Such a crack will be excessively wide and formation of several cracks with limited width does not take place. This is true when cracking is induced by applied forces or imposed displacements. The minimum reinforcement cross-section area $A_{s,\min,y}$, and the corresponding steel ratio $\rho_{\min,y}$ to ensure that wide isolated cracks do not occur due to yielding is given by the following expression:

$$\rho_{\min,y} = \frac{A_{s\min,y}}{b\,d} \cong 0.24\frac{f_{ct}}{f_y} \tag{2.7}$$

where b is the width of the tension side, d is the height of the cross section, f_{ct} is the tensile strength of concrete determined from split cylinder tests, f_y is the yield strength of steel and A_c is the cross sectional area. This equation is suitable for members subjected to significant amounts of flexural tensile forces. Hence, it is suitable for offshore applications.

2.3 Effect of Member Size on Minimum Reinforcement Ratio

Most design codes, with the exception of the Norwegian code (NS 3473 E 1989), specify minimum reinforcement requirements that are depth independent, although ACI 318-89 does have different requirements for beams and slabs.

2.3.1 Slab Size Effect

Bosco et al. (1990) evaluated the minimum flexural reinforcement corresponding to a condition at which the formation of first flexural cracking and yielding of the steel reinforcement occur simultaneously. Linear elastic fracture mechanics (LEFM) model was able to capture the most relevant aspects and trends in the mechanical and failure behaviour of lightly reinforced HSC beams in flexure. The brittleness number is derived from linear elastic fracture mechanics concepts as:

$$\frac{A_s}{A} = \frac{N_p K_{IC}}{f_y h^{0.5}} \tag{2.8}$$

where A_s/A is the steel ratio based on the gross section of the beam, K_{Ic} is the critical stress intensity factor calculated as $(G_f E_c)^{0.5}$ where G_f is the fracture energy and E_c is the modulus of elasticity determined by standard methods, f_y is the yield strength of the steel and h is the overall depth of the beam.

Carpinteri (1984) and Bosco et al. (1991) found that the brittleness of structural concrete increases as the size increases and/or the reinforcement ratio decreases. Physically similar

behaviour has been revealed in cases where the brittleness number N_P is the same. Different sizes of beams with HSC (compressive strength 91.2 MPa) have been tested. At a value of N_P equal to 0.26, the yielding moment is more or less equal to the first cracking moment of the beam. The reinforcement corresponding to this condition was considered for predicting the minimum reinforcement in flexural members. The percentage of reinforcement established by many codes is conservative for large size beams, whereas it tends to be insufficient for small size beams. The minimum percentage of reinforcement tends to be inversely proportional to the beam depth, while the values specified by the codes are independent of the beam depth. Hillerborg (1990) considered strain localization in concrete while analyzing the reinforced concrete beams. Strain localization is a fact in tension in concrete and the stresses pass through the peak. The descending portion occurs due to crack formation within the fracture process zone. From the analysis of reinforced concrete beams, the balanced reinforcement ratio decreases with increasing beam depth. Based on experimental results (Bosco et al. 1990), the following relationship between the critical values of the transitional brittleness number N_{PC}, corresponding to the minimum reinforcement condition and the concrete compressive strength has been determined:

$$N_{PC} = 0.1 + 0.0023 f_{cm} \tag{2.9}$$

N_{PC} is the critical value of the brittleness number, which distinguishes two failure modes (brittle and ductile) and f_{cm} is the cylinder compressive strength of concrete. By substituting this expression in Equation (2.8), the following formula for the evaluation of the minimum reinforcement can be derived as follows:

$$\rho_{\min} = \frac{K_{IC}}{f_y h^{0.5}}\left(0.1 + 0.0023 f_{cm}\right) \tag{2.10}$$

2.4 Minimum Flexure Reinforcement for HSC Plates

In studying the cracking for restrained HSC members due to temperature and shrinkage strains, Bergner (1994) presents an equation predicting the tensile load at first cracking:

$$F_{crack} = A_i \, f_{ctm} \, k_{z,t} \, \lambda_{Reinf} \tag{2.11}$$

where, F_{crack} is the tensile load producing first crack, A_i is the area of concrete member including reinforcement (transformed), A_s is the area of reinforcement, f_{ctm} is the mean tensile strength of concrete at 28 days, $k_{z,t}$ is a time factor (suggested values given by Bergner 1994), λ_{Reinf} is a factor of inherent stress caused by reinforcement and chemical (basic) shrinkage = 0.85 for $0 \leq \mu \leq 1.0$ %, = 0.90 - 0.05 μ for $\mu \geq 1.0$ %, μ = reinforcement ratio. Bergner (1994) also estimated the minimum reinforcement that will produce distributed cracking without yielding of the reinforcement as follows:

$$A_{s,rec} = F_{crack} / \sigma_{s,zul} \tag{2.12}$$

where, $A_{s,req}$ is minimum reinforcement and $\sigma_{s,zul}$ is steel stress.

A few tests were conducted to determine the amount of reinforcement required to prevent brittle failure in high-strength concrete slabs. Twenty four one-way slabs subjected to pure flexure were tested by Battista (1992). The test variables were concrete compressive strength, slab thickness, and ratio of ultimate stress to yield stress of reinforcement. While the 150 mm thick high-strength concrete slab with a reinforcement ratio of 0.2% showed an undesirable response, a companion specimen that was 300 mm thick made from the same concrete, also having a reinforcement ratio of 0.2%, displayed a very ductile response, with the post-cracking capacity exceeding the cracking moment by about 60%. After cracking, it is important to guarantee that, the forces resisted by concrete in tension are transmitted to tensile longitudinal steel. The 300 mm thick slabs

tested by Battista (1992) cracked at a lower calculated stress than the 150 mm thick slabs, which had the same minimum reinforcement ratio, this implies that the minimum reinforcement ratio required to carry the applied forces for thicker members could be less than that required for thinner members, which is known as the size effect factor.

The fact that larger beams crack at lower values of flexural tensile stresses is recognized in the CEB-FIP (1990), where the flexural cracking stress is assumed to be inversely proportional to the fourth root of the depth, up to depths of one meter. It has been recommended that the code requirement of CSA-A23.3-94 (Clause 7.8.1), which requires $A_{smin} = 0.002\ A_g$, can be sufficient in producing a ductile failure for slabs with strengths up to 85 MPa.

2.5 Minimum Shear Reinforcement

Thick concrete plates (250-500 mm) without shear reinforcement usually exhibit brittle shear failure under an axial force that transferred between the column and the plate. Conventional design methods consider potential shear failures of a slab as a wide beam as well as punching failures in the vicinity of concentrated loads. Nominal shear stresses at well-defined critical sections are limited to guard against such failure modes. With the extensive use of thick plates of more than 250 mm thickness, made of high strength concrete for offshore structures, different design codes must provide minimum shear reinforcement requirements for such thick plates. There have been several research investigations to study the effectiveness of different types of shear reinforcement used in two-way slabs. Different tests proved that the use of shear reinforcement in the form of stirrups, bent-up bars, or structural shear heads enhanced the ductility and energy absorption of tested specimens.

2.5.1 Minimum Shear Reinforcement for Plates and Two-Way Slabs

Shear reinforcement assembly, composed of vertical bars with forged anchor heads at their top ends and welded to a steel strip at their bottom ends, was originally developed at the University of Calgary. Extensive tests conducted in Canada and Germany (Elgabry and Ghali 1987; Andrä 1981; Dilger et al. 1981; Mokhtar et al. 1985) on full-size slab-column connections verified that stud type reinforcements can substantially increase the strength of slabs and prevent brittle failure. Marzouk and Jiang (1997) conducted an experimental investigation of six high strength concrete plates. The punching shear behavior of high strength concrete plates with different types of shear reinforcement was examined. The test investigation included five different types of shear reinforcement with a shear reinforcement ratio around 0.7 to 1.0 percent by volume. Several types of shear reinforcements were used to enhance the punching shear capacity, such as single-bend, U-stirrups, double-bend, shear-stud and T-headed shear reinforcement. It was concluded that double bend, shear-stud and T-headed shear reinforcement were the most efficient shear enhancement for punching shear capacity of high-strength concrete plates. The punching shear of slabs provided with shear reinforcement was eliminated and the failure mode was transformed into flexural failure for the high-strength concrete plates utilizing the flexural reinforcement in a much better fashion. In the mean time, both ductility and energy absorption of the two-way slabs are significantly increased by using shear reinforcement.

Thick concrete slabs were investigated by the US Army Engineer Waterways Experiment Station (Woodson 1994); thirteen one-way reinforced concrete slabs were statically loaded. The study emphasized primary parameters that affect the large-deflection

behavior of one-way slabs such as: support conditions, quantity and spacing of principal reinforcement, quantity and spacing of shear reinforcement, and span-to-effective-depth (L/d) ratio. The experimental program was designed to study the behavior of uniformly-loaded deep slabs and, in particular, to compare the effects of lacing bars and stirrups on the behavior. Lacing bars are reinforcing bars that extend in the direction parallel to the principal reinforcement and are bent into a diagonal pattern between mats of principal reinforcement. It is generally known that the cost of using lacing reinforcement is considerably greater than that of using single-leg stirrups due to the more complicated fabrication and installation procedures. The tests verified that shear reinforcement has a significant contribution to the ultimate resistance, and lacing and single-leg stirrups are about as equally as effective.

Kordina and Meichsner (1996) tested slabs having depths of 150, 250 and 450 mm; tests included slabs without any shear reinforcement and slabs provided with the minimum shear reinforcement calculated according to Eurocode 2 provisions (1992). The slabs had spans at least ten times their depth, their width being equivalent to four times their depth. The objective of the tests was to demonstrate the extent to which the provided shear reinforcement improves the load-bearing capacity of reinforced concrete slabs. Because of the minimum shear reinforcement provided, the shear failure loads remained practically unaffected.

Broms (2000) tested seven slab-column connections, all of which had the same dimensions and approximately the same flexural capacity, but with different reinforcement arrangements. The tests have demonstrated that flat plates with shear reinforcement arranged using bent bar as a hanger and stirrup combination exhibited a very

ductile behavior similar to that of ordinary reinforced concrete slabs supported by beams or walls. One of the advantages of using such arrangement is that it is easy to fabricate and install in a stable way.

More recently, an experimental research investigation of punching behavior of reinforced concrete footings were conducted by Hegger et al. (2006). Five reinforced concrete footings were tested to investigate the punching shear failure of footings realistically supported on sand. Four footings had no shear reinforcement, whereas the remaining specimen included shear reinforcement that consisted of vertical bars mechanically anchored at the top and bottom by welded anchor plates. The thickness of the footings ranged from 200 mm to 300 mm. The experimental results indicated that the angle of the shear failure crack is steeper than observed by punching tests of flat slabs. Based on the results of the experimental investigation, the observed angle of the failure cone is approximately 45° for all of the tested specimens.

Birkle and Dilger (2008) studied the influence of slab thickness on punching shear strength. A total of nine slab-column assemblies were tested to investigate the influence of the slab thickness on the shear strength of slab-column connections in three series. Each of the three test series had slabs with thicknesses of 160, 230, and 300 mm. It was concluded that a slab without shear reinforcement of 230 mm thickness may not have a high factor of safety if designed in accordance to ACI 318-05. For thick slabs with shear reinforcement, the shear stress resistance provided by concrete is also reduced, but to a lesser degree. Slabs with shear reinforcement resulted in significant increases in shear capacity and ductility in comparison with slabs without shear reinforcement. It was also recommended

that there is a significant decrease of the shear stress resistance with increasing slab thickness.

Twenty-eight large-scale tests were conducted by Jaeger and Marti (2009) to investigate the shear strength and deformation capacity of orthogonally reinforced concrete slabs. It was concluded that all tests without transverse reinforcement exhibited brittle shear failures; the addition of transverse reinforcements with reinforcement ratios of approximately 0.3% and 0.6% changed the failure modes to ductile flexural failures; and the tests without transverse reinforcement showed a significant influence of slab thickness on shear strength. The size effect was not observed for the tests with transverse reinforcement. The tests without transverse reinforcement also showed a reduced strength, no such reduction was observed in the tests with transverse reinforcement.

Vaz et al. (2009) performed a study that aims to define the minimum shear reinforcement of flat slabs that, leading to a punching shear failure surface that crosses that reinforcement, to avoid a sudden failure. In the attempt to define the minimum punching reinforcement of the slabs, a parameter k, equal to the total force in the transverse reinforcement inside a truncated cone bounded by the shear crack divided by the punching strength of a similar slab without shear reinforcement, was used. The punching failure surface crossed the shear reinforcement when k was smaller than around 0.70. The results of the analyzed tests point out that the value of k corresponding to the minimum reinforcement should be around 0.5 to 0.7.

2.6 Shear Strength of Two-Way Slabs

One of the early outstanding investigations of the two-way slab system was conducted by Kinnunen and Nylander in 1960. Tests were conducted on circular concrete slabs without

shear reinforcement. The specimens were circular shaped subjected to a uniformly distributed load along the circumference of the slabs. The mechanical model presented by researchers (Kinnunen and Nylander 1960) has been the basis of many subsequent rational models of analyzing two-way slabs.

Marzouk and Hussein (1991) reported tests of seventeen slabs with varying concrete strength of 30-80 MPa. Major conclusions derived from this investigation included that punching failure of high strength concrete slabs can be classified into two modes, "flexure-punching" and "punching-shear" failures. Flexural-punching occurs in the slabs with relatively low reinforcement ratio. As the steel reinforcement ratio is increased, slab stiffness increased and deformation capacity decreased. It was concluded that the ACI equations overestimate the shear capacity of a high-strength concrete slab. Relating connection shear strength to the square root of concrete strength, results in an overestimation of the effect of the concrete strength.

Alexander and Simmonds (1986) suggested a space truss model composed of steel tension ties and concrete compression struts inclined at an angle α to the slab plane. Although a straight-line compression strut was initially suggested, Alexander and Simmonds (1992) later concluded that a curved compression strut with varying α along the slab depth was more consistent with the test data.

An earlier strut-and-tie model was recommended by Tiller (1995) to model the punching shear behaviour of concrete slabs. The model can provide a quick and simple approach to punching shear behaviour. It is also applicable for both normal and high strength concrete under symmetric and nonsymmetric loading with and without shear reinforcement. In this research, the proposed strut-and-tie model for symmetric punching consists of a "bottle-

shaped" compressive zone in the upper section of the slab depth leading to a "rectangular-stress" compressive zone in the lower section depth.

2.7 Shear Design of Two-Way Slabs

Most code provisions with regards to two-way shear design of a slab-column connection use the critical section (control perimeter) approach. According to this method, the nominal shear stress due to gravity load is determined at an assumed vertical critical section around the column. The shear stress should be limited to a nominal shear strength that is usually assumed to be a function of concrete strength and geometric parameters. Although, such a method lacks physical reality, it is simple and leads to reasonable estimates if properly formulated.

Marzouk and Hussein (1991) and Gardner (1990) recommended the CEB-FIP (1990) code assumption, where the shear stress is proportional to the cubic root of concrete compressive strength, as a better option than the use of the square root for high strength concrete specimens with concrete strength more than 40 MPa. The analysis of the present results is made in relation to ACI 318-08, CEB-FIP (1990) and BS 8110-97.

2.7.1 Canadian Standard 2004 (CSA-A23.3-04) Requirements

The CSA-A23.3-04 code does not consider the effect of steel reinforcement ratio or the slab's effective depth less than 300 mm in its limiting shear stress. CSA-A23.3-04 requires that the ultimate shear strength for slabs without prestress is given by, for non-prestressed slabs and footings, v_c, which shall be the smallest of:

$$v_c = 0.38\lambda\phi_c\sqrt{f_c'} \tag{2.13}$$

$$v_c = 0.19\left(1+\frac{2}{\beta_c}\right)\lambda\phi_c\sqrt{f_c'} \tag{2.14}$$

$$v_c = \left(\frac{\alpha_s d}{b_o} + 0.19 \right) \lambda \phi_c \sqrt{f_c'} \tag{2.15}$$

where ϕ_c is resistance factors of concrete, λ is modification factor of lightweight concrete, β_c is the aspect ratio of the column, α_s = 40 for an interior column; f_c' is uniaxial compressive strength of concrete. If the effective depth, d, used in two-way shear calculations exceeds 300 mm, the value of v_c obtained from Equations (2.13) to (2.15) shall be multiplied by 1300/(1000+d), this size effect factor is not effective for slabs less than 300 mm thick. Fracture mechanics concepts suggest that the size effect factor is not related to the member thickness only but must be related to the concrete strength as well.

2.7.2 ACI 318-08

In ACI 318-08, the control perimeter is only 0.5 d from the loaded area. The ACI code has no influence from either the main steel ratio or the effective depth of the slab in its limiting shear stress. ACI 318-08 requires that the ultimate shear resistance for slabs without prestress is given by, for non-prestressed slabs and footings, v_c shall be the smallest of:

$$v_c = 0.33 \lambda \sqrt{f_c'} \tag{2.16}$$

$$v_c = 0.083 \left(\frac{\alpha_s d}{b_o} + 2 \right) \lambda \sqrt{f_c'} \tag{2.17}$$

$$v_c = 0.17 \left(1 + \frac{2}{\beta} \right) \lambda \sqrt{f_c'} \tag{2.18}$$

where β is the ratio of the long side to short side of the column, concentrated load or reaction area; α_s is 40 for interior columns, 30 for edge columns, 20 for corner columns, and

2.7.3 European Codes

Modern European codes in practice, treat punching in terms of shear stresses calculated for control perimeters at relatively large distances from columns or loaded areas. According to the CEB-FIP (1990) model code equation, the distance is 2.0 *d*. In BS 8110-97, it is 1.5 *d*, but the perimeter has square corners in comparison to the rounded corners of the CEB-FIP (1990) model code. The CEB-FIP code recommends that the punching shear resistance, V_{CEB}, is expressed as proportional to $(f_{ck})^{1/3}$ where f_{ck} is the characteristic compressive strength of concrete. The highest concrete grade considered in the CEB-FIP (1990) model code is C80 that corresponds to f_{ck} equal to 80 MPa. Influences of reinforcement ratio and slab depth are also considered in this design code. The relevant punching resistance in accordance to the CEB-FIP (1990) code is:

$$V_{CEB} = 0.18\sqrt[3]{100\rho \times f_{ck}}\left(1+\sqrt{200/d}\right)u_1 d \qquad (2.19)$$

where: $\left(1+\sqrt{200/d}\right)$ is a size-effect coefficient, u_1 is the length of the control perimeter at 2 *d* from the column and $\rho = \sqrt{\rho_x \rho_y}$, where ρ is the ratio of flexure reinforcement; ρ_x and ρ_y are the flexure reinforcement ratios in orthogonal directions.

The punching resistance in accordance to BS 8110-97 is:

$$V_{BS} = 0.79(100\rho)^{1/3}\left(f_c'/0.8\right)^{1/3}\sqrt[4]{400/d}\,u\,d \qquad (2.20)$$

where: $\sqrt[4]{400/d}$ is a size-effect coefficient, u for both circular and square loaded areas being the length of a square perimeter 1.5 *d* from the loaded area, and ρ is the ratio of flexure reinforcement.

2.8 Cracking in Reinforced Concrete Structures

Cracking in reinforced concrete structures is unavoidable due to the low tensile strength of concrete. Wider cracks may not only destroy the aesthetics of the structure, but also expose steel reinforcement to the environment leading to corrosion. To control the crack width at the member surface, designers may use the guidelines prescribed in various building codes. These guidelines are based on certain crack width prediction formulae developed by various researchers.

Cracking in a reinforced concrete member also causes a significant increase in deflection. This is a result of the reduction of bending stiffness at cracked sections when the contribution of tensile concrete below the neutral axis diminishes. However, at successive sections between cracks, some tensile stress is retained in the concrete around steel bars due to bond, contributing to the bending stiffness of the member. This phenomenon is called "tension-stiffening" effect. If the tension stiffening effect is neglected, the calculated deflection may be overestimated by a large proportion. In simplified methods of deflection calculation, the tension stiffening effect is incorporated in a semi-empirical manner by using the effective moment of inertia method. In analytical methods, the deflection is calculated using the curvature values, evaluated by adopting a non-linear stress-strain relationship for tensile concrete. This relationship allows the concrete to retain some tensile stress beyond the cracking strain.

Crack width models clearly illustrate that the crack spacing and width are functions of the distance between the reinforcing steel. Therefore, crack control can be achieved by limiting the spacing of the reinforcing steel. Maximum bar spacing can be determined by limiting the crack width to acceptable limits.

2.9 Crack Spacing

The average spacing of cracks normal to the reinforcement, S_m, may be calculated using the following equation:

$$S_m = 2.0(C_c + 0.1s) + k_1 k_2 d'_{be} h_{ef} b / A_s \text{ (CSA-S474-04 and NS 3473 E 1989)} \quad (2.21)$$

where S_m is the average crack spacing, C_c is concrete cover, s is bar spacing of outer layer, k_1 is coefficient that characterizes bond properties of bars, k_1 = 0.4 for deformed bars, k_1 = 0.8 for plain bars, this is related to the deformed rips on bars; k_2 is coefficient to account for strain gradient, k_2= 0.25 (ε_1 + ε_2) / 2 ε_1, where ε_1 and ε_2 are the largest and the smallest tensile strains in the effective embedment zones; d'_{be} is bar diameter of outer layer, h_{ef} is effective embedment thickness (see Figure 2.1) as the greater of $(C_c + d'_{be}) + 7.5d'_{be}$ and $a_2 + 7.5d'_{be}$ but not greater than the tension zone or half slab thickness, b is width of the section and A_s is area of reinforcement within the effective embedment thickness.

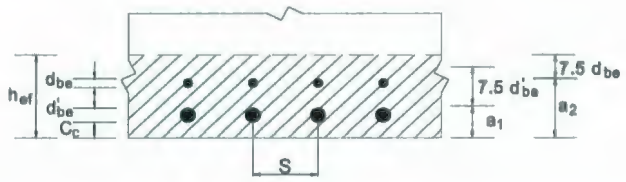

Figure 2.1: Effective embedment thickness (effective tension area)

The crack spacing expression of CEB-FIP (1990) is different compared with other codes (CSA-S474-04 and NS 3473E 1989). Meanwhile, the bond effect of CEB-FIP (1990) is treated in a different manner. For a cracked reinforced concrete section, an increase in loading will result in an increase in steel strain. This will cause an elongation of the reinforcing bar in which the bar ribs will tend to move toward the nearest crack relative to

the surrounding concrete. The stress in the steel caused by steel strain will be reduced due to the bond stress τ_{bk} between the steel and surrounding tensile concrete. Therefore, instead of using the factor k_1 to account for the bond effect, the CEB-FIP (1990) model code uses the bond stress τ_{bk} directly in the expression as shown in Equation (2.22).

$$l_{s,\max} = 2\frac{\sigma_{s2} - \sigma_{sE}}{4\tau_{bk}}\phi_s \tag{2.22}$$

$$l_{s,\max} = \frac{\phi_s}{3.6\rho_{s,ef}} \text{ for stabilized cracking} \tag{2.23}$$

$$l_{s,\max} = \frac{\sigma_{s2}}{2\tau_{bk}}\phi_s \frac{1}{1+\alpha_e \rho_{s,ef}} \text{ for a single crack formation} \tag{2.24}$$

$$S_{rm} = \frac{2}{3} l_{s,\max} \text{ for stabilized cracking} \tag{2.25}$$

where $l_{s,max}$ is the length over which slip between steel and concrete occurs, steel and concrete strains, which occur within this length, contribute to the width of the crack, σ_{s2} is steel stress at crack, σ_{sE} is steel stress at point of zero slip, ϕ_s is bar diameter, τ_{bk} is the lower fractile value of the average bond stress, α_e is the ratio (E_s/E_{ci}), E_s is steel modulus of elasticity, E_{ci} is the tangent modulus of elasticity of concrete, $\rho_{s,ef}$ is the effective reinforcement ratio ($A_s/A_{c,ef}$), $A_{c,ef}$ is the effective area of concrete in tension limited by slab width and height equal to the lesser of 2.5 ($c + \phi/2$) or ($h - c$)/3 is defined in Figure (2.2); and S_{rm} is the average crack spacing.

2.9.1 ACI 318-99 Approach

A reevaluation of cracking data (Frosch 1999) provided a new equation based on the physical phenomenon for the determination of the flexural crack widths of reinforced concrete members. This study showed that previous crack width equations are valid for a

relatively narrow range of covers (up to 63 mm). Frosch (1999) introduced this phenomenon into a new expression that was adopted by ACI 318-99.

ACI 318-99 does not make a distinction between interior and exterior exposure. It requires that for crack control in beams and one-way slabs, the spacing of reinforcement closest to a surface in tension shall not exceed that given by:

$$s = \frac{95000}{f_s} - 2.5C_c \tag{2.26}$$

But not greater than 300 (280 / f_s) or 300 mm, where f_s is calculated stress in reinforcement at service load = unfactored moment divided by the product of steel area and internal moment arm. Alternatively, f_s can be taken as 0.60 f_y, C_c is clear cover from the nearest surface in tension to the flexural tension reinforcement, and s is center-to-center spacing of flexural reinforcement nearest to the surface of the extreme tension face.

2.9.2 ACI 318-05 Major Changes

Equation (2.26), for maximum bar spacing to control cracking, was modified to provide results consistent with previous editions of the code while maintaining similar level of crack control. The default steel stress at service load in the equation was increased from 0.6 f_y to (2 / 3) f_y. The modified equation is intended to recognize the increase in service load stress level in flexural reinforcement resulting from the use of the load combinations introduced in the 2002 code. According to the new method, the spacing of reinforcement closest to a tension surface shall not exceed that given by:

$$s = 380\left(\frac{280}{f_s}\right) - 2.5C_c \tag{2.27}$$

but not greater than 300 (280 / f_s), where s is center-to-center spacing of flexural tension reinforcement nearest to the extreme tension face, f_s is calculated stress in reinforcement

at service load computed as the unfactored moment divided by the product of steel area and internal moment arm. It is permitted to take f_s as (2 / 3) f_y, and C_c is clear cover from the nearest surface in tension to the surface of flexure tension reinforcement.

2.9.3 Eurocode EC2 Provisions

The characteristic crack width is estimated by the next expression as:

$$w_k = \beta S_{rm} \xi \varepsilon_{sm} \tag{2.28}$$

where w_k is design crack width, S_{rm} is average stabilized crack spacing, ξ is a dimensionless coefficient between 0 and 1, representing the effect of the participation of concrete in the tension zone to stiffness of the member, ε_{sm} is mean strain under relevant combination of loads and allowing for effects, such as tension stiffening or shrinkage, β is coefficient relating the average crack width to the design value and equals to 1.7 and 1.3, respectively, for a section where the minimum dimensions exceed 800 mm or smaller than 300 mm. The average stabilized mean crack spacing S_{rm} is evaluated from the following expression:

$$S_{rm} = 2C_c + k_1 k_2 \frac{d_b}{4\rho_r} \tag{2.29}$$

where, d_b is bar diameter, mm, ρ_r is effective reinforcement ratio = A_s / A_{ct}, the effective concrete area in tension A_{ct} is generally the concrete area surrounding the tension reinforcement of depth equal to 2.5 times the distance from the tensile face of the concrete section to the centroid of the reinforcement. For slabs where the depth of the tension zone may be small, the height of the effective area should not be taken greater than [($c - d_b$) / 3], where C_c is clear cover to the reinforcement, mm, k_1 is 0.8 for deformed bars and 1.6 for plain bars, and k_2 is 0.5 for bending and 1.0 for pure tension. In cases of eccentric tension or for local areas, an average value of $k_2 = (\varepsilon_1 + \varepsilon_2) / 2\ \varepsilon_1$ can be used, where ε_1 is the

greater and ε_2 the lesser tensile strain at the section boundaries, determined on the basis of cracked section.

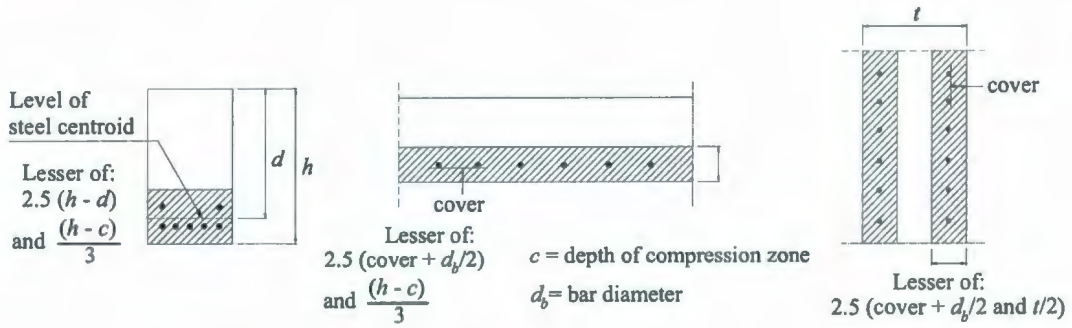

Figure 2.2: Effective area, $A_{c,ef}$ for use in equations (2.6): (*a*) beam; (*b*) slab; (*c*) member in tension (CEB-FIP Model code 1990)

2.10 Research on Cracking in Beams and One-Way Slabs

A total of twelve simply-supported beams and one-way slabs were subjected to constant sustained service loads for a period of 400 days by Gilbert and Nejadi (2004). The parameters varied in the tests were the shape of the section *b*/*h*, the number of reinforcing bars, the spacing between bars *s*, the concrete cover C_c, and the sustained load level. Experimental observations indicated that the bond stress reduces as the stress in the reinforcement increases and, consequently, the tensile stresses in the concrete between the cracks reduce (that is, tension stiffening reduces with increasing steel stress).

Frosch et al. (2003) tested ten one-way bridge deck slabs; the specimens were designed to represent a full scale cut section from a bridge deck. The primary variables evaluated in the study were the spacing of the reinforcement and the epoxy coating thickness. The parameters varied in the tests were the reinforcing bars type, the spacing between bars *s*

and the sustained load level. It was concluded that as the reinforcement spacing decreased, the spacing of primary cracks decreased and the number of primary cracks increased. As the reinforcement spacing increased, there was a corresponding increase in crack width.

2.11 Research on Cracking in Plates and Two-Way Slabs

Crack-control equations for beams underestimate the crack width developed in plates and two-way slabs (Nawy and Blair 1971). Desayi and Kulkarni (1976) developed an approximate method to predict the maximum crack width in two-way reinforced concrete slabs. The researchers calculated the maximum crack width based on an estimation of the crack spacing at any given stage of loading, which is between that stage and the ultimate load. Because, from the two-way action of slabs, when the stretching of bars in direction X and the concrete surrounding them are considered, the bars in the perpendicular direction can be assumed to bear against the concrete surrounding them. The spacing of cracks formed in direction X can be calculated using the following formula:

$$a_1 = \frac{k_t f_t A_{ct1}}{(\pi \phi_1 k_b f_b / S_1) + (\phi_2 f_{bb} / S_2)} \tag{2.30}$$

where f_b is the bond strength, k_b is constant to account for the surface characteristics of the bar and the distribution of bond stress, f_{bb} is the bearing stress, k_t *is* constant to account for the distribution of tensile stress, and f_t is the tensile strength of the concrete. The diameter of the bars in direction X is ϕ_1 and the spacing between bars is S_1. In direction Y, the diameter is ϕ_2 and the spacing is S_2. At any given stage of loading, the maximum crack width is obtained from:

$$w_m^s = a_{\max 1} \varepsilon_s R_1 \tag{2.31}$$

where a_{max1} is the maximum spacing of cracks that corresponds to that at M_{cr}, and R_1 is the cover ratio given by, this follows an assumption of linear variation of strain:

$$R_1 = \frac{d - d_{n1}}{d_1 - d_{n1}} \tag{2.32}$$

Rizkalla et al. (1983) conducted two extensive experimental programs to study the cracking behavior of reinforced concrete members subjected to pure tension in the presence of transverse reinforcement. The measured average values of the final crack spacing were compared to the values presented by other researchers. Based on this comparison, the researchers proposed a simplified expression for the prediction of crack spacing. The average crack spacing S_m may be calculated using the following equation:

$$S_m = 5(d - 7.2) + 1.33c + 0.08d / \rho \tag{2.33}$$

where d is the bar diameter, c is the clear concrete cover, and ρ is the steel reinforcement ratio. Hossin and Marzouk (2009) tested eight square specimens to investigate the crack width and spacing of high strength concrete slabs, five high strength concrete slabs (HSC) and three normal strength concrete slabs (NSC). Details of the eight specimens are provided later in Table 7.3. The structural behaviour with regards to the deformation and strength characteristic of high strength concrete slabs of various thicknesses and different reinforcement ratios (0.40-2.68%) were studied. The test results showed that as the concrete cover increases by 67%, the average crack width becomes larger by 90% experimentally. While increasing the bar spacing by 67%, increases the crack width by 19%. However, increasing the bar spacing further does not affect the crack width.

2.12 Crack Width

Crack width depends on the amount and distribution of reinforcing steel across the crack, concrete cover thickness and characteristics of the bond between the concrete and

reinforcement bars. Using thick concrete covers in offshore and nuclear containment applications is increasing. Most crack width models indicate that increasing concrete covers results in increased crack spacing and hence increased crack width this means that using thick concrete covers is detrimental to crack control.

2.13 Factors Affecting Crack Width

The following general trend can be seen in every prediction formula: an increase in the bar diameter and concrete cover, as well as a decrease in the reinforcement ratio will increase the crack width, if all other variables are kept constant. The following section includes discussion on the effects of various variables on the measured crack width, observed by different investigators.

2.13.1 Effect of Concrete Cover

As mentioned in the previous paragraph, an increase in concrete cover will result in a larger calculated crack width, according to all prediction formulae. In spite of this fact, provision of larger concrete cover is considered the most practical means of protecting reinforcement against corrosion. To investigate the effect of varying concrete cover, Makhlouf and Malhas (1996) carried out tests on 16 beams and compared the measured and calculated crack widths. Results of these tests revealed that the measured crack width increased by about 16% when the concrete cover was doubled from 30 mm to 60 mm. However, more than an 80% increase was predicted by the equations recommended in ACI 318-95 and BS 8110: Part 2 (1985), are based on expressions developed by Gergley and Lutz (1968) and Beeby (1979), respectively. It was concluded that, based on the above test results, the equations recommended in both the above building codes are too sensitive with respect to concrete cover. Further, as reported by Frosch (1999), concrete

covers only up to 65 mm have been used in experiments considered by Gergely and Lutz (1968) in the development of the prediction formula. As a result, the applicability of ACI 318-95 prediction procedure that is based on Gergely and Lutz (1968) formula is questionable in cases where the concrete cover exceeds 65 mm. An alternative approach for the calculation of crack width is proposed for thicker concrete covers ($d_c \geq 63$ mm) by Frosch (1999). In his approach, a flexural cracking model is considered and the crack width is assumed as a function of the bar spacing and the distance between the reinforcing steel. Therefore, crack control can be achieved by limiting the spacing of the reinforcing steel. The equation for the maximum crack width of uncoated reinforcement is:

$$w_c = 2\frac{f_s}{E_s}\beta\sqrt{d_c^2 + \left(\frac{s}{2}\right)^2} \tag{2.34}$$

where w_c is limiting crack width, s is maximum permissible bar spacing, d_c is bottom cover measured from the center of the bar, $f_s = 0.6 f_y$, $\beta = 1.0 + 0.08\, d_c$.

2.13.2 Effect of Reinforcement Ratio and Bar Diameter on Crack Width

Individual effects of bar diameter and reinforcement ratio on the crack width have not been investigated separately due to the interdependency of these two variables. It is very difficult to design a series of test specimens where only the bar diameter or the reinforcement ratio is changed one at a time. As reported by Kaar (1966), this difficulty has contributed to large differences in test results of the various investigators. It may also lead to differing conclusions on the relative significance of some of the variables.

2.14 Crack Width and Crack Spacing Based on Fracture Mechanics

Byung and Young (1986) developed formulae to calculate crack spacing and crack width based on cracking theory developed by Bazant and Byung (1984). The cracking theory is

based on the energy criterion of fracture mechanics as well as the strength criterion. An experimental program was set up and five reinforced concrete test beams have been designed to investigate crack width and crack spacing of reinforced concrete beams. The cracking theory indicates that the crack spacing depends mainly on the axial tensile strain of bars ε_s, bar diameter d_b, bar spacing b_1 fracture energy of concrete G_f, and its elastic modulus E_c. The general expression for the crack width may be written from the cracking theory as follows:

$$w = a_o\left(\varepsilon_s - a_1\right) \tag{2.35}$$

in which w represents the crack width, a_o and a_1 are the coefficients that are functions of certain important variables. It is now necessary to determine the parameters a_o and a_1 that give the best prediction. The maximum crack width equation that gives the best prediction is found as follows:

$$\frac{w_{\max}}{d_b} = a_o\left(\varepsilon_s - 0.0002\right)R \tag{2.36}$$

in which

$$a_o = 159\left(\frac{t_b}{h_2}\right)^{4.5} + 2.83\left(\frac{A_1}{A_{s1}}\right)^{1/3} \tag{2.37}$$

$$R = h_2 / h_3 \tag{2.38}$$

The value $w_{\max}$ represents the maximum crack width at the extreme tension face, R represents the ratio between the distance h_2 and h_3, h_2 is the distance from the extreme tension fiber to the neutral axis, h_3 is the distance from the centroid of steel to the neutral axis, A_{s1} is the average area of one tensile reinforcing bar, A_1 is the effective area of concrete surrounding one reinforcing bar, and t_b is the bottom concrete cover.

2.15 Tension Chord Method

Based on an analytical model developed previously to study the problem by Gilbert (2008), a simplified model to predict crack spacing and crack width was developed.

The researcher proposed the following expression for the average crack width w:

$$w = -\left[\frac{\sigma_{c1}^{*}}{E_e^{*}}\left(s - \frac{2}{3}s_o\right) + \varepsilon_{sh}^{*}\, s\right] \tag{2.39}$$

where E_e^{*} is the final effective modulus for concrete and is given by $E_e^{*} = E_c / 1 + \varphi^{*}$

The final concrete stress is given by:

$$\sigma_{c1}^{*} = \frac{N(\infty) - \sigma_{s1}^{*} A_s}{A_c} \tag{2.40}$$

where $N(\infty)$ is the final restraining force. The distance s_o in which stresses vary on either side of a crack was taken to be (Gilbert 2008):

$$s_o = \frac{d_b}{10\rho} \tag{2.41}$$

where d_b is the bar diameter and ρ is the reinforcement ratio (A_s / A_c).

2.16 Codes Provisions for Crack width Calculations

2.16.1 Norwegian Code

The Norwegian code, NS 3473E (1989), provides the following equation for calculating the crack width. It uses factor r to account for tension stiffening effect.

$$w_k = 1.7\, w_m \tag{2.42}$$

$$w_m = r\, \varepsilon_1\, S_{rm} \tag{2.43}$$

$$r = 1 - \frac{\beta}{2.5 k_1}\left(\sigma_{sr} / \sigma_s\right)^2 \geq 0.4 \tag{2.44}$$

where w_k is the characteristic maximum crack width, w_m is the average crack width, ε_1 is the principal tensile strain at level of tensile reinforcement, $\varepsilon_1 = \varepsilon_s = \sigma_s / E_{sk}$, σ_s is the stress in the reinforcement in the crack, σ_{sr} is the stress in the reinforcement at calculated crack, E_{sk} is the characteristic modulus of elasticity of steel, k_1 is a coefficient that characterizes bond properties of bars, β is a coefficient accounts for type of action, and S_{rm} is the mean crack spacing. The NS 3473E (1989) code calculates the maximum characteristic crack width w_k at the level of steel reinforcement. The characteristic crack width is defined in most of the European codes as the width that only 5% of the cracks will exceed. This characteristic crack width is taken as 70% more than the average crack width. The NS 3473E (1989) code provides more detailed regulations for crack width limitations depending on the environmental conditions. Four environment classes are identified; namely, especially aggressive, severely aggressive, moderately aggressive and mildly aggressive environment.

2.16.2 CEB-FIP (1990) Code

The CEB-FIP (1990) model code gives the following equation for calculation of the characteristic crack width:

$$w_k = l_{s,\max}\left(\varepsilon_{s2} - \beta\,\varepsilon_{sr2} - \varepsilon_{cs}\right) \tag{2.45}$$

Where $l_{s,\max}$ is the length over which slip between steel and concrete occurs, w_k is characteristic maximum crack width, w_m is average crack width, ε_{s2} is steel strain of transformed section in which the concrete in tension is ignored, ε_{cs} is the free shrinkage of concrete, generally a negative value, ε_{sr2} is the steel strain at crack, under a force causing stress equal to f_{ctm}, within A_{cef}, β is an empirical factor to assess average strain within $l_{s,max}$.

To account for tension stiffening in the CEB-FIP (1990) code, an empirical shape factor β is used to assess the average strain.

2.17 Summary

- Most concrete codes have semi-empirical equations to estimate the minimum steel reinforcement requirements for flexural members. The use of thick concrete plates requires further examination of the empirical-based building design codes formulae that are based on the results of experimental tests performed mostly on thin slabs.
- Research results suggest that the minimum reinforcement ratio is member size dependent. However, the exact tendency performance criterion is not very clear due to lack of experimental results. Most design codes deal with the minimum steel reinforcement ratio independent of member size. Only a few codes, such as the NS 3473 E (1989), suggest that the minimum reinforcement ratio is a size dependent factor.
- Most design codes do not provide guidance for thick plates over 250 mm thickness and do not account for the fact that the shear stress can cause failure of thick members. This means that by increasing the member size the behavior of the member becomes more brittle, hence shear reinforcement is required to enhance the behavior of such thick plates.
- Conventional design methods consider potential shear failures of a slab as a wide beam as well as punching failures in the vicinity of concentrated loads. Most of design codes try to avoid minimum shear reinforcement requirements for slabs by limiting nominal shear stresses at well-defined critical sections to guard against

such failure modes.

- Different codes have different formulae to calculate crack spacing and crack width developed in flexural members. Most of these formulae are based on the analysis of results of tested beams or one-way slabs. Crack control equations for beams underestimate the crack width developed in plates and two-way slabs.
- The use of thick concrete covers in offshore and nuclear containment structures applications is increasing for reasons of durability. Most crack width models indicate that increasing concrete covers results in increased crack spacing and hence increased crack width this means that using thick concrete covers is detrimental to crack control.

Chapter 3

The Experimental Program

3.1 General

This chapter gives a detailed description of the experimental program that was carried out to investigate the structural behavior of plates reinforced with steel bars. It includes sections describing the preparation of the form work, the steel cages and mixing concrete. The test program consisted of testing and evaluation of the structural performance of seven high-strength and five normal-strength concrete two-way slabs. Test setup and different instrumentations used to measure the deformations and strains throughout the testing program are described in this chapter. The test set-up includes the loading test frames and the loading equipment that has been used to apply the loads. In addition, a description of the data acquisition system is also provided in this chapter. Detailed description of the material properties utilized in this investigation is given in Table 3.1.

3.2 Test Parameters

The variables considered in the current investigation are the concrete cover, slab effective depth, and steel reinforcement ratio for normal and high strength concrete. The main objective was to study the structural behavior of thick plates with regard to deformation, strains, ultimate capacity, ductility, and energy absorption.

A total of twelve concrete plates were tested. Five normal strength concrete plates (NS) and seven high strength concrete plates (HS) were selected for the experimental investigation as detailed in Table 3.2. The details of typical test specimens are shown in Figures 3.1, 3.2 and 3.3. Minimum flexural reinforcement ratios, which are required by

different codes and proposed equation by Rizk and Marzouk (2009) for the actual material strengths are given in Table 3.3.

The test specimens were classified into two groups. The first group (Group A) was designed to investigate the effect of small reinforcement ratios and effective depth on the behaviour of two-way slabs. The group is made of seven slabs designated as NS1, NS2, NS3, NS4, HS1, HS2 and HS3. The slabs of this group had different slab thicknesses, 150 mm to 300 mm; different concrete covers 40 mm to 70 mm, different bar diameters, 10M, 15M, 20M and 25M, and different bar spacing of 210 mm, 240 mm and 368 mm. The second group (Group B) was designed to investigate the effect of plate effective depth, reinforcement ratio and concrete strength on the structural behavior of reinforced thick plates, usually designed for offshore structures. The group was made of five slabs designated as NS5, HS4, HS5, HS6 and HS7. The slabs of this group had the same thick concrete cover 70 mm, different slab thicknesses, 300 mm, 350 mm and 400 mm, different bar diameters, 25M and 35M, and different bar spacing of 217 mm, 289 mm and 368 mm. Slab HS5 included T-headed shear stud reinforcement and was designed to examine the effect of shear reinforcement on structural behavior of thick concrete plates. The shear reinforcement consisted of vertical bars with a diameter of 15 mm and specified yield strength of 400 MPa anchored at the top and bottom by welded anchor plates. The layout of the shear reinforcement is shown in Figure 3.4. All the specimens of the first group (Group A) were designed to fail under flexure failure as recommended by Marzouk and Hussein (1991). However, the second group (Group B) was designed to investigate the effect of other modes of failure on crack width and crack spacing. The specimens in this series were designed to fail under punching.

Table 3.1–Mix proportions

Material	Series I, $f_c' = 35$ MPa	Series II, $f_c' = 70$ MPa
Cement (kg)	400	400
Water (Liter)	2201	1301
Silicafume (kg)	---	50
Fine Aggregate (kg)	830	713
Coarse Aggregate (kg)	1245	1070
Water Reducer (Liter)	---	2.25
Superplasticizer (Liter)	---	12
Retarder (Liter)	---	0.5

Table 3.2–Details of test specimens

Group No.	Slab No.	Compressive strength f_c', MPa	Bar size, mm	Bar spacing, mm	Concrete cover C_c, mm	Slab thickness, mm	Depth, mm	Steel ratio ρ%	Shear reinforcement ρ_z%
A	NS1	45	10	210	40	150	105.0	0.48	---
	NS2	50	15	240	40	200	152.5	0.54	---
	NS3	35	20	368	60	250	182.5	0.35	---
	HS1	70	35	368	60	250	182.5	0.35	---
	NS4	40	20	368	70	300	217.5	0.73	---
	HS2	65	25	368	70	300	217.5	0.73	---
	HS3	75	20	368	70	300	220.0	0.43	---
B	HS4	76	25	368	70	350	267.5	0.56	---
	HS5	70	25	217	70	300	217.5	1.42	0.68
	HS6	70	35	289	70	350	262.5	1.42	---
	NS5	40	35	217	70	400	312.5	1.58	---
	HS7	60	35	217	70	400	312.5	1.58	---

*NS-Normal strength slabs; HS-High strength slabs

Table 3.3–Minimum reinforcement ratios required by different codes for test slabs

Group No.	Slab No.*	Compressive strength f_c', MPa	Actual steel ratio ρ%	CSA-A23.3-04 ACI 318-08 ρ%	CSA-S474-04 ρ%	NS 3474 E-89 ρ%	CEB-FIP-90 ρ%	Rizk and Marzouk (2009) ρ%
A	NS1	45	0.48	0.60	0.39	0.62	0.18	0.59
	NS2	50	0.54	0.58	0.38	0.59	0.19	0.55
	NS3	35	0.35	0.51	0.33	0.49	0.15	0.40
	HS1	70	0.35	0.72	0.47	0.74	0.24	0.48
	NS4	40	0.73	0.55	0.36	0.52	0.17	0.37
	HS2	65	0.73	0.69	0.46	0.69	0.23	0.45
	HS3	70	0.43	0.71	0.47	0.72	0.24	0.42
B	HS4	76	0.56	0.52	0.45	0.67	0.24	0.43
	HS5	70	1.42	0.52	0.45	0.67	0.24	0.43
	HS6	70	1.42	0.52	0.45	0.67	0.24	0.43
	NS5	40	1.58	0.37	0.31	0.43	0.24	0.34
	HS7	60	1.58	0.52	0.44	0.64	0.24	0.40

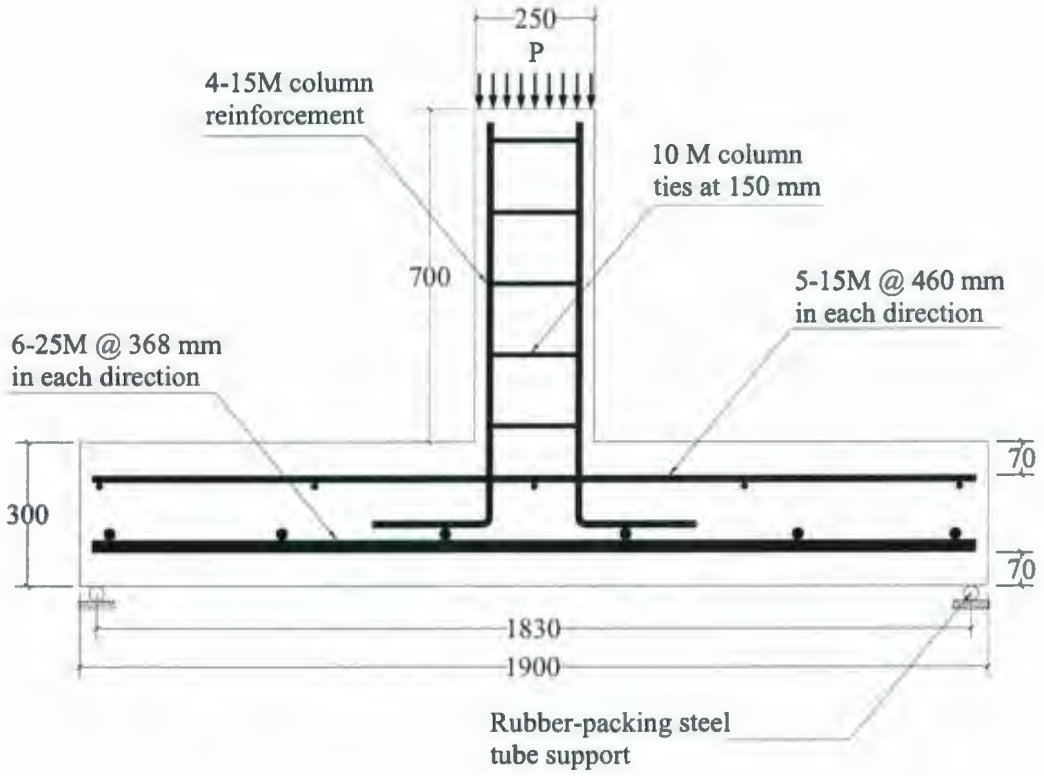

Figure 3.1: Details of typical test specimen HS2 (h = 300 mm)

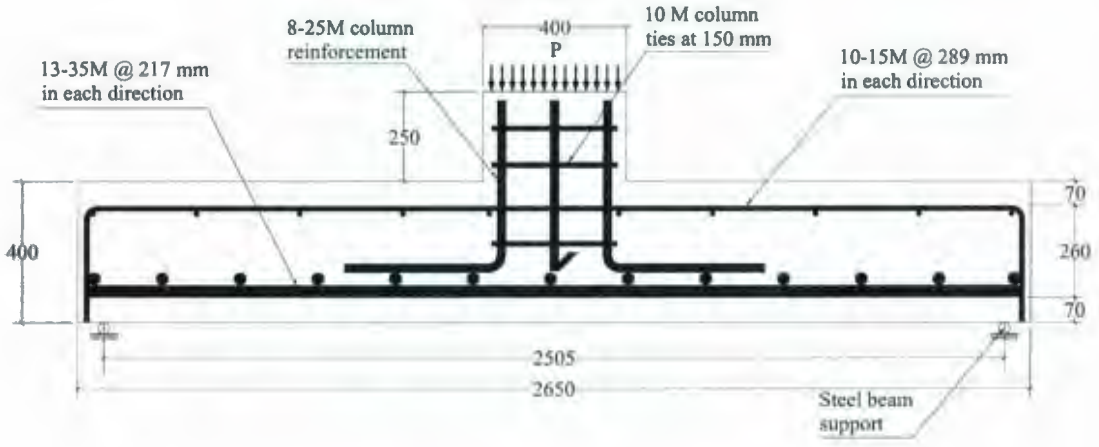

Figure 3.2: Details of typical test specimen HS7 (h = 400 mm)

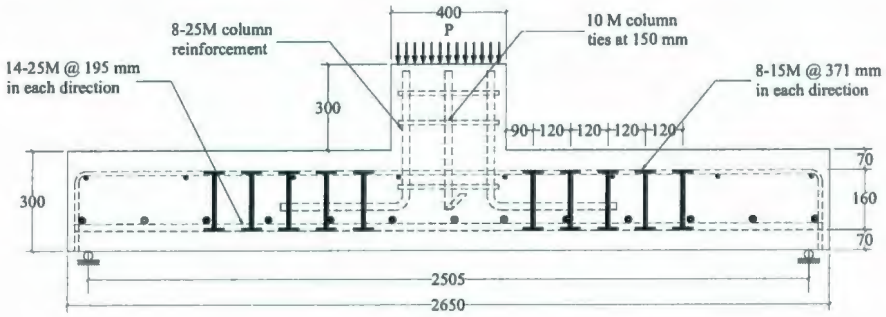

Details of T-headed shear reinforcement

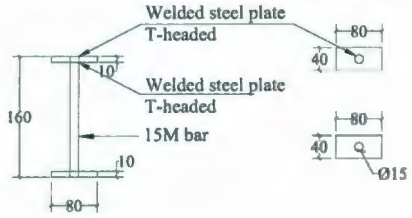

Figure 3.3: Dimensions and reinforcement details of slab HS5 with T-headed shear reinforcement (h = 300 mm)

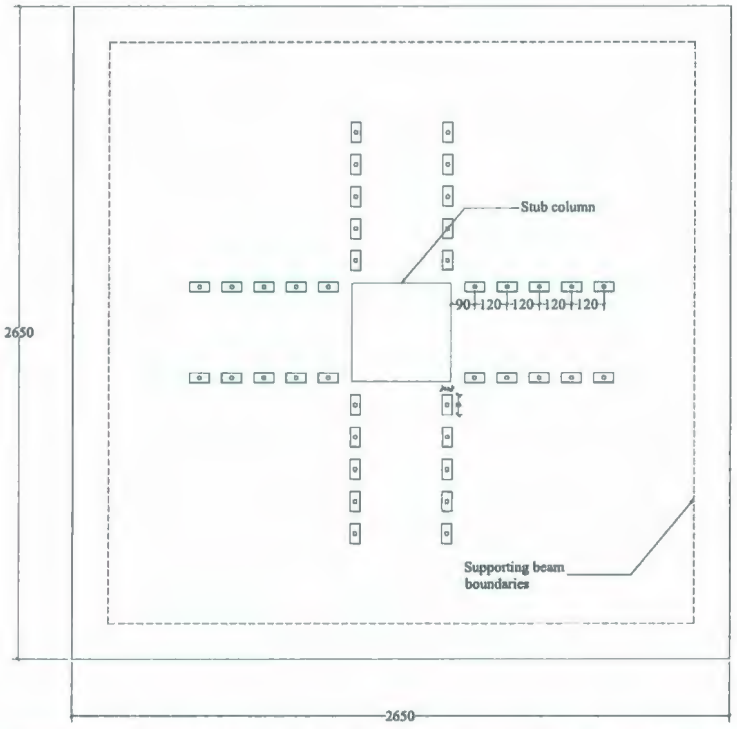

Figure 3.4: Arrangement of T-headed shear reinforcement in slab HS5 (h = 300 mm)

3.3 Test Specimens

A summary of the different specimens is presented in Table 3.2. Details of the concrete dimensioning, reinforcement details, and materials properties are presented in Tables 3.1 and 3.2 as illustrated before. Twelve full-scale specimens were instrumented and tested in the described experimental program. The first tested slabs group (Group A) had a side dimension of 1900 mm in both directions. The test specimens were simply supported along all four edges with the corners free to lift. The test slabs represent the region of negative bending moment around an interior column in a flat slab system and the simply supported edges simulate the lines of contra-flexure. A concentric load was applied on each slab through a 250 × 250 mm column stub. The dimensions and reinforcement details of a typical test slab are shown in Figure 3.1. Reinforcement ratios of 0.35%, 0.43%, 0.5% and 0.7% were selected for bottom reinforcement, the top reinforcement ratios were selected to satisfy the CSA-A23.3-04 code for minimum reinforcement ratio for controlling shrinkage. Minimum reinforcement ratios were chosen to investigate the structural behaviour of thick slabs (size effect) having minimum reinforcement ratios. All specimens were square with total thickness ranging from 150 - 300 mm. The dimensions were chosen to give shear span to depth ratio (a/d) equal to 3.5 to 7.5. The main variables in this investigation were the reinforcement ratio, concrete strength and effective depth as shown in Table 3.2.

The punching shear strength is influenced by the shear span, a, from the loaded area to the support. Regan and Braestrup (1985) studied the effect of the ratio a/d known as the shear span to depth ratio on the shear strength. Although the data in this area is limited, it could be concluded that the shear strength rises quite sharply when a/d is less than about

1.5 but is relatively constant for larger values of the ratio. For very short shear spans, *a*, the support location significantly interferes with the failure surface. According to Gardner (1990), for punching shear failure to occur, at least three times the slab thickness is necessary between the punching surface and the support. This ratio could be used to distinguish between thick and thin slabs. According to Hallgren (1996), slender slabs are those slabs with shear-span to depth ratios of more than 3 to 4.

The second test plates group (Group B) had a side dimension of 2650 mm in both directions. The tested specimens were simply supported along all four edges with the corners free to lift. A concentric load was applied on each slab through a 400 × 400 mm column stub. The dimensions and reinforcement details of a typical test slab are shown in Figure 3.2. Reinforcement ratios of 0.56%, 1.42% and 1.58% were selected for bottom reinforcement, which is a common practice in offshore platform structures, the top reinforcement ratios were selected to satisfy the CSA-A23.3-04 code for minimum reinforcement ratio for controlling shrinkage. Heavy reinforcement ratios were chosen to investigate the behaviour of thick plates (size effect) in punching. All specimens were square with total thickness ranging from 300 - 400 mm. The dimensions were chosen to give shear span to depth ratio (*a*/*d*) equal to 3.33 to 4.8. The T-headed shear reinforcement specimen consisted of 15 mm bar as a stem, two 40 × 80 mm steel plates individually welded on both sides as anchor plates. A total of 40 T-headed studs were placed in slab HS5 as shown in Figure 3.4. The top anchors were in the form of rectangular plates, the areas of which are at least 10 times the area of the stem (Elgabry and Ghali 1990). The stud spacing *s* was chosen to be 0.5 *d*, this value is recommended by the ACI-ASCE 421 joint committee (2008) as the upper limit for *s*, and the shear studs

were extended to approximately 2.0 d from the column faces as recommended by Marzouk and Jiang (1997). The distance between the first row of studs and the column face s_o was taken as 0.4 d to avoid shear failure between the column and the first row of shear studs. The main variables in this investigation were the reinforcement ratio, concrete strength and effective depth as illustrated in Table 3.2.

3.4 Properties of Material

Two concrete mixes with compressive strength of 35 MPa and 70 MPa after 28 days were used. The concrete mix proportions are listed in Table 3.1. Reinforcing bars consisted of Grade 400 steel conforming to CSA standards with specified yield strength of 400 MPa was used. In the next sections, the properties of the material utilized are detailed.

3.4.1 Normal Strength Concrete Mixture

The normal strength concrete (NSC) used in casting the tested slabs was supplied from a local batch plant. The concrete had a nominal compressive strength of 35 MPa. The NSC mixture was designed to achieve a target compressive strength of 35 MPa after 28 days. Type 10 SF cement blended with silica fume as produced by Holcim Canada, was used for all the mixes. The maximum aggregate size was 20 mm. The mixture proportions are listed in Table 3.1.

3.4.2 High Strength Concrete Mix Design

The high strength concrete (HSC) used in casting the tested slabs was supplied from a local batch plant. The concrete had a nominal compressive strength of 70 MPa. The HSC used in casting column stubs was produced in the concrete laboratory at Memorial University of Newfoundland (MUN). The HSC mixture was designed to achieve a target

compressive strength of 70 MPa after 28 days. Type 10 SF cement blended with silica fume as produced by Holcim Canada, was used for all the mixes. Local fine aggregate that had a composition similar to that of the coarse aggregate was used. The fine aggregate consisted mainly of quartzite sandstone with a fineness modulus of 3.1. Crushed sandstone fine aggregate and crushed sandstone coarse aggregate of 20 mm maximum nominal size were used. The water/cement ratio was 0.29. A non-chloride water reducing agent of polycarboxlate base, and a retarder of organic base, conforming to ASTM C494 type C and D, was adopted.

3.5 Curing

Curing the HSC specimens is an essential way to avoid evaporation from the surface of the slab and to achieve the design properties. Without proper curing, significant shrinkage can be found in the specimen. This could lead to a large number of shrinkage cracks on the surface of the slab. It was noted that covering HSC specimen with burlap sheets after casting was an effective way to reduce shrinkage. After 18 hours, the concrete mixture began to consolidate and produced a lot of heat due to the chemical reaction. Pouring water on the HSC specimen at this stage reduced the heat of hydration and did not impair the concrete strength development. By keeping the burlap sheets wet, it kept the surface of the specimen moistures and prevents the evaporation of water. The HSC slabs were cured in this way for seven days and then kept in the laboratory until the day of testing.

3.6 Compressive Strength of the Test Slabs

The concrete compressive strength of the tested slabs was measured according to the ASTM C39-04. Three standard concrete cylinders (100 × 200 mm) were cast from each batch at the same time of casting each slab. The cylinders were cured and kept at the

same location as the slabs in the lab in a temperature around 20 degrees. The control cylinders were tested at the same time of testing the slab. A compressive test machine was used to apply the load on the cylinders up-to-failure under a stress rate of 0.25 MPa/second. Figure 3.5 shows a photo of the concrete compression testing machine.

3.7 Slab Formwork and Fabrication

The first group (group A) of tested slabs was cast in a temporary wood formwork at the structural lab at MUN. The formwork was supported directly on lab structural floor. A square wood 1900 mm × 1900 mm sheet with 18 mm thickness stiffened with 25 mm lumbers was supported directly on lab structural floor. Four removable wooden sheets with a height of 300 mm were installed on the wooden base as the sides of the formwork, as shown in Figure 3.6

The second group (group B) of tested slabs was cast in a temporary wood formwork at the structural lab at MUN. The formwork was supported directly on lab structural floor. A square wood 2650 mm × 2650 mm sheet with 18 mm thickness stiffened with 3/8″ plywood sheets was supported directly on lab structural floor. Four removable wooden sheets with a height of 500 mm were installed on the wooden base as the sides of the formwork, as shown in Figure 3.7 and Figure 3.8. Care was taken in order to keep the slab and the column reinforcement mutually perpendicular while the ready mix concrete was being poured. The steel bars were tied together into a sturdy mat and lifted into the form. The reinforcing mat rested upon chairs made of cement mortar. The chairs were placed far away from the punching zone in order to eliminate their effect on the observed shear strength. However, during concrete preparation great care was taken to insure that the cover provided was uniform.

Steel bars were cut in the same length of 2600 mm that allowed for a distance of 25 mm from each side of the formwork edges. The strain gauges were mounted at predetermined locations on the steel bars. The steel bars were arranged together to form a reinforcement cage. For the stub reinforcement, eight 950 mm long steel bars bent at a right angle with horizontal legs of 450 mm were used. Four 25 mm (2090 mm long) steel hooks were placed on one side of each tested slab for lifting purposes. The wooden forms were strengthened with horizontal metal straps to protect the thick concrete from spalling during casting.

During casting, the concrete was vibrated using a vibrator. When full compaction was attained, the top face of the slab was leveled and finished with a steel trowel. In the next day, a steel mould used for construction of the column stub was placed at the center of the slab. The column stub was cast using a concrete mix that was produced in MUN lab.

Figure 3.5: The concrete compression testing machine

Figure 3.6: A reinforcement cage in the formwork for a typical slab (group A)

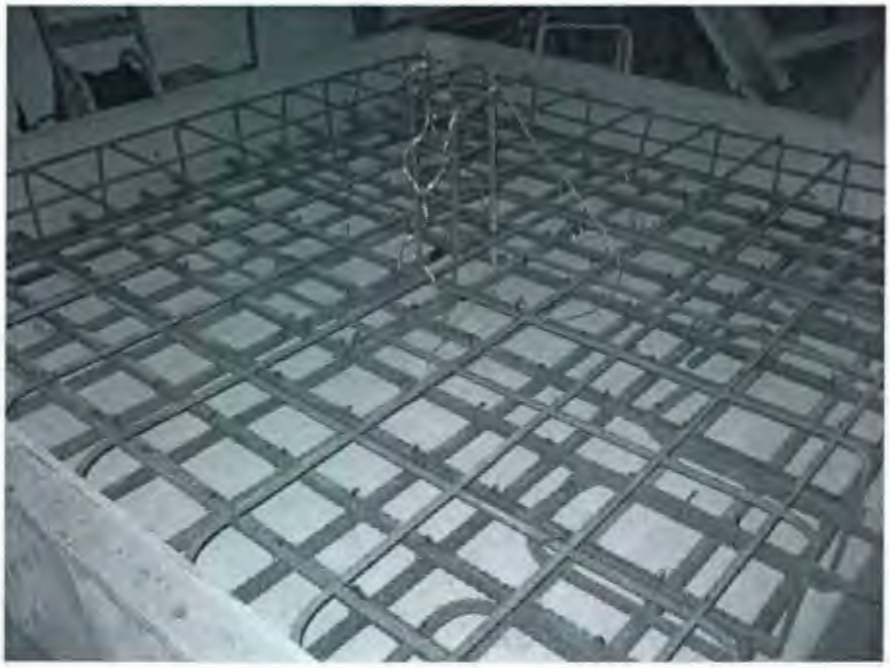

Figure 3.7: A reinforcement cage in the formwork for a typical slab (group B)

Figure 3.8: A reinforcement cage in the formwork for slab HS5 with T-headed shear stud reinforcement (h = 300 mm)

3.8 Test Set-up

All the slabs were cast in a horizontal position and were tested in a vertical position in order to detect and mark the cracks as it develops at the structural lab at MUN. The first test frame was a space frame made of steel wide flange beams and channel sections as shown in Figure 3.9. The frame was anchored to the concrete floor and was self-reacting. Four 32 mm diameter rods were welded on the vertical W-shape sections to form the four sides of the slab support system. A 3 mm packing rubber was placed on the supports that were made of steel tubes to minimize the friction between the support and the slab.

A hydraulic jack was fixed to the frame and was used to apply a concentric load on the column stub in a horizontal position. CLRG-30012 Series hydraulic jack cylinders with a maximum capacity of 3110 kN (700 kips) and a maximum displacement of 300 mm was

used. The applied load and the displacement of the actuator were measured by its internal load cell and linear variable differential transducer (LVDT), respectively.

For the purpose of testing second specimens group (Group B), a new test setup was designed and fabricated in the structural laboratory at MUN. The main function of this setup is to apply direct transverse load through hydraulic jack. The maximum capacity of the new setup is 4450 kN (1000 kips). The test setup consisted of four reaction walls; two of them were used for supporting wide flange steel beams that were welded together to form a support to carry the applied load on the tested slabs. Four wide flange steel beams were anchored to the retaining walls that were anchored to the structural floor. The third and fourth retaining walls were used to carry the hydraulic jack that used to apply the load directly on the column-stub. The retaining walls were braced using two self supporting (closed) frames, one at the top and one at the bottom. These two rigid frames were designed using heavy wide flange steel beams. In order to resist torsional moment due to eccentricity of applied load, 10 mm steel plates were welded between beam flanges. This transformed the wide flange beam cross section into a closed section that was very effective in resisting high bending and torsional moments. In designing self-supporting frames, consideration was made to minimize lateral deformation of retaining walls as possible. The details of this test setup are shown in Figures 3.10 and 3.11.

A hydraulic jack was fixed to the frame and was used to apply a central load on the column stub in a horizontal position. CLRG-50012 Series hydraulic jack cylinders with a maximum capacity of 4893 kN (1100 kips) and a maximum displacement of 300 mm was used. The applied load and the displacement of the actuator were measured by its internal load cell and linear variable differential transducer (LVDT), respectively. In the current

experimental program, the actuators were used in a load control mode. The loading system was executed through a 407 MTS load controller.

Figure 3.9: The test set-up for group A

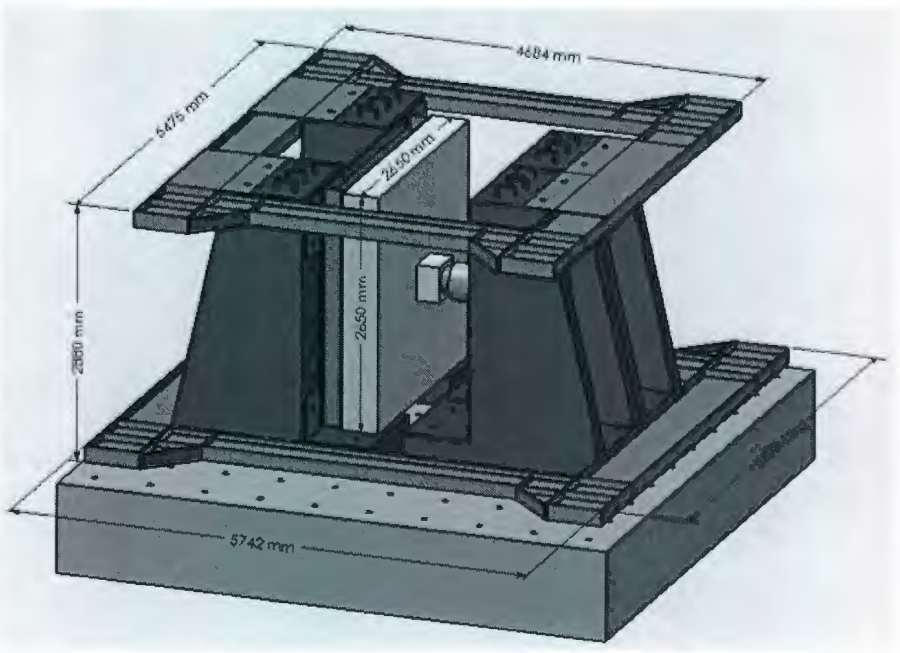

(*a*) Isometric view

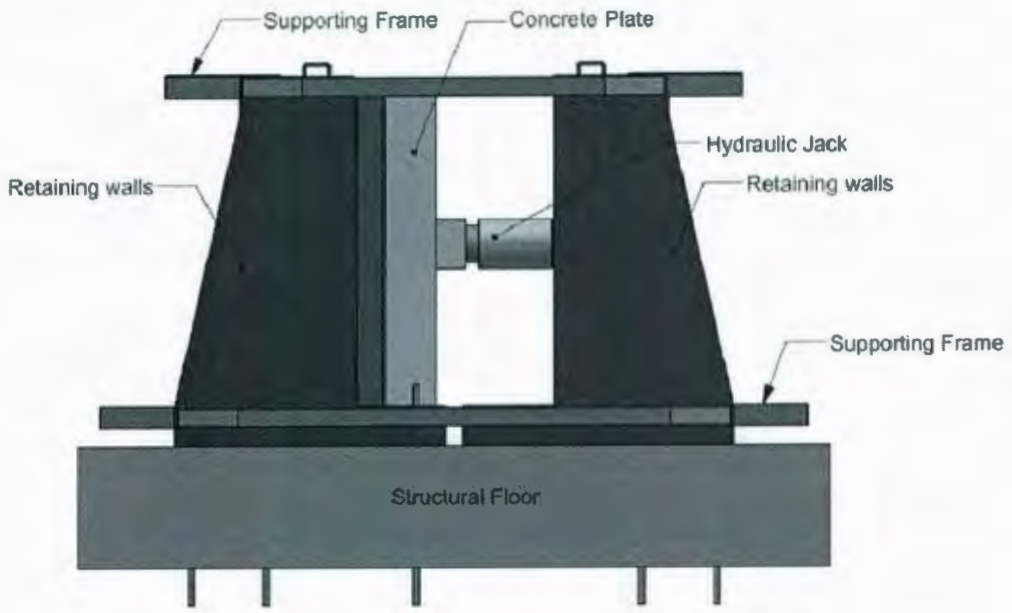

(*b*) Front view

Figure 3.10: Test setup for group B: (*a*) Isometric view; (*b*) Front view

(*a*) A Specimen during testing

(*b*) Typical specimen indicates size effect challenge

Figure 3.11: Test set-up for group B: (*a*) A Specimen during Testing; (*b*) Typical specimen indicates size effect challenge

3.9 Instrumentation and Measurements

3.9.1 Deflections

The deflection of the slabs was measured during loading by three linear variable differential transducers (LVDTs) and two linear potential differential transducers (LPDTs) at five predetermined locations on the tension surface as shown in Figure 3.12. The readings from the LVDTs and LPDTs were logged into a data acquisition system. The measured deformation values were readjusted by relating all the deformations to the deformation measured with the LVDT that was placed just above the support.

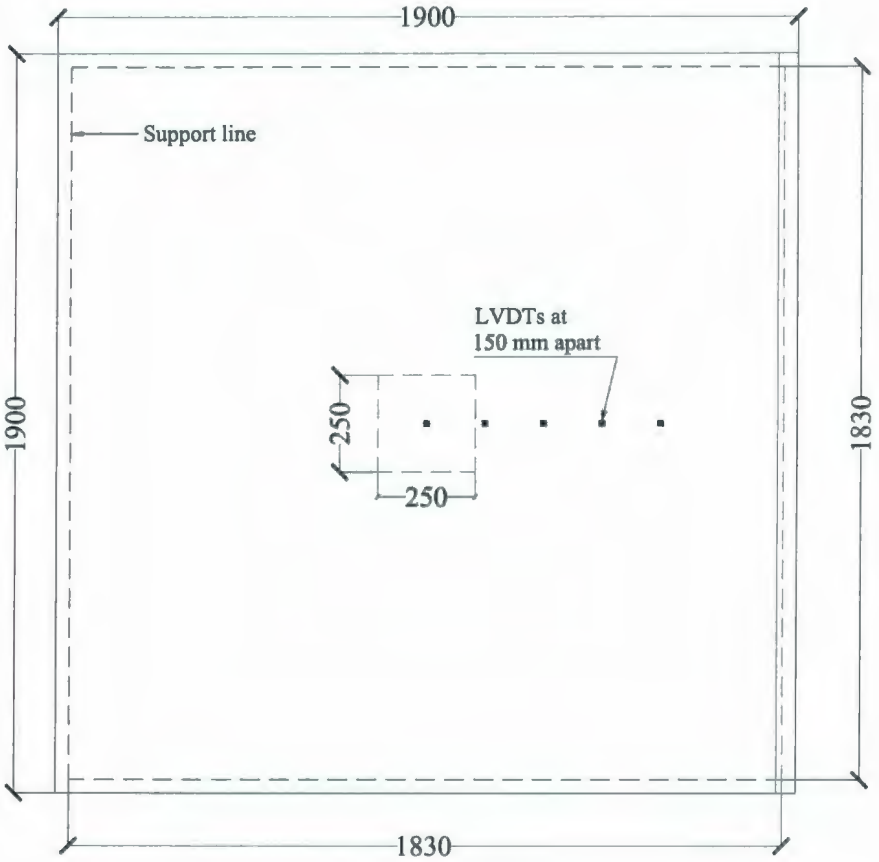

Figure 3.12: A typical arrangement of LVDT's

3.9.2 Steel Strains

The steel strains were measured in each connection at different locations by, with means of electrical strain gauges. Figure 3.13 shows a typical arrangement of the steel strain gauges. The strain gauges were 6 mm long, with a strain limit of approximately 5%. The resistance of strain gauge is 120 Ω ± 0.2% at 24° c and the gauge factor is 2.075 ± 0.5% at the same temperature. The normal use temperature range for the static strain measurement is -75° c to 175° c. For protection against any possible water damage during casting, the strain gauges were coated with a protective sealant and then covered with a shrink tube waxed at the ends.

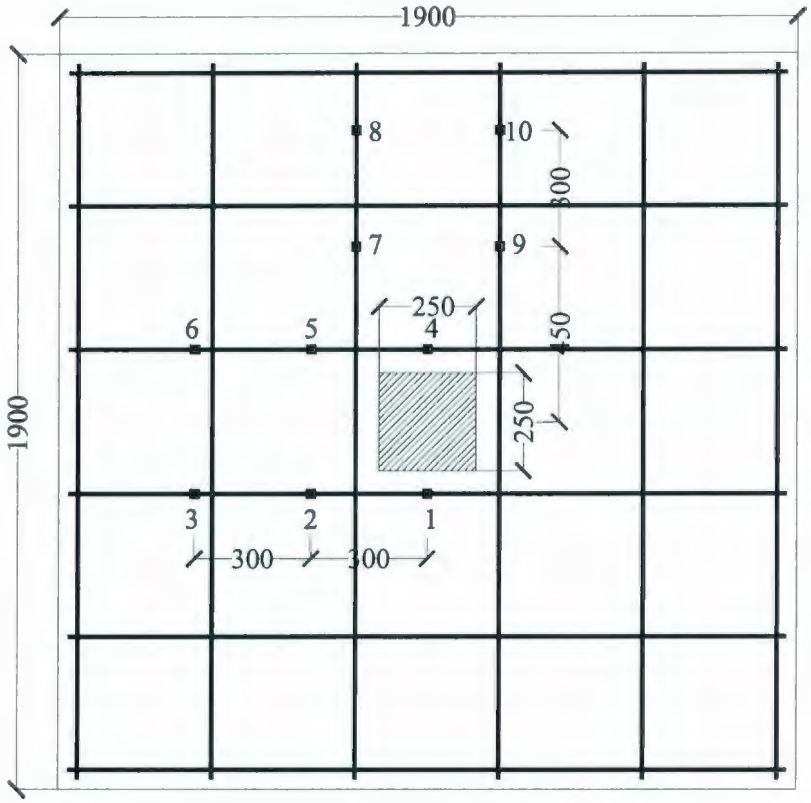

Figure 3.13: A typical arrangement of the steel strain gauges

3.9.3 Concrete Strains

The concrete strains were measured at eight locations in the tangential directions on the compression side of the tested slabs. The strains were measured using electrical resistance strain gauges glued to the concrete surface at various distances from the column face as shown in Figure 3.14. The locations of the strain gauges were marked on the concrete surface. The concrete surface at the specified locations was ground with a hand grinder, and a very thin film of epoxy resin was placed on the concrete surface in order to make the surface even. Each strain gauge was placed in position and the wire connections were connected to the data acquisition system.

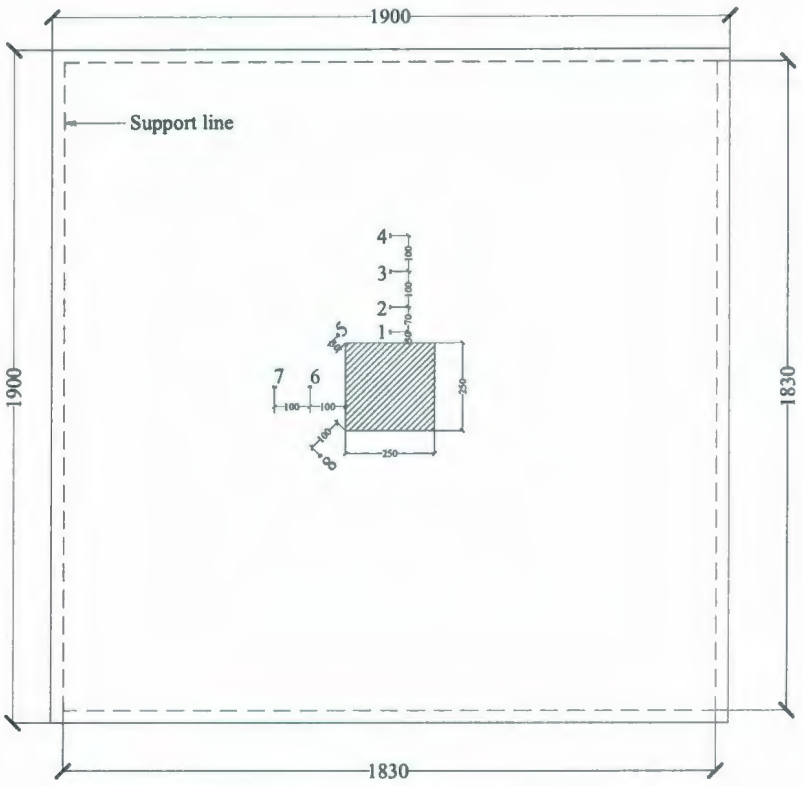

Figure 3.14: Concrete Strain gauge locations (The strain gauges were located at 100 mm apart)

3.9.4 Crack Measurements

Each slab was carefully inspected at each load step. The cracks were marked and the maximum visible crack width was measured using a crack width measuring gauge. Crack Displacement Transducer (CDT) was mounted to concrete surface cracks and joints in order to measure opening displacement as shown in Figure 3.15. It is a waterproof instrument that enables accurate measurements in range of ± 2mm. The accuracy of the measurements improved as the cracks started to widen.

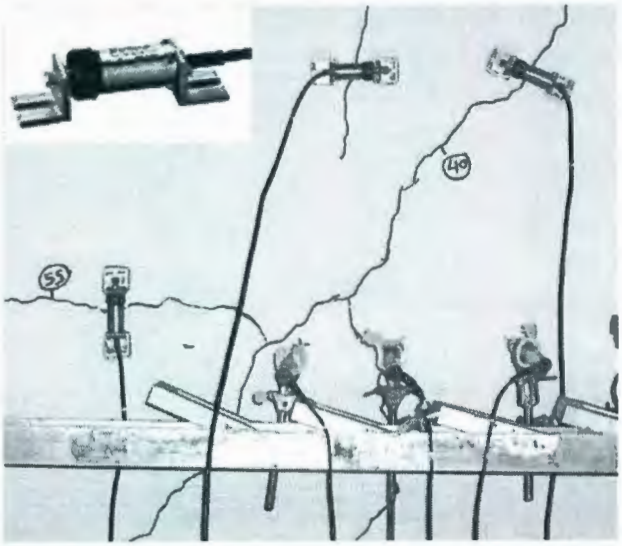

Figure 3.15: Crack Displacement Transducer (KG-A)

3.9.5 Data Acquisition System

The electrical strain gauges, LVDT's and the load readings were logged to a high speed data acquisition system. This system can be divided into two broad categories, analog systems and digital systems. In analog systems, the measurement information is processed and displayed in analog form. In digital systems, the original information may also be acquired in the form of an analog electrical signal, but the signal is then converted to a digital signal for further processing and display. A digital electrical signal has the form of a group of discrete and discontinuous pulses. Typically, the instrument first subjects the analog signal to amplification. Next, the amplified signal is converted into digital form by an analog-to-digital (A/D) conversion circuit. Finally, the digital signal is either displayed on a digital display device or is made available for transmission to other digital instruments such as a computer for further processing and display. All measurements were stored in a computer file. The software (Lab-View, 2005) was used

and the data scanning and saving rate was set to record the readings every 1 second during the period of testing.

3.10 Test Procedure

The test slabs were placed in the frame in a vertical position using a 10-ton capacity crane. At the beginning of the test, an initial load equal to 10 % of the ultimate load was applied until the slab started cracking. Then, crack gauges were installed using epoxy glue on the tension surface of the slab and left for one hour in order to enable the epoxy to dry. Then the test was resumed after epoxy hardened, the load was applied at selected load increments of 44.8 kN (10 kips). The slab was carefully inspected at each load step and the cracks were marked as shown in Figure 3.16.

Crack mapping of the specimen was depicted by, with means of photographs at each stage of loading throughout the experiment. These photographs were inserted in a computer aided AutoCAD software drafting package on a two-dimensional grid with a scale one to one. Cracks were retraced on the computer using AutoCAD, tools and the spacing was measured and averaged using the software. For all the specimens, the first crack forms along the rebar and passes through the slab center or close to the slab center. The second crack forms along the perpendicular rebar in the other direction.

Figure 3.16: Marking the cracks on a typical slab

Chapter 4

Structural Behaviour of Two-Way Slabs Reinforced with Minimum Reinforcement Ratios

4.1 Introduction

The results and observations obtained from the experimental program of the specimens in Group A are given in this chapter. The following parameters were examined in this investigation; concrete strength, concrete covers, bar spacing and slab effective depth on the crack properties. A large volume of data was recorded and the related graphs were prepared. Few data was important for interpretation of the cracking test results, as presented here. The behavior of the slabs was presented in terms of load-deflection relationship at different load stages, service, ultimate load, and crack width-steel strain relationship. Failure modes and crack patterns were also depicted with means of photographs.

A total of seven concrete slabs were tested in Group A. Four normal strength concrete slabs (NS) and three high strength concrete slabs (HS) were selected for the experimental investigation as detailed in Table 4.1. The seven reinforced concrete slabs were divided into three series. The first series (Series A1) was designed to investigate the effect of minimum reinforcement ratio on the structural behaviour of two-way slabs. The series was made of two slabs designated as NS1 and NS2. The slabs had the same concrete cover, the same reinforcement ratio but different bar spacing. The second series (Series A2) was designed to investigate the effect of concrete strength when the reinforcement ratio was kept constant on the structural behavior of tested slabs. The series was made of two slabs designated as NS3 and HS1. The slabs of this series had the same effective

depth, the same reinforcement ratio, the same thick concrete cover of 60 mm with different concrete strength. The third series (Series A3) was designed to investigate the size effect on the structural behavior of normal and high strength concrete slabs. The third series was made of three specimens designated as NS4, HS2 and HS3 with thick concrete cover. The slabs of this series had the same effective depth, the same bar spacing and the same thick concrete cover of 70 mm but with different concrete strength and different reinforcement ratio. All the specimens of Series A1, series A2 and Series A3 were designed to fail in flexure.

The variables considered in the current section of the investigation were the concrete cover, slab effective depth, and steel reinforcement ratio for normal and high strength concrete. The main objective was to study the effect of small reinforcement ratio on the structural behavior of thick two-way concrete slabs with regard to deformation, strains, ultimate capacity, ductility, and energy absorption.

Table 4.1–Details of Group A test specimens

Series No.	Slab No.*	Compressive Strength f_c', MPa	Bar diameter, mm	Bar Spacing, mm	Concrete Cover C_c, mm	Slab Thickness, mm	Depth, mm	Steel ratio ρ%
A1	NS1	45	10	210	40	150	105.0	0.48
	NS2	50	15	240	40	200	152.5	0.54
A2	NS3	35	15	368	60	250	182.5	0.35
	HS1	70	15	368	60	250	182.5	0.35
A3	NS4	40	25	368	70	300	217.5	0.73
	HS2	65	25	368	70	300	217.5	0.73
	HS3	75	20	368	70	300	220.0	0.43

*NS-Normal strength slabs; HS-High strength slabs

4.2 Test Results

The first crack of each specimen was visually inspected and the corresponding load was recorded as the first crack load. The yield steel strain was assumed to occur at a value of

2000 με, which produced a stress in the steel rebar equal to 400 Mpa. The yield strain was measured at location 150 mm from the center of the slab. The value of 2000 με was suggested based on experimental observations of the stress-strain curve of a single rebar. In all tested slabs, the initial observed cracks were first formed tangentially under the edge of the column stub, followed by radial cracking extending from the column edge toward the edge of the slab. As the load was increased, the tension reinforcement yielded and this resulted in a significant increase in the crack width and the deflection. It was noted that the ratio of the yield load to the cracking load increased with increasing reinforcement ratio.

4.2.1 Load-Deflection Characteristics

The load-deflection curves were obtained using LVDT measurements during loading by three linear variable differential transducers (LVDTs) and two linear potential differential transducers (LPDTs) at five predetermined locations on the tension surface. The readings from the LVDTs were logged into a data acquisition system. Table 4.2 illustrates the measured deflection at first crack, first yield of tension steel, ultimate load and at post ultimate load. Post-ultimate loading capacity refers to slab capacity at ultimate deflection. The applied load versus the deflection at the center of the slab for different test series is shown in Figure 4.1. The load-deflection curves of slabs NS1, NS2, NS3, HS1 and HS3 indicated that the specimens failed in flexure. All of these slabs reached the state of steadily increasing deflections at constant load, all slabs displayed a very ductile behavior characterized by a continuously increasing capacity with increasing deflection after overall yield of the flexural reinforcement, which is a normal characteristic for a lightly reinforced concrete specimen experiencing flexural failure.

Slabs NS4 and HS2 failed in punching shear failure this is indicated by a sudden drop in the load-deflection curve. Slab HS2 had a reinforcement ratio equal to 0.73% and was designed using ACI 318-08 requirements for minimum flexural reinforcement while slab HS3 had a reinforcement ratio equal to 0.43% and was designed using formula proposed by Rizk and Marzouk (2009). This means that using ACI 318-08 design guidelines for slabs more than 250 mm thickness can result in a brittle response and hence no adequate warning of an impending failure at extreme overloads and this is due to neglecting size effect.

Table 4.2–Deflection characteristics of test slabs

Slab No.	Concrete Strength f_c', Mpa	Steel ratio, ρ%	First crack load, kN	First crack deflection, mm	Yield load P_y, kN	Yield load deflection Δ_y, mm	Ultimate load P_u, kN	Ultimate load deflection ΔP_u, mm	Post-ultimate load $P\Delta_u$, kN	Post-ultimate load deflection Δ_u, mm
NS1	45	0.48	118	5.5	153	9.2	219	29.8	215	32.5
NS2	50	0.54	206	6.9	409	15.4	491	29.7	200	29.6
NS3	35	0.35	211	8.9	256	10.9	438	27.6	347	36.1
HS1	70	0.35	156	6.8	358	16.3	574	35.8	294	53.0
NS4	40	0.73	210	5.1	837	13.7	882	14.3	72	29.4
HS2	65	0.73	176	9.3	801	16.1	1023	22.3	255	23.6
HS3	75	0.43	295	3.6	708	10.2	886	24.7	735	39.8

*NS-Normal strength slabs; HS-High strength slabs

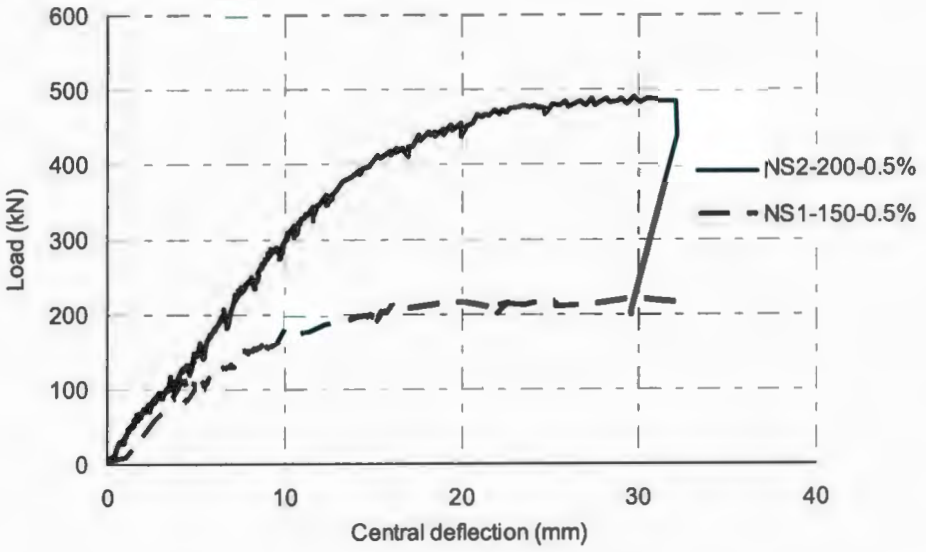

(*a*) Series A1

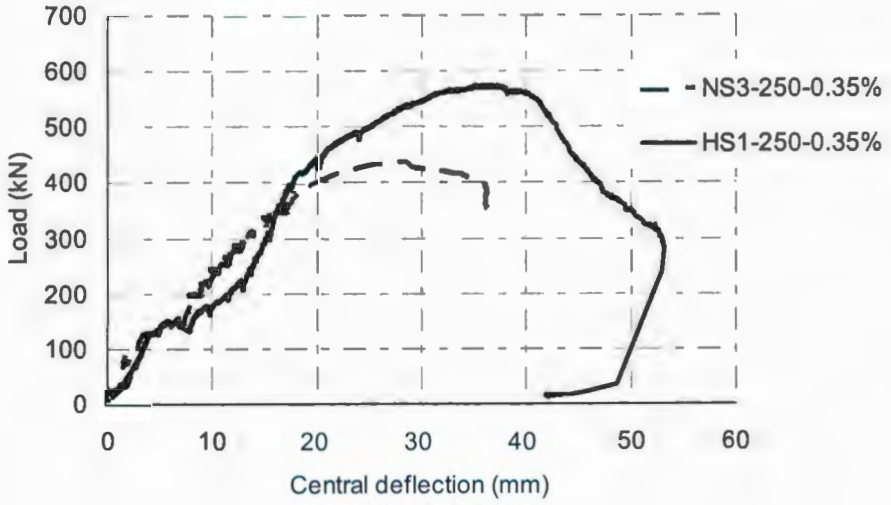

(*b*) Series A2

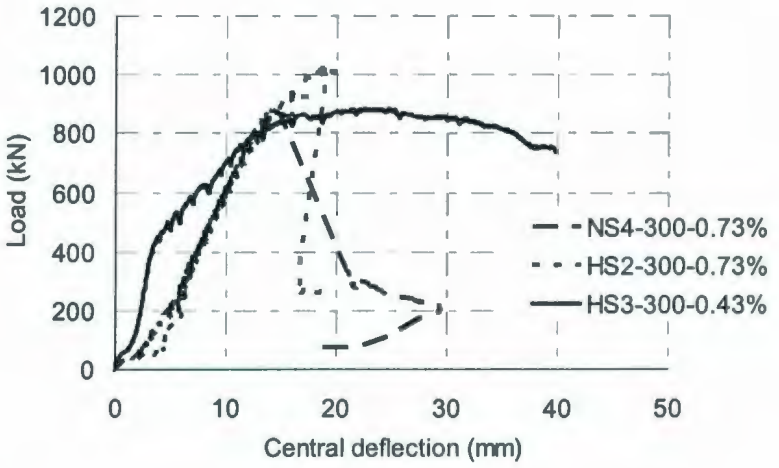

(*c*) Series A3

Figure 4.1: Typical load-deflection characteristics at center span of tested slabs: (*a*) Series A1; (*b*) Series A2; (*c*) Series A3

4.2.2 Deflection Profiles

Measuring the deflection at different locations along a specimen's width was used to construct the deflection profile for such a specimen. Deflection profiles give a global indication of the deformational response to the application of load not just at the location of the application of load but also along the slab width. The deflection values were measured at five different locations on one side of the symmetrical specimen as shown in Figure 3.10. Values of the deflection at each increment were recorded and used to determine the deflection profile at the increment. Figures 4.2 to 4.4 show the deflection profiles of specimens NS1, NS2, NS3, HS1, NS4 and HS2.

Figures 4.3a and 4.2b indicate that specimen HS1 required more load to reach the same level of deformation as that of specimen NS1. It is also clear that the zone of high deformation of specimen HS2 is extending over a less distance from the center of the slab

than that of HS1. This is a clear indication that specimen HS2 tended to deform more severely due to shear unlike specimen HS1. Moreover, the failure load occurred right after the yield of bottom steel reinforcement in specimen HS2 while in specimen HS1 it took more stages of loading before failure occurred. This support the idea that specimen HS2 tended to fail in shear more severely than HS1. Figures 4.3a and 4.4b show that NS3 and HS2 reached the same range of deflection prior to failure. This is due to the small reinforcement ratio used for NS3.

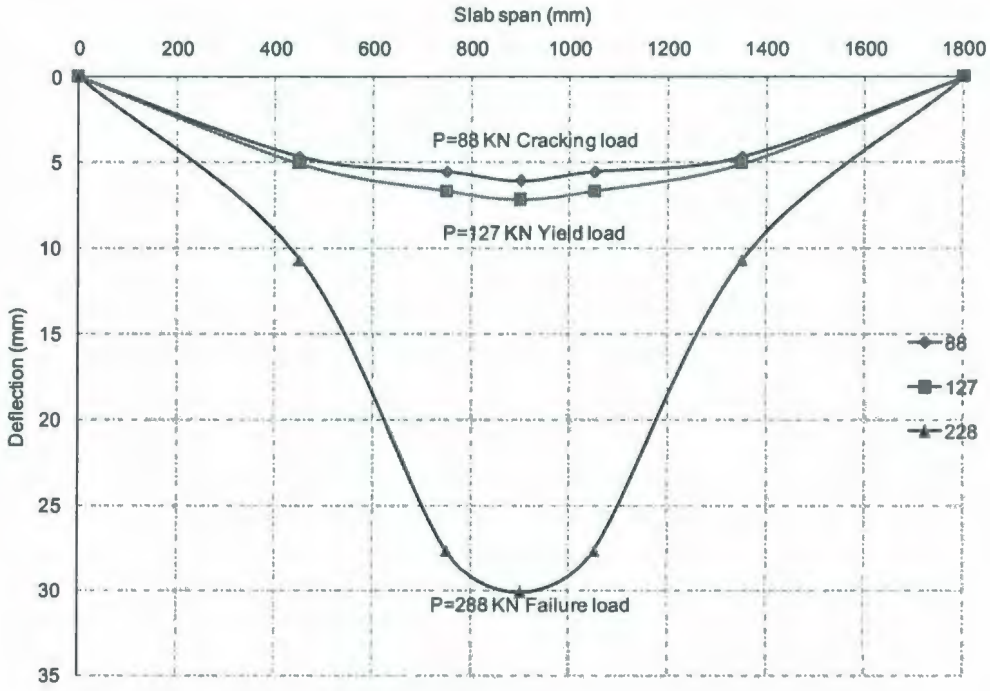

(*a*) NS1

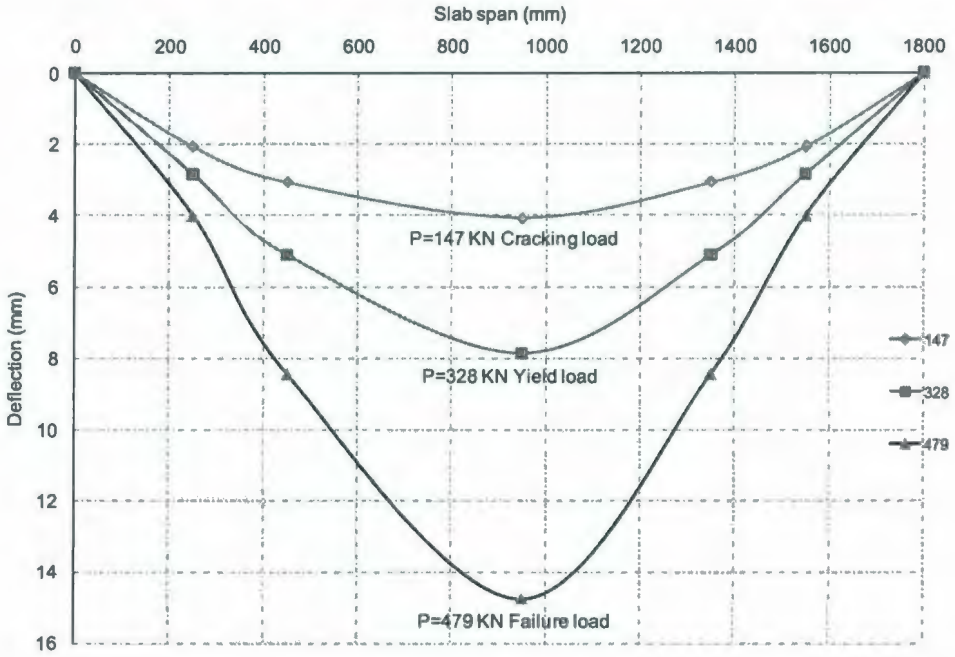

(*b*) NS2

Figure 4.2: Deflection profile for tested slabs: (*a*) NS1 and (*b*) NS2

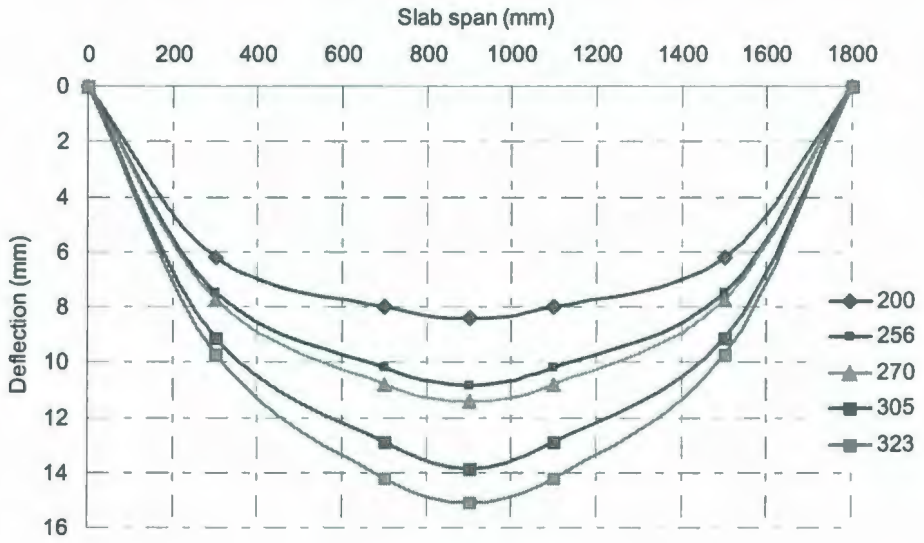

(*a*) NS3

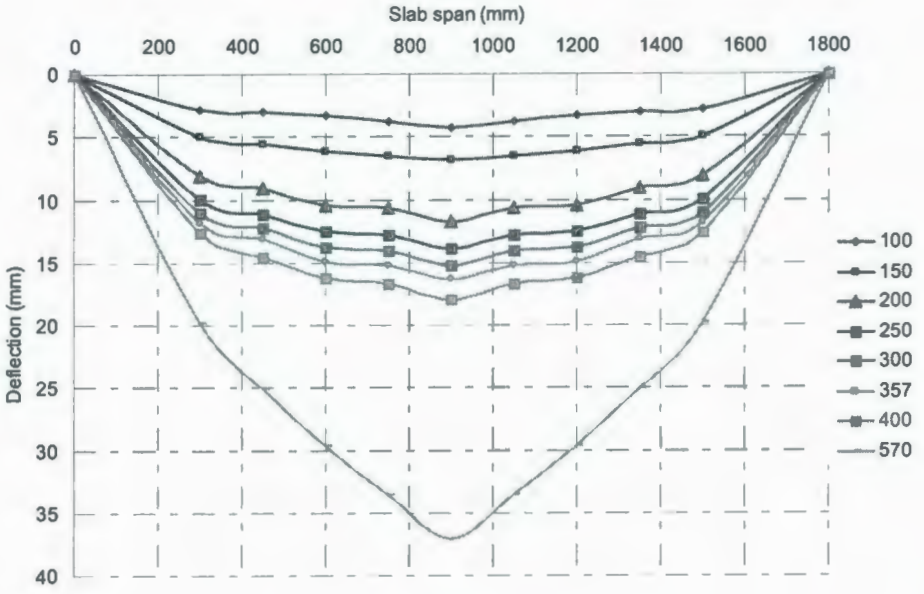

(*b*) HS1

Figure 4.3: Deflection profile for tested slabs: (*a*) NS3 and (*b*) HS1

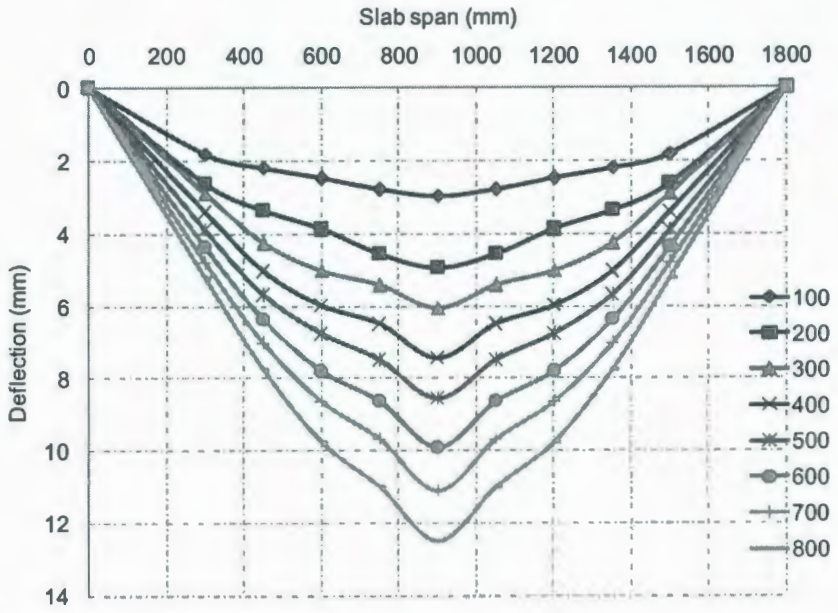

(*a*) NS4

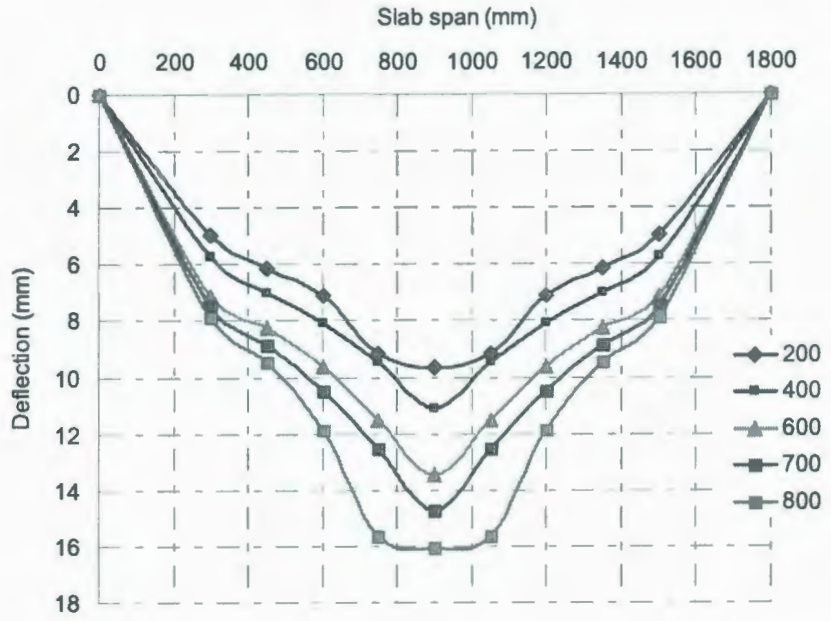

(*b*) HS2

Figure 4.4: Deflection profile for tested slabs: (*a*) NS4 and (*b*) HS2

The deflection profiles for specimens NS1, NS2, NS3 and HS1 indicate that the zone of high deformation was extended over a large distance from the center of the slab, beside there were more stages of loading between the yield load point and the failure load point. This is a clear indication that specimens NS1, NS2, NS3 and HS1 tended to deform due to flexure unlike specimens NS4 and HS2 that deformed due to local punching-shear at location of the applied load.

4.2.3 Ductility and Energy Absorption Characteristics

Ductility is a term that reflects the deformation capacity of a structural member before failure. Ductility U is defined as the ratio of the ultimate deflection Δ_U to the deflection at first yield Δ_y. The energy-absorption capacity is defined as the area under the load-deflection curve. The ductility at failure and the energy-absorption capacity of all test

slabs, as defined above, are given in Table 4.3. Test results revealed that as the steel reinforcement ratio is increased, the ductility is decreased. For example, increasing the reinforcement ratio from 0.35 to 0.73% decreased the ductility by 75%. Test results revealed that as the depth of the slab increased ductility was decreased. Comparing the test results of Series A1, Series A2 and Series A3, it is evident that as the depth increased the slab ductility decreased. Normal strength slabs NS3 and NS4 were identical, in size and reinforcement ratio to high-strength concrete slabs HS1 and HS2, respectively. Test results showed that the ductility decreased with increasing concrete strength. The energy absorption capacity for slabs NS2, NS3, and NS4 is as follow 11.07, 11.32, and 11.95 respectively, all values are multiplied by 10^3 N.m; this means that by increasing the thickness, the slab structural behaviour becomes more brittle.

The energy absorption capacity for slab HS2 is 10.1×10^3 N.m, and is smaller than the energy absorption value for slab NS4 which has the same reinforcement ratio, which reflects the brittle behavior of high strength concrete slabs. However, structural behavior for slab HS2 could be enhanced by using a smaller reinforcement ratio, and this is also due to the size effect. This is clear when comparing the values of ductility and energy absorption capacity for slab HS3 which has a reinforcement ratio equal to 0.43 % to identical slab HS2 which has a reinforcement ratio equal to 0.73%. The values of ductility and energy absorption capacity for slab HS3 are more than twice the same values for slab HS2, i.e. much better structural behavior resulted by reducing the reinforcement ratio from 0.73% to 0.43% for the 300 mm HSC concrete slab. This proves the previous assumption, which states that the structural behavior for slab HS2 could be enhanced by using a smaller reinforcement ratio. Using the same analogy for the size effect for slabs with

thickness over 250 mm, the structural behavior of slab NS4 could be enhanced by using a smaller reinforcement ratio.

Table 4.3–Observed ductility and energy absorbtion

Slab No.	Concrete Strength f_c', MPa	Slab Thickness, mm	Depth, mm	Steel ratio, ρ%	Ductility $\frac{\Delta_u}{\Delta_y}$	Energy absorption capacity, N.m × 10^3
NS1	45	150	105.0	0.48	3.54	5.76
NS2	50	200	152.5	0.54	1.92	11.07
NS3	35	250	182.5	0.35	3.31	11.32
HS1	70	250	182.5	0.35	3.25	20.27
NS4	40	300	217.5	0.73	3.81	11.95
HS2	65	300	217.5	0.73	1.68	10.11
HS3	75	300	220.0	0.43	3.89	28.91

4.2.4 Concrete Strains

For all the test slabs, measurements were made to determine the distribution of the concrete strain along a radius of the slab. Figures 4.5 to 4.11 present the load-versus-concrete strain measured at two different positions. Neither the concrete strains in the tangential or the radial directions reached a limiting value of 3000 με for any of the tested slabs except for specimens HS1 and HS2 the concrete strain at a distance equal to 100 mm from the column edge reached almost 3000 με. It can be concluded that the maximum concrete strain occurred at a distance almost equal to *d*/2 from the column face. The load-concrete strain curves for NS1, NS2, NS3, HS1 and HS3 were linear until the cracking point beyond that with every increase in loading the concrete strain was relatively high.

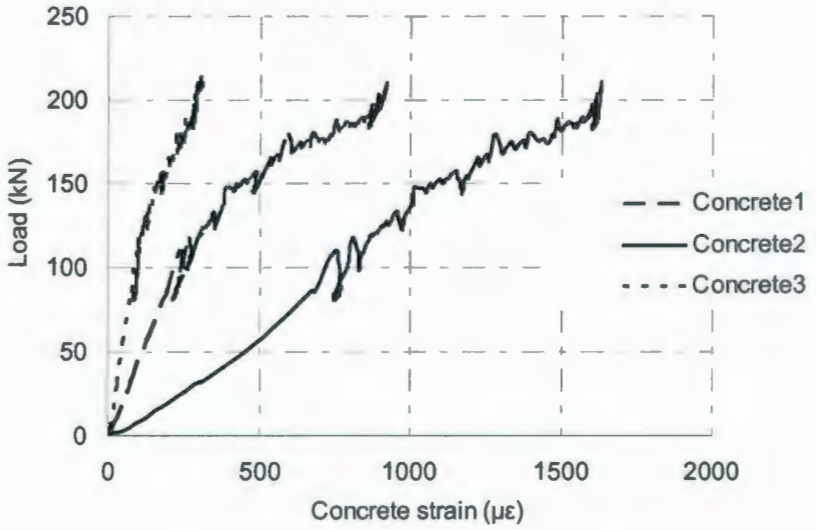

Figure 4.5: Load versus concrete strain for NS1

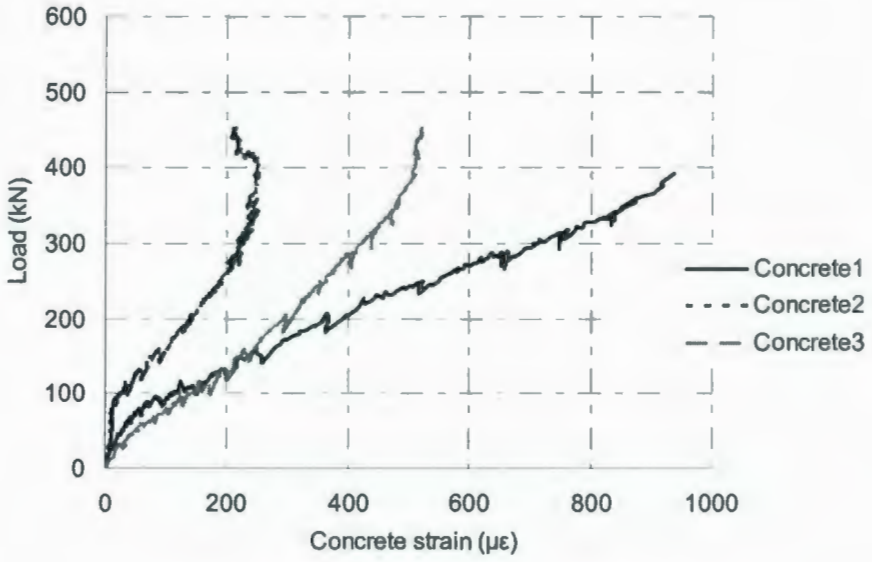

Figure 4.6: Load versus concrete strain for NS2

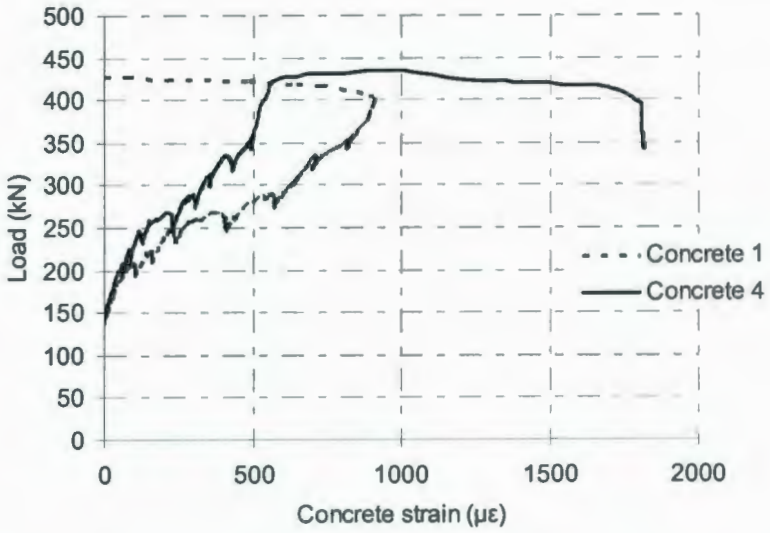

Figure 4.7: Load versus concrete strain for NS3

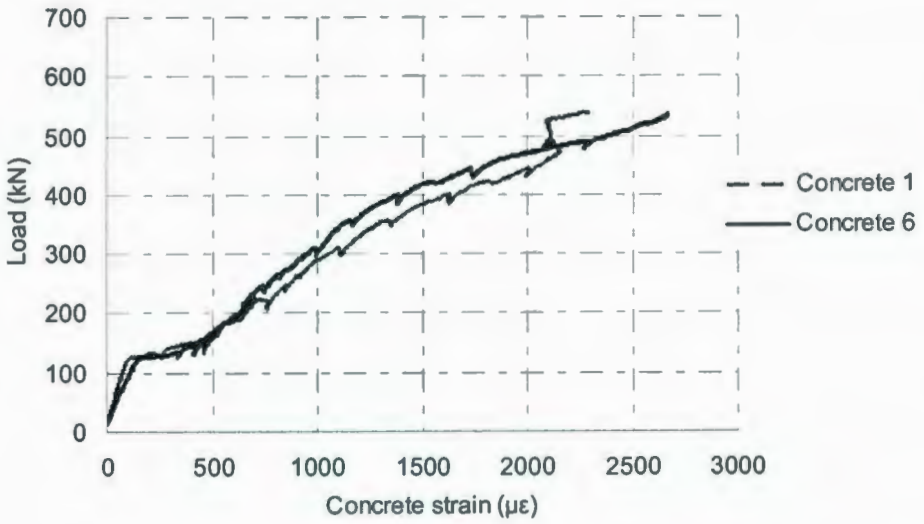

Figure 4.8: Load versus concrete strain for HS1

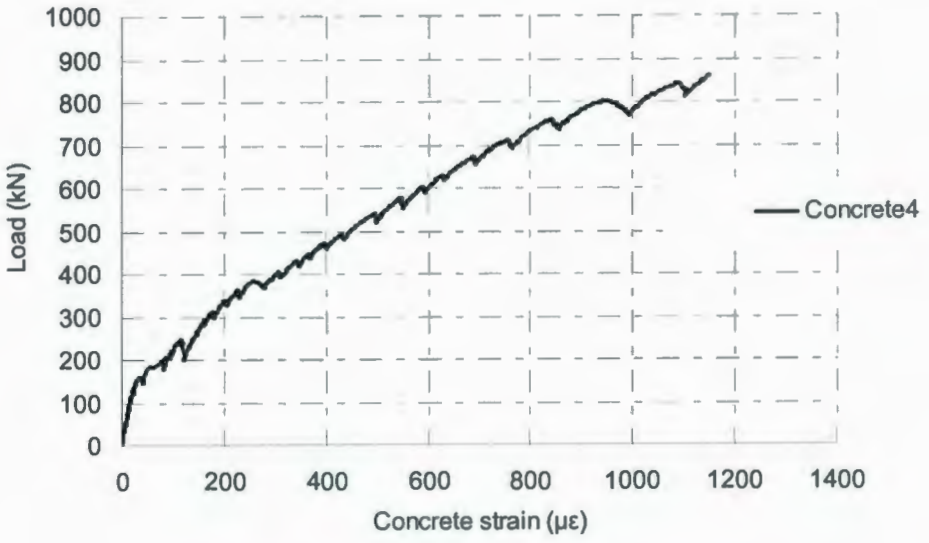

Figure 4.9: Load versus concrete strain for NS4

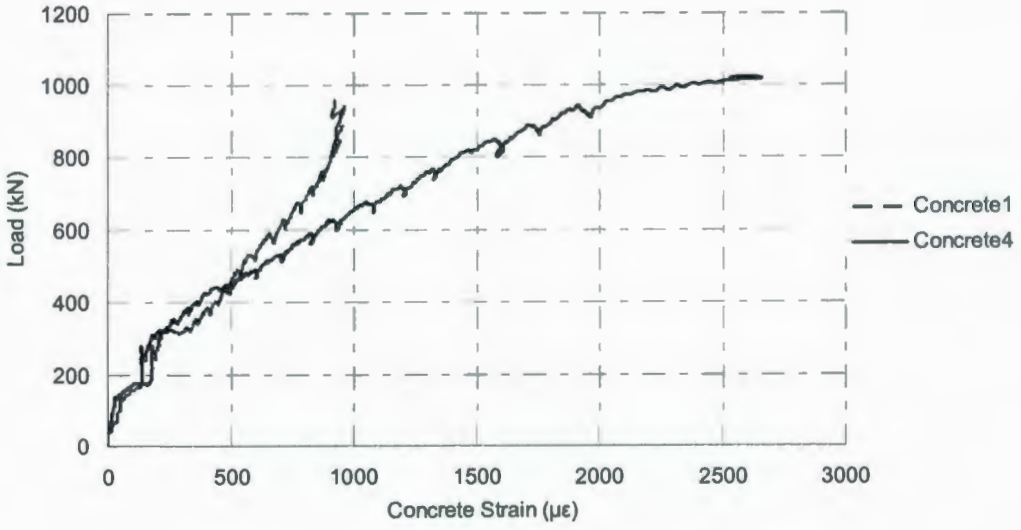

Figure 4.10: Load versus concrete strain for HS2

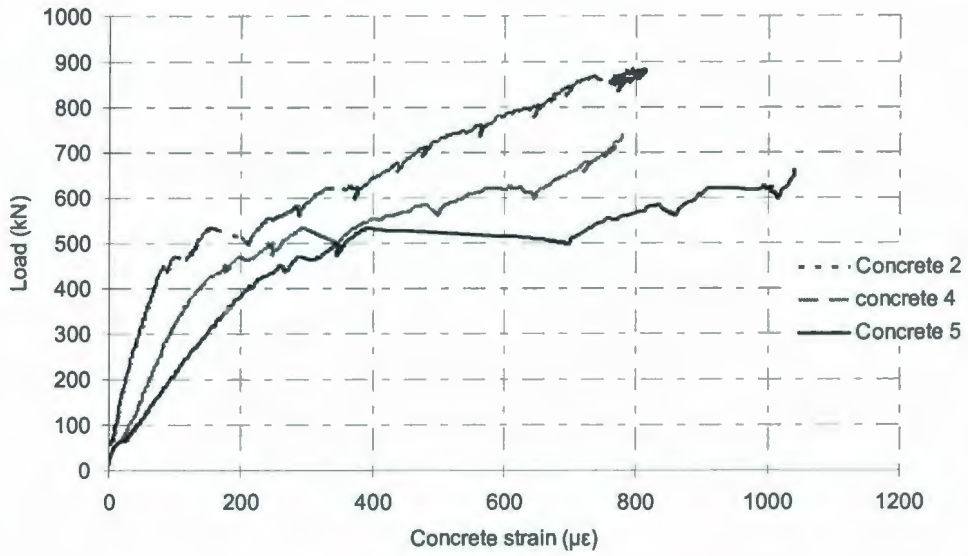

Figure 4.11: Load versus concrete strain for HS3

4.2.5 Steel Strains

Measurements were made to determine the strain distribution along a radius for all the tested slabs. Typical test results of these measurements are presented in Figures 4.12 to 4.14. For all test slabs, the tension reinforcement yielded before punching took place. The degree to which yielding spread in the tension steel varied as reinforcement ratio changed. At high reinforcement levels, the yielding of the tension reinforcement occurred at higher applied loads and was localized at the column stub. For lightly reinforced slabs, yielding initiated at the column stub and gradually progressed throughout the whole tension reinforcement.

The highest stain that resulted in initial yielding occurred below the stub-column. In all the tested slabs the tension reinforcement yielded prior punching took place except specimen NS4 that experienced ductile shear failure, for specimen HS1 that experienced ductile flexural failure, the yielding load occurred at almost 50% of the failure load.

In general, the slope of load-strain graph is very high for high-strength concrete slabs that failed in shear compared to normal-strength concrete and after a certain load level the slope gradually decreased. This could be attributed to the concrete contribution at the initial stage. In NS1, NS2, NS3, HS1 and HS3, yielding initiated at the column stub and gradually progressed through the whole tension reinforcement. Moreover, specimens NS1, NS2, NS3, HS1 and HS3 reached the state of steadily steel strain at a constant load that is a normal behavior for slabs failed in flexure.

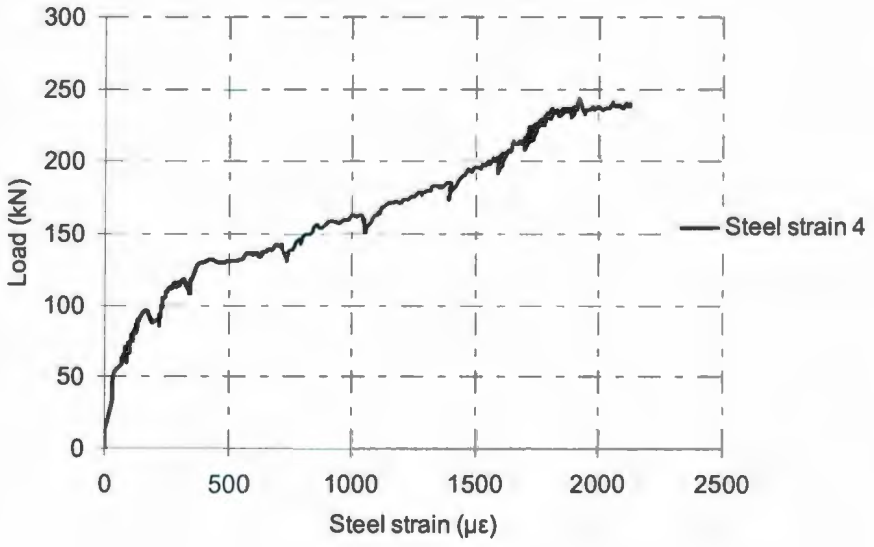

(*a*) NS1

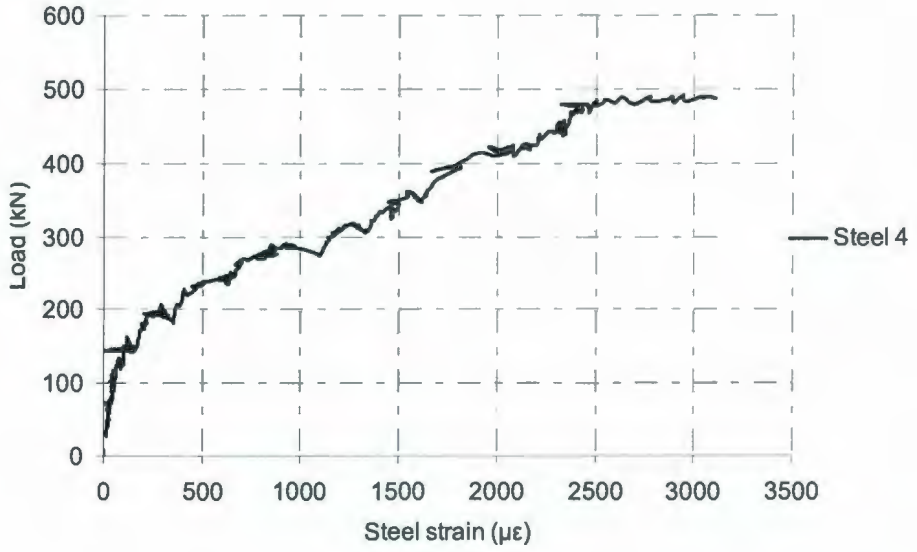

(*b*) NS2

Figure 4.12: Typical load-tension steel strain behavior at the column periphery for Series A1: (*a*) NS1; (*b*) NS2

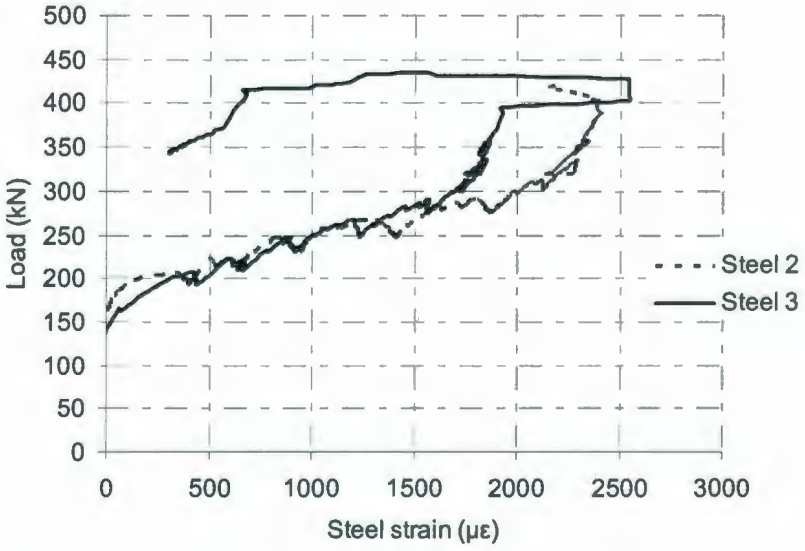

(*a*) NS3

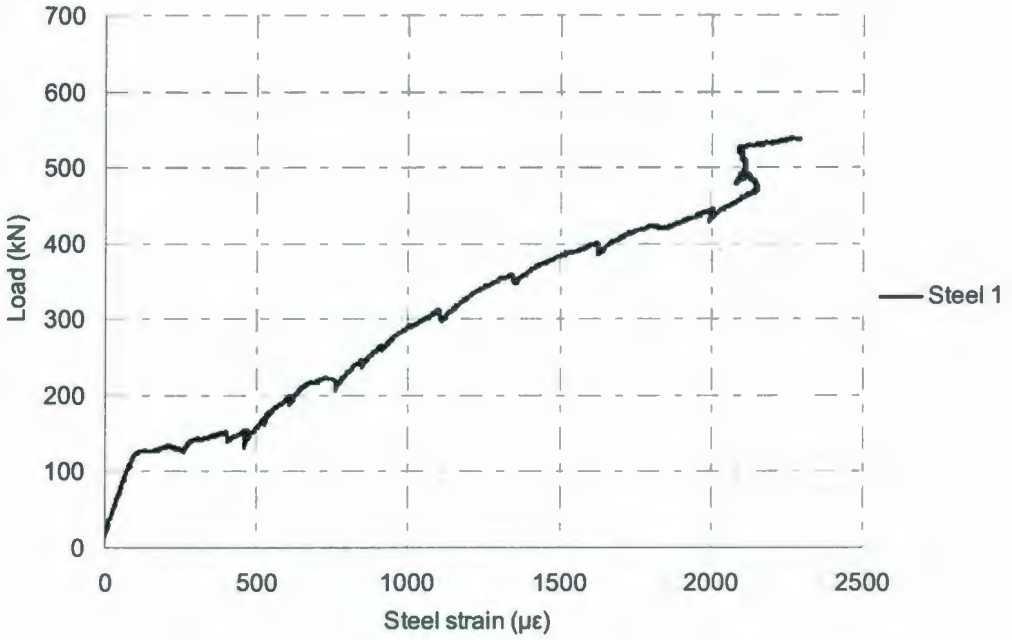

(*b*) HS1

Figure 4.13: Typical load-tension steel strain behavior at the column periphery for Series A2: (*a*) NS3; (*b*) HS1

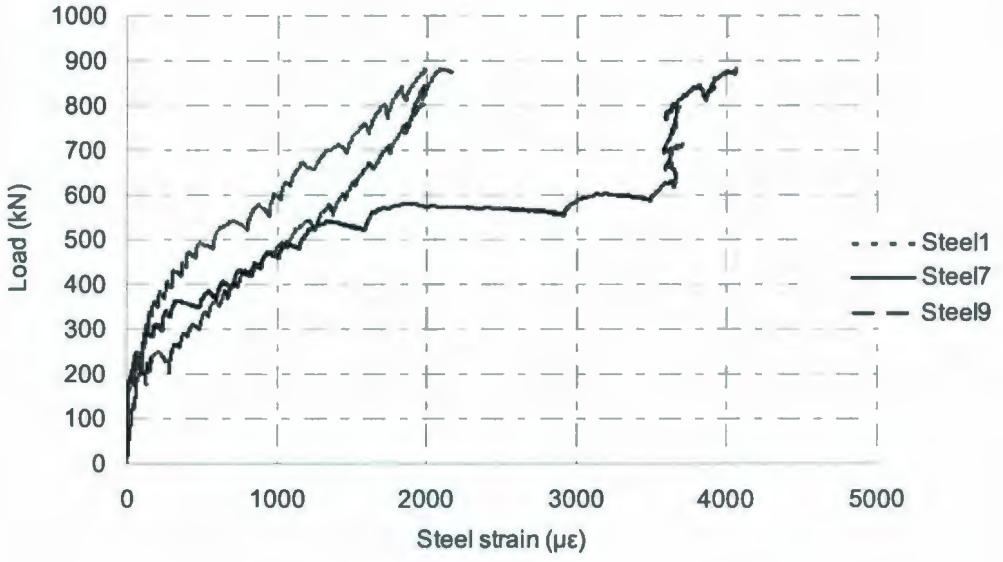

(*a*) NS4

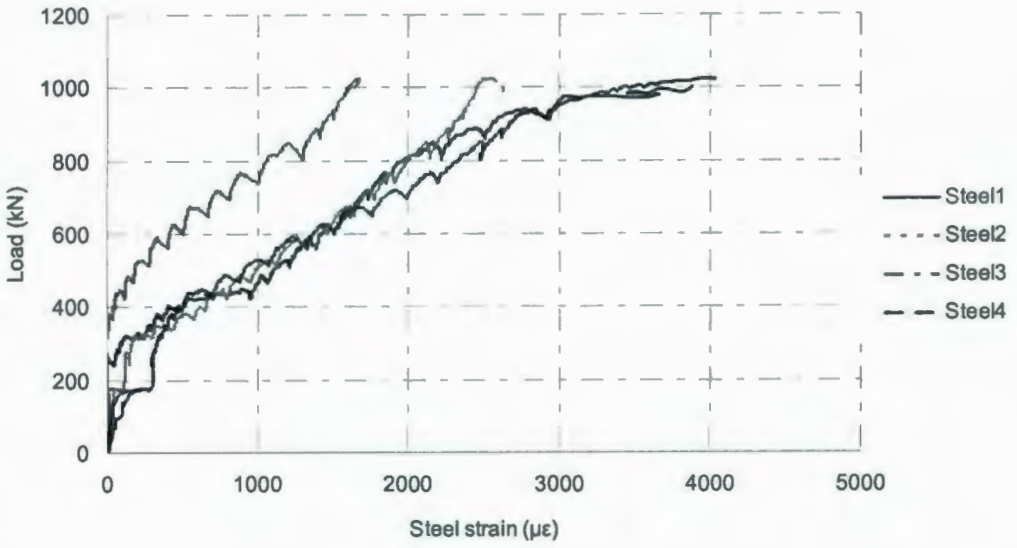

(*b*) HS2

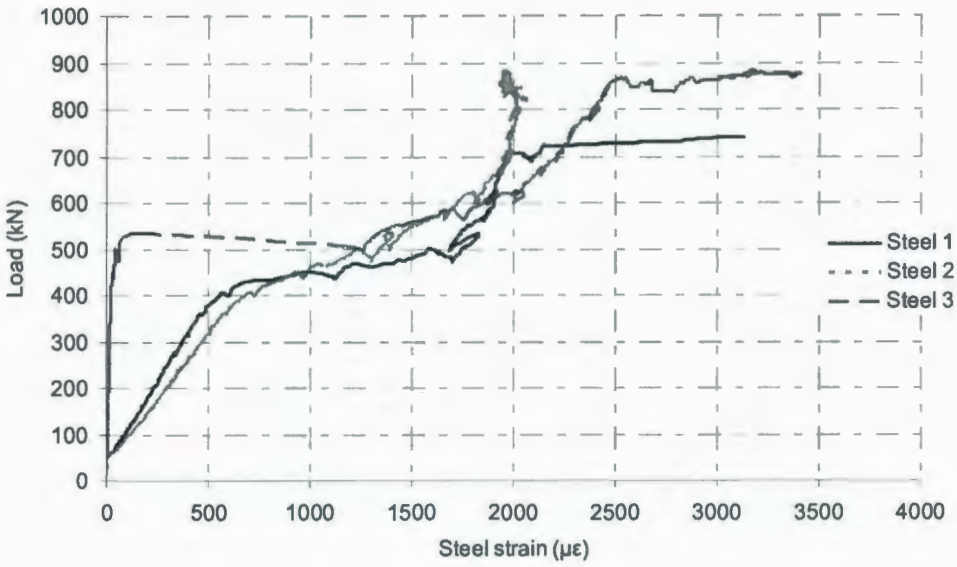

(*c*) HS3

Figure 4.14: Typical load-tension steel strain behavior at the column periphery for Series A3: (*a*) NS4; (*b*) HS2; (*c*) HS3

4.3 Cracking and Failure Characteristics

The first crack of each specimen was visually inspected and the corresponding load was recorded at the first crack load. In all tested slabs, the initial observed cracks were first formed tangentially under the edge of the column stub, followed by radial cracking extending from the column edge toward the edge of the slab.

For the slabs failing in flexure (NS1, NS2, NS3, HS1 and HS3), the crack pattern observed prior to punching consisted of one tangential crack, roughly at the column outline, followed by radial cracking extending from the column. In all slabs, flexure yield lines were well developed. This failure can be classified as flexure failure. For the slabs failing by flexure-punching or punching, the crack pattern observed prior to punching consisted of almost no tangential crack, radial cracking extending from the column were the most dominant crack pattern.

4.3.1 Crack Spacing

Numerous cracks developed on the tension face of slab at the time of failure. Photographs of all test slabs with crack marks are shown in Figures 4.15 to 4.17. For all the specimens, the first crack formed along the rebar passes through the slab center or close to the slab center. The second crack formed along the similar rebar in other direction. Crack Displacement Transducers (CDT) were mounted on the concrete surface of the first, second and third visible cracks in order to measure opening displacement. The corresponding load of each crack was recorded accurately. The cracks formed in this stage have no effect on the characteristics of the crack pattern and primarily depend on the concrete strength. The first crack of each specimen was visually inspected and the corresponding load was recorded as the first crack load.

It was noticed that increasing the concrete cover resulted in increased crack spacing. Test results of Series A2 and A3 indicated that increasing the concrete cover from 60 mm to 70 mm increased the crack spacing from 245 mm to 261 mm. The test results of Series A1 (NS1, NS2) indicated that as the bar spacing is increased from 210 mm to 240 mm, the crack spacing increased from 201 mm to 221 mm, respectively.

Series A2 and A3 included five specimens; all specimens had the same bar spacing 368 mm. It is interesting to point out that the average crack spacing almost equal to 253 mm was much smaller than the bar spacing. Table 4.4 presents the experimental measured crack spacing and crack width for tested slabs.

Table 4.4–Experimental measured crack spacing and crack width for tested slabs

Series No.	Slab No.	Concrete cover C_c, mm	Slab thickness, mm	Bar spacing s, mm	f_c', MPa	Average crack spacing S_{rm}, mm	Characteristic crack width w_k, mm
A1	NS1	45	150	210	45	201	-----
	NS2	40	200	240	50	221	-----
A2	NS3	60	250	368	35	245	0.465
	HS1	60	250	368	35	263	0.402
A3	NS4	70	300	368	70	261	0.714
	HS2	70	300	368	65	246	0.596
	HS3	70	300	368	75	247	0.362

*NS-Normal strength slabs; HS-High strength slabs

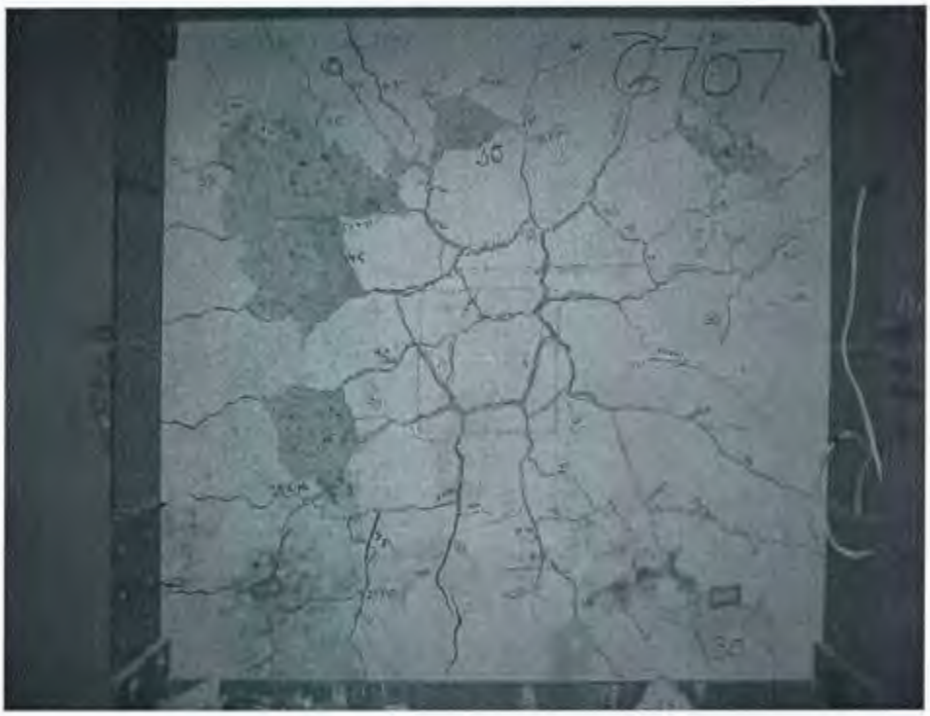

(*a*) NS1

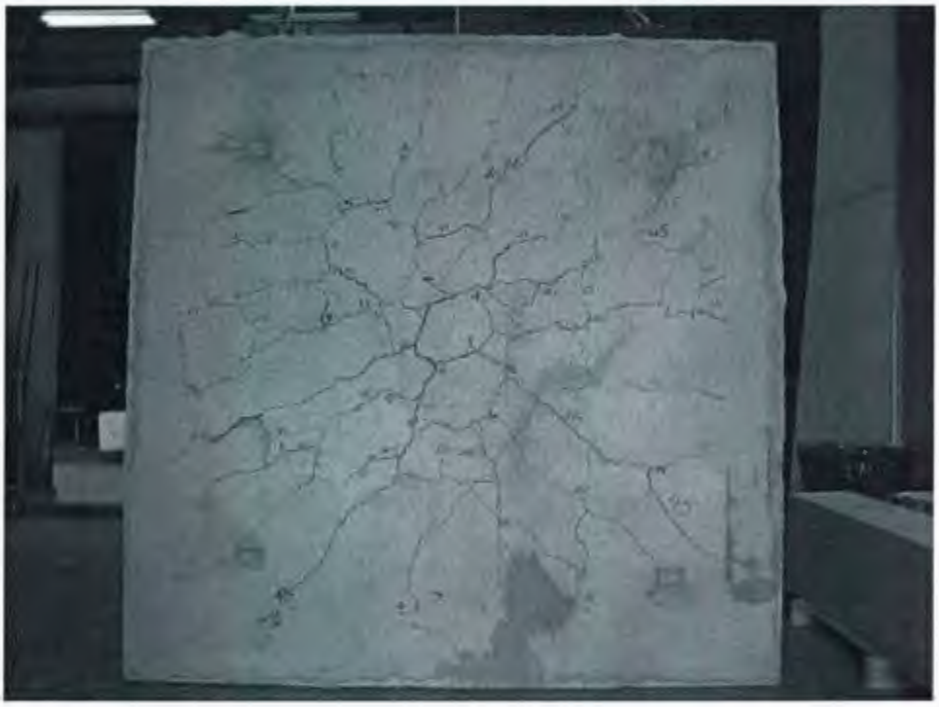

(*b*) NS2

Figure 4.15: Crack patterns of Series A1: (*a*) NS1; (*b*) NS2

(*a*) NS3

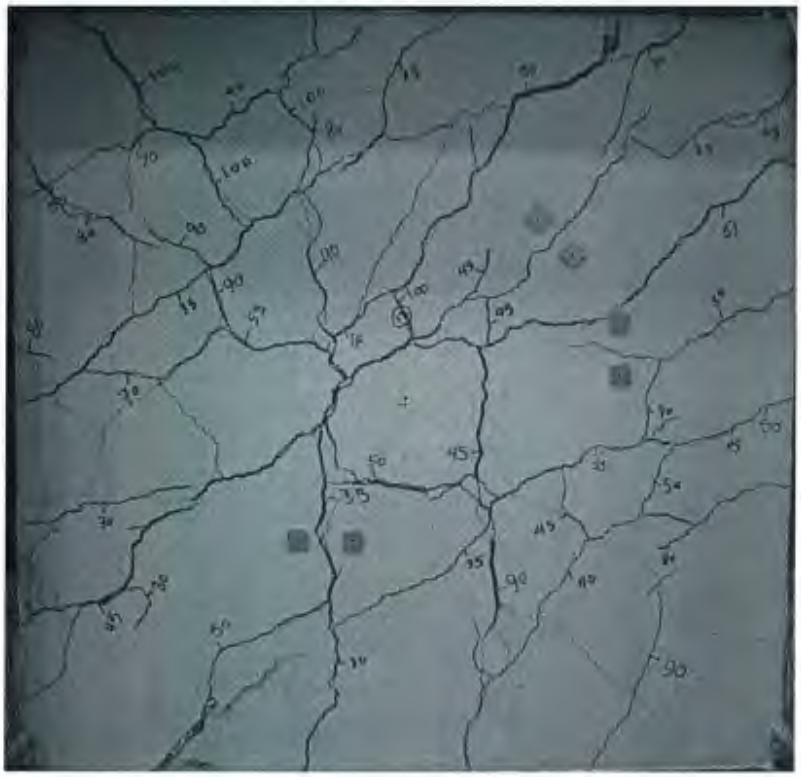

(*b*) HS1

Figure 4.16: Crack patterns of Series A2: (*a*) NS3; (*b*) HS1

(*a*) NS4

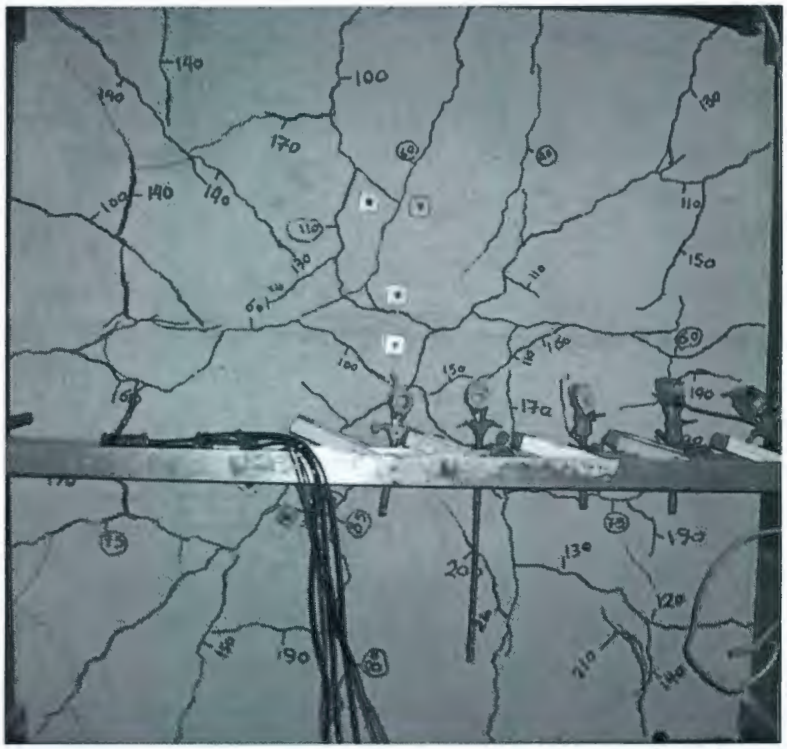

(*b*) HS2

(*c*) HS3

Figure 4.17: Crack patterns of Series A3: (*a*) NS4; (*b*) HS2; (*c*) HS3

4.3.2 Crack Width

This section is focused on evaluating the effect of using thick concrete covers and big bar spacing on crack widths and crack properties of tested two-way slabs. Each slab was carefully inspected at each load step. The cracks were marked and the maximum visible crack width was measured using a crack width measuring gauge. The Crack Displacement Transducer (CDT) is mounted to concrete surface cracks in order to measure the opening displacement as shown in Figure 3.14. It is a waterproof enabled gauge. The range of the gauge is ±2 mm. The accuracy of the measurements improved as the cracks started to widen.

4.3.2.1 Crack Width Measurements

The following study tries to assess the effect of thick covers on crack widths. Also, one of the objectives of this experimental investigation is to evaluate the accuracy of design codes models for crack width estimate when dealing with thick plates having thick concrete covers. This will help in identifying the conflict between the code specifications and the recommended practices of durable concrete. Provisions based on limiting crack width need to be re-examined in light of the requirements for a durable concrete in aggressive environments. This study will address the two issues of controlled crack width and increased concrete cover and their influence on each other. The objective is to achieve an efficient economical design and durable concrete in aggressive environments.

The crack width was measured at each load increment. In Figure 4.18 through 4.22, the opening of the crack width is plotted versus the steel strain. The crack width increased as the applied load was increased. However, this increase was not very smooth as concrete is not a homogenous material. It was noticed that the crack width versus steel strain can be represented by one straight line up to value that ranges between 1500 and 2000 με of steel strain except for slab HS1. This value of strain produces a stress in the steel bars equal to 300-400 MPa. In most of the slabs, the crack width versus steel strain curve tends to behave nonlinearly after the steel strain reaches the value 1800 με. In slabs NS3, HS1 and HS3, the crack width continues to increase after the steel strain reaches the yield point that is an expected behavior for a slab that failed in flexure.

All measurements reported in Table 4.4 are taken at a steel stress level of 267 MPa (0.67 f_y). The data showed that as the concrete cover increases the crack width increases. The maximum crack width can be influenced by as much as 28% when the concrete cover

increases from 60 to 70 mm for the same bar spacing. A comparison of the experimental results of the average crack width measurements of the two tested series indicated that the mode of failure has no effect on the size of the crack width.

Most design codes neglect the effect of concrete strength on crack width size; however, the CEB-FIP (1990) model code is the only code that takes into account the effect of concrete strength when calculating crack width. Test results indicated that increasing the concrete strength from 35 MPa to 70 MPa resulted in about 10-15% decrease in crack width.

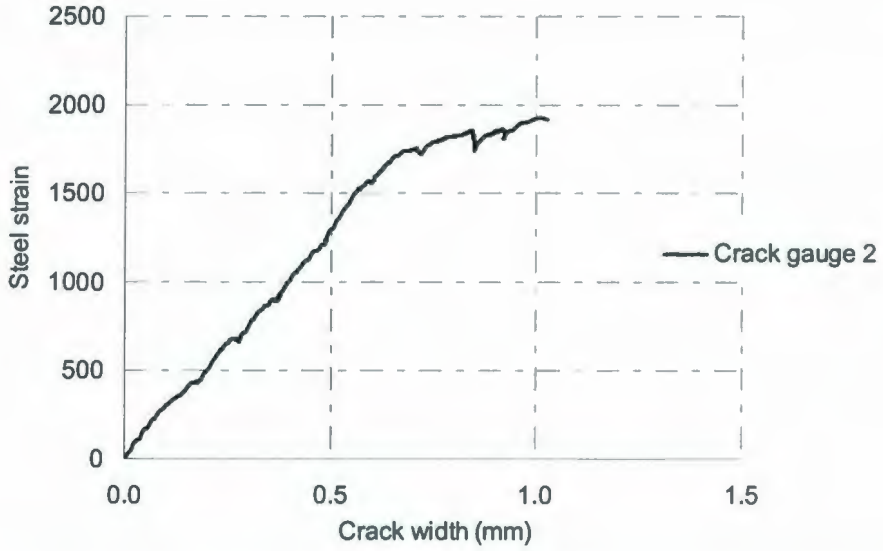

Figure 4.18: Crack width expansion versus steel strain for NS3 (h = 250 mm)

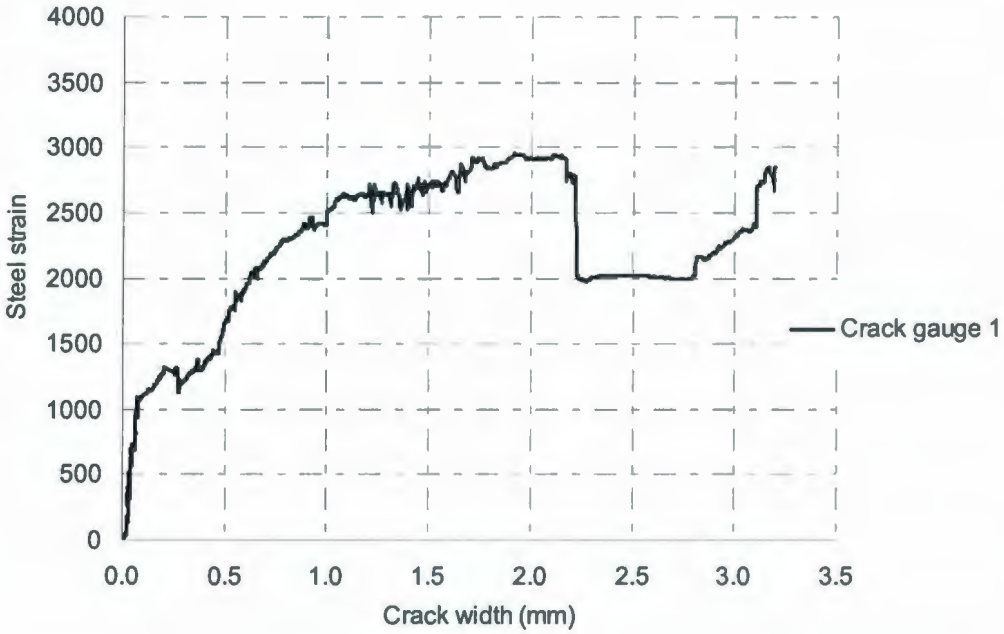

Figure 4.19: Crack width expansion versus steel strain for HS1 (h = 250 mm)

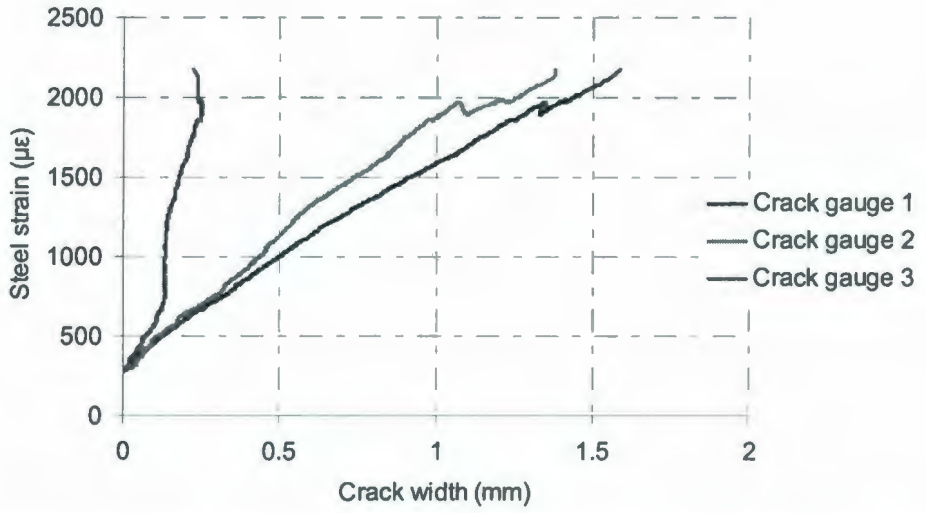

Figure 4.20: Crack width expansion versus steel strain for NS4 (h = 300 mm)

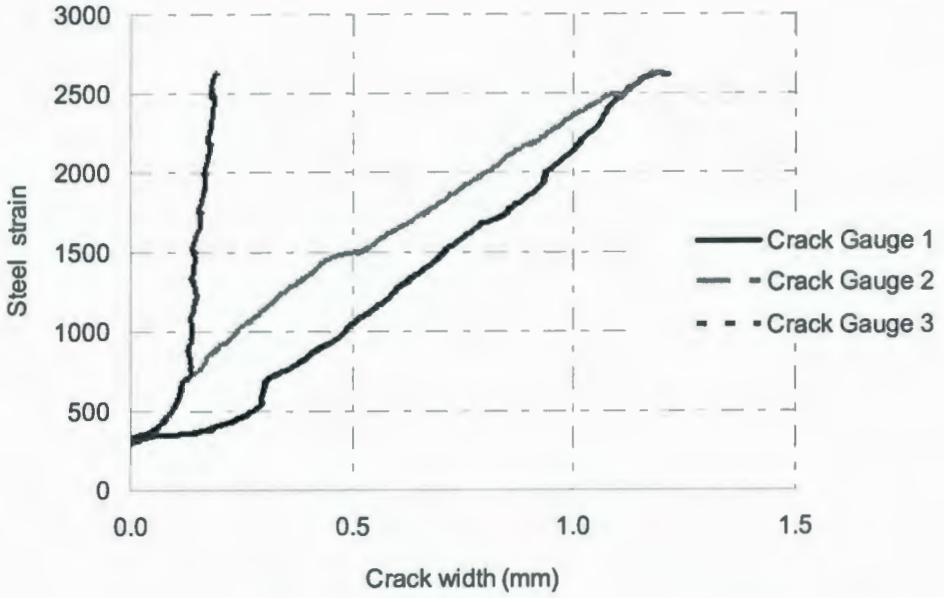

Figure 4.21: Crack width expansion versus steel strain for HS2 (h = 300 mm)

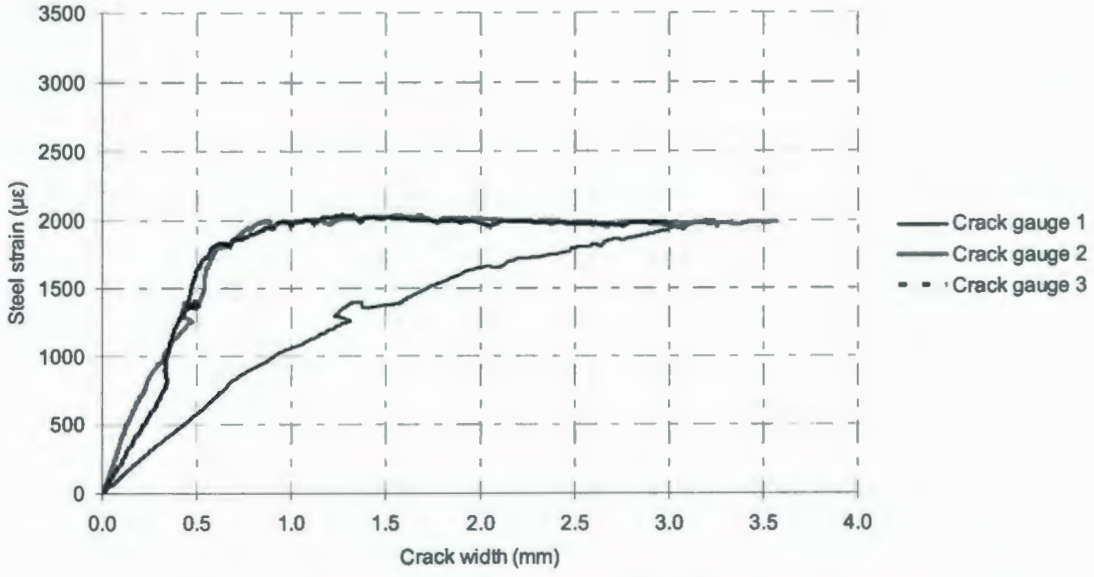

Figure 4.22: Crack width expansion versus steel strain for HS3 (h = 300 mm)

4.4 Modes of Failure

All the test specimens except specimen NS4 and HS2 failed in flexure. All these slabs utilized full flexural capacity as it will be discussed later in Chapter 8. However, slab NS4 and slab HS2 failed in punching, with the slab failing before the flexural strength exceeded. The test specimens NS4 and HS2 had a reinforcement ratio (ρ = 0.73 %) while slab HS3 had a reinforcement ratio (ρ = 0.43 %) and was designed to fail in flexure, however, both the load-deflection curve and the strain distribution indicated that slab NS4 and slab HS2 failed in a brittle punching manner. Structural behaviour of slabs NS4 and HS2 could be enhanced by using a smaller reinforcement ratio; this is due to the size effect. Failure patterns of the tested slabs are shown in Figures 4.15 to 4.17. Provision of shear reinforcement can possibly improve the structural behaviour of NS4 and HS2; but this has not been investigated in Group A tests.

4.5 Summary

- The energy absorption capacity for slabs NS2, NS3, and NS4 is almost the same. These slabs have different thicknesses; this means that by increasing the thickness, the slab structural behavior becomes more brittle. This confirms the assumptions that the size effect for slabs over 250 mm has an effect on the structural behavior on slabs and must be considered in design.
- Test specimens NS3 and HS1 are identical with the exception of concrete strength and both specimens displayed flexure failure. However, the energy absorption capacity for slab HS1 is higher than that for slab NS3. This confirms that the size effect factor cannot be taken as a constant number related to the member depth only but it must be related to the concrete strength as well as represented by

fracture mechanics size effect factor proposed by Marzouk et al. (1998).

- The values of ductility and energy absorption capacity for slab HS3 are more than twice the same values for slab HS2. This proves the previous conclusion that states that the structural behaviour for slab HS2 could be enhanced by using a smaller reinforcement ratio. The flexural reinforcement ratio chosen for slab HS2 was designed using ACI 318-08 formula while the flexural reinforcement ratio chosen for slab HS3 was designed using a formula proposed by the Rizk and Marzouk (2009).
- The Canadian offshore code CSA-S474-04 underestimates the minimum reinforcement ratio required for thin concrete slabs less than or equal to 200 mm.
- The ACI 318-08 and CSA-A23.3-04 design codes overestimate the minimum reinforcement ratio required for thick concrete slabs greater than 200 mm; this is due to the fact that none of these codes contain a size effect factor, and this can result in a lot of money savings.
- Using ACI 318-08 design guidelines for slabs more than 250 mm depth can result in a brittle response and hence no adequate warning of an impending failure at extreme overloads and this is due to neglecting size effect.
- The test results of Group A show that as the concrete cover increases, the maximum crack width increases. The data shows that the maximum crack width can be influenced by as much as 28% when the concrete cover increases from 60 to 70 mm for the same bar spacing.

Chapter 5

Structural Behaviour of Thick Plates

5.1 Introduction

The results and observations obtained from the second phase of experimental program are given in this chapter. Group B is designed to investigate the effect of bar spacing and thick concrete cover on crack width and crack spacing; it is also designed to investigate the effect of slab effective depth (size effect) on the structural behavior of heavily reinforced thick plates, common for offshore structures. The group contains five thick plates designated as specimens HS4, HS5, HS6, NS5 and HS7. The slabs of this group have slab thicknesses: 300 mm, 350 mm and 400 mm, two bar sizes, 25M and 35M, and three bar spacing of 217 mm, 289 mm and 368 mm but have the same thick concrete cover 70 mm. Slab specimen HS5 included T-headed shear stud reinforcement and was designed to examine the effect of shear reinforcement on the maximum punching capacity. The shear reinforcement consisted of vertical bars with a diameter of 15 mm and specified yield strength of 400 MPa anchored at the top and bottom by welded anchor plates. The layout of the shear reinforcement is shown in Figure 3.4. All the specimens of this group (Group B) were designed to investigate the effect of punching mode of failure on crack width and crack spacing. The specimens in this group were designed to fail in punching mode according to Osman et al. (2000).

The five reinforced concrete plates were divided into two groups. The following parameters were examined in this investigation; bar spacing and the slab effective depth on the crack properties. A large dataset was recorded and the related graphs were prepared. Few data were important for interpretation of the cracking test results, as

presented here. The behavior of the slabs was presented in terms of load-deflection relationship at different load stages, service load, ultimate load, and steel strain-crack width relationship. Failure mode and crack patterns were also depicted by photographs.

The test slabs were classified into two series. The first series (Series B1) was designed to investigate the effect of the reinforcement ratio on the structural behavior of thick plates. The group was made of three slabs designated as HS4; HS5 and HS6.The slabs of this group had the same thick concrete cover of 70 mm but with different slab thickness and different reinforcement ratios. The second series (Series B2) was designed to investigate the effect of concrete strength on the structural behaviour of thick plates. The group was made of two slabs designated as NS5 and HS7. The two slabs had the same concrete cover, the same reinforcement ratio and the same effective depth but with different concrete strength. All the specimens were designed to fail in punching failure except specimen HS4 that was designed to fail in flexure.

The main objective was to study the effect of slab effective depth (size effect) and shear reinforcement on the structural behavior of thick plates designed for offshore applications with regard to deformation, strains, ultimate capacity, ductility, and energy absorption.

5.2 Test Specimens

A summary of the different specimens is presented in Table 5.1. The test slabs have a side dimension of 2650 mm in both directions. The test specimens were simply supported along all four edges with the corners free to lift. A concentric load was applied on the slab through a 400 × 400 mm column stub. Reinforcement ratios of 0.56%, 1.42% and 1.58% were selected for bottom reinforcement, the top reinforcement ratios were selected to satisfy the CSA-A23.3-04 code for minimum reinforcement ratio for controlling

shrinkage. Heavy reinforcement ratios were chosen to investigate the behaviour of thick plates in punching. All specimens were square with total thickness ranging from 300-400 mm. The dimensions were chosen to give a shear-span to depth ratio (a/d) of 3.33 to 4.8. The T-headed shear reinforcement specimen consisted of 15 mm bar as a stem, two 40 × 80 mm steel plates individually welded on both sides as anchor plates. A total of 40 T-headed studs were placed in slab HS5 as shown in Figure 3.6. The top anchors are in the form of rectangular plates, the areas of which are at least 10 times the area of the stem (Elgabry and Ghali 1990). The stud spacing s was chosen to be 0.5 d, as the lower of two spacings recommended by the ACI-ASCE 421 joint committee (2008), and the shear studs were extended to approximately 2.0 d from the column faces as recommended by Marzouk and Jiang (1996). The distance between the first row of studs and the column face s_o was taken as 0.4 d to avoid shear failure between the column and the first row of shear studs. The shear reinforcement ratio in the cross-pattern arrangement (Figure 3.4) is equal to the cross-sectional area of the studs on a peripheral line divided by d times the periphery of the column. For walls, the shear reinforcement ratio is equal to the cross-sectional area of a stud divided by d times the product of the two spacings in orthogonal directions. For slab HS5, the shear reinforcement has a ratio of 0.68% by volume; this ratio is equal to the area of 12 shear studs divided by slab depth d times the periphery of the column (i.e. $(12\times200)/(4\times400\times217.5)$)

5.3 Test Setup

A new test setup was designed and fabricated in the structural laboratory at MUN. The main function of this setup is to apply direct transverse load through hydraulic jack. The test setup consists of four reaction walls; two of the walls were used for supporting steel

beams that carried the load applied on the tested slabs. The steel beams were anchored to the retaining walls that were anchored to the structural floor. The third and fourth retaining walls were used to carry the hydraulic jack that applied the load directly on the column stub. The retaining walls units were restrained at the top and lower edges by self supporting closed rigid steel frames; the object of theses steel frames was to minimize the lateral displacement of the supporting retaining walls and hence ensuring that the test setup would act as a very rigid self supporting unit capable of resisting lateral applied loads. The test setup is shown in Figure 3.11. A hydraulic jack was mounted to the third and fourth retaining walls and was used to apply a concentric load on the column stub in a horizontal position. The jack was a CLRG-30012 Series hydraulic jack cylinder with a maximum capacity of 3110 kN (700 kips) and a maximum displacement of 300 mm.

5.4 Test Procedure

The test slabs were placed in the frame in a vertical position. The test slabs were simply supported along all four edges with the corners free to lift and were loaded concentrically through a column stub. Test specimens were instrumented to measure the applied load, central deflection, strains on concrete and reinforcement. The load was applied at a selected load increment of 44.0 kN. The test slabs were carefully inspected at each load step. The cracks were marked manually after mapping all the cracks on the specimen. Deflection at the slabs centers was measured with an LVDT gage. Steel strains at ten locations were monitored, as shown in Figure 3.12a. Concrete strains were recorded at eight locations on the compression faces of the concrete slabs. The concrete strains were measured with electrical 50 mm strain gages, as shown in Figure 3.12b. For all the specimens, the first crack formed along the rebar and passes through the slab center or

close to the slab center. The second crack formed along the perpendicular rebar in the other direction. All tests were terminated after punching had occurred and the load had dropped considerably.

Table 5.1–Details of Group B test specimens

Series No.	Slab No.	Compressive Strength f_c', MPa	Bar Size, mm	Bar Spacing, mm	Concrete Cover C_c, mm	Slab Thickness, mm	Depth, mm	Steel ratio ρ%	Shear reinforcement ρ_z%
B1	HS4	76	25	368	70	350	267.5	0.56	---
	HS5	79	25	217	70	300	267.5	1.42	0.68
	HS6	65	35	289	70	350	262.5	1.42	---
B2	NS5	40	35	217	70	400	312.5	1.58	---
	HS7	60	35	217	70	400	312.5	1.58	---

*NS-Normal strength slabs; HS-High strength slabs

5.5 Test Results

The first crack of each specimen was visually inspected and the corresponding load was recorded as the first crack load. The yield steel strain was assumed to occur at a value of 2000 με, which produced a stress in the steel rebar equal to 400 MPa. The yield strain was measured at a location 150 mm from the center of the slab. The value of 2000 με was suggested based on experimental observations of the stress-strain curve of a single rebar. In all test slabs, the initial observed cracks were first formed tangentially under the edge of the column stub, followed by radial cracking extending from the column edge toward the edge of the slab. As the load was increased, tension reinforcement yielded, which resulted in a significant increase in the crack width and the deflection. It was noted that the ratio of the yield moment to the cracking moment increased with increasing reinforcement ratio.

5.5.1 Load-Deflection Characteristics

The load-deflection curves were obtained using LVDT measurements during loading by three linear variable differential transducers (LVDTs) and LPDT at four predetermined locations on the tension surface. All the readings were logged into a data acquisition system. The applied load versus the deflection at the center of the slab for different test specimens is shown in Fig. 5.1. Table 5.2 illustrates the measured deflection at first crack, first yield of tension steel, ultimate load and at post-ultimate load.

The load-deflection curve of slab HS4 indicated that it failed in flexure. The test slab reached the state of steadily increasing deflection at constant load. Thus, it displayed a very ductile behavior characterized by a continuously increasing capacity with increasing deflection after overall yield of the flexural reinforcement, which is a normal characteristic for a lightly reinforced concrete specimen experiencing flexural failure. Slab HS5 failed in a ductile flexure failure as indicated by its load-deflection curve. Slabs HS6, NS5 and HS7 failed in punching this is indicated by a sudden drop in the load-deflection curve.

Table 5.2–Deflection characteristics of test slabs

Slab No.	Concrete Strength f_c', MPa	Steel ratio, ρ%	First crack load, kN	First crack deflection, mm	Yield load P_y, kN	Yield load deflection Δ_y, mm	Ultimate load P_u, kN	Ultimate load deflection ΔP_u, mm	Post-ultimate load $P\Delta_u$, kN	Post-ultimate load deflection Δ_u, mm
HS4	76	0.50	312	5.9	790	7.3	1722	22.5	360	32.0
HS5	79	1.42	320	5.7	1219	18.9	2172	35.5	1067	43.5
HS6	65	1.42	258	7.0	1381	17.3	2090	24.1	617	35.1
NS5	40	1.58	276	4.1	2094	11.5	2234	13.1	549	24.6
HS7	60	1.58	317	4.4	2081	9.4	2513	13.1	507	25.7

*NS-Normal strength slabs; HS-High strength slabs

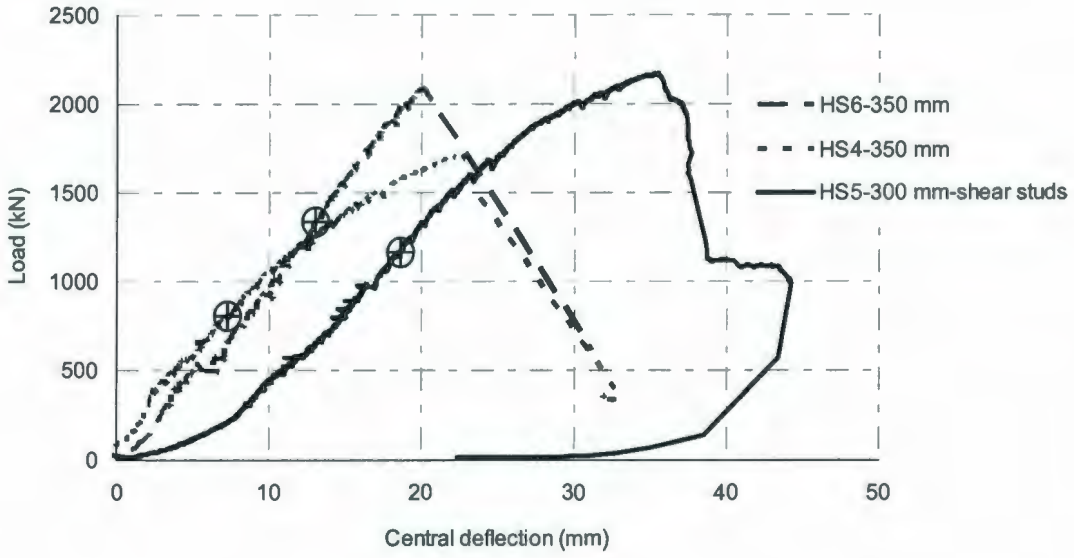

(*a*) Series B1

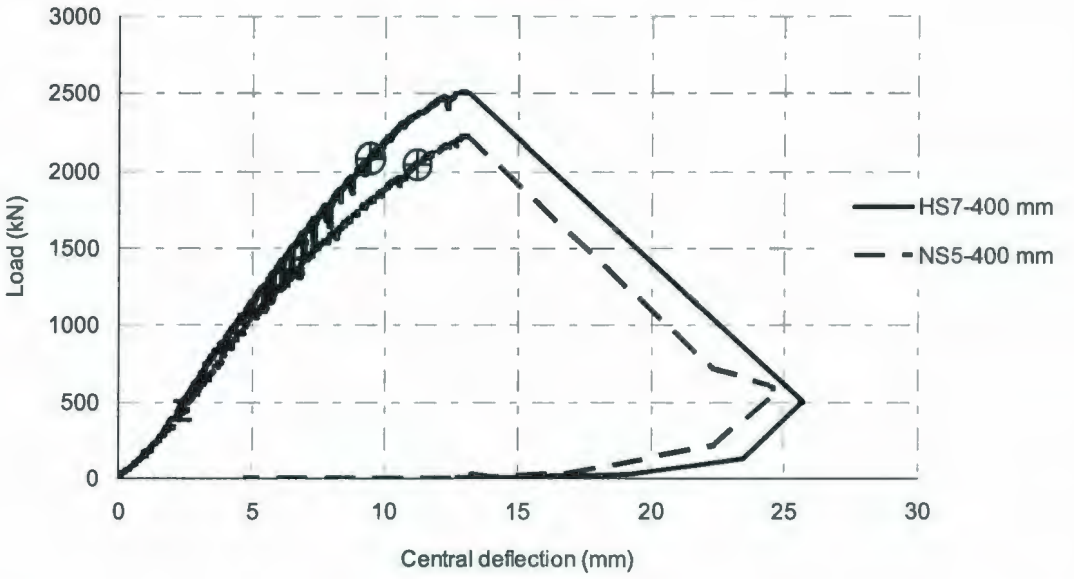

(*b*) Series B2

Figure 5.1: Typical load-deflection characteristics at center span of test slabs: (*a*) Series B1; (*b*) Series B2

5.5.2 Deflection Profiles

Measuring the deflection at different locations along a specimen's width is used to construct the deflection profile for such a specimen. Deflection profiles give a global indication of the deformational response to the application of load not just at the location of the application of load but also along the slab width. The deflection values were measured at four different locations on one side of the symmetrical specimen as show in Figure 3.10. Values of the central deflection at each increment were recorded and used to determine the deflection profile at the increment. Figures 5.2 to 5.3 show the deflection profiles of the specimens HS4, HS5, HS6, NS5 and HS7.

Figures 5.2a and 5.2c indicate that specimen HS6 require more load to reach the same level of deformation compared to that of specimen HS4. It is also clear that the zone of high deformation of specimen HS6 is extending over a less distance from the center of the slab than that of HS4. This is a clear indication that specimen HS6 tends to deform more severely due to shear unlike specimen HS4. Moreover, the failure load occurred right after the yield of bottom steel reinforcement in specimen HS6 while in specimen HS4 it took more stages of loading before failure occurred. This supports the idea that specimen HS6 tends to fail in shear more suddenly than HS4. Figure 5.2b indicates that specimen HS5 with T-headed shear reinforcement failed in flexure mode. It is also clear that the zone of high deformation of specimen HS5 is extending over a significant distance from the slab center; this is due to the existence of T-headed shear studs.

Figures 5.2a and 5.3b show that HS4 and HS7 reached almost the same range of deflection prior to failure. This is due to the small reinforcement ratio used for HS4.

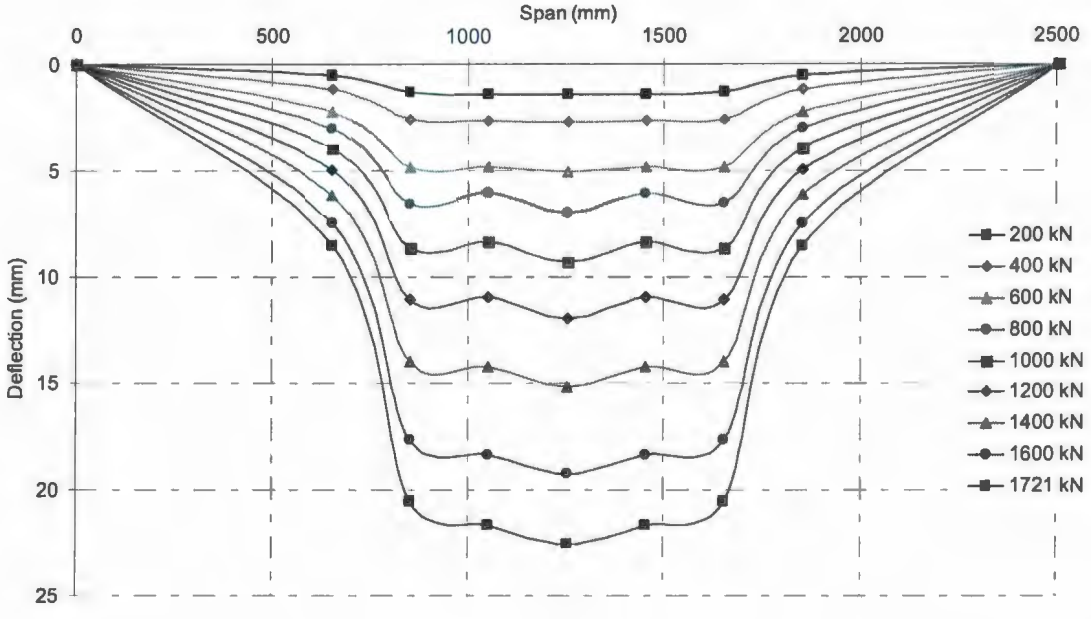
Span (mm)
0
500
1000
1500
2000
2500
Deflection (mm)
0
5
10
15
20
25
200 kN
400 kN
600 kN
800 kN
1000 kN
1200 kN
1400 kN
1600 kN
1721 kN

(*a*) HS4

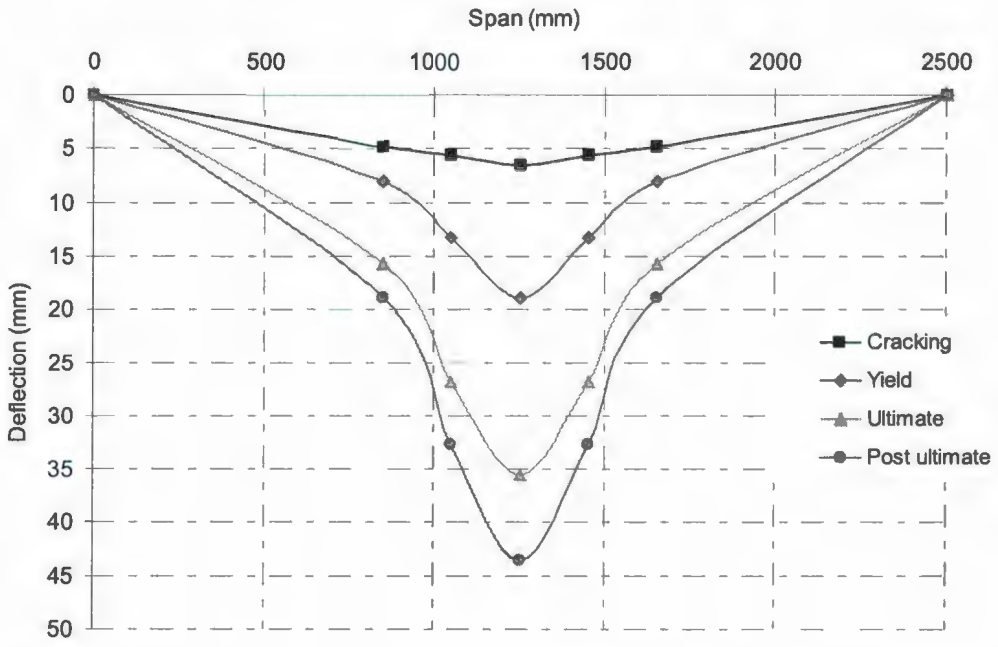
Span (mm)
0
500
1000
1500
2000
2500
Deflection (mm)
0
5
10
15
20
25
30
35
40
45
50
Cracking
Yield
Ultimate
Post ultimate

(*b*) HS5

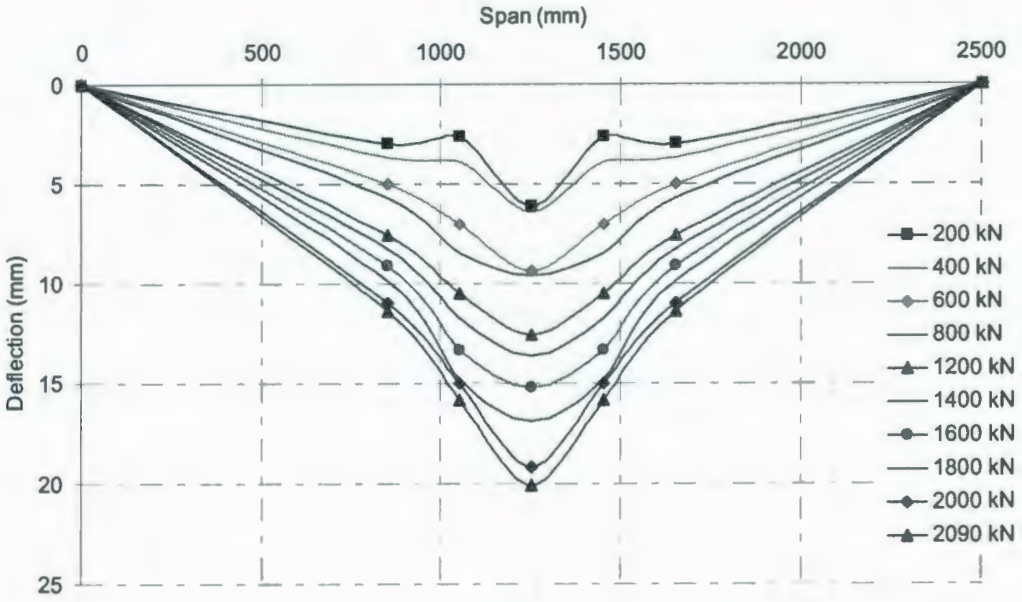

(*c*) HS6

Figure 5.2: Deflection profile for slabs: (*a*) HS4; (*b*) HS5; (*c*) HS6

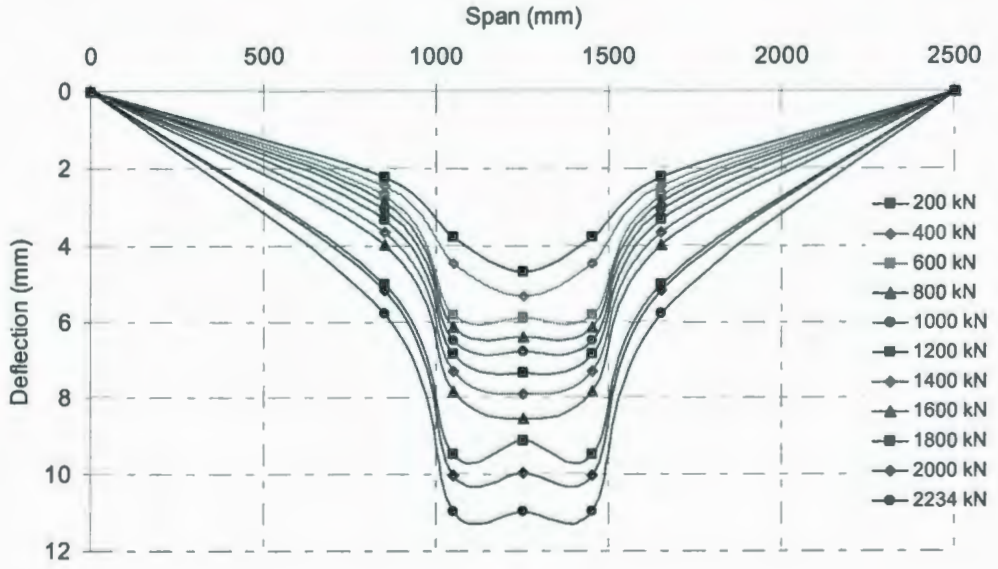

(*a*) NS5

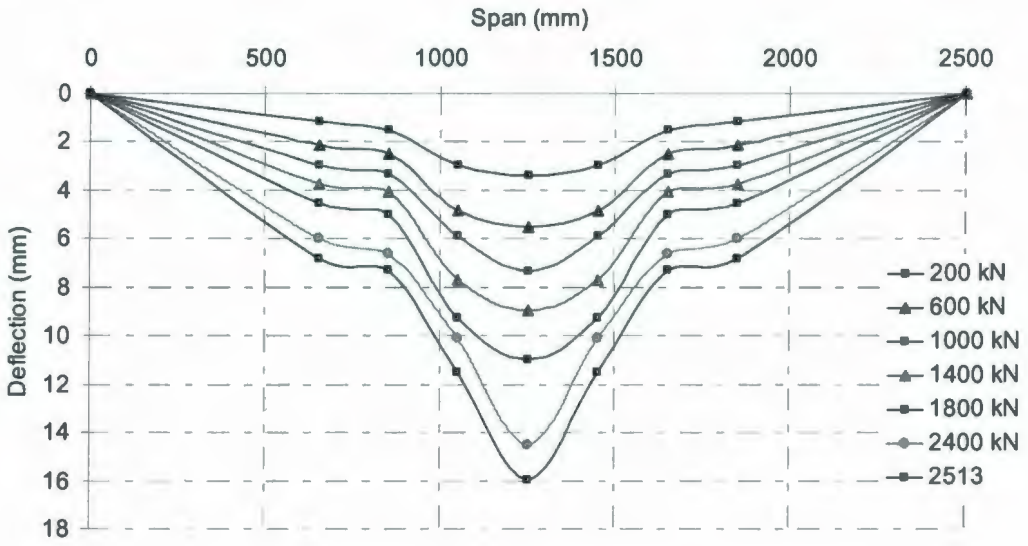

(*b*) HS7

Figure 5.3: Deflection profile for slabs: (*a*) NS5; (*b*) HS7

The deflection profiles for specimen HS4 and HS5 indicate that the zone of high deformation is extended over a large distance from the center of the slab beside there were more stages of loading between the yield loading point and the failure loading point. This is a clear indication that specimens HS4 and HS5 failed due to flexure unlike specimens HS6, NS5 and HS7 that failed due to local punching-shear at location of the application load.

5.5.3 Ductility and Energy Absorption Characteristics

Ductility is a term that reflects the deformation capacity of a structural member before failure. Ductility U is defined as the ratio of the ultimate deflection Δ_U to the deflection at first yield Δ_y. The energy-absorption capacity is defined as the area under the load-deflection curve. The ductility at failure and the energy-absorption capacity of all tested slabs, as defined above, are given in Table 5.3. Within a given series as the steel

reinforcement was increased, the ductility was decreased. For example, increasing the reinforcement ratio from 0.56 to 1.42% decreased the ductility by more than 50%. Test results revealed that as the depth of the slab increased, ductility was decreased. High strength slab HS6 was almost identical, in reinforcement ratio, to high-strength concrete slab HS7. Test results showed that the ductility and energy absorption capacity for slabs HS6 and HS7 were almost the same; this means that after a certain depth limit (d = 260 mm) increasing the effective depth resulted in increasing the punching capacity but at the same time did not result in significant increase in ductility and energy absorption. In addition, by increasing the slab effective depth, the structural behaviour became more brittle. This is known as the size effect.

The ductility of slab HS5 was almost the same as the ductility of slab HS7. At the same time, the energy absorption capacity of slab HS7 was about 80% of slab HS5. This reflected the enhanced structural behaviour of slab HS5 by using shear reinforcement; brittle structural behaviour of slab HS7 could be transformed to ductile structural behaviour by using shear reinforcement. Adding shear reinforcement would ensure utilizing the full benefit due to increasing the slab effective depth. The test results indicated that increasing the slab thickness from 350 mm to 400 mm resulted in increased punching capacity and at the same time resulted in only 25% increase in ductility characteristics. The possible explanation for the slight increase in ductility ratio for specimen HS7 compared to specimen HS6 is the increase in brittleness of specimen HS7 and this is due to size effect factor.

Flexural reinforcement alone cannot provide adequate ductility of slab-column connections especially when deformations are large, for example, during seismic events.

Adding shear reinforcement to the slabs at the column area can substantially increase the punching shear capacity and ductility, which was shown by several researchers (Dilger and Ghali 1981; Megally and Ghali 2000). To make sure that shear reinforcement significantly increase both the strength and the ductility of the connection, it is recommended that the flexural reinforcement ratio be more than or equal to 1% (Megally and Ghali 2000).

Table 5.3–Observed ductility and energy absorbtion

Slab No.	Concrete strength f_c', MPa	Slab Thickness, mm	Depth, mm	Steel ratio, ρ%	Ductility $\frac{\Delta_u}{\Delta_y}$	Energy absorption capacity, N.m $\times 10^3$
HS4	76	350	267.5	0.50	4.38	33.44
HS5	79	300	267.5	1.42	2.30	50.00
HS6	65	350	262.5	1.42	2.03	35.19
NS5	40	400	312.5	1.58	2.14	29.98
HS7	60	400	312.5	1.58	2.73	39.53

5.5.4 Concrete Strains

For all the tested slabs, measurements were made to determine the distribution of the concrete strain along a radius of the slab. Figures 5.4 to 5.8 show the load-versus-concret strain measured at different positions. Neither the concrete strains in the tangential or the radial directions reached a limiting value of 3000 με for any of the test slabs except for specimens HS5, which were reinforced with shear reinforcement, the concrete strain at a distance equal to 100 mm from the column edge reached almost 3000 με. The load-concrete strain curves for HS4, HS5, HS6 and HS7 were linear until the first cracking point.

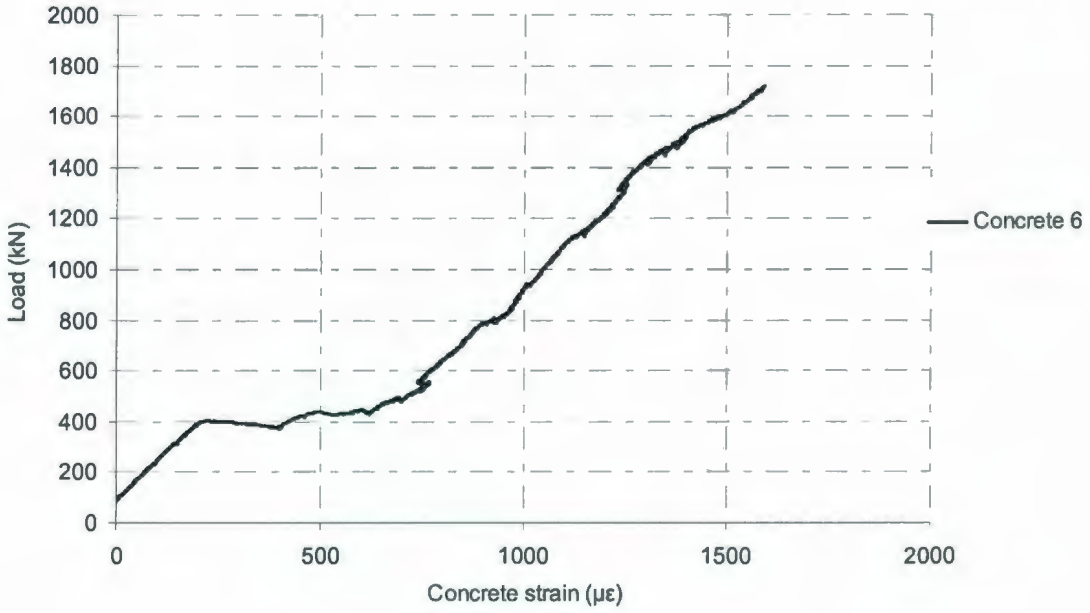

Figure 5.4: Load versus concrete strain for HS4

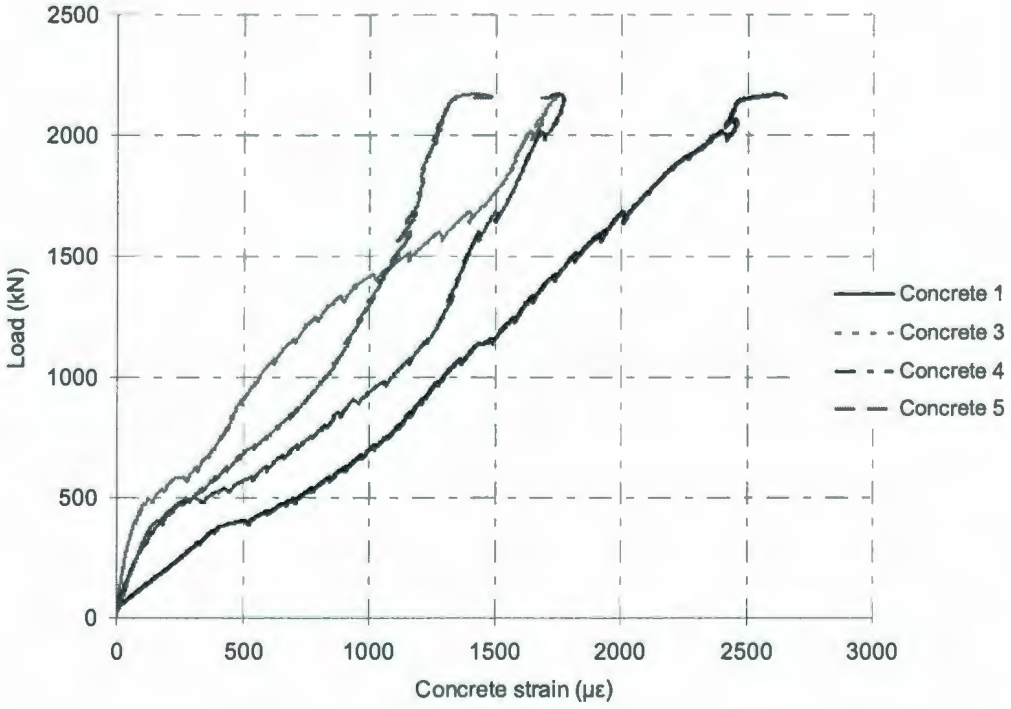

Figure 5.5: Load versus concrete strain for HS5

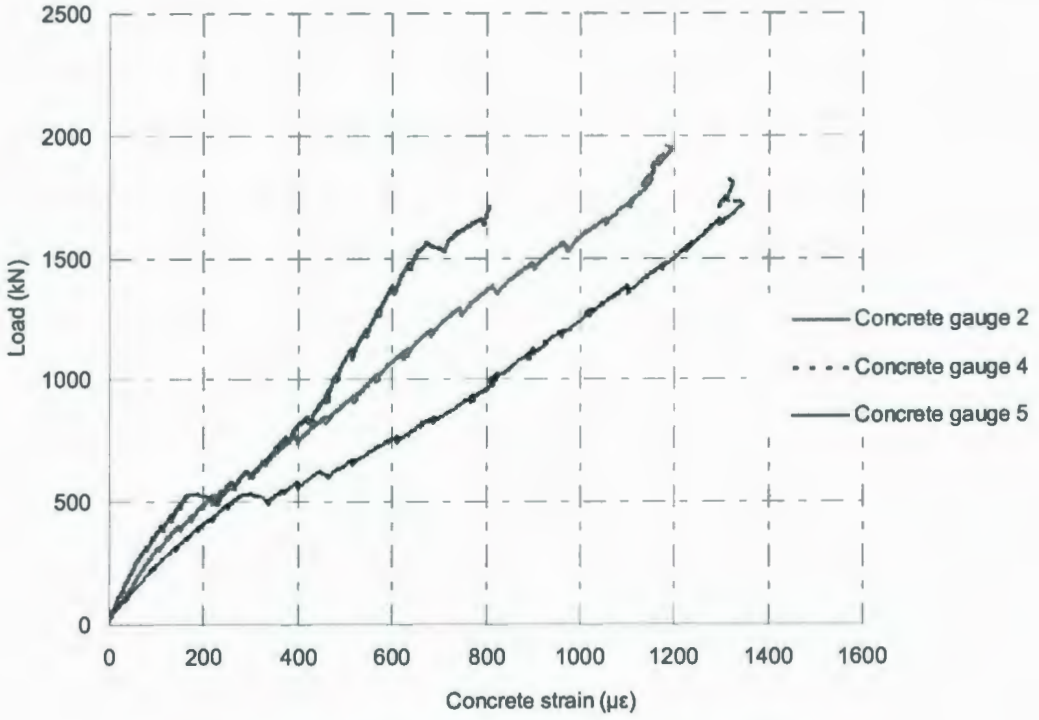

Figure 5.6: Load versus concrete strain for HS6

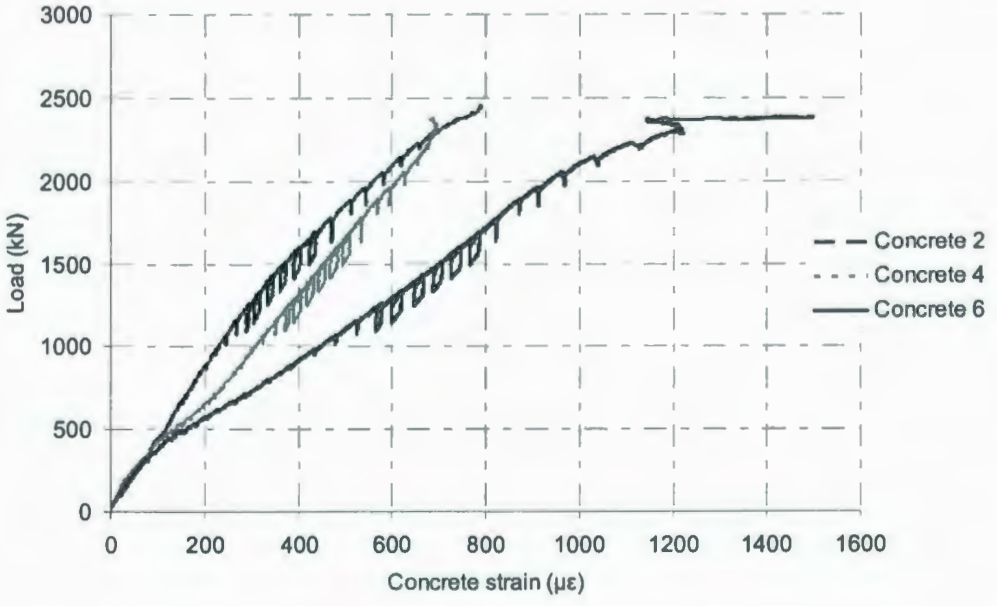

Figure 5.7: Load versus concrete strain for HS7

5.5.5 Steel Strains

Measurements were made to determine the strain distribution along a radius for all the tested slabs. Typical test results of these measurements are presented in Figures 5.8 to 5.10. For all test slabs, the tension reinforcement yielded before punching took place. The degree to which yielding spread in the tension steel varied as the reinforcement ratio changed. At high reinforcement levels, the yielding of the tension reinforcement occurred at higher applied loads and was localized at the column stub. For lightly reinforced slabs, HS4, yielding initiated at the column stub and gradually progressed throughout the whole tension reinforcement. The highest stain consequently initial yielding occurred below the stub-column. In all the tested slabs, the tension reinforcement yielded prior punching took place except HS5 that experienced ductile flexure failure. For slab HS5 that experienced flexure failure, the yielding load occurred at almost 50% of the flexure failure load. The existence of T-headed shear reinforcement converted the brittle failure mode into flexure failure mode with utilizing all the flexure reinforcement. For slabs HS6, NS5 and HS7 that experienced punching failure, the yielding load occurred at almost 75% to 85% of the failure load. In general, the slope of load-strain graph is very high for high-strength concrete slabs that failed in shear compared to normal-strength concrete and after a certain load level the slope gradually decreased. This could be attributed to the concrete contribution at the initial stage. In slab HS4, yielding initiated at the column stub and gradually progressed through the whole tension reinforcement. Moreover, specimen HS4 reached the state of steadily steel strain at a constant load that is a normal behavior for slabs failed in flexure. None of the T-headed shear studs reached yielding. Figure 5.10 indicates the load versus shear stud strain for slab HS5. It is obvious that the contribution

of shear reinforcement did not take place before the slab reached 60% of the ultimate load. The slope of load-strain graph for shear studs is very small and gradual.

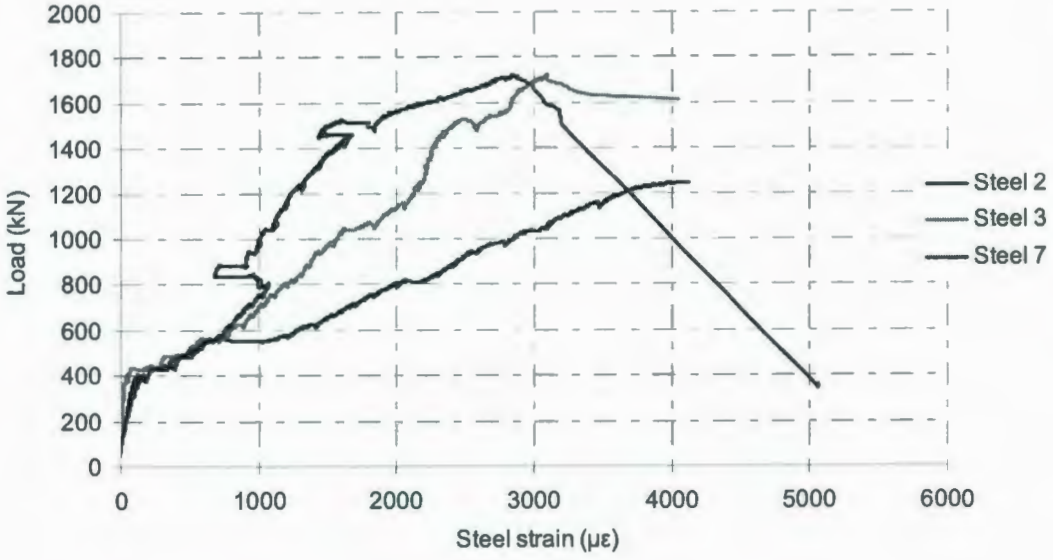

(*a*) HS4

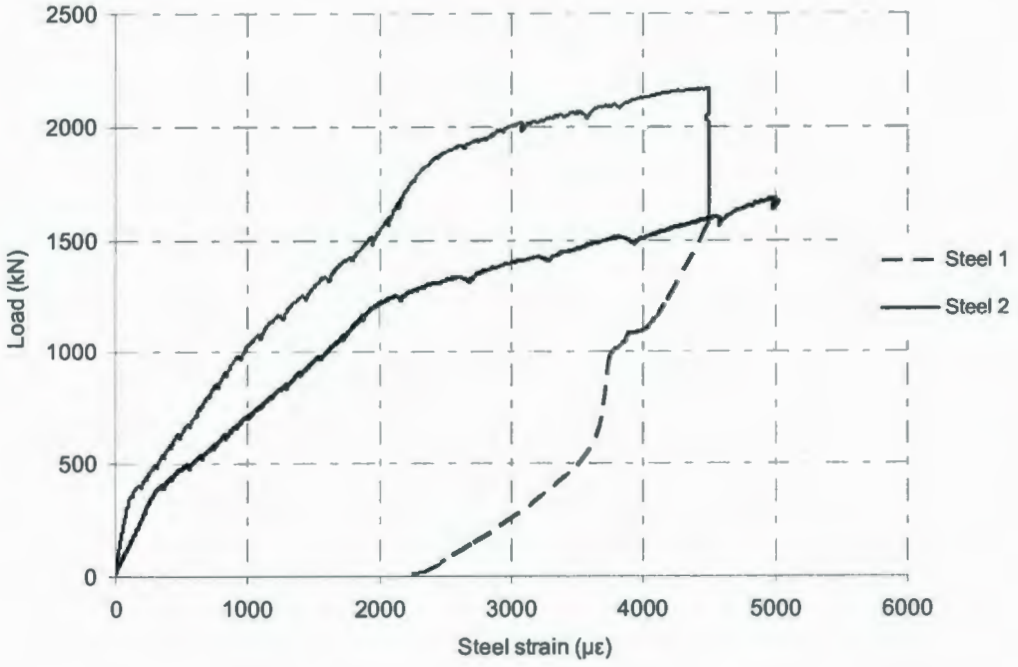

(*b*) HS5

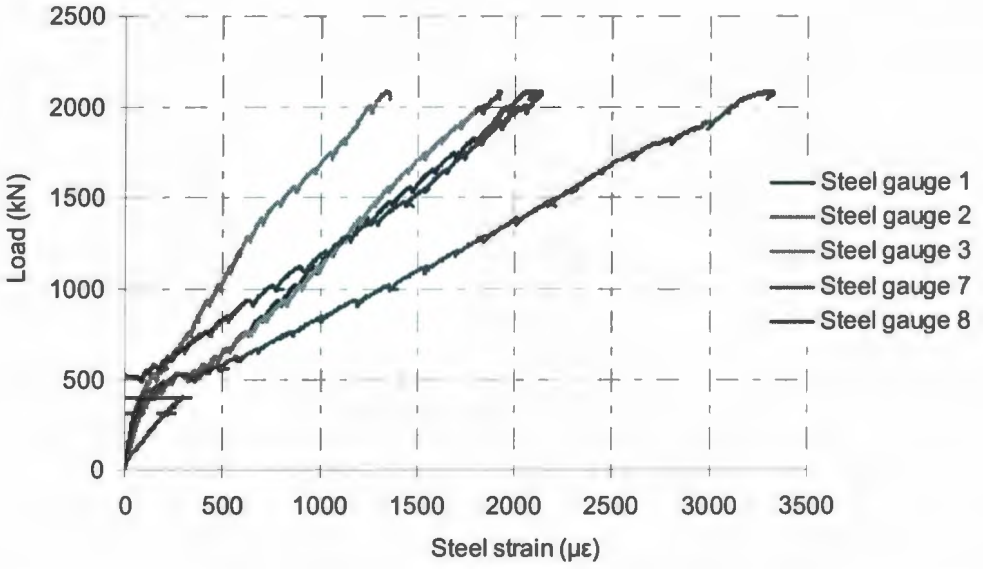

(*c*) HS6

Figure 5.8: Typical load-tension steel strain behavior at the column periphery for Series B1: (*a*) HS4; (*b*) HS5; (*c*) HS6

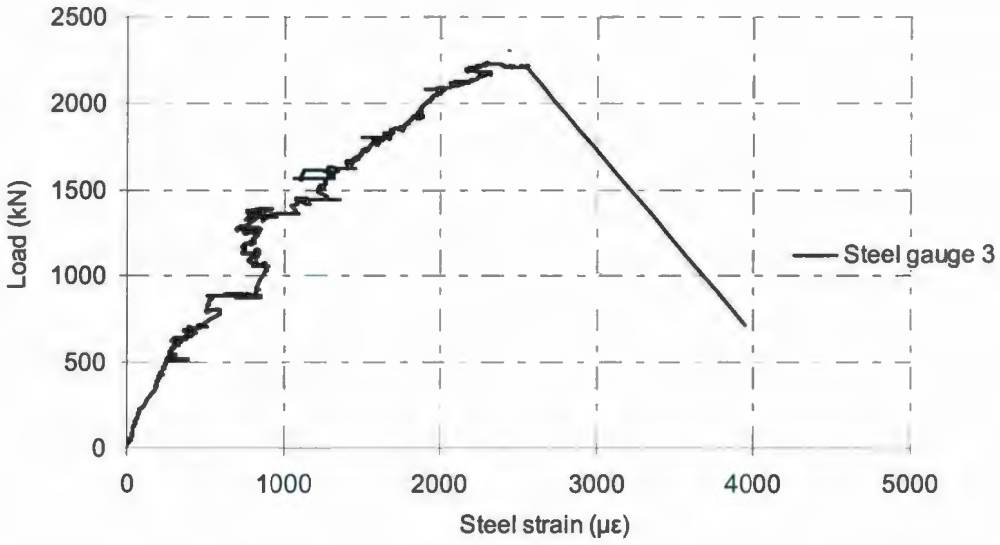

(*a*) NS5

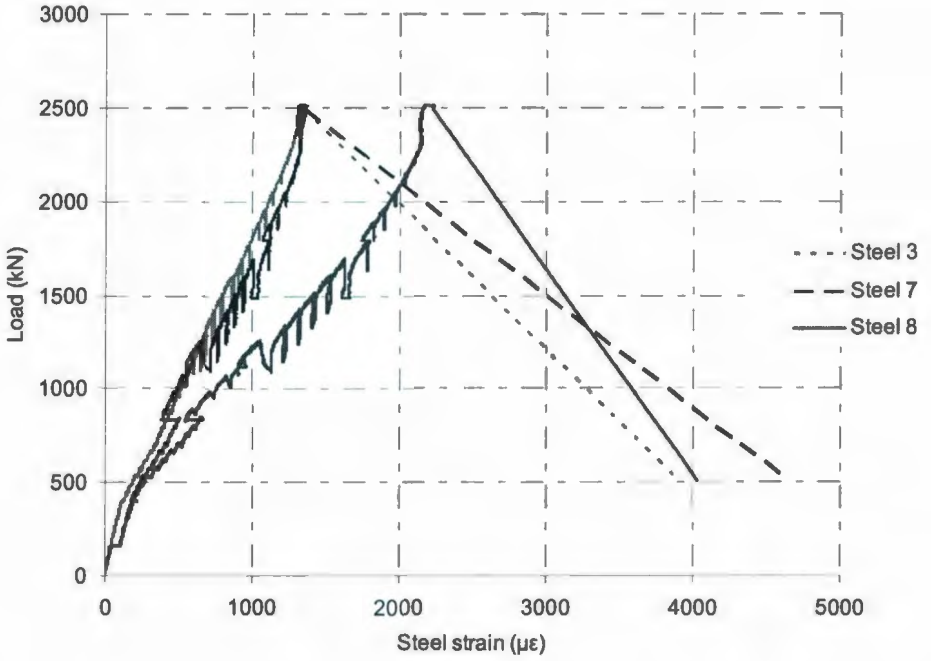

(*b*) HS7

Figure 5.9: Typical load-tension steel strain behavior at the column periphery for Series B2: (*a*) NS5; (*b*) HS7

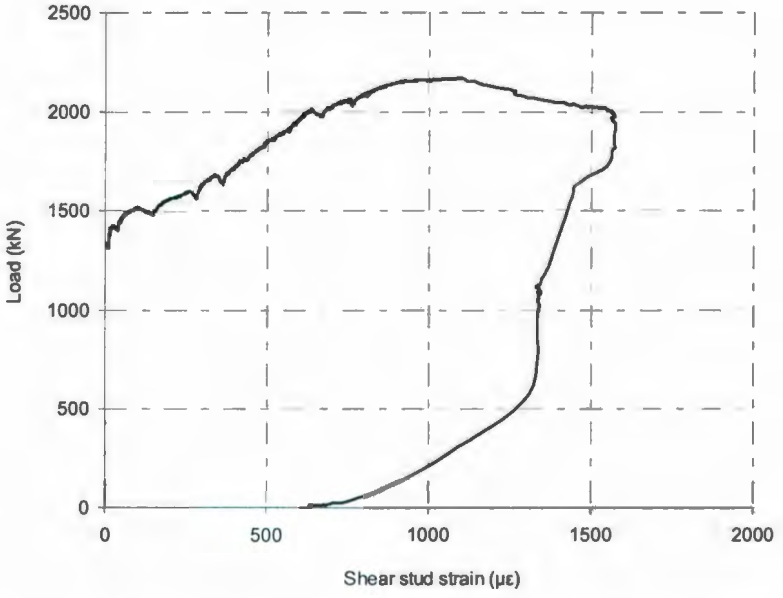

Figure 5.10: Load-shear stud steel strain behavior for slab HS5

5.6 Cracking and Failure Characteristics

The first crack of each specimen was visually inspected and the corresponding load was recorded at the first cracking load. The first cracking load values for all tested slabs are reported in Table 5.2. The first cracking load for slab NS5 is equal to 276 kN that is 12% of the maximum failure load while the first cracking load for slab HS7 is equal to 317 kN that is 13% of the maximum failure load. Both slabs NS5 and HS7 have the same reinforcement ratio and the same slab thickness. This means that increasing the concrete compressive strength from 40 MPa to 60 MPa (increasing the concrete compressive strength by 50%) resulted in increasing the first cracking load by about 15%. The first cracking load for slab HS6 is equal to 257 kN that is 12% of the maximum failure load while the first cracking load for slab HS4 is equal to 312 kN that is 18% of the maximum failure load. Both slabs HS4 and HS6 have the same slab thickness but different reinforcement ratio. This means that increasing the concrete compressive strength from 65 MPa to 79 MPa (increasing the concrete compressive strength by 20%) resulted in increasing the first cracking load by about 23%. For all test slabs, the first cracking load occurred at an average value of 14% of the maximum failure load. In all test slabs, the initial observed cracks were first initiated tangentially under the edge of the column stub, followed by radial cracking extending from the column edge toward the edge of the slab. For slab HS4 that failed in flexure, the crack pattern observed prior to punching consisted of one tangential crack, roughly at the column outline, followed by radial cracking extending from the column. Flexure yield lines were well developed. For slabs failing by punching, the crack pattern observed prior to punching consisted of almost no tangential

crack, orthogonal cracking extending from the column were the most dominant crack pattern.

5.6.1 Crack Spacing

Numerous cracks developed on the tension face of slab at the time of failure. Photographs of all test slabs with crack marks are shown in Figures 5.11 to 5.12. For all the specimens, the first crack formed along the rebar passes through the slab center or close to the slab center. The second crack formed along the similar rebar in other direction. Crack Displacement Transducers (CDT) were mounted on the concrete surface of the first, second and third visible cracks in order to measure opening displacement. The corresponding load of each crack was recorded accurately. The cracks formed in this stage had no effect on the characteristics of the crack pattern and primarily depend on the concrete strength.

In the current test program, two parameters; namely, the concrete cover and bar spacing were examined separately to investigate their effect on crack spacing and crack width. All the reinforced concrete slabs in Series B2 exhibited an orthogonal crack pattern that formed along the direction of the reinforcement. The orthogonal cracks are function of the bar spacing as it was noticed for slabs HS6, NS5 and HS7. Once the bar spacing was increased, the average orthogonal crack spacing increased. For slabs HS4 and HS7, the average crack spacing was less than the bar spacing (Table 5.4). In HS5, the crack pattern was radial that is a normal behavior of a slab exhibits a large deflection. Most of the slabs that failed in punching exhibited a big punching radius at the tension face of the slab.

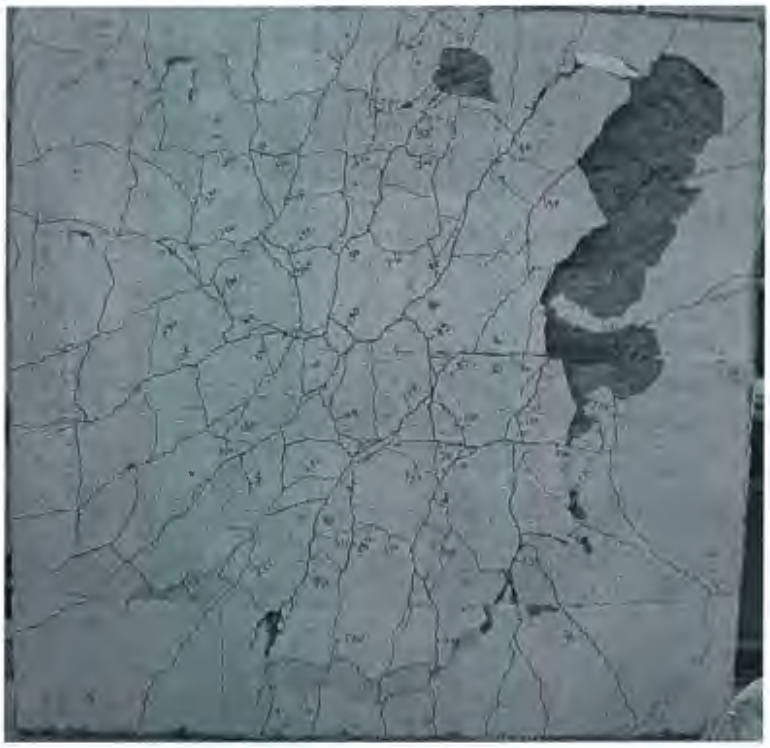

(*a*) HS4

(*b*) HS5

(*c*) HS6

Figure 5.11: Crack patterns of Series B1: (*a*) HS4; (*b*) HS5; (*c*) HS6

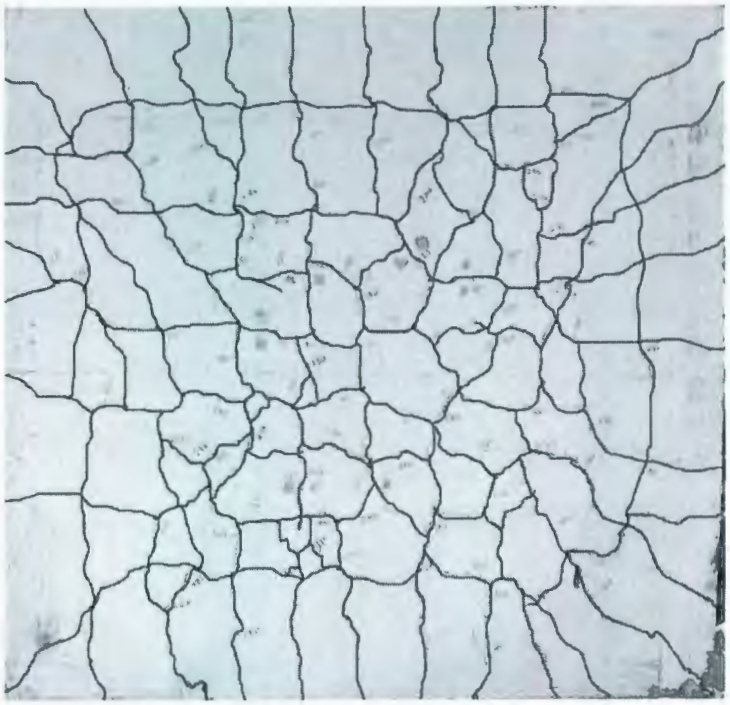

(*a*) NS5

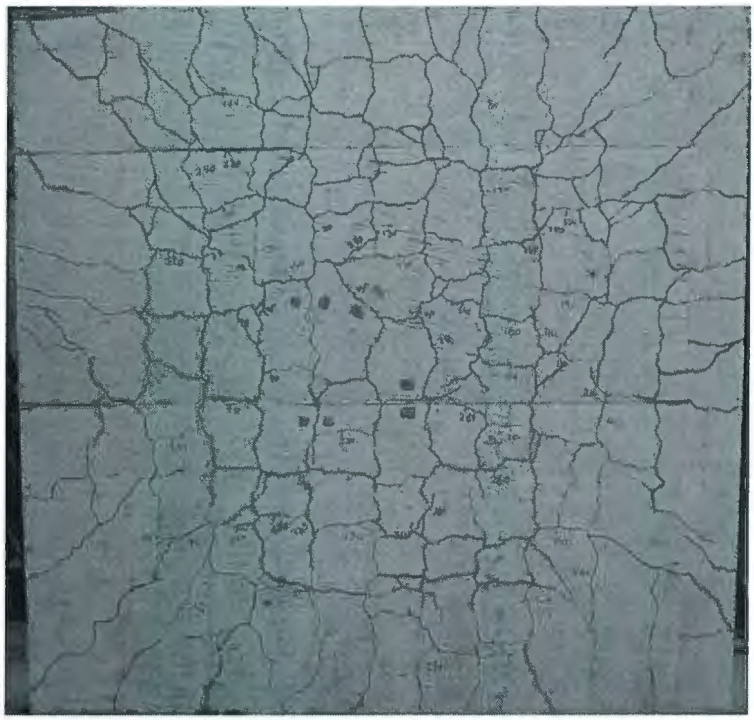

(*b*) HS7

Figure 5.12: Crack patterns of Series B2: (*a*) NS5; (*b*) HS7

5.6.2 Crack Width

The crack width was measured at each load stage. In Figure 5.13 through 5.17, the opening of the crack width is plotted versus the steel strain. The crack width increased as the applied load was increased. However, this increase was not very smooth as concrete is not a homogenous material. It was noticed that the crack width versus steel strain can be represented by one straight line up to value approximately equal to 2000 με except for slab HS4. This value of strain produced a stress in the steel bars equal to 400 MPa. In most of the slabs, the crack width versus steel strain curve tends to behave nonlinearly after the steel strain reached the yield point. In slab HS4, the crack width continues to increase after the steel strain reached the yield point that is an expected behavior for a

slab that failed in flexure. All measurements reported in Table 5.4 are taken at a steel stress level of 267 MPa (0.67 f_y). The data of test results shows that the maximum crack width can be influenced by as much as 50% when the bar spacing increased from 217 mm to 368 mm, this means that for the same concrete cover increasing the bar spacing by about 70% results in increasing the crack width by about 50%.

Series B2 included two specimens (NS5 and HS7) reinforced with a heavy steel reinforcement ratio 1.58 %, all specimens had the same bar spacing 217 mm. Test results revealed that crack control (crack width) can still be achieved by limiting the spacing of the reinforcing steel despite using thick concrete cover. At sections between successive cracks, some tensile stress is retained in the concrete around steel bars due to the action of bond, contributing to the bending stiffness of the member and this is reflected by a reduction in tensile strain in the reinforcement. This is called the "tension-stiffening" effect. The crack width can be calculated by multiplying the crack spacing by the average steel strain after reducing the crack width due to tension-stiffening. The steel strain can be determined at any loading by determining the neutral axis and assuming linear strain distribution.

Table 5.4–Measured crack spacing and crack width

Slab No.	Concrete cover, C_c, mm	Slab thickness, h, mm	Bar spacing s, mm	f_c', MPa	Average crack spacing, S_m, mm	Maximum crack width, w_k, mm
HSS1	70	350	368	76	221	0.581
HSS2	70	300	217	79	228	0.876
HSS3	70	350	289	65	264	0.435
NSS1	70	400	217	40	250	0.439
HSS4	70	400	217	60	210	0.469

*NS-Normal strength slabs; HS-High strength slabs

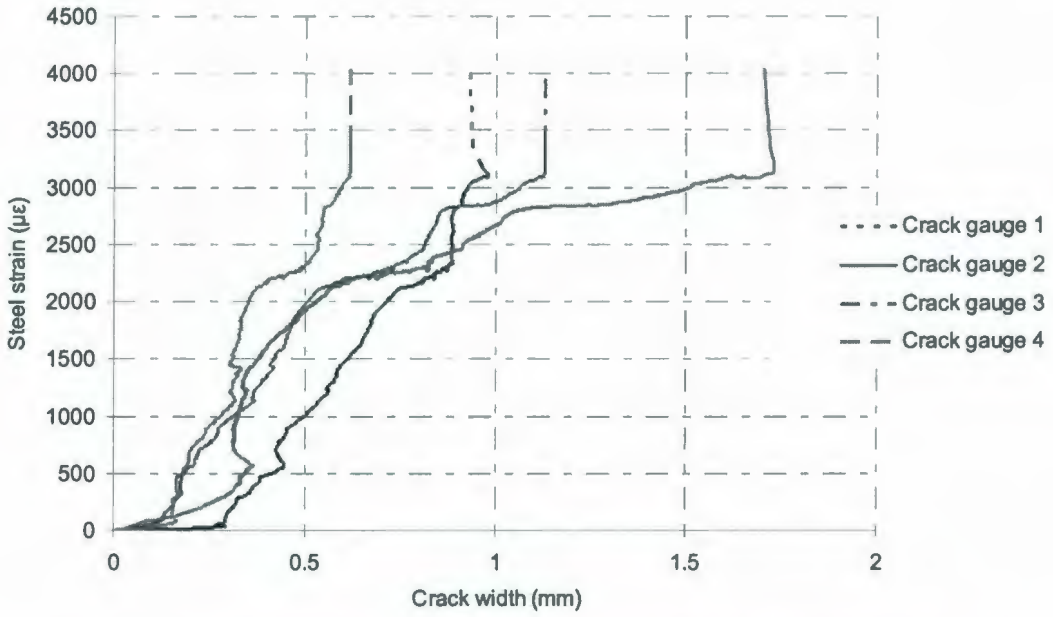

Figure 5.13: Crack width expansion versus steel strain for HS4 (h = 350 mm)

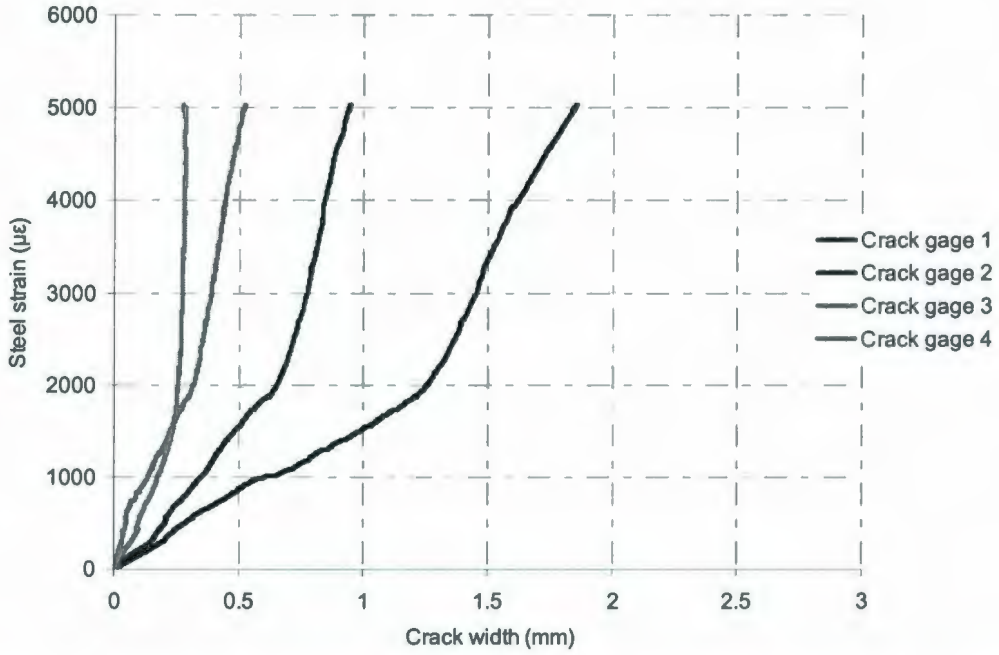

Figure 5.14: Crack width expansion versus steel strain for HS5 reinforced with T-headed shear reinforcement (h = 300 mm)

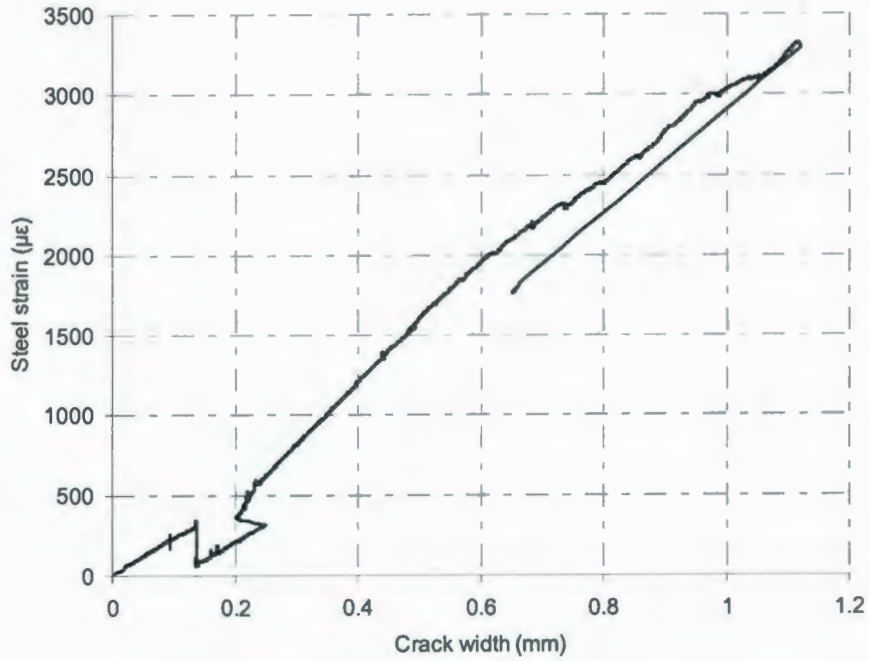

Figure 5.15: Crack width expansion versus steel strain for HS6 (h = 350 mm)

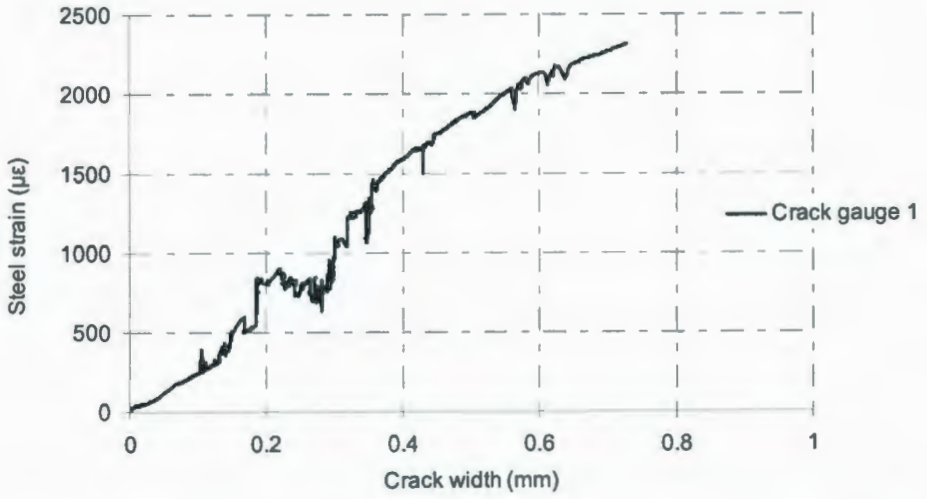

Figure 5.16: Crack width expansion versus steel strain for NS5 (h = 400 mm)

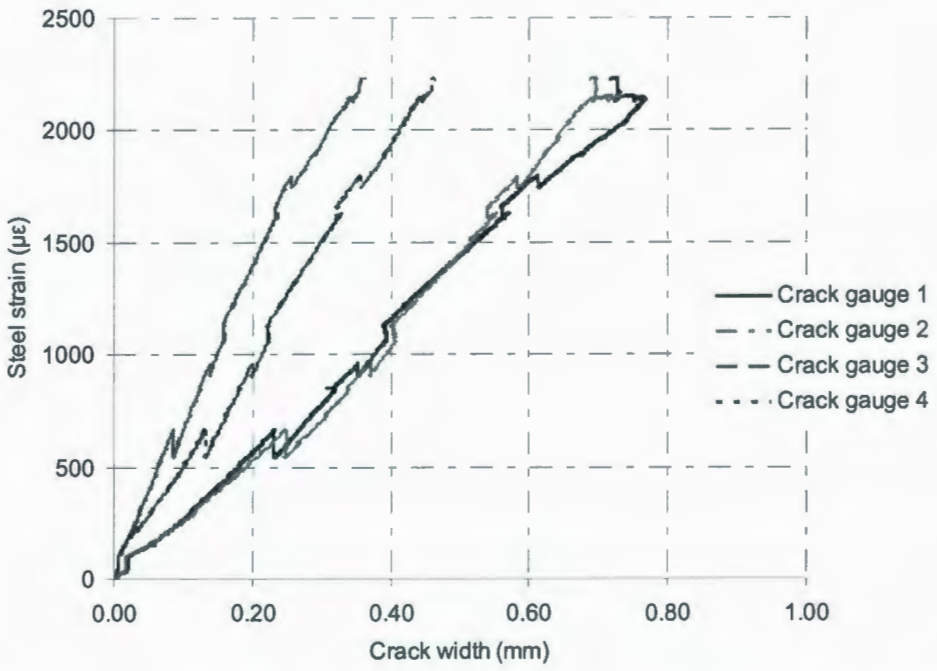

Figure 5.17: Crack width expansion versus steel strain for HS7 (h = 400 mm)

5.7 Modes of Failure

All the test specimens except HS4 and HS5 failed in punching. Slab HS5 showed a ductile punching failure; with the slab failing before the flexure strength was exceeded. While, slab HS4 failed in flexure. The test slab HS4 had a reinforcement ratio (ρ = 0.56%) and was designed to fail in flexure. Test results indicate that slab HS4 utilized full flexural capacity while slab HS5 utilized 100% of its flexural capacity. Both the load-deflection curve and the strain distribution indicated that slab HS5 exhibited a gradual and ductile punching failure. Failure patterns of the tested slabs are shown in Figures 5.11 to 5.12. Slabs NS5 and HS7 failed in punching these slabs utilized only 50% of its flexural capacity.

5.8 Effectiveness of Shear Reinforcement

The shear reinforcement has little effect before the occurrence of the inclined shear cracks inside the slab. However, after the development of the inclined shear cracks, shear

reinforcement transfers much of the forces across the shear crack and delays the further widening of the shear crack, thus increasing the punching shear capacity and ductility of the slab. To achieve this, the reinforcement needs to be well anchored and have enough ductility to allow the mobilization of many legs of the reinforcement. In the case of specimen HS5 with T-headed shear reinforcement, none of the shear studs were intersected by inclined shear cracks. The existence of T-headed shear reinforcement forced the shear crack to develop outside the shear reinforcement zone, resulting in increasing the punching perimeter, and this resulted in increasing the ultimate load capacity. But at the same time the existence of T-headed shear reinforcement did not result in increasing the ductility of specimen HS5, since the shear studs were not intersected by inclined shear cracks. A possible reason for the low ductility for specimen HS5 is the wide (large) coverage area of T-headed shear stud reinforcement, the coverage zone extended to more than $2d$ from the column face as shown in Figure 3.4, and this did not give the chance for flexure reinforcement to be fully mobilized after occurrence of shear crack. As a result, the failure mode was less ductile as indicated by the load-deflection curve (Figure 5.1a). Structural behavior of specimen HS5 could be enhanced by either increasing the flexure reinforcement development length or decreasing the shear reinforcement ratio to force the shear crack to develop inside the shear reinforcement zone.

5.8 Summary

- This chapter presents a unique experimental work. Five full-scale, normal and high-strength concrete thick plate-column connections tested under concentric punching loading. The test specimens had different plate thicknesses. Four

specimens had no shear reinforcement, whereas the remaining one included T-headed shear reinforcement consisting of vertical bars mechanically anchored at top and bottom by welded anchor plates.

- Increasing the effective depth more than a certain depth limit (d = 260 mm) resulted in increased punching capacity and at the same time resulted in only 25 % increase in ductility characteristics. This means that by increasing the slab depth, the structural behaviour becomes more brittle, this is known as the size effect as proposed by fracture mechanics concepts. Hence shear reinforcement requirements should be provided by design codes of practice for slabs having effective depth more than or equal to 260 mm.
- The enhanced structural behavior of slab HS5 reflects the benefit of using shear reinforcement, structural behaviour for slab HS7 could be enhanced by adding shear reinforcement, adding shear reinforcement will ensure utilizing full benefit due to increasing slab effective depth. Test results revealed wasted ductility and energy absorption despite increasing the effective depth; the wasted ductility characteristics could be fully utilized by adding shear reinforcement.
- The inclusion of T-headed shear reinforcement improved the ultimate loading capacity. Provision of shear enhancement also provided a post-ultimate behaviour when the ultimate loading capacity was reached, and eliminated the so-called punching shear failure.
- For all tested slabs, the first cracking load occurred at an average value of 14% of the maximum failure load.

- The data of group B showed that the maximum crack width can be influenced by as much as 50% when the bar spacing is increased from 217 mm to 368 mm, this means that for the same concrete cover increasing the bar spacing by about 70% results in increasing the crack width by about 50%.
- Test results of group B revealed that crack control can still be achieved by limiting the spacing of the reinforcing steel despite using thick concrete cover.

Chapter 6

Minimum Flexural Reinforcement for Thick HSC Plates

6.1 Introduction

The amount of reinforcement that is required for crack control is not easily determined. Since the formation of cracks is a complex behaviour, the present minimum reinforcement guidelines are empirical and do not normally considers the effect of member effective depth (size effect). An accurate estimate of the minimum flexural steel reinforcement ratio can result in saving millions of dollars for a single project (e.g. Hibernia oil platform). In this chapter, a new model is developed to calculate minimum flexure reinforcement for thick plates and two-way slabs. The main contributions of this research investigation are accounting for the torsional moment and the size effect factor in estimating the minimum reinforcement of concrete plates.

6.2 Slab Size Effect

For design engineers, the size effect is a useful concept that is based on fracture mechanics. The size of the fracture process zone is represented by a material property called the characteristic length, l_{ch}. It expresses the fracture properties of the concrete, such as the modulus of elasticity, E_c, the fracture energy, G_f and the tensile strength, f_{ct}, where f_{ct} is the direct tensile strength of concrete.

$$l_{ch} = \frac{E_c G_f}{f_{ct}^2} \tag{6.1}$$

G_f is defined as the amount of energy required to cause one unit area of a crack, it can be obtained as the area under the "load-crack width curve." However, the characteristic length has no physical correspondence, i.e., it is not a real length that can be measured. A

higher value of l_{ch} reflects that the material is less brittle and a smaller value means that the material is more brittle. In an earlier investigation by Marzouk and Chen (1995), the fracture energy, G_f, was determined experimentally for high-strength concrete to be 160 N/m compared to 110 N/m for normal strength concrete. These values have been estimated according to the results of the direct tension test. The fracture energy is calculated as the area under the descending portion of the stress-crack width curve. The characteristic length, l_{ch} was estimated to have an average value of 500 mm and 250 mm for normal and high-strength concrete, respectively. In this research, the term $(l_{ch}/h)^{0.33}$ was chosen to account for the size effect. The exponent $\alpha = 0.33$ represents a sensitivity number, it was found by Marzouk et al. (1998) that a value of 0.25 may be taken for concrete strength less than 35 MPa, and a value of 0.33 may be taken for concrete strength of 75 MPa. For concrete strength between 35 and 75 MPa, a linear interpolation may be taken between the values of 0.25 and 0.33. For concrete strength higher than 75 MPa, α may be considered to be higher than 0.33 but without exceeding the limit of 0.5. In the present research, a value of 0.33 was found to be more consistent. A similar expression was developed in Germany on punching shear capacity of point supported, reinforced concrete normal and high strength slabs by Staller (2000).

6.3 Analytical Investigation

An elastic solution is not suitable for reinforced concrete structure after cracking, before the onset of cracking the behavior of reinforced concrete can be based on elastic solutions or based on the study of plain concrete because the contribution of reinforcement at this stage is negligible. In evaluating minimum reinforcement ratio, it is important to guarantee that if the cracking moment M_{cr} is reached due to eventual overloading, the

forces resisted by concrete in tension are transmitted to tensile longitudinal steel capable of resisting M_{cr}. Calculation of cracking moments is usually based on the behavior of uncracked concrete sections (stage I), so using elastic solutions to compute cracking moment M_{cr} is acceptable.

6.3.1 Effect of Torsional Moment on Minimum Reinforcement of Thick Plates

An approximate solution for a rectangular plate problem subjected to uniform loading has been presented by many authors. This problem requires the solution of the deferential equation:

$$\frac{\partial^4 w}{\partial x^4} + 2\frac{\partial^4 w}{\partial x^2 \partial y^2} + \frac{\partial^4 w}{\partial y^4} = \frac{q(x,y)}{D} \tag{6.2}$$

subject to the boundary conditions

$$w = 0 \quad \frac{\partial w}{\partial x} = 0 \quad (x = -a, x = a) \tag{6.3a}$$

$$w = 0 \quad \frac{\partial w}{\partial y} = 0 \quad (y = -b, y = b) \tag{6.3b}$$

The moment components are related to the deflection w as follows:

$$M_x = -D\left(\frac{\partial^2 w}{\partial x^2} + \nu\frac{\partial^2 w}{\partial y^2}\right) \tag{6.4}$$

$$M_y = -D\left(\frac{\partial^2 w}{\partial y^2} + \nu\frac{\partial^2 w}{\partial x^2}\right) \tag{6.5}$$

$$M_{xy} = -D(1-\nu)\frac{\partial^2 w}{\partial x \partial y} \tag{6.6}$$

where D is the bending rigidity of the plate defined as:

$$D = \frac{E h^3}{12(1-\nu^2)} \tag{6.7}$$

with E as the modulus of elasticity, ν as orthotropic Poisson's ratio and h as the plate thickness. The problem of a rectangular plate clamped at four sides with a uniform load is considered. The sides of the rectangular section are at $x = \pm a$, and $y = \pm b$. It is supposed throughout the paper that $a \geq b$. Several approaches (Timoshenko and Woinowsky-Krieger 1959) exist to approximately solve the biharmonic problem governing the plate's deflection w in a convenient manner for direct use in engineering applications. In all of them, the boundary conditions are satisfied identically.

The most common way of solving equations (6.4), (6.5) and (6.6) is to use a finite element analysis. Such an analysis gives values of M_x, M_y, and M_{xy} in each element where M_x, M_y, and M_{xy} are moments per unit width. A portion of an element bounded by a diagonal crack is shown in Figure 6.1. The moments on the x and y faces from the finite element analysis are shown in Figure 6.1b. The moment about an axis parallel to the crack is M_c given by

$$M_c\, ds = \left(M_x\, dy + M_{xy}\, k\, dy\right)\cos\theta + \left(M_y\, k\, dy + M_{xy}\, dy\right)\sin\theta \tag{6.8a}$$

or

$$M_c = \left(\frac{dy}{ds}\right)^2 \left(M_x + k^2\, M_y + 2k\, M_{xy}\right) \tag{6.8b}$$

This slab is to be reinforced with bars in the x and y direction with positive moment capacities M_{rx} and M_{ry} per unit width. The corresponding moment capacity at the assumed crack is

$$M_{rc} = \left(\frac{dy}{ds}\right)^2 \left(M_{rx} + k^2\, M_{ry}\right) \tag{6.9}$$

where M_{rc} must equal or exceed M_c to provide adequate strength. Equating Equation (6.8b) and (6.9), and solving for minimum we get

$$M_{ry} = M_y + \frac{1}{k} M_{xy} \tag{6.10}$$

Since M_{ry} must equal or exceed M_y to account for the effects of M_{xy}, $(1/k)M_{xy} \geq 0$, which gives

$$M_{ry} = M_y + \frac{1}{k}\left|M_{xy}\right| \tag{6.11a}$$

$$M_{rx} = M_x + k\left|M_{xy}\right| \tag{6.11b}$$

where k is a positive number. This must be true for all crack orientations (i.e., for all values of k). As k is increased, M_{ry} goes down and M_{rx} goes up. The smallest sum of the two (i.e., the smallest total reinforcement) depends on the slab in question, but $k = 1$ is the best choice for a wide range of moment values (Hillerborg 1975 and Randal et al. 1968). The reinforcement at the bottom of the slab in each direction is designed to provide positive moment resistances of

$$M_{ry} = M_y + \left|M_{xy}\right| \tag{6.12a}$$

$$M_{rx} = M_x + \left|M_{xy}\right| \tag{6.12b}$$

If either of these two bottom reinforcements is negative, it is set equal to zero. Similarly, the steel at the top of the slab is designed to provide negative moment resistances of

$$M_{ry} = M_y - \left|M_{xy}\right| \tag{6.13a}$$

$$M_{rx} = M_x - \left|M_{xy}\right| \tag{6.13b}$$

In this chapter, a simply supported uniformly loaded rectangular clamped plates with different aspect ratios, a/b = 1, a/b =1.5, a/b =2 and a/b =2.5, were solved using the structural analysis program (SAP) to evaluate the value of the bending moments M_x; M_y and the torsional moment M_{xy} within the plate. The value of the torsional moment M_{xy} is

added to the value of the bending moment M_x at each point and compared with the maximum positive bending moment $M_{x,\max+ve}$. It is found that for simply supported square plates or clamped square plates, the ratio is:

$$\frac{M_x + |M_{xy}|}{M_{x,\max+ve}} \leq 1.0 \tag{6.14}$$

However, for a clamped rectangular plate with an aspect ratio a/b=1.5, the same ratio is found equal to 1.04; for a/b =2.0, the same ratio is found equal to 1.27 and finally, for a/b =2.5, the same ratio is found equal to 1.13. The difference between the normalized calculated torsional moment vs. the aspect ratio for different clamped rectangular plates is shown graphically in Figure 6.2 as $\left(M_x + |M_{xy}|\right)/M_{x,\max+ve}$ vs. a/b. in the case of square clamped plates, the location of the maximum bending moment is at the center of the plate, while for rectangular clamped plates with an aspect ratio $a/b \geq 1.0$, the location of maximum positive bending moment $M_{x,\max+ve}$ is shifted from the center of the plate, this means that there are two points of maximum positive moment instead of one point at the center of the plate. For an aspect ratio a/b = 2.0, the location of the points of maximum positive moment is almost at the quarter points of the plate in the long direction. The drop in the moment ratio for the aspect ratio a/b of 2.5, is due to the fact that the load tends to be transferred in the short direction (one-way action) instead of two-way action, this minimizes the effect of torsional moment.

Based on the previous findings, it can be concluded that neglecting the effect of the torsional moment M_{xy} in calculating the minimum reinforcement ratio for clamped rectangular plates with an aspect ratio a/b = 2.0 results in about a 25% error. Therefore,

using an empirical code formula in calculating the minimum reinforcement ratio for clamped rectangular plates with an aspect ratio $a/b > 1.0$ is unsafe.

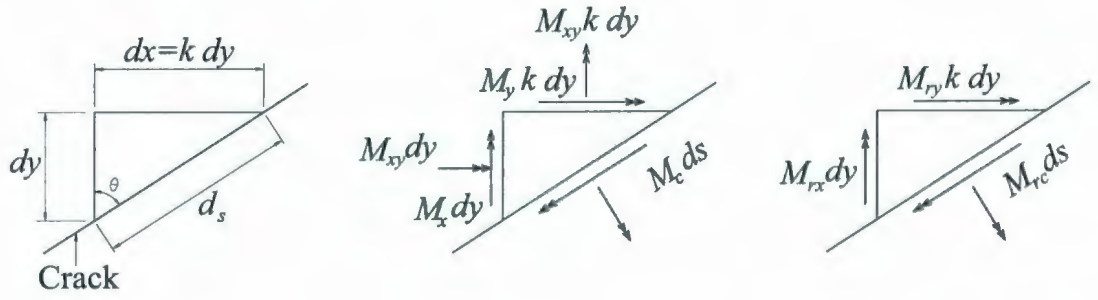

(*a*) (*b*) (*c*)

Figure 6.1: Resolution of moments

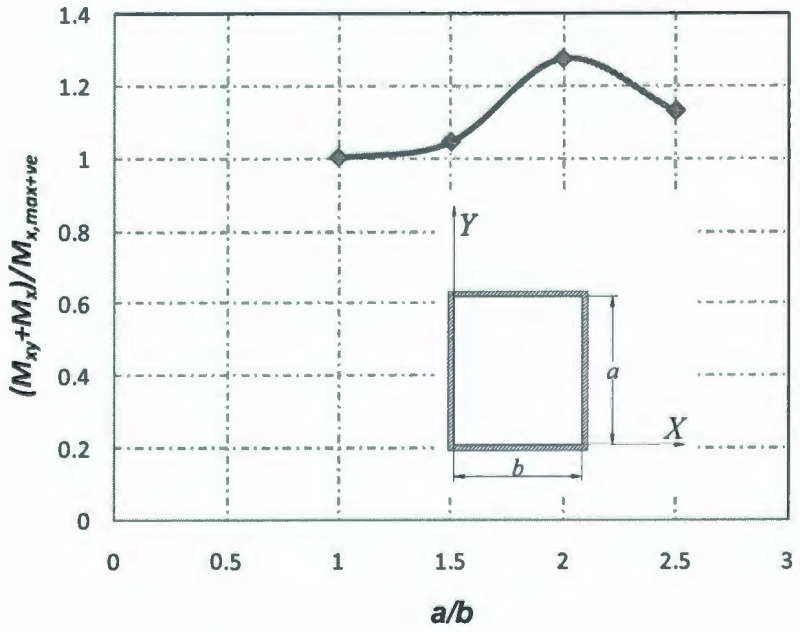

Figure 6.2: Normalized torsional moment vs. aspect ratio ($\left(\left(M_x+\left|M_{xy}\right|\right)\right)/M_{x,\max+ve}$ vs. *a*/*b*) for clamped rectangular plates

6.3.2 Marti's Shear Sandwich Model (1990)

Generally, slab elements are subjected to eight stress resultants, i.e., the three membrane force components N_x, N_y, and $N_{xy} = N_{yx}$, two transverse shear force components V_x, and V_y, two flexural moments M_x and M_y, and torsional moment $M_{xy} = M_{yx}$ (see Figure 6.3*a*). Marti (1990) introduced a sandwich model where the covers are assumed to carry moments and membrane forces, while the transverse shear forces are assigned to the core (see Figure 6.3*b*). As a simple approximation, Marti (1990) assumed that the middle planes of the cover elements coincide with the middle planes of the reinforcing meshes close to the slab surfaces. Assuming equal cover element thicknesses at top and bottom c, the lever arm of the in-plane forces in the cover elements d_v, equal to the effective shear depth of the core, equal to the distance from the center of the top concrete cover element to the center of the bottom concrete cover element, is given by $d_v = h\text{-}c$, where h = slab thickness. For the dimensioning of the in-plane reinforcement, the well-known limit-design method for reinforced concrete membrane elements can be employed.

Accordingly, the necessary resistances of the reinforcements in the two orthogonal directions x and y are equal to $N_x + k\,[N_{xy}]$ and $N_y + [N_{xy}]/k$, respectively, where k denotes an arbitrary positive factor and N_x, N_y, and N_{xy}, are the applied membrane force components. Hence, from Figure 6.3, we obtain the requirements

$$a_x f_y \geq \frac{M_x}{d_v} + \frac{N_x}{2} + \frac{V_x^2}{2V_o \tan\theta} + k\left[\frac{M_{xy}}{d_v} + \frac{N_{xy}}{2} + \frac{V_x V_y}{2V_o \tan\theta}\right] \tag{6.15}$$

and

$$a_y f_y \geq \frac{M_y}{d_v} + \frac{N_y}{2} + \frac{V_y^2}{2V_o \tan\theta} + \frac{1}{k}\left[\frac{M_{xy}}{d_v} + \frac{N_{xy}}{2} + \frac{V_x V_y}{2V_o \tan\theta}\right] \quad (6.16)$$

where a_x and a_y denote the cross-sectional areas of the orthogonal bottom reinforcements per unit width of the slab, and V_o is the principal diagonal shearing force carried by the core.

6.3.2.1 Uncracked Core

Provided that the nominal shear stress due to the principal shear force, v_o/d_v, does not exceed the limit of $0.17\sqrt{f_c'}$ (MPa) ($2\sqrt{f_c'}$ (psi)), one may assume that there are no diagonal cracks in the core. In this case, a state of pure shear develops within the core as shown in Figure 6.3*c*, and the transverse shear force at a section has no effect on the in-plane forces in the sandwich covers. Thus, no transverse reinforcement has to be provided, and the in-plane reinforcement must not be strengthened to account for transverse shear.

6.3.2.2 Cracked Core

If v_o/d_v exceeds $0.17\sqrt{f_c'}$ (MPa) ($2\sqrt{f_c'}$ (psi)), diagonal cracking of the core must be considered. Transverse reinforcement is necessary and the in-plane reinforcement must be strengthened to account for transverse shear.

The considered model is depicted in Figure 6.3*d*, the horizontal component of the diagonal compression in the core, $v_o \cot\theta$, must be compensated by membrane forces in the sandwich covers that can be determined from the free-body diagram of Figure 6.3*d*.

Using transverse reinforcement normal to the plane of the slab, the necessary transverse reinforcement ratio amounts to

$$\rho_z = \frac{V_o \tan\theta}{d_v f_y} \quad (6.17)$$

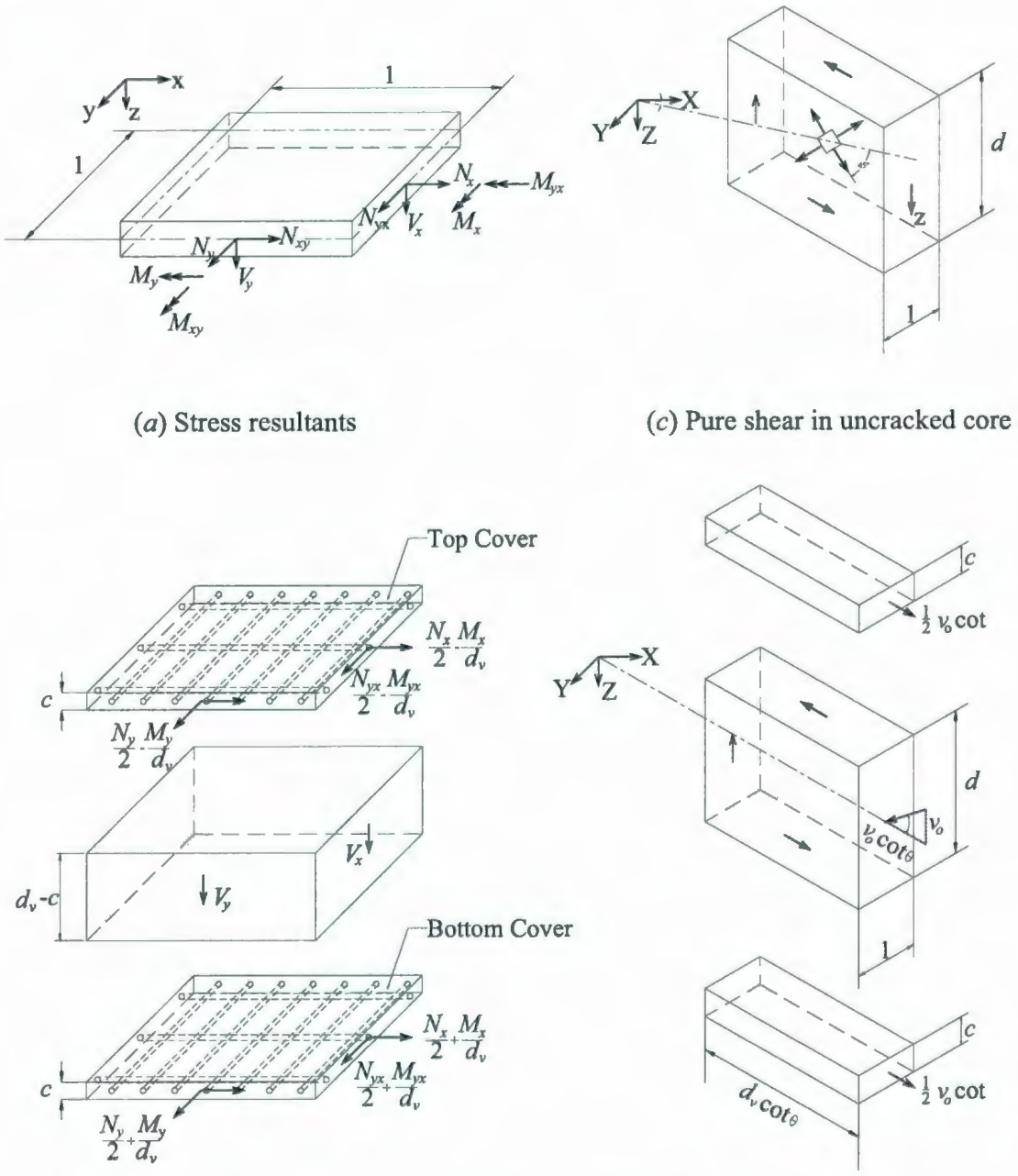

(*a*) Stress resultants

(*c*) Pure shear in uncracked core

(*b*) Sandwich model

(*d*) Diagonal compression field in cracked core

Figure 6.3: Statics of slab elements: (*a*) Stress resultants; (*b*) Sandwich model; (*c*) Pure shear in uncracked core; (*d*) Diagonal compression field in cracked core

6.3.3 Modified Sandwich Model

Based on the shear sandwich model proposed by Marti (1990), a new modified sandwich model is proposed. The new model accounts for the slab size effect through the term $(l_{ch}/h)^{0.33}$.

It is important to guarantee that if the cracking moment M_{cr} is reached due to eventual overloading, the forces resisted by concrete in tension are transmitted to tensile longitudinal steel capable of resisting M_{cr}. With reference to Figure 6.4 shown below, we can calculate the illustrated forces. Taking moments about the point of action of C_1:

$$M_{cr} = A_{s,\min} f_y \left(d - \frac{kd}{3} \right) + \frac{f_t}{2} s b \left(\frac{2kd}{3} + \frac{2s}{3} \right) \tag{6.18}$$

where $A_{s,\min}$ is the minimum flexure reinforcement area, f_t is the tensile strength of concrete, f_y is the yield strength of steel, d is the distance from extreme compression fiber to centroid of longitudinal tension reinforcement, kd is the distance from extreme compression fiber to the neutral axis calculated using the first moment equation of area, s is the height of uncracked concrete in tension as illustrated in Figure 6.4 and b is the width of the tension side.

The second term on the right-hand side of Equation (6.18), is very small, so it can be neglected. From a linear elastic stress distribution, cracking moment, M_{cr}, could be calculated as follows:

$$M_{cr} = \frac{f_r b h^2}{6} \tag{6.19}$$

where f_r is the rupture strength of concrete

$$f_r = 0.6 \lambda \sqrt{f_c'} \text{ (MPa) (CSA-A23.3-04)} \tag{6.20a}$$

$$f_r = 7.5\lambda\sqrt{f_c'} \text{ (psi) (ACI 318-08)} \tag{6.20b}$$

where λ is the modification factor reflecting the reduced mechanical properties of lightweight concrete (λ = 1.0 for normal weight concrete, 0.85 for sand-lightweight concrete, and 0.75 for all-lightweight concrete). Now, considering equilibrium equations using the modified sandwich model (neglecting the effect of transverse shear components) as shown in Figure 6.5, Figure 6.5 illustrates the modified sandwich assumptions and using Equations (6.15) and (6.16) to calculate the required reinforcement as follows:

$$a_{x,\min} f_y \frac{1}{(l_{ch}/h)^{0.33}} \geq \frac{M_x}{d} + k\left[\frac{M_{xy}}{d}\right] \tag{6.21}$$

and

$$a_{y,\min} f_y \frac{1}{(l_{ch}/h)^{0.33}} \geq \frac{M_y}{d} + \frac{1}{k}\left[\frac{M_{xy}}{d}\right] \tag{6.22}$$

where $a_{x,\min}$ and $a_{y,\min}$ denote the cross-sectional minimum areas of the orthogonal bottom reinforcements per unit width of the slab, k denotes an arbitrary positive factor taken equal to unity, M_{xy} is the torsional moment, in the case of a clamped plate with an aspect ratio a/b=2.0, M_{xy}=0.27 M_x. Hence the value of $a_{x,\min}$ can be calculated by substitution in Equation (6.21) as follows:

$$a_{x,\min} f_y \frac{1}{(l_{ch}/h)^{0.33}} \geq \frac{1.27M_x}{d} \tag{6.23}$$

where M_x is equal to the cracking moment. After cracking moment M_{cr} is reached, it is assumed that all forces resisted by concrete in tension are transmitted to tensile longitudinal steel capable of resisting M_{cr}

$$a_{x,\min} f_y \frac{1}{(l_{ch}/h)^{0.33}} \geq \frac{1.27 M_{cr}}{d} \tag{6.24}$$

substituting for the value of M_{cr}

$$a_{x,\min} f_y \frac{1}{(l_{ch}/h)^{0.33}} \geq \frac{1.27 f_r b h^2}{6d} \tag{6.25}$$

$$\rho_{x,\min} \geq \frac{1.27}{6} \frac{f_r}{f_y} \frac{(l_{ch}/h)^{0.33}}{(d/h)^2} \tag{6.26}$$

It should be noted that Eq. (6.26) can be employed for any dimensions, concrete strength or cover. For plates and concrete slabs with 100-200 mm having concrete covers up to 50 mm, it can be assumed that $h = 1.4\ d$. It can also be assumed that $h \approx 2\ h_{ef}$, where h_{ef} is effective embedment thickness as the greater of $(C_c + d'_{be}) + 7.5 d'_{be}$ and $a_2 + 7.5 d'_{be}$ but not greater than the tension zone or half slab thickness (Figure 2.2). Substituting in Equation (6.25), the expression proposed for minimum steel reinforcement is given as follows:

$$\rho_{\min} = \frac{0.415 f_r}{f_y} (l_{ch}/2h_{ef})^{0.33} \tag{6.27}$$

For plates and concrete slabs with 200-400 mm having concrete covers up to 75 mm, we can assume that $h = 1.3\ d$. Substituting in Equation (6.25), the expression proposed for minimum steel reinforcement is given as follows:

$$\rho_{\min} = \frac{0.358 f_r}{f_y} (l_{ch}/2h_{ef})^{0.33} \tag{6.28}$$

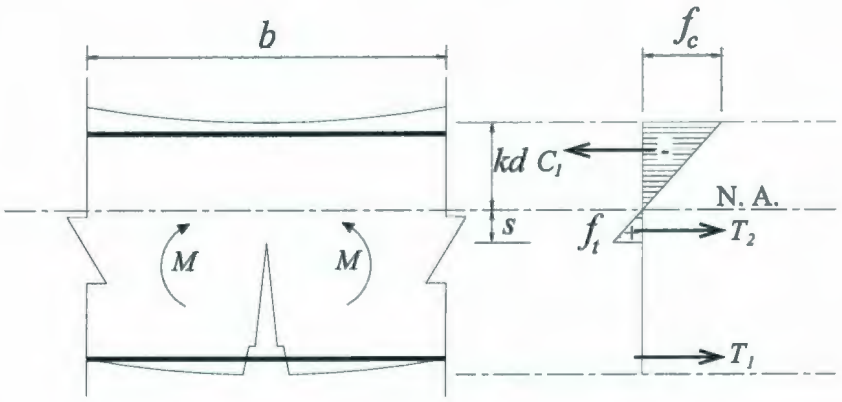

Figure 6.4: Schematic of reinforced concrete section in bending

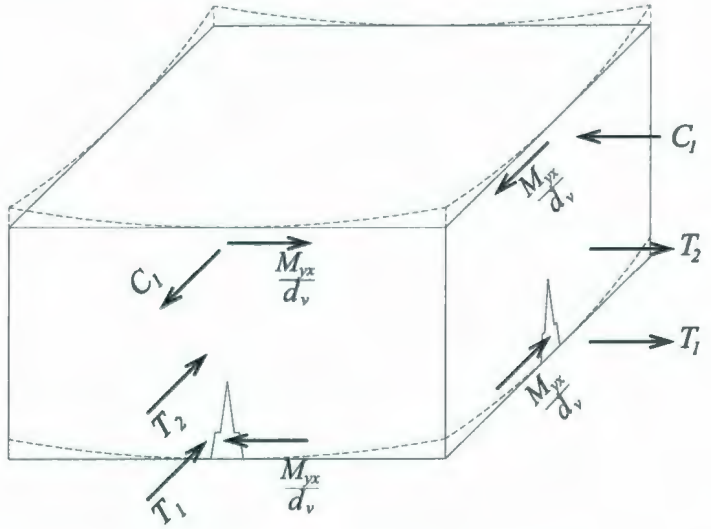

Figure 6.5: Modified sandwich model

6.4 Comparison of Proposed Model with Different Code Predictions

To verify the validity of the new proposed equation, a comparison between the proposed equation with Battista (1992) experimental results and with different code formulae for calculating minimum reinforcement for flexural members is presented in the following sections.

6.4.1 Comparison between the Values of Proposed Model with Experimental Results

Twenty four one-way slabs subjected to pure flexure were tested by Battista (1992). The test variables were concrete compressive strength, slab thickness, and ratio of ultimate stress to yield stress of reinforcement. Details of the tested slabs are presented in Table 6.1. Minimum flexural reinforcement ratios, which are required by different codes and proposed Equations (6.27); (6.28), are given in Table 6.2. All slabs had the same reinforcement ratio. Battista (1992) found that the cracking loads of the high-strength and the very high-strength specimens were greater than those of the normal-strength specimens, the brittleness of the very high-strength concrete slabs increased as the slab thickness increased, and as the concrete compressive strength increased for the 300 mm thick specimens, the total deformation decreased. This means that structural behavior for 300 mm thick high strength concrete slabs could be enhanced by using a smaller reinforcement ratio; this is due to the size effect. This is verified by the minimum reinforcement ratio required by the proposed equation for example investigating the first group of specimens S1, S13 and S19, which had thicknesses equal to 150 mm, 200 mm and 300 mm the minimum reinforcement ratio required by equation decreases as the slab thickness increases, also as the concrete strength increases the required minimum reinforcement ratio increases. This is confirmed by the values required by the NS 3474 E (1989) code as well as formula proposed by Bosco and Carpinteri (1992). It can be concluded that Eurocode 2 (2004) underestimates the minimum reinforcement ratio required by almost 75%, also it can be concluded that Eurocode 2 (2004) as well as ACI-318-08 code does not account for size effect factor. ACI 318-08 code overestimates minimum reinforcement ratio required for thick concrete slabs. In general, it can be

noticed that the Canadian offshore code (CSA-S474-04) does not account for size effect factor and the concrete strength.

Table 6.1–Details of test specimens by Battista (1992)

Slab No.*	Compressive strength f_c', MPa	Bar size d_b, mm	Concrete cover C_c, mm	Slab thickness h, mm	Depth d, mm	Steel ratio ρ_{min}%
S1	35	10 M	20	150	125.0	0.24
S7	35	10 M	20	200	175.0	0.23
S13	35	15 M	20	200	172.5	0.23
S19	35	15 M	20	300	272.5	0.22
S4	35	10 M	20	150	125.0	0.24
S10	35	10 M	20	200	175.0	0.23
S16	35	15 M	20	200	172.5	0.23
S22	35	15 M	20	300	272.5	0.22
S2	55	10 M	20	150	125.0	0.24
S8	55	10 M	20	200	175.0	0.23
S14	55	15 M	20	200	172.5	0.23
S20	55	15 M	20	300	272.5	0.22
S5	55	10 M	20	150	125.0	0.24
S11	55	10 M	20	200	175.0	0.23
S17	55	15 M	20	200	172.5	0.23
S23	55	15 M	20	300	272.5	0.22
S3	85	10 M	20	150	125.0	0.24
S9	85	10 M	20	200	175.0	0.23
S15	85	15 M	20	200	172.5	0.23
S21	85	15 M	20	300	272.5	0.22
S6	85	10 M	20	150	125.0	0.24
S12	85	10 M	20	200	175.0	0.23
S18	85	15 M	20	200	172.5	0.23
S21	85	15 M	20	300	272.5	0.22

Table 6.2–Minimum reinforcement ratios required by proposed equation and different codes formulae for tested slabs by Battista (1992)

Slab No.*	Compressive strength f_c', MPa	f_y, MPa	CSA-A23.3-04 ACI 318-08, ρ_{min}%	CSA-S474-04 ρ_{min}%	NS 3474 E-1989 ρ_{min}%	EC2-2004 ρ_{min}%	Bosco & Carpinteri 1992	Proposed eq. by Rizk and Marzouk 2009, ρ_{min}%
S1	35	584	0.25	0.20	0.31	0.08	0.15	0.38
S7	35	584	0.25	0.19	0.29	0.08	0.13	0.34
S13	35	619	0.24	0.18	0.27	0.07	0.12	0.32
S19	35	619	0.24	0.17	0.25	0.07	0.10	0.28
S4	35	545	0.27	0.21	0.33	0.08	0.16	0.40
S10	35	545	0.27	0.20	0.31	0.08	0.14	0.37
S16	35	571	0.26	0.20	0.30	0.08	0.13	0.35
S22	35	571	0.26	0.19	0.27	0.08	0.11	0.31
S2	55	584	0.32	0.25	0.40	0.10	0.23	0.42
S8	55	584	0.32	0.24	0.37	0.10	0.20	0.38
S14	55	619	0.30	0.23	0.36	0.09	0.19	0.36
S20	55	619	0.30	0.22	0.32	0.09	0.16	0.32
S5	55	545	0.34	0.27	0.43	0.11	0.25	0.45
S11	55	545	0.34	0.26	0.40	0.11	0.22	0.41
S17	55	571	0.32	0.25	0.39	0.10	0.21	0.39
S23	55	571	0.32	0.24	0.35	0.10	0.17	0.34
S3	85	584	0.39	0.31	0.52	0.12	0.38	0.40
S9	85	584	0.39	0.30	0.48	0.12	0.33	0.37
S15	85	619	0.37	0.28	0.46	0.11	0.31	0.35
S21	85	619	0.37	0.27	0.42	0.11	0.25	0.30
S6	85	545	0.42	0.33	0.56	0.12	0.41	0.43
S12	85	545	0.42	0.32	0.52	0.12	0.35	0.39
S18	85	571	0.40	0.31	0.50	0.12	0.34	0.38
S21	85	571	0.40	0.29	0.46	0.12	0.27	0.33

6.4.2 Proposed Model versus Different Codes Formulae

To verify the validity of the new proposed model, a comparison between the proposed formula versus different codes formulae for calculating minimum reinforcement for flexural members is implemented as shown Figures 6.6, 6.7 and 6.8. The new proposed equation accounts for the size effect; this agrees with the Norwegian code (NS 3474 E 1989) as well as Bosco and Carpinteri (1992). It can be concluded from Figures 6.7, 6.8 and 6.9 that, the Canadian offshore code (CSA-S474-04) underestimates the minimum reinforcement ratio required for all slabs thicknesses. It can be concluded also that the

American (ACI 318-08) and Canadian (CSA-A23.3-04) codes overestimate the minimum reinforcement ratio required for thick concrete slabs greater than 200 mm, this is due to the fact that, none of these codes contain a size effect factor, this can result in a huge saving in steel reinforcement. Eurocode 2 (2004) underestimates the minimum reinforcement ratio required by as much as 75%, hence using Eurocode 2 (2004) formula resulting in unsafe design for very thick plates.

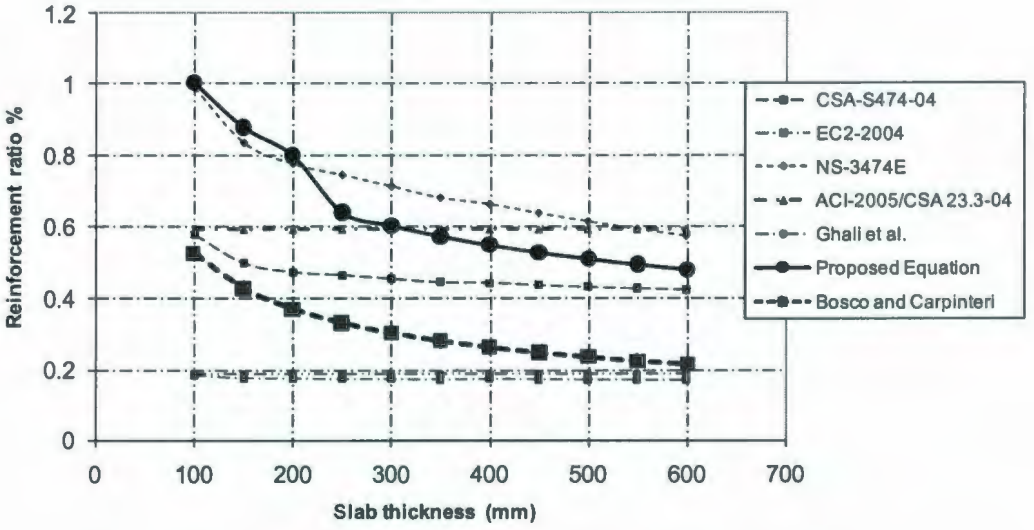

Figure 6.6: Comparison of minimum reinforcement ratios calculated by different codes

$f_c' = 35\,\text{MPa}$

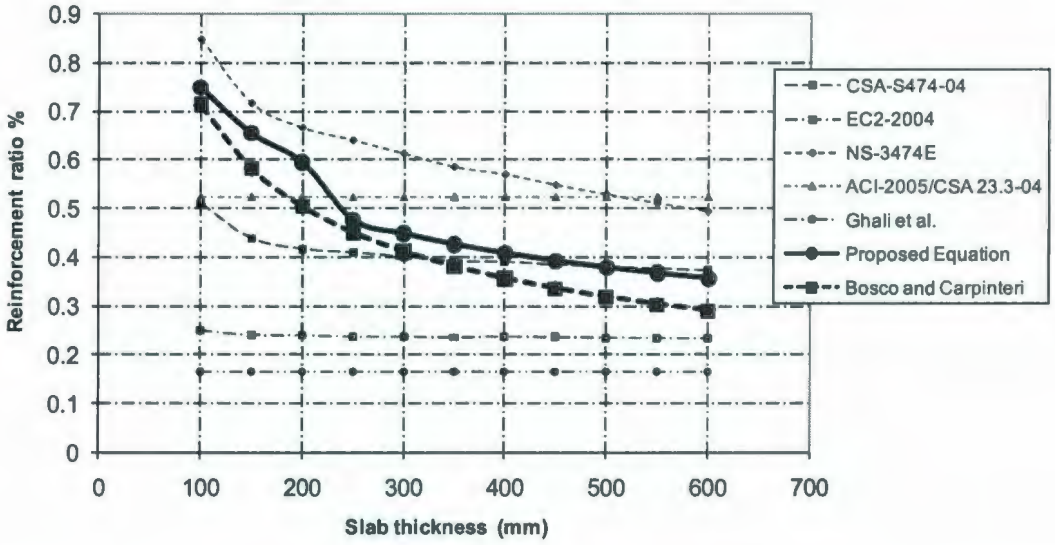

Figure 6.7: Comparison of minimum reinforcement ratios calculated by different codes

$f_c' = 70$ MPa

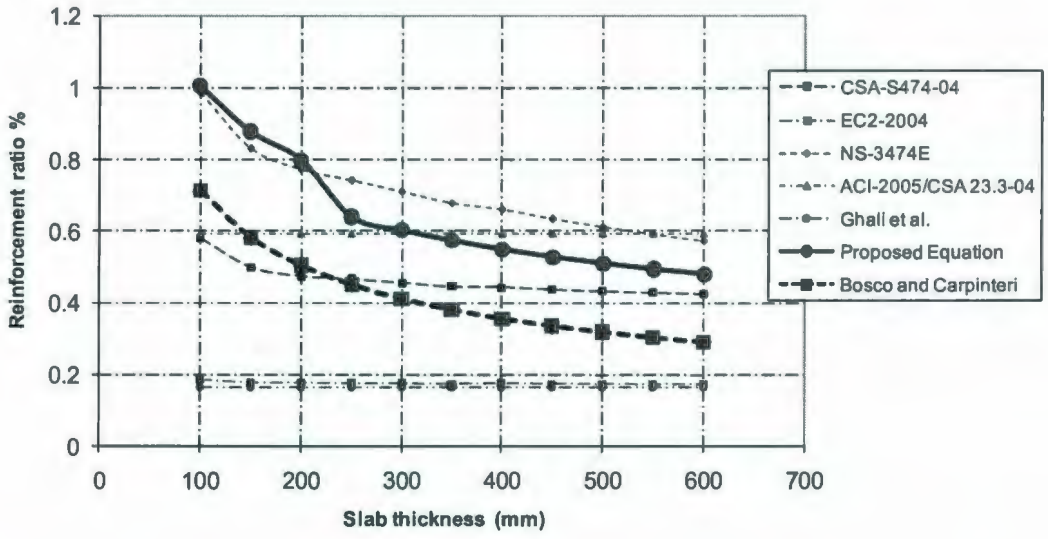

Figure 6.8: Comparison of minimum reinforcement ratios calculated by different codes

$f_c' = 90$ MPa

6.5 Minimum Shear Reinforcement for Thick Plates and Two-Way Slabs

Slabs without shear reinforcement usually exhibit brittle shear failure under a concentric force. Conventional design methods consider potential punching failures in the vicinity of concentrated loads. Nominal shear stresses at well-defined critical sections are limited to guard against such failure modes. With the extensive use of thick plates of more than 250 mm thick for offshore and nuclear containment structures, design codes must provide special provisions for shear reinforcement requirements. There have been several research investigations to study the effectiveness of different types of shear reinforcement used in two-way slabs. Different tests proved that the use of shear reinforcement in the form of stirrups, or headed shear studs prevented brittle failure of test specimens.

6.6 Development of Minimum Shear Reinforcement Ratio for Two-Way Slabs

6.6.1 North American Codes Requirements

Canadian standard CSA-A23.3-04 allows using shear reinforcement consisting of headed shear reinforcement, stirrups, or shear heads to increase the shear capacity of slabs and footings. Shear reinforcement should be extended to the section where V_f is not greater than $0.12\lambda\sqrt{f_c'(\text{MPa})}$, but at least a distance $2d$ from the column face. In the zone reinforced by headed shear reinforcement, the factored shear stress resistance of the concrete, V_c, shall be $0.18\lambda\sqrt{f_c'(\text{MPa})}$. Stirrups could be used as shear reinforcement provided that, the overall thickness of the slab not less than 300 mm. For slabs without shear reinforcement, the value of $\sqrt{f_c'}$ used to calculate factor shear resistance, v_r, shall not exceed 8 MPa.

ACI 318-08 sets out the principles of design for slab shear reinforcement but does not make specific reference to mechanically anchored shear reinforcement, also referred to as shear studs. ACI 421.1R-08 gives recommendations for the design of shear reinforcement using shear studs in slabs. Shear studs have proven to be effective in increasing the strength and ductility of slab-column connections. ACI 421.1R-08 suggests treating a shear stud as the equivalent of a vertical branch of a stirrup and to use higher limits on some of the design parameters used in ACI 318-08. In particular, ACI 421.1R-08 suggests higher allowable values for v_n, v_c, s, and f_{yv}, as follows:

$$v_n = v_c + v_s \leq 8\sqrt{f_c'} \text{ (psi) or } 0.66\sqrt{f_c'} \text{ (MPa)} \tag{6.29}$$

$$v_c = 3\sqrt{f_c'} \text{ (psi) or } 0.25\sqrt{f_c'} \text{ (MPa)} \tag{6.30}$$

The allowable values recommended in ACI 421.1R-08 have been adopted in ACI 318-08. The justification for these higher values is mainly due to the almost slip-free anchorage of the studs and that the mechanical anchorage at the top and bottom of the stud is capable of developing forces in excess of the specified yield strength at all sections of the stud stem.

6.6.2 European Codes Requirements

EC 2 (2004) requires that reinforced concrete slabs be provided with minimum shear reinforcement equal to that needed for the same cross section to be designed as a beam. For solid one-way and two-way slabs, shear reinforcement is not normally required provided the design ultimate shear force V_{Ed} does not exceed V_{Rd1}.

$$V_{Rd1} = 0.12k\left(100\rho f_{ck}\right)^{1/3} b_w d \tag{6.31}$$

but not less than:

$$V_{Rd2} = 0.035\sqrt{f_{ck}}\, k^{3/2} b_w d \tag{6.32}$$

$$k = \sqrt{1+\frac{200}{d}} \le 2 \text{ and } \rho = \frac{A_{sl}}{b_w d} \le 2\% \tag{6.33}$$

where k is a size effect factor, A_{sl} is the area of tensile reinforcement, which extends beyond the section considered taking account of the "shift rule," shift rule is the recommended method for working out curtailment points for beam reinforcement, which at the same time ensures the provision of sufficient steel near to supports, to accommodate the additional tensile forces generated by the strut-and-tie shear action, b_w is the web width and d is the effective depth of a cross-section. The area of a link leg (or equivalent), $A_{sw,\min}$, is given by:

$$A_{sw,\min}\frac{1.5}{s_r s_t} \ge 0.08\frac{\sqrt{f_{ck}}}{f_{yk}} \tag{6.34}$$

where s_r is the spacing of shear links in the radial direction, s_t is the spacing of shear links in the tangential direction, f_{ck} is the characteristic compressive cylinder strength of concrete at 28 days (MPa), f_{yk} is the characteristic yield strength of reinforcement (MPa). A slab in which shear reinforcement is provided should have a depth of at least 200 mm.

6.7 Shear Transfer in the Interior of a Slab

Using Cartesian coordinates with axes X and Y in the plane of the slab, and Z perpendicular to this plane, Figure 6.9 illustrates the positive directions for slab element internal forces V_{xz} and V_{yz}. Note that these slab element internal forces are forces per unit length acting on the mid-surface of the slab element. Figure 6.10 illustrates the positive direction for slab element maximum transverse shear force, $V_{\max}$. Knowing the values of V_{xz} and V_{yz}

from a plate analysis, the maximum transverse shear force, V_{max}, can be calculated using the following equation for the transverse shear force components:

$$V_{max} = \sqrt{V_{xz}^2 + V_{yz}^2} \tag{6.35}$$

The angle, at which principal shear force V_{max} occurs, is found by solving the following equation:

$$\varphi_{max} = \tan^{-1}\left(V_y / V_x\right) \tag{6.36}$$

In the same manner maximum shear stress could be found using Equation (6.35)

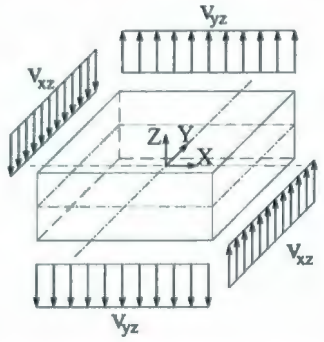

Figure 6.9: Slab element internal forces V_{xz} and V_{yz}

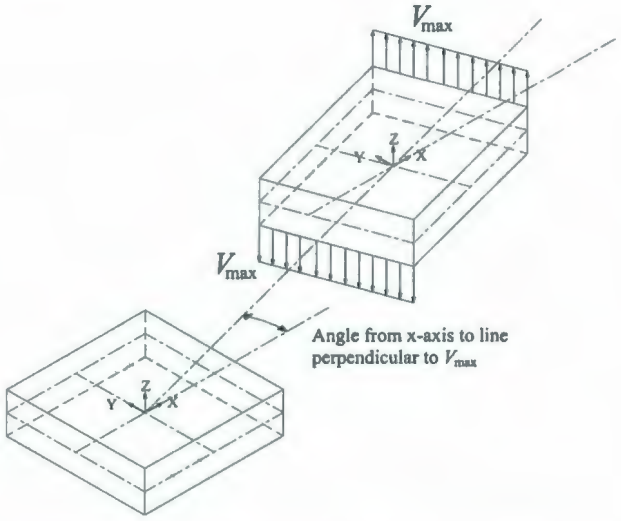

Figure 6.10: Maximum transverse shear force

6.8 Dimensioning of Sandwich Model Core

The inner core must transmit transverse shear forces as assumed by sandwich model. In the following discussion, we shall analyze the behavior of the core with unit length along the X and Y axes, thickness of the core is d_v, subjected to shear forces orthogonal to the element's plane (V_{xz} and V_{yz}), as in Figure 6.3*b*. The thickness of the core is d_v, but it is accepted that the shear forces act over a lever arm $jd = d_v + c$. The principal shear force and its direction can be determined from the values of V_{xz} and V_{yz} [Eq. (6.35) and (6.36)]. In the following subsections, we distinguish two possible mechanisms for the shear forces transfer.

6.8.1 Slabs without Shear Reinforcement

When dimensioning slab, we usually limit the nominal shear stress acting on critical defined sections as to omit shear reinforcement steel. Most codes present formulae, where the design punching load is a product of design nominal shear strength and the area of a chosen control surface. Depending on the method used, the critical section for checking punching shear in slabs is usually situated between 0.5 to 2 times the effective depth from the edge of the load or the reaction. For example, ACI 318-08 requires that the nominal shear stress for slabs without shear reinforcement to be not more than:

$$V_c = 0.33\lambda\sqrt{f_c'}\, b_o\, d \quad \text{(MPa)} \tag{6.37a}$$

$$V_c = 4\lambda\sqrt{f_c'}\, b_o\, d \quad \text{(psi)} \tag{6.37b}$$

where d is the effective depth of the slab; b_o is the length of the perimeter at an assumed shear critical section at a distance $d/2$ from the column faces.

6.8.2 Slabs with Shear Reinforcement

When the Eq. (6.37) cannot be applied, the resisting mechanism should be analogous to that of a beam (Figure 6.3*b*), locally oriented according to the principal shear direction. The diagonal compression field, v_o / sin θ, makes an angle φ with the *XY* plane, and is the resultant of the sum of two component forces: v_o cot θ parallel to the *XY* plane, and v_o, parallel to the *Z* axis. Assuming that vertical studs are used, the following equations must be verified:

$$F_{cw} = \frac{v_o}{\sin\theta} \leq f_2 \, d_v \cos\theta \tag{6.38}$$

where F_{cw} is the diagonal compressive force in concrete, f_2 is the crushing strength of diagonal cracked concrete given by the following equation:

$$f_2 = \frac{f_c^{'}}{0.8 + 170\,\varepsilon_1} \leq 0.85\, f_c^{'} \tag{6.39}$$

where ε_1 is the principal tensile strain in cracked concrete due to factored loads.

Tensile forces in the shear reinforcement:

$$F_{sz} = v_o \leq \frac{A_{sz}\, f_{yz}}{s} d_v \cot\theta \tag{6.40}$$

Additional truss axial force in the tension and compression covers (outer layers of the model):

$$\Delta F = v_o \cot\theta \tag{6.41}$$

Angle θ is subjected to the same limitations that apply to linear elements subjected to shear forces. According to EC 2 (2004), angle θ can be chosen freely within the limits of $22° \leq \theta \leq 45°$ ($1 \leq \cot\theta \leq 2.5$). The selection of θ must be based primarily on practical

considerations in detailing. A low value of θ allows for large shear reinforcement spacing and facilitates the casting of concrete, but requires more longitudinal reinforcement.

6.9 Punching Shear Distribution

The investigation of transverse shear stress distribution under the ultimate load, referred to as punching shear, was carried out by Marzouk and Jiang (1996) using 3D Finite Element analysis since it was difficult to measure this distribution and its associated value from the experimental investigation. The numerical investigation by researchers revealed that the punching shear in the slabs provided with shear reinforcement was located out of a distance 0.5 d to the loading stud face. The test observation from the slabs with vertical types of shear reinforcement supports the provision by the FEA with the three-dimensional model.

In terms of punching shear value, a comparison of the FEA with punching shear resistance, revealed that τ_{max}, the maximum shear stress, provided by shear stress contour diagrams v_r, unfactored shear resistance, is equal to $0.4\sqrt{f_c'}$ (MPa) ($4.8\sqrt{f_c'}$ (psi)) for the slab without shear reinforcement and $0.6\sqrt{f_c'}$ (MPa) ($7.2\sqrt{f_c'}$ (psi)) for the slab with different types of shear reinforcement, respectively. The ratio of predicted maximum shear stress to punching shear resistance, (τ_{max}/v_r), was 1.24 to 1.27, respectively for slabs without shear reinforcement. The corresponding ratio for slabs with different types of shear reinforcement ranged from 0.72 to 0.93 with a mean value of 0.86 and a standard deviation of 0.08.

6.10 Minimum Shear Reinforcement Based on Truss Model

In this model, it is assumed that the column force is transferred to slab through four analogues trusses as shown in Figure 6.11, each truss has an effective width equal to the

column side dimension, all stirrups are lumped into one vertical member, the dashed truss members in compression are rather forces in concrete and are not really separate truss members, the idealized truss model does not assign any shear forces to the concrete, and truss is statically indeterminate.

Before concrete shear cracking is induced, shear forces are carried equally by diagonal tensile and compression stress fields. Cracking is assumed to occur when the principal tensile strength reaches the tensile strength of concrete in biaxial tension-tension. After cracking, all shear forces are carried by stirrups. To simplify calculations it can be assumed that stirrups have yielded to make the truss statically determinate, as shown in Figure 6.12. The compression diagonals originating at the load, and are referred to as a compression fan. The number of such diagonals in the fan must be such that the entire vertical load is resisted by the vertical force components in these diagonals. A similar compression fan exists at the support. Between the compression fans is a compression field consisting of parallel diagonal struts. The angle ϕ of the compression field (Figure 6.12) is determined by the number of stirrups needed to equilibrate the vertical loads in the fans.

6.10.1 Evaluation of Minimum Shear Reinforcement

In this section, minimum shear reinforcement is evaluated based on truss model assumptions. Figure 6.12 illustrates the stress fields in the core of two-way slab after cracking. Prior to cracking, shear is carried equally by diagonal tensile and compressive stresses at 45°. After cracking, shear is carried by tensile strength of vertical members. Transverse shear reinforcement is necessary and flexural reinforcement must be increased

to account for transverse shear and reduce diagonal crack opening (Marti 1990). The minimum shear reinforcement can be evaluated as follows:

$$A_{z,\min} f_y \cos\theta = f_{ct} \frac{h}{\sin\theta} c \tag{6.42}$$

$$A_{z,\min} = \frac{h f_{ct}}{f_y \sin\theta \cos\theta} c \tag{6.43}$$

$$\rho_{z,\min} = \frac{A_{z,\min}}{c\, h \cot\theta} \tag{6.44}$$

$$\rho_{z,\min} = \frac{f_{ct}}{f_y} \frac{1}{\cos^2\theta} \tag{6.45}$$

where c is the width of the diagonal compression strut that is taken equal to the truss width; f_{ct} is the direct tensile strength of concrete (Marzouk and Chen 1995), $f_{ct} = 0.33\sqrt{f_c'}$, and f_y is the specified yield strength. The angle of the failure plane θ normally varies between 22° and 45° (Marzouk and Jiang 1997). It can be assumed that θ tends to be a small value for small slab thicknesses less 300 mm and equal to 22°. For medium slab thicknesses of 300-500 mm, θ can be taken equal to 30°. For thick slabs greater than 500 mm of thickness, θ can be taken equal to 45°. In this research, θ is taken equal to 30° based on experimental findings (Marzouk and Jiang 1997; Hegger et al. 2006).

Introducing the term $(l_{ch}/h)^{0.33}$ to account for the size effect, equation (6.45) could be written as follows:

$$\rho_{z,\min} = \frac{f_{ct}}{f_y} \sin^2\theta \frac{1}{(l_{ch}/h)^{0.33}} \tag{6.46}$$

where h is the slab thickness.

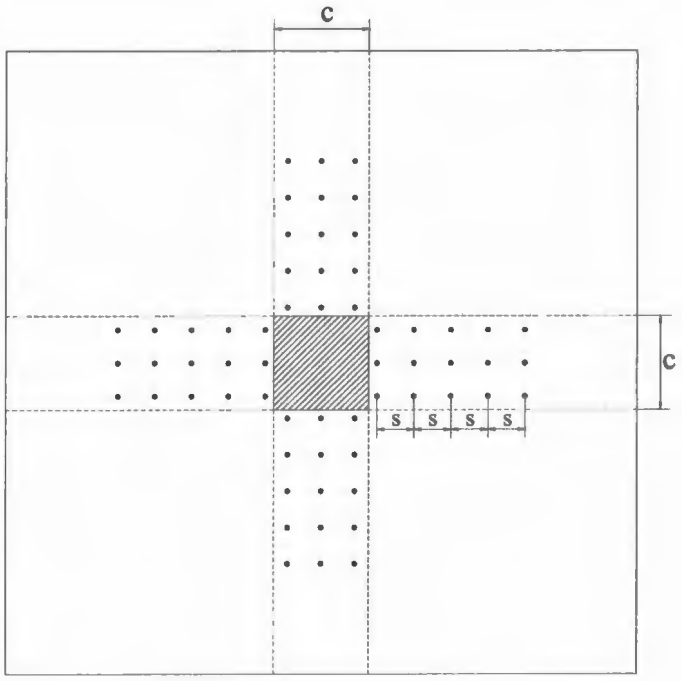

Figure 6.11: Effective width of truss model idealization for slab column connection

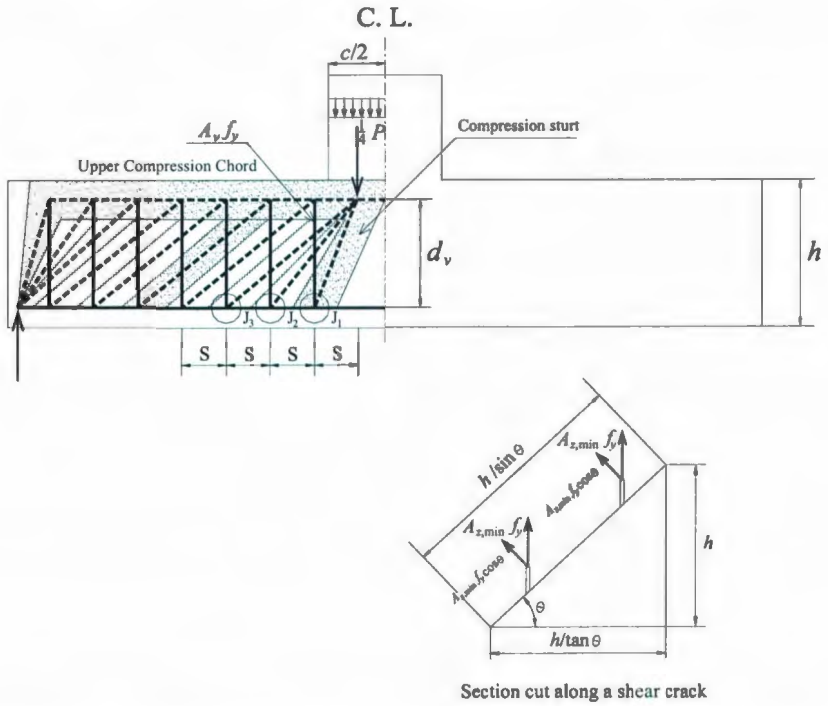

Figure 6.12: Equivalent plastic truss model idealization and equilibrium of bottom chord joints

6.11 Minimum Shear Reinforcement Ratio Based on the Diagonal Cracking Load

Consider a rectangular cross section subjected to shearing force; from the elastic shear stress distribution (second degree parabola, Figure 6.13), the shear crack appears when $\tau_{max} = 1.25\, f_{ct}$ (Marzouk and Jiang 1996), where f_{ct} is the tensile strength of concrete, $f_{ct} = 0.33\sqrt{f_c'}$, and f_c' is the cylinder compressive strength of concrete in MPa. According to the compression field theory approach, the shear crack appears when $\tau_{max} = 2\, f_{ct}$ (Angelakos et al. 2001). Hence, the associated shear force is calculated as:

$$V_{cr} = \frac{2}{3} b h \tau_{max} = \frac{2}{3} b h f_{ct} \tag{6.47}$$

where b is the unit slab width, h is the height of the slab and f_{ct} is the tensile strength of concrete. For slabs subjected to shearing forces V_{xz} and V_{yz}:

$$V_{cr} = \sqrt{V_{xz}^2 + V_{yz}^2} \tag{6.48}$$

Given that, when the cracking shear force reaches V_{cr}, a sudden rupture of the slab will occur with a total loss of strength. It is important that the slab contains the minimum shear reinforcement for certain ductility at failure. Considering the failure plane is considered to be inclined at an angle θ to the slab surface and the shear studs are in normal directions. From equilibrium of forces in the vertical direction along a projected length of the failure plane ($h \cot \theta$), the minimum shear reinforcement is calculated as follows:

$$V_{cr} = A_{z,min}\, f_y \tag{6.49}$$

$$A_{z,min} = \rho_{z,min}\, b h \cot\theta \tag{6.50}$$

$$\rho_{z,min} = \frac{A_{z,min}}{b h \cot\theta} = \frac{V_{cr}}{b h \cot\theta\, f_y} \tag{6.51}$$

$$\rho_{z,\min} = 0.83\frac{f_{ct}}{f_y}\tan\theta \tag{6.52}$$

where $A_{z,\min}$ is the area of minimum shear reinforcement and $\rho_{z,\min}$ is the minimum shear reinforcement ratio. ACI 318-08 design code does not account for the fact that the shear stress that can cause failure of members without shear reinforcement decreases as the depth of the member increases, which is known as the size effect factor. Modern European codes of practice such as EC 2 (2004) provide a factor $k = \sqrt{1+(200/d)}$ to account for size effect and as the depth of the member increases the value of k as well as the predicted punching shear resistance decreases. This means that by increasing the member size, the behavior of the member becomes more brittle, and hence more shear reinforcement is required to enhance the behavior of thick members. The previous equation, Eq. (6.52), could be modified to account for the size effect factor by the inclusion of the brittleness ratio (h/l_{ch}) as proposed earlier by Marzouk et al. (1998). However, it should be noted that any size effect factor that is derived using LEFM could be applied. Introducing the term $(l_{ch}/h)^{0.33}$ to account for the size effect, Eq. (6.52) can be modified as follows:

$$\rho_{z,\min} = 0.83\frac{f_{ct}}{f_y}\tan\theta(l_{ch}/h)^{0.33} \tag{6.53}$$

$$\text{For } \theta=30°, \rho_{z,\min} = 0.16\frac{\sqrt{f_c'}}{f_y}(l_{ch}/h)^{0.33} \tag{6.54}$$

The angle of the failure plane θ normally varies between 22° and 45°, it can be assumed that θ tending to be small value for the normal slab thicknesses less 300 mm and could be taken equal to 22°, for medium slabs thicknesses 300-500 mm, θ could be taken equal to 30°, for thick slabs greater than 500 mm thickness, θ could be taken equal to 45°.

6.12 Minimum Shear Reinforcement Ratio Based on Compression Field Theory

Figure 6.14 illustrates the stress fields in the core of the two-way slab before and after cracking. Prior to cracking, the shear is carried equally by diagonal tensile and diagonal compressive stresses at 45° (Angelakos et al. 2001).

$$V_{cr} = f_2 (b d_v \cos\theta)\sin\theta + f_1 (b d_v \sin\theta)\cos\theta \tag{6.55}$$

Just prior to cracking

$$f_1 = f_2 = f_{ct} \tag{6.56}$$

where f_1 and f_2 are the principal tensile and compressive stresses and f_{ct} is the direct tensile strength of concrete as determined by the direct tension test (Marzouk and Chen 1995) or any other fracture mechanics test.

Cracking is assumed to occur when the principal tensile strength reaches the tensile strength of concrete in biaxial tension-tension.

$$V_{cr} = 2 f_{ct} b d_v \sin\theta\cos\theta \tag{6.57}$$

$$V_{cr} = A_{z,\min} f_y = \rho_{z,\min} b h \cot\theta f_y \tag{6.58}$$

$$\rho_{z,\min} b h \cot\theta f_y = 2 f_{ct} b d_v \sin\theta\cos\theta \tag{6.59}$$

$$\rho_{z,\min} b h \cot\theta f_y = 1.44 f_{ct} b h \sin\theta\cos\theta \tag{6.60}$$

$$\rho_{z,\min} = \frac{1.44 f_{ct}}{f_y}\sin^2\theta \tag{6.61}$$

where d_v is the effective shear depth taken as the greater of 0.9 d or 0.72 h.

Introducing the term $(l_{ch}/h)^{0.33}$ to account for the size effect, Equation (6.61) could be modified as follows:

$$\rho_{z,\min} = \frac{1.44 f_{ct}}{f_y}\sin^2\theta (l_{ch}/h)^{0.33} \tag{6.62}$$

For $\theta=30°$, $\rho_{z,\min} = 0.12\frac{\sqrt{f_c'}}{f_y}(l_{ch}/h)^{0.33}$ (6.63)

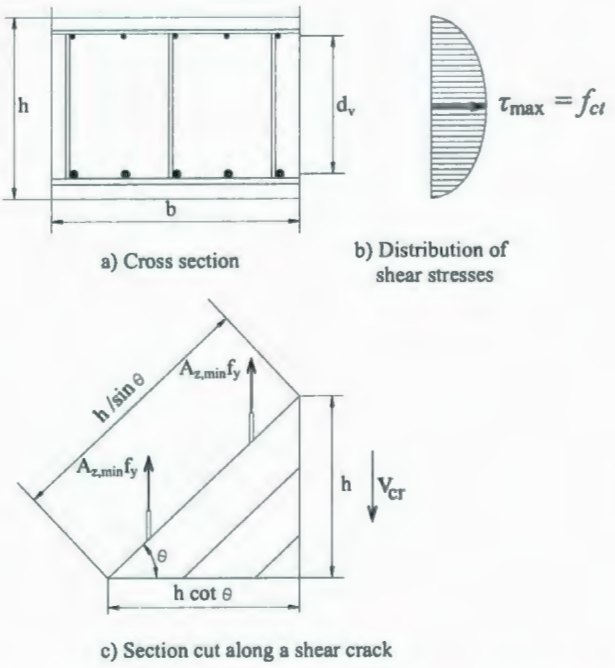

Figure 6.13: Shear stress distribution in a slab cross section just before the formation of shear cracks

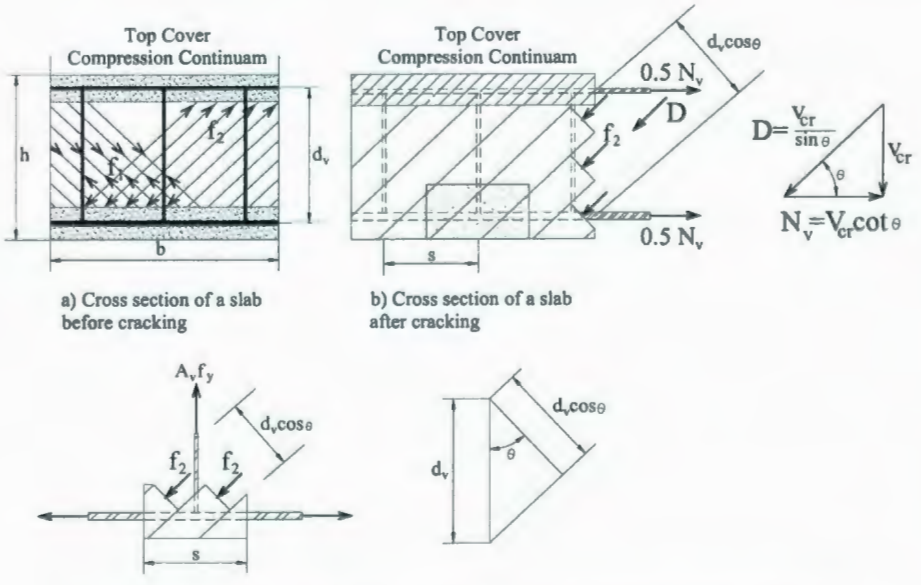

Figure 6.14: Stress fields in the core of reinforced concrete slab

6.13 Comparison of Proposed Formula with Different Design Codes formulae

To verify the validity of the proposed formula, a comparison between the proposed formula [Eq. (6.63)] with different design codes formulae for calculating minimum shear reinforcement for beams and two-way slabs is presented in Figure 6.15 and Figure 6.16 for three different heights (250, 500 and 1000 mm). A summary of the minimum shear reinforcement requirements provided by most popular design concrete codes is presented in Table 6.3. In this comparison, yield strength of shear reinforcement, f_{yv}, is assumed to be equal to 400 MPa. Analyzing the results of the comparison, it is obvious that $\rho_{z,\min}$ increases as the concrete strength increases. The amount of shear reinforcement calculated by proposed formula [Eq. (6.63)] is slightly higher than the amount of shear reinforcement calculated by EC2 (2004) design code requirement. It could be noted also that as the beam height increases the value of minimum shear reinforcement required by proposed formula decreases. The ACI 318-08 and CSA-A23.3-04 expressions give similar amounts of shear reinforcement, while the EC 2 (2004) expression gives a larger amount of minimum shear reinforcement for all concrete strengths. Both ACI 318-08 and CSA-A23.3-04 require that a minimum amount of shear reinforcement be provided in all reinforced concrete flexural members where the factored shear force exceeds one-half the factored shear resistance of the concrete, except for slabs and footings. In contrast, EC 2 (2004) requires that all beams that contribute significantly to the overall resistance and stability of the structure must contain at least a minimum amount of shear reinforcement. The following section presents an experimental validation required to verify the proposed theoretical analysis done.

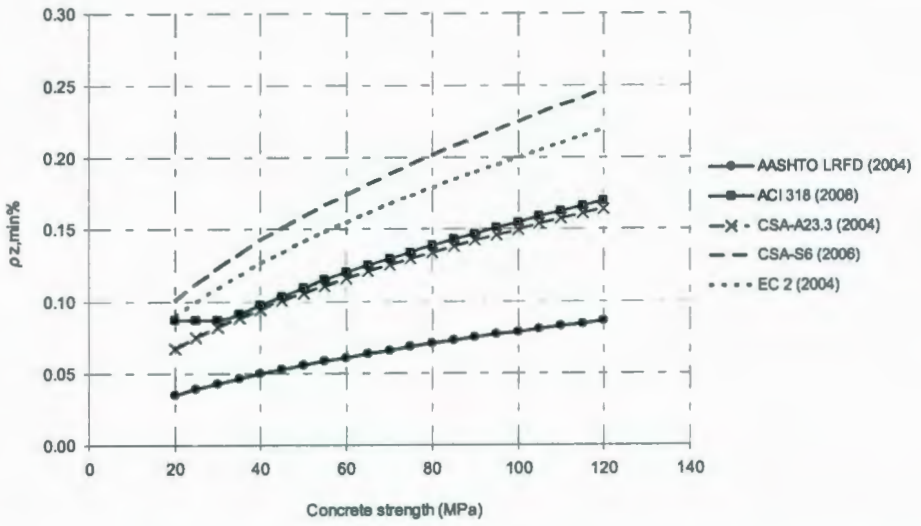

Figure 6.15: Comparison of minimum shear reinforcement requirements for beams by various design codes as a function of concrete compressive strength f_c'

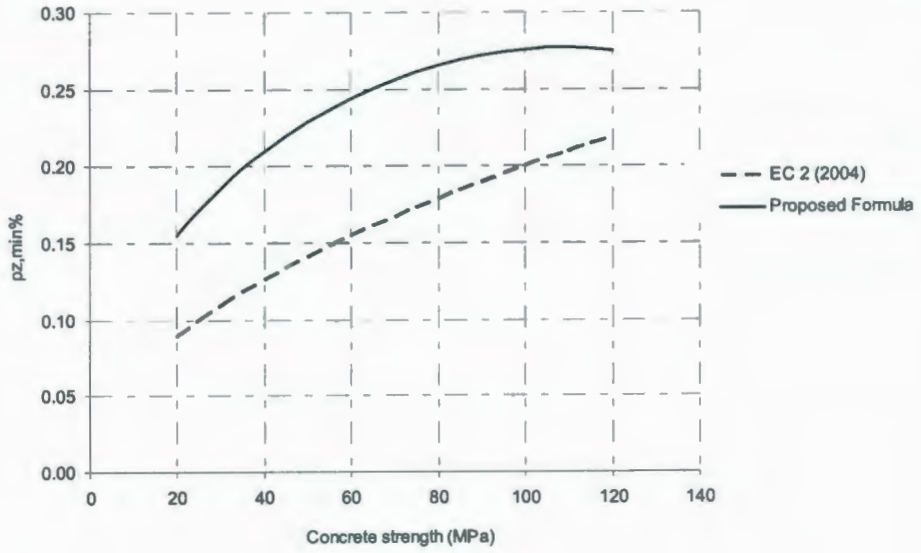

(*a*) h = 250 mm

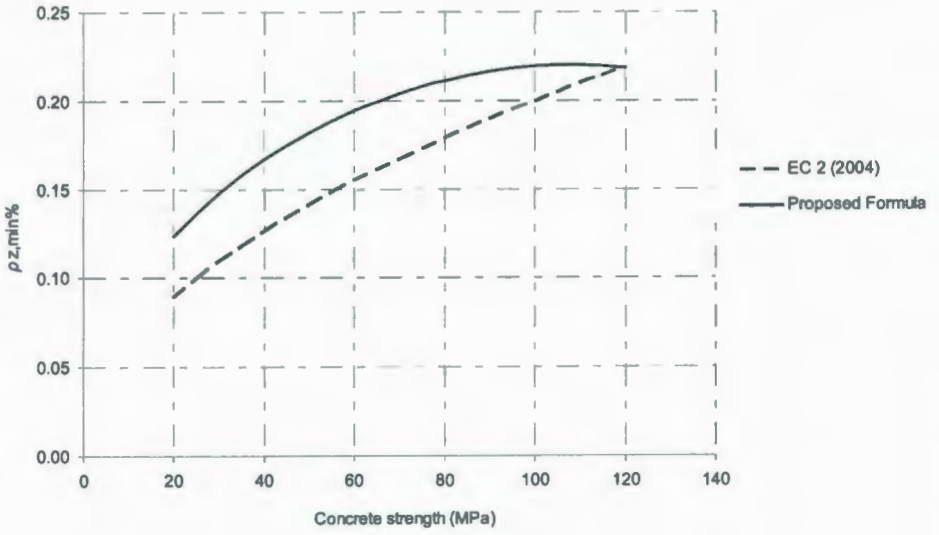

(*b*) $h = 500$ mm

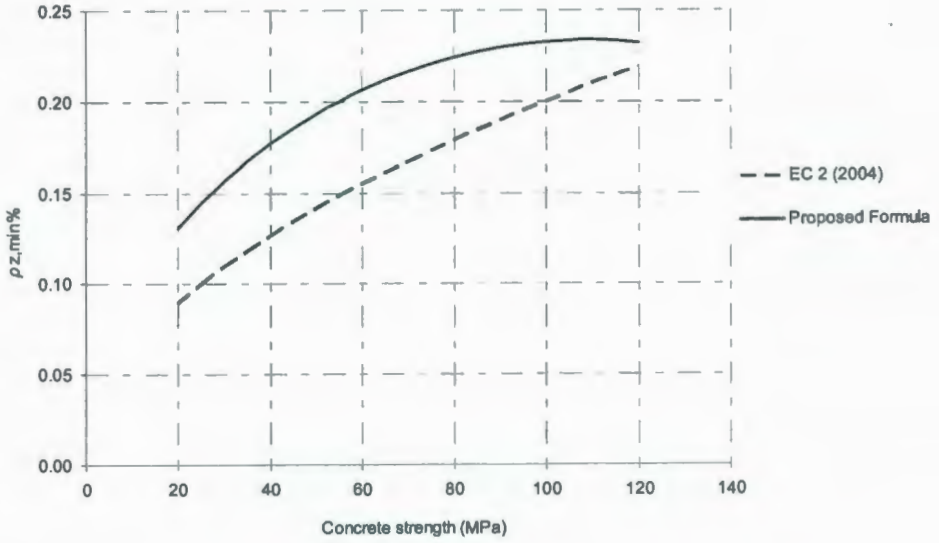

(*c*) $h = 1000$ mm

Figure 6.16: Comparison of minimum shear reinforcement requirements for two-way slabs by EC2 and proposed formula as a function of concrete compressive strength $f_c^{'}$: (*a*) $h = 250$ mm; (*b*) $h = 500$ mm; (*c*) $h = 1000$ mm

Table 6.3–Minimum shear reinforcement requirements in different design codes

Code	Minimum area of shear reinforcement	Maximum spacing of shear reinforcement	Shear strength reduction factor	Shear type
ACI 318-08 (2008)	$A_{v\min} = 0.062\sqrt{f_c'}\frac{bs}{f_y} \geq \frac{0.35 b_w s}{f_y}$	$s \leq \frac{d}{2} \leq 600\,\text{mm}$ If $\phi_v V_s > 0.33\phi_v \sqrt{f_c'}\, b_w d$ Then $s \leq \frac{d}{4} \leq 300\,\text{mm}$	$\phi_v = 0.75$	One-way shear
CSA-A23.3 (2004)	$A_{v\min} = 0.06\sqrt{f_c'}\frac{b_w s}{f_y}$	$s \leq 0.7 d_v \leq 600\,\text{mm}$ If $V_f > 0.125\lambda\phi_c f_c' b_w d_v$ Then $s \leq 0.35 d_v \leq 300\,\text{mm}$	$\phi_c = 0.65$	One-way shear
CAN/CSA-S6 (2006)	$A_{v\min} = 0.15 f_r \frac{bs}{f_y}$ $f_r = 0.6\lambda\sqrt{f_c'}$	$s \leq 0.75 d_v \leq 600\,\text{mm}$ If $V_f > 0.10\phi_c f_c' b d_v$ Then $s \leq 0.33 d_v \leq 300\,\text{mm}$	$\phi_c = 0.75$	One-way shear
NS 3473 E (1989)	$A_s \geq 0.2 A_c \frac{f_{tk}\,(\text{MPa})}{f_{sk}} \sin\alpha$	$s_{\max} = 0.6h'(1+\cot\alpha) \leq h'$ $s_{\max} = 500\,\text{mm}$		One-way shear
EC 2 (2004)	$A_{sw,\min}\frac{1.5\sin\alpha + \cos\alpha}{S_r S_t} \geq 0.08\frac{\sqrt{f_{ck}}}{f_{yk}}$	$s_{t,\max} \leq 0.75 d \leq 600\,\text{mm}$ $s_{\max} = 0.75 d(1+\cot\alpha)$		One-way shear and two-way shear

6.14 Discussion

Most design codes provide simple or general methods for beams along with simple rules on the required minimum shear reinforcement, and such requirements are usually sufficient enough for beam designs. The situation is different for slab designs, as most design codes generally try to avoid shear reinforcement requirements. However, such simple and conservative design methods provided by different design codes are not sufficient for thick plates where there is a good possibility of brittle failure due to punching shear cracks. A consistent procedure for design along with minimum shear

reinforcement requirements for such thick plates is practically sufficient. Minimum shear reinforcement is provided for plates to avoid shear cracks, help maintain the aggregate interlock after shear cracking, reduce shear crack openings and increase the strength by10 % to 30 % (Vaz et al. 2009). One more reason to provide shear reinforcement requirements is to allow using a slab with a large amount of flexural reinforcement ratio. Tests performed by Jaeger and Marti (2009) revealed that the addition of transverse reinforcements with reinforcement ratios of approximately 0.3% and 0.6% changed the failure modes to ductile flexural failures; the tests without transverse reinforcements showed a significant influence of slab thickness on shear strength. No such size effect was observed for the tests with transverse reinforcement. Codes thus specify upper limits to the shear capacity (V_u), which is a function of the concrete compressive strength. It should also be noted that due to the difficulties of anchoring shear reinforcement in thin slabs, the EC 2 (2004) stipulate a minimum slab thickness of 200 mm. Below this minimum slab thickness, one is not permitted to increase the shear capacity by providing shear reinforcement. In order that the presence of shear reinforcement may enhance the shear strength of a section, it is necessary that it should raise the shear capacity above the shear cracking load. Codes of practice give the minimum amount of shear reinforcement that is necessary to satisfy the requirements for beams, but in general, this does not apply to slabs. This is because, very often, in past practice, shear reinforcement has not been provided in slabs that have performed satisfactorily in service. In addition, it is thought that a slab has the ability to redistribute shear forces from weak to adjoining strong areas.

6.15 Summary

- The analytical study revealed that the torsional moment (M_{xy}) effect is an important factor in determining the minimum flexural reinforcement ratio for thick concrete plates and should be taken into account.
- In this chapter a new equation is developed to calculate minimum flexure reinforcement for thick concrete plates. The main contribution of this equation is to account for the torsional moment and the size effect factor. The proposed equation [Eq. (6.28)] can be applied to calculate minimum flexural reinforcement in each of the two orthogonal directions on both faces for thick concrete plates or walls more than 200 mm thickness.
- This chapter also presents two methods that can be used to calculate minimum shear reinforcement required to prevent brittle shear failure for thick concrete plates and walls in the vicinity of concentrated loads. The first method is based on the diagonal shear cracking load while the second method is based on the modified compression field theory. Both methods account for the slab size effect by using principles of fracture mechanics.
- It is recommended that the shear reinforcement zone be extended to a distance of $2d$ from the column face.
- It is recommended also that a slab in which minimum shear reinforcement is provided to have a depth of at least 250 mm, this value is equal to the measured characteristic length for normal strength concrete. This recommendation is also based on previous research done at Memorial University.

Chapter 7

Estimate of Crack Spacing and Crack Width for Thick Concrete Plates and Two-Way Slabs

7.1 Introduction

The use of thick concrete covers in offshore applications is increasing because it is a durability issue. Most crack width models indicate that increasing concrete covers results in increased crack spacing and hence increased crack width. This means thick concrete covers are detrimental to crack control. One of the objectives of this research is to evaluate the accuracy of design codes models when dealing with thick plates having thick concrete covers. Little attention has been paid in determining the crack spacing and width in reinforced concrete thick plates. A lack of available research data on the prediction of crack properties results in unnecessary over design of steel reinforcement to satisfy conservative crack requirements in codes for offshore structures.

This chapter provides a rational method for designers to calculate crack spacing for thick plates and two-way concrete slabs. An accurate estimate of the crack spacing and crack width of thick concrete plates used for offshore and nuclear power plant structures can result in reduction of steel reinforcement. The saving of steel reinforcement to satisfy the crack width limitations can be estimated in millions of dollars for a single project (Hibernia oil platform). A new analytical equation to calculate crack spacing for plates and two-way concrete slabs has been developed. The new equation combines the known bond stress effect with the contribution of splitting bond stress in the transverse direction due to the action of two-way slabs. The new equation gives a good estimate for crack

spacing in plates and two-way slabs with concrete covers equal to ($C_c < 2.5\ d_b$). The proposed method can also be modified and used for thick concrete covers, C_c=2.5–5.0 d_b.

7.2 Crack Spacing

Crack control equations for beams underestimate the crack width developed in plates and two-way slabs (Nawy and Blair 1971). The behaviour of reinforced concrete plates and two-way slabs is different from that of one-way slabs and beams. Hence, the methods developed for beams cannot be directly applied to plates and two-way slabs. The expression for crack spacing is based on the beam theory in several codes, such as the Canadian offshore code CSA-S474-04, Norwegian Code 3473E (1989) and European CEB-FIP (1990) model code. With the extensive use of thick concrete plates with thick concrete covers for offshore and nuclear containment structures, the development of new formulae is needed to predict crack spacing and width for plates and two-way concrete slabs.

7.3 Mechanism of Bond Transfer

Although adhesion and friction are present when a deformed bar is loaded for the first time, these bond transfer mechanisms are quickly lost, leaving the bond to be transferred by bearing on deformations as shown in Figure 7.1a.

Equal and opposite bearing stresses act on the concrete as shown in Figure 7.1b. The forces on the concrete have a longitudinal and a radial component (Figure 7.1c and 7.1d). The latter causes circumferential tensile stresses in the concrete around the bar. Eventually, the concrete will split parallel to the bar and the resulting crack will propagate out to the surface of the section. Once these cracks develop, the bond transfer

drops rapidly unless reinforcement is provided to restrain the opening of the splitting crack.

The load at which splitting failure develops is a function of: the minimum distance from the bar to the surface of the concrete or to the next bar. The smaller this distance, the smaller the splitting load; the tensile strength of the concrete; and the average bond stress. As the average bond stress increases, the wedging forces increase, leading to a splitting failure.

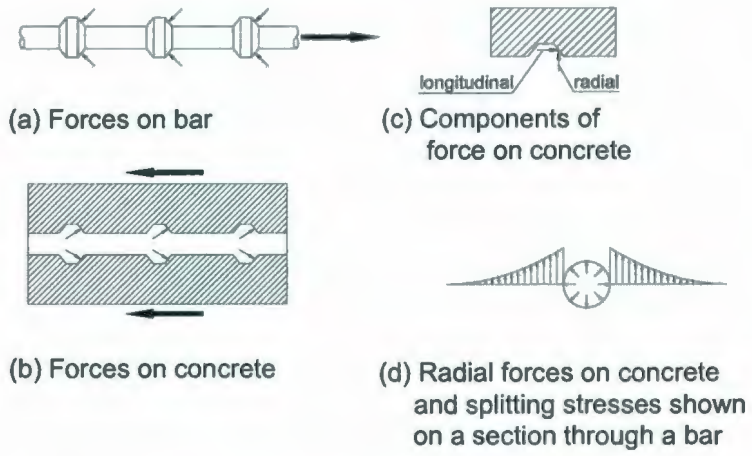

Figure 7.1: Bond transfer mechanism

If the cover and bar spacing are large compared to the bar diameter, a pull-out failure can occur, where the bar and the annulus of concrete between successive deformations pull out along a cylindrical failure surface joining the tips of the deformations

7.4 Analytical Model

7.4.1 Bond Stress Distribution

For a concrete section between two successive cracks in a tensile test specimen, zero bond stresses at the two cracked sections and at the mid-point can be assumed. Variation of the bond stress between these two zero-points (between the mid-point and the nearest cracked section) was established by many researchers (Jiang et al. 1984 and Kankam 1997) based on experimental results. In the present research, it is further assumed that the peak bond stress occurs at the mid section between the two zero points, with a parabolic variation. These two assumptions greatly simplify the mathematical formulation in calculating the bond stress. The resulting bond stress distribution closely agrees with the experimental observations (Jiang et al. 1984 and Kankam 1997). The resulting parabolic bond stress distribution between two successive flexural cracks is shown in Figure 7.2b.

Figure 7.2 shows a cross-section of a slab and the layout of reinforcement in the directions X and Y. As shown in Figure 7.2, stretching bars in direction X with the concrete surrounding the bars will result in another crack at a distance $x = s_{mx}$. At the same time because, from the two-way action of slabs, stretching the bars in a perpendicular direction results in splitting circumferential forces in direction X. A sufficient bond force is developed at this location ($x = s_{mx}$) that together with the splitting stresses along the transverse bars is just large enough to induce a maximum tensile stress equal to the tensile strength of concrete.

7.4.2 Longitudinal Steel Reinforcement (Loading Direction)

The equilibrium of forces acting on concrete to the left and right of section 1-1 in direction X as shown in Figure 7.2a for a unit width of the slab in direction Y is considered:

$$\frac{2}{3}\pi d_{bx} f_{bo} s_{mx} n_x + \text{contribution of transverse steel reinforcement} = k_t f_{ctm} A_{ctx} \quad (7.1)$$

The constant k_t accounts for the distribution of tensile stress in section 1-1 on the effective area of concrete, A_{ctx} and f_{ctm} is the mean tensile strength value of the concrete that is calculated according to the CEB-FIP (1990) model code.

The number of bars per unit width in X direction is n_x, the peak bond strength is f_{bo}, calculated using the CEB-FIP (1990) Model Code equation. The CEB-FIP (1990) Model Code (table 3.1.1) provides the following expression for calculating peak bond stress for confined and unconfined concrete for different bond conditions:

$$f_{bo} = \mu\sqrt{f_c'} \quad \text{(MPa)} \quad (7.2)$$

For cases where failure is initiated by splitting of the concrete (unconfined concrete), the coefficient μ is taken equal to unity and hence f_{bo} is calculated as follows:

$$f_{bo} = 1.0\sqrt{f_c'} \quad \text{(MPa)} \quad (7.3)$$

It should be noted that Eq. (7.3) is only valid for concrete covers equal or less than 2.5 d_b ($C_c \leq 2.5\ d_b$), C_c is the clear concrete cover; for plates and two-way slabs with thick concrete covers greater than the radius of the effective embedment zone ($C_c > 2.5\ d_b$), a value of 0.75 for the coefficient μ will be more consistent, so Eq. (7.3) can be written as follows:

$$f_{bo} = 0.75\sqrt{f_c'} \quad \text{(MPa)} \quad (7.4)$$

This is due to the fact that such plates act as cross sections that contain two separate materials, a reinforced concrete part and a plain concrete part.

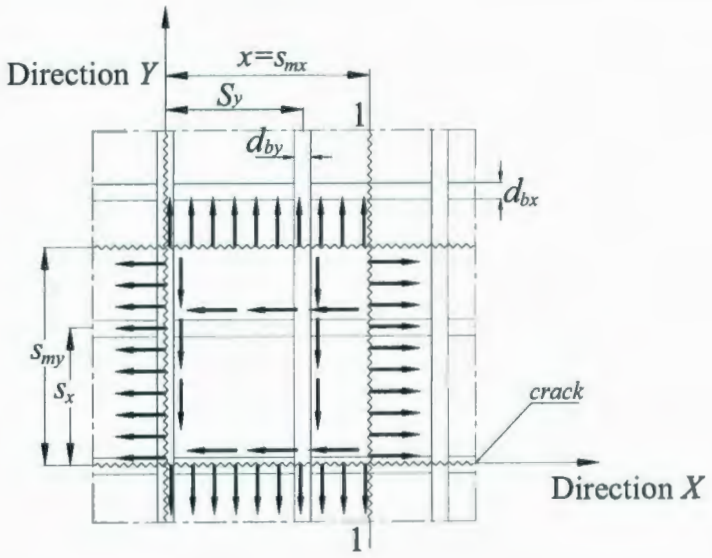

(*a*) A plan of a two-way plate

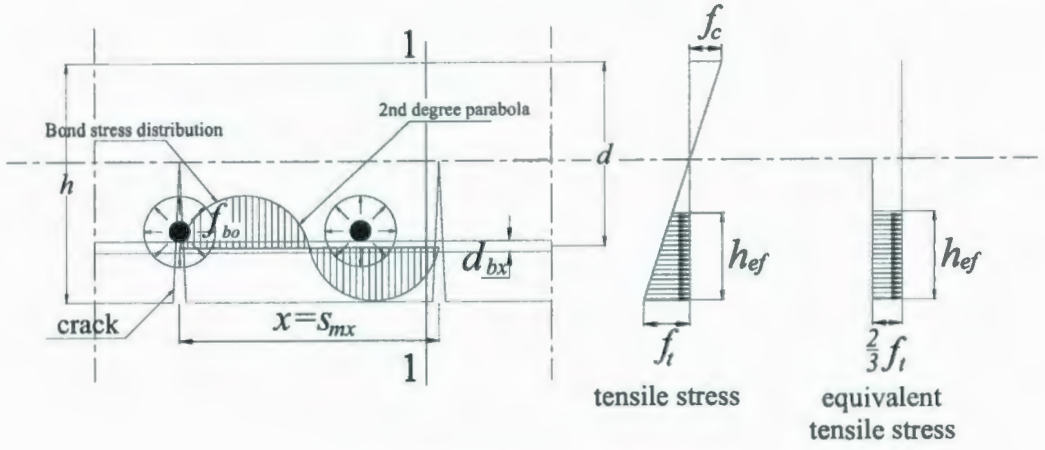

(*b*) Cross section of two-way plate

Figure 7.2: Distribution of bond stress, splitting stress and tensile stress over a section: (*a*) A plan of a two-way plate; (*b*) Cross section of two-way plate

7.4.3 Transverse Steel Reinforcement and Splitting Bond Stress

The contribution of the transverse steel reinforcement is considered through splitting bond stress. A concrete cylindrical prism with a diameter of c_s (diameter of effective

embedment zone), containing a bar with a diameter of d_b, as shown in Figure 7.3c is considered. The radial components of the forces on the concrete, shown in Figure 7.3a and 7.3b, cause a pressure p on a portion of the cross section of the prism. This is equilibrated by tensile stresses in the concrete on either side of the bar. In Figure 7.3a, the distribution of these stresses has been previously assumed to be parabolic, this assumption has been found to provide more consistent values compared to the experimental results. Splitting is assumed to occur when the maximum stress is equal to the tensile strength of the concrete f_{ctm}. For equilibrium in the transverse direction in a prism with a length equal to l_y,

$$\frac{P d_b l_y}{2} = K\left(\frac{c_s}{2} - \frac{d_b}{2}\right) f_{ctm} l_y \tag{7.5}$$

where K is the ratio of the average tensile stress to the maximum tensile stress and equals 0.33 for the parabolic stress distribution. A rearrangement gives:

$$P = 0.33\left(\frac{c_s}{d_b} - 1\right) f_{ctm} \tag{7.6}$$

where c_s is the diameter of the effective embedment zone where the reinforcing bar can influence the concrete bond, is also known as the diameter of the splitting cylinder, arbitrarily taking c_s = (3.0-3.5) d_b, and d_b is the bar diameter. For a triangular stress distribution, K can be assumed equal to 0.5 (Macgregor and Bartlett 2000).

The contribution of the transverse splitting bond can be estimated by considering the equilibrium of forces acting on concrete to the left and right of section 1-1(Figure 7.2a), and the unit width of the slab in transverse direction Y:

$$\text{Contribution of transverse steel reinforcement} = K\left(c_s - d_{by}\right) f_{sp,t} l_y \tag{7.7}$$

The different components of the right hand side of Eq. (7.7) can be estimated as follows: The splitting bond stress $f_{sp,t}$ can be assumed to be equal to f_{ctm}. The diameter of the effective embedment zone $c_s = 3.0\ d_{by}$. The length of the effective embedment zone l_y is taken equal to the slab unit width. Therefore, Eq. (7.7) can be written as follows for a unit width in the Y direction:

$$\text{Contribution of transverse steel reinforcement} = 0.33\left(3\,d_{by} - d_{by}\right) f_{ctm} \tag{7.8}$$

The contribution of the splitting bond stress determined from Eq. (7.8) can be substituted into Eq. (7.1), representing the equilibrium forces in direction X to determine the crack spacing as follows:

$$\frac{2}{3}\pi\, d_{bx}\, f_{bo}\, s_{mx}\, n_x + 0.33\left(2\,d_{by}\right) f_{ctm} = k_t\, f_{ctm}\, A_{ctx} \tag{7.9}$$

The crack spacing formed in direction X, can be estimated as follows:

$$s_{mx} = \frac{k_t\, f_{ctm}\, A_{ctx} - 0.67\, d_{by}\, f_{ctm}}{\frac{2}{3}\pi\, d_{bx}\, f_{bo}\, n_x} \tag{7.10a}$$

Similarly, the spacing of cracks formed in direction Y, can be estimated as follows:

$$s_{my} = \frac{k_t\, f_{ctm}\, A_{cty} - 0.67\, d_{bx}\, f_{ctm}}{\frac{2}{3}\pi\, d_{by}\, f_{bo}\, n_y} \tag{7.10b}$$

Eq. (7.10a) and (7.10b) give the crack spacing in directions X and Y respectively at a given stage of loading. The proposed model suggests that increasing bar diameter d_b will result in decreased crack spacing and hence decreased crack width. Also increasing the number of bars (decreasing bar spacing) will result in decreasing crack spacing and hence achieving required crack control. In order to use the above expression, values of k_t, A_{ctx}, A_{cty}, f_{ctm} and f_{bo} must be estimated. The constant k_t is a tensile stress factor that depends on

the distribution of tensile stress on concrete areas A_{ctx} and A_{cty}. k_t is the ratio of the average tensile stress area to the actual tensile stress area within the effective embedment thickness h_{ef}. For thick plates, the tensile stress distribution within the effective embedment thickness is trapezoidal and hence k_t could be assumed equal to 0.67-1.0. In the proposed expression, for plates and two-way slabs having concrete covers of ($C_c < 2.5$ d_b), tensile stress on the concrete is assumed to be uniformly distributed and hence k_t can be taken as equal to unity (Desayi and Kulkarni 1976). For thick plates and two-way slabs with thick concrete covers that are greater than 2.5 d_b and less than 5.0 d_b, tensile stress distribution on the concrete is assumed to be trapezoidal and hence k_t can be taken as equal to 0.67, this assumption was found more convenient. The values of A_{ctx} and A_{cty}, which are the effective stretched area of concrete in the X and Y direction, are assumed to be:

$$A_{ctx} = h_{efx}\, b \tag{7.11a}$$

$$A_{cty} = h_{efy}\, b \tag{7.11b}$$

where h_{ef} is the effective embedment thickness (as shown in Figure 2.3) as the greater of $a_1 + 7.5d_{be}^{'}$ and $a_2 + 7.5d_{be}^{'}$ but not greater than the tension zone or half slab thickness (mm); and b is the width of the section (mm).

7.5 Crack Spacing for Beams and One-Way Slabs

The proposed equation can be used to calculate the crack spacing for beams and one-way slabs by modifying the peak bond strength f_{bo}, according to the CEB-FIP (1990) Model Code provisions (table 3.1.1). For cases where failure is initiated by shearing of the concrete between the ribs (all other bond conditions), f_{bo} is calculated as follows:

$$f_{bo} = 1.25\sqrt{f_c^{'}} \quad \text{(MPa)} \tag{7.12}$$

The crack spacing can be estimated as follows:

$$s_m = \frac{k_t f_{ct} A_{ct}}{\frac{2}{3}\pi d_b f_{bo} n} \tag{7.13}$$

where n is the number of bars per unit width. The constant k_t is a tensile stress factor that depends on the distribution of tensile stress on concrete areas A_{ct}. In the present research, a value of 0.67 for the coefficient k_t was found to provide more consistent values for beams and one-way slabs compared to the experimental results.

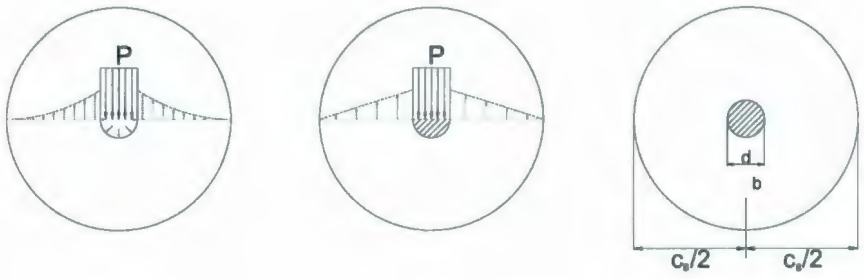

(*a*) (*b*) (*c*)

Figure 7.3: Stresses in a circular concrete prism subjected to bond stresses: (*a*) parabolic stress distribution; (*b*) triangular stress distribution; (*c*) diameter of the effective embedment zone

7.6 Discussion

7.6.1 Verification of Proposed Model

A total of twelve simply-supported beams and one-way slabs were subjected to constant sustained service loads for a period of 400 days by Gilbert and Nejadi (2004). Each specimen was prismatic, with a rectangular cross section (b = 250 mm and h = 348 mm for the six beams and b = 400 mm and h = 161 mm for the six one-way slabs) and a span of 3500 mm, and was carefully monitored throughout the test to record the time-

dependent deformation, together with the gradual development of cracking and the gradual increase in crack widths with time. The parameters varied in the tests were the shape of the section b/h, the number of reinforcing bars, the spacing between bars s, the concrete cover C_c, and the sustained load level. Details of Gilbert and Nejadi (2004) test specimens are provided in Table 7.1. The measured elastic modulus, compressive strength, and tensile strength of the concrete at the age of first loading were E_c = 22820 MPa, f_c' = 18.3 MPa, and f_{ct} = 2.00 MPa. A comparison between beam series 1 and 2 (Table 7.4) demonstrates that increasing the clear concrete cover increases the average crack spacing. This can be explained by the fact that the crack spacing s_{rm} is inversely proportional to the effective reinforcement ratio ρ_{eff}. Increasing the bottom cover increases the effective tension area of the concrete, and decreases the effective reinforcement ratio that results in larger crack spacing. In addition, increasing the tensile reinforcement area decreases crack spacing and reduces crack width (because crack spacing is inversely proportional to the effective reinforcement ratio).

Frosch et al. (2003) tested ten one-way slabs to determine the effects of bar spacing and epoxy coating thickness on crack width and spacing. The ten bridge deck specimens were designed to represent a full scale cut section from a bridge deck. Each specimen was prismatic, with a rectangular cross section (b = 914 mm and h = 203 mm and a span of 2438 mm. The primary variables evaluated in the study were the spacing of the reinforcement and the epoxy coating thickness. Complete details of all specimens are provided in Table 7.2. The parameters varied in the tests were the reinforcing bars type, the spacing between bars s and the sustained load level. The measured crack width and spacing were also compared to calculated crack width and spacing. Major conclusions

derived from this investigation included; load-deflection behavior was not affected by epoxy coating thickness; spacing of reinforcement significantly affected the width and spacing of cracks. As the reinforcement spacing decreased, the spacing of primary cracks decreased and the number of primary cracks increased; epoxy coating thickness significantly affected the width and spacing of primary cracks. In general, as epoxy coating thickness increased, both average and maximum crack widths also increased; and to calculate crack widths of epoxy coated bars, the calculation procedure must account for epoxy coating thickness. Crack widths for epoxy coated bars can be computed by multiplying a factor times the crack width computed for black bars.

In order to verify the validity of the new proposed model, the model was applied to predict the average crack spacing of normal weight concrete test slabs reported in the literature. The results indicate that there exists a very good correlation between theoretical and measured average crack spacing values and between theoretical and calculated average spacing values using CSA-S474-04 and NS 3474 E (1989) codes were very close to the experiments with about 5% error. In this chapter, the model has been applied to thirty tests, to predict the average crack spacing of beams, one-way and two-way concrete slabs. The geometry of test slabs, analysis and the results are shown in Tables 7.1-7.6 and include twelve test results of Gilbert and Nejadi (2004), ten test results of Frosch et al. (2003) with different concrete covers and different bar spacing, eight test results of Marzouk and Hossin (2009) with different concrete strengths, different concrete covers and different bar spacing.

For the proposed model, the overall average theory/test ratio was 1.03 with a S.D. of 0.15, giving strong support to the ability of the proposed model to evaluate the average

crack spacing in tested slabs. It is also worth emphasizing that the slabs analyzed and presented in Tables 7.1-7.3 cover many variables that influence crack spacing such as concrete strength, bar spacing and concrete cover. Bearing this in mind as well as the fact that the tests themselves are one-to-one scale models of the prototype and the inevitable scatter of test results in concrete behavior, the theoretical model developed here is an excellent representation of the physical behavior of tested specimens.

Tables 7.4-7.6 show a comparison between the calculated values of crack spacing with the measured experimental values reported by different researchers (Gilbert and Nejadi 2004; Frosch et al. 2003; and Marzouk and Hossin 2008). Analysis of the results given in Table 7.4-7.6 indicates that the new proposed model provides good estimates for crack spacing in slabs having small and thick concrete covers.

Figure 7.4 and 7.5 shows a comparison in the calculations for crack spacing between the new proposed model and different codes with the measured experimental values by Marzouk and Hossin (2008). Figures 7.4 and 7.5 indicate that the crack spacing values estimated using the presented model, CSA-S474-04, NS 3473 E (1989) and EC2 (2004) codes were very close to the experiments with about 5-9 % error. Codes expressions for crack spacing are based on the beam theory while the rational present model is based on two-way action.

Table 7.1–Details of test specimens by Gilbert and Nejadi (2004)

Beam	d_b, mm	No. of bars	A_s, mm^2	C_c, mm	s, mm	f_{st}, MPa
B1-a	16	2	400	40	150	227
B1-b	16	2	400	40	150	155
B2-a	16	2	400	25	180	226
B2-b	16	2	400	25	180	153
B3-a	16	3	600	25	90	214
B3-b	16	3	600	25	90	129
Slab	d_b, mm	No. of bars	A_s, mm^2	a	s, mm	f_{st}, MPa
S1-a	12	2	226	25	308	252
S1-b	12	2	226	25	308	195
S2-a	12	3	339	25	154	247
S2-b	12	3	339	25	154	171
S3-a	12	4	452	25	103	216
S3-b	12	4	452	25	103	159

Table 7.2–Details of test specimens by Frosch et al. (2003)

Slab*	Bar diameter d_b, mm	No. of bars	Clear cover C_c, mm	Spacing s, mm	f_y, MPa	Width b, mm	Height h, mm	f_c', MPa
B-6	16	6	38	152	469	914	203	47
B-9	16	4	38	229	469	914	203	44
B-12	16	3	38	305	469	914	203	45
B-18	16	2	38	457	469	914	203	47
E12-6	16	6	38	152	510	914	203	47
E12-9	16	4	38	229	510	914	203	46
E12-12	16	3	38	305	510	914	203	46
E12-18	16	2	38	457	510	914	203	47
E6-9	16	4	38	229	510	914	203	46
E18-9	16	4	38	229	510	914	203	46

*B-Black bars; E-Epoxy coated bars

Table 7.3–Details of test specimens by Hossin and Marzouk (2008)

Series No	Slab No.*	f_c', MPa	Bar size, mm	Bar spacing, mm	Clear cover C_c, mm	Slab thickness, mm	Steel ratio, ρ %
Series I	NSC1	35	25	150	30	200	2.17
	HSC1	69	25	150	50	200	2.48
	HSC2	70	25	150	60	200	2.68
Series II	HSC3	67	25	200	30	200	1.67
	HSC4	61	25	250	30	200	1.13
Series III	HSC5	70	15	100	30	150	1.88
	NSC2	33	15	240	30	200	0.52
	NSC3	34	10	210	40	150	0.40

*NSC-Normal strength slabs; HSC-High strength slabs

Table 7.4–Comparison between the calculated crack spacing values using code formulae with the measured experimental values for test specimens by Gilbert and Nejadi (2004)

Slab No.	Clear cover C_c, mm	Height h, mm	Bar spacing s, mm	f_c', MPa	NS/CSA	CEB	New proposed model	Exp. results
Beam 1-a	40	348	150	36	179	190	173	192
Beam 1-b	40	348	150	36	179	190	173	186
Beam 2-a	25	333	180	36	151	190	157	149
Beam 2-b	25	333	180	36	151	190	157	163
Beam 3-a	25	333	90	36	105	127	105	109
Beam 3-b	25	333	90	36	105	127	105	104
Slab 1-a	25	161	308	36	184	178	177	131
Slab 1-b	25	161	308	36	184	178	177	128
Slab 2-a	25	161	154	36	124	119	118	92
Slab 2-b	25	161	154	36	124	119	118	131
Slab 3-a	25	161	103	36	100	89	88	89
Slab 3-b	25	161	103	36	100	89	88	117

Table 7.5–Comparison between the calculated crack spacing values using code formulae with the measured experimental values for test specimens by Frosch et al. (2003)

Slab No.	Clear cover C_c, mm	Height h, mm	Bar spacing s, mm	f_c', MPa	NS/CSA	CEB	New proposed model	Exp. results
B-6	46	203	152	47	167	118	136	175
B-9	46	203	229	44	213	177	211	229
B-12	46	203	305	45	260	236	282	249
B-18	46	203	457	47	352	355	411	310
E12-6	46	203	152	47	167	118	136	170
E12-9	46	203	229	46	213	177	206	226
E12-12	46	203	305	46	260	236	278	257
E12-18	46	203	457	47	352	355	414	338
E6-9	46	203	229	46	213	177	207	203
E18-9	46	203	229	46	213	177	207	188

Table 7.6–Comparison between the calculated crack spacing values using code formulae with the measured experimental values for test specimens by Hossin and Marzouk (2008)

Slab No.	Clear cover C_c, mm	Slab thickness, mm	Bar spacing s, mm	f_c', MPa	NS/CSA	CEB	New proposed model	Exp. results
NSC1	30	200	150	35	125	77	126	134
HSC1	50	200	150	69	165	68	187	171
HSC2	60	200	150	70	186	63	188	185
HSC3	30	200	200	67	146	100	182	163
HSC4	30	200	250	61	167	125	184	172
HSC5	30	150	100	70	107	56	111	120
NSC2	30	200	240	33	204	204	225	223
NSC3	40	150	240	34	228	182	230	239

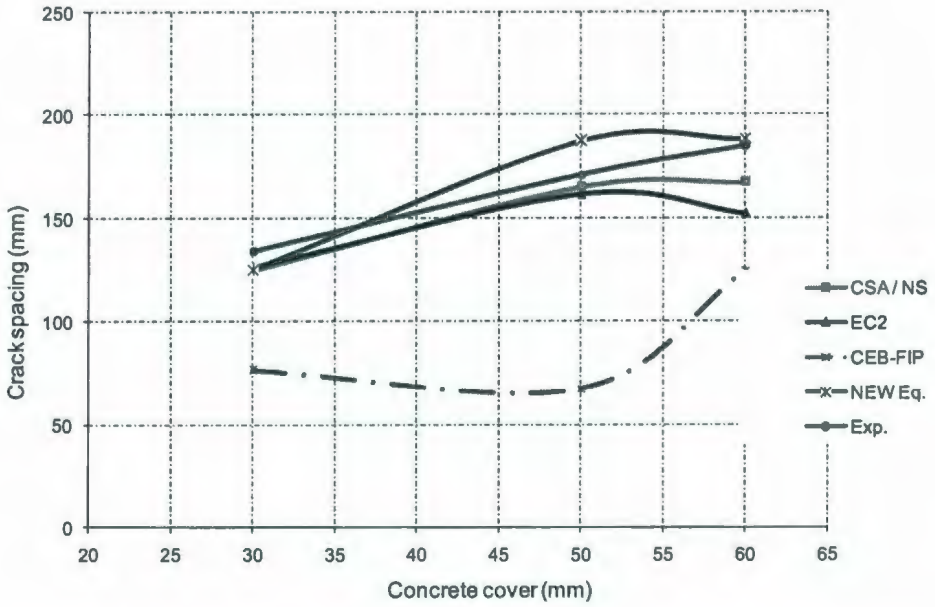

Figure 7.4: Comparison of crack spacing equations at 150 mm bar spacing

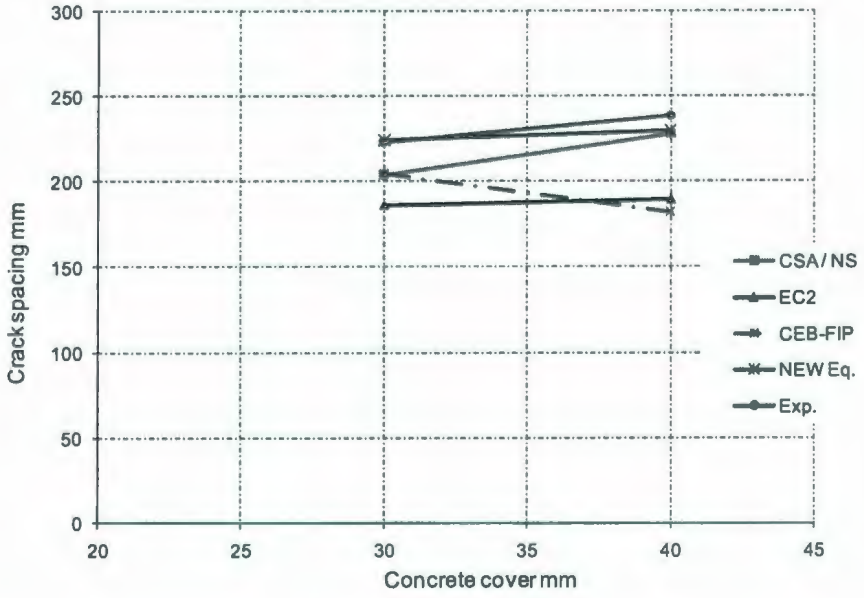

Figure 7.5: Comparison of crack spacing equations at 250 mm bar spacing

7.6.2 Comparison of Experimental and Theoretical Estimates of Crack Spacing

Table 7.7 shows a comparison between the calculated values of crack spacing with the measured experimental values. For bar spacing greater than 300 mm, the Norwegian code NS 3474 E (1989) and the Canadian offshore code CSA-S474-04 overestimates the average crack spacing by about 33%. In general, the calculated average crack spacing was higher than test results, and as both the concrete cover and bar spacing increased, the crack spacing increased theoretically and experimentally. For bar spacing less than 250 mm, the CEB-FIP (1990) model code underestimates the average crack spacing by about 31% compared to the one measured during testing.

Table 7.7–Comparison between the calculated crack spacing values using codes formulae with the measured experimental values

Group No.	Slab No.	Concrete cover C_c, mm	Slab thickness, mm	Bar spacing s, mm	f_c', MPa	NS 3474 /CSA-S474-04	CEB	New proposed model	Test results
A	NS1	45	150	210	45	211	137	248	201
	NS2	40	200	240	50	216	176	234	221
	NS3	60	250	368	35	341	279	320	245
	HS1	60	250	368	70	341	279	361	263
	NS4	70	300	368	40	331	225	273	261
	HS2	70	300	368	65	331	225	304	246
	HS3	70	300	368	75	371	300	386	247
B	HS4	70	350	368	76	301	176	304	221
	HS5	70	300	217	70	244	118	215	228
	HS6	70	350	289	70	276	160	273	264
	NS5	70	400	217	40	252	145	226	250
	HS7	70	400	217	60	252	145	249	210
Average						1.21	0.82	1.19	
Stdev						0.18	0.23	0.29	
Cov						0.14	0.27	0.17	

7.7 Crack Width

The crack width depends on the amount and distribution of reinforcing steel across the crack, concrete cover thickness and characteristics of the bond between the concrete and reinforcement bars. Using thick concrete covers in offshore applications is increasing because it is a durability issue, and also thick concrete covers resist and delay steel reinforcement corrosion. Most crack width models indicate that increasing concrete covers results in increased crack spacing and hence increased crack width this means that thick concrete covers are detrimental to crack control.

Experimental findings by Makhlouf and Malhas (1996) indicate that increasing concrete covers results in increased crack widths but at much smaller rate than the rate of increasing concrete covers, as suggested by most design codes. This means that thick concrete covers can be used to increase durability of offshore structures and at the same time crack control requirements are not violated.

An analytical investigation is presented in this chapter. The main focus of this study is to evaluate the available code models for estimating the crack width of concrete plates. The investigation focused on the suitability of available crack width expressions for thick concrete plates having thick concrete covers used for offshore concrete structure applications.

7.8 Characteristic Crack Width

7.8.1 Maximum Crack Width

The two important factors that determine the width of the crack are the crack spacing and the steel strain; both of these depend on the external loading on the slab. Crack spacing decreases with increasing load and stabilizes after reinforcement reaches a critical stress.

Further stress increases act only to widen existing cracks. The cracks that form at the stage of cracking moment are farthest apart, at this stage the spacing of cracks is the maximum crack spacing, S_{max}. With increased load, more cracks develop. When steel stress reaches a critical value, crack spacing stabilizes. Increasing the load acts only to widen the existing cracks.

Crack width at the level of reinforcement is determined as the relative difference in elastic extensions of steel and surrounding concrete, both extensions are measured with respect to the zero-slip point. The extension of steel at the cracked section ε_s is evaluated as follows:

$$\varepsilon_s = \frac{f_s}{E_s} \tag{7.14}$$

The corresponding contraction of concrete ε_c at the cracked section is determined as follows:

$$\varepsilon_c = \frac{2\pi f_{bo} S_m}{9 E_c h_{ef}} \tag{7.15}$$

where E_c is concrete modulus of elasticity. The average crack width at the extreme tension surface can be calculated as follows:

$$w_m = S_m \xi \varepsilon_{sm} \tag{7.16a}$$

$$w_m = S_m \xi \left(\varepsilon_s \frac{h_2}{h_1} - \varepsilon_c \right) \tag{7.16b}$$

where S_m is the average crack spacing (stabilized crack stage) obtained from Eq. (7.10), ξ is a dimensionless coefficient between 0 and 1, representing the effect of the participation of concrete in the tension zone to stiffness of the member [Eurocode 2 (2004)], ε_{sm} is the average strain in steel at the stage at which the crack width is determined, h_1 is the

distance from centroid of the tension steel to the neutral axis and h_2 is the distance from extreme tension fiber to the neutral axis. This follows from an assumption of linear variation of strain.

The tension stiffening contribution is estimated without consideration for the steel reinforcement ratio, size of the concrete cover and concrete member thickness. A tension stiffening model based on fracture mechanics concepts and tension properties of high-strength concrete was developed by Marzouk and Chen (1993). The model can account for the concrete mix design properties and the steel reinforcement contribution through two sets of constants.

The ratio between maximum crack width w_{max} and average crack width w_m had been suggested by Rizkalla and Hwang (1984) to be equal to 1.55. CEB-FIP (1990) recommended a value of 1.70 for flexural members. The maximum crack width at the extreme tension fiber is obtained from:

$$w_{max} = 1.55\, w_m \tag{7.17}$$

7.8.2 Crack Width for Beams and One-Way Slabs

The proposed equation can be used to calculate the maximum crack width for beams and one-way slabs by modifying the peak bond strength f_{bo}, according to the CEB-FIP (1990) Model Code provisions (clause 3.1.1). The average crack width can be calculated using Equation (7.14), (7.15) and (7.16).

7.9 Comparison of Calculated Crack Width Values with Different Code Predictions

In order to verify the validity of the proposed crack control model, the model was applied to predict the average crack width of normal weight concrete test slabs reported in the literature. The results indicate that there exists a very good correlation between

theoretical and measured average crack width values and between theoretical and calculated average crack width values using different codes formulae. In this chapter, the model has been applied to thirty tests, to predict the characteristic crack width of beams, one-way and two-way concrete slabs. The geometry of test slabs can be found in references (Gilbert and Nejadi 2004; Frosch et al. 2003; Marzouk and Hossin 2009), analysis and the results are shown in Tables 7.8-7.10 and include twelve test results of Gilbert and Nejadi (2004), ten test results of Frosch et al. (2003) with different concrete covers and different bar spacing, eight test results of Marzouk and Hossin (2008) with different concrete strengths, different concrete covers and different bar spacing.

For the proposed model, the overall average theory/test ratio was 1.04 with a S.D. of 0.33, giving strong support to the ability of the proposed model to evaluate the characteristic crack width in tested slabs. It is also worth emphasizing that the slabs analyzed cover many variables that influence crack width such as concrete strength, bar spacing and concrete cover. Bearing this in mind as well as the fact that the tests themselves are one-to-one scale models of the prototype and the inevitable scatter of test results in concrete behavior, the theoretical model developed here is an excellent representation of the physical behavior of tested specimens.

Table 7.8–Comparison between the calculated crack width values using code formulae with the measured experimental values for test specimens by Gilbert and Nejadi (2004)

Slab No.*	f_c' (MPa)	Bar spacing, mm	Concrete cover (mm) C_c	ACI w_k	CSA w_m	NS w_k	CEB-FIP w_k	EC2 w_k	Experiment w_k (mm)	Proposed Eq. w_k (mm)
B1-a	36	150	40	0.192	0.365	0.632	0.381	0.492	0.33	0.346
B1-b	36	150	40	0.192	0.365	0.632	0.381	0.492	0.38	0.346
B2-a	36	180	25	0.230	0.313	0.541	0.381	0.418	0.30	0.315
B2-b	36	180	25	0.230	0.313	0.541	0.381	0.418	0.43	0.315
B3-a	36	90	25	0.116	0.228	0.393	0.290	0.333	0.20	0.210
B3-b	36	90	25	0.116	0.228	0.393	0.290	0.333	0.20	0.210
S1-a	36	308	25	0.393	0.367	0.634	0.319	0.392	0.33	0.353
S1-b	36	308	25	0.393	0.367	0.634	0.319	0.392	0.28	0.353
S2-a	36	154	25	0.197	0.256	0.442	0.255	0.312	0.25	0.235
S2-b	36	154	25	0.197	0.256	0.442	0.255	0.312	0.25	0.235
S3-a	36	103	25	0.132	0.210	0.363	0.207	0.273	0.18	0.177
S3-b	36	103	25	0.132	0.210	0.363	0.207	0.273	0.23	0.177

*B-Beam; S-Slab

Table 7.9–Comparison between the calculated crack spacing values using code formulae with the measured experimental values for test specimens by Frosch et al. (2003)

Slab No.*	f_c' (MPa)	Bar spacing, mm	Concrete cover (mm) C_c	ACI w_k	CSA w_m	NS w_k	CEB-FIP w_k	EC2 w_k	Experiment w_k (mm)	Proposed Eq. w_k (mm)
B-6	47	152	38	0.229	0.368	0.373	0.330	0.462	0.381	0.304
B-9	44	229	38	0.343	0.469	0.477	0.430	0.560	0.483	0.471
B-12	45	305	38	0.456	0.571	0.580	0.487	0.657	0.457	0.630
B-18	47	457	38	0.684	0.773	0.786	0.473	0.852	0.381	0.919
E12-6	47	152	38	0.249	0.401	0.406	0.367	0.503	0.406	0.331
E12-9	46	229	38	0.373	0.511	0.519	0.485	0.609	0.635	0.501
E12-12	46	305	38	0.497	0.622	0.631	0.561	0.715	0.584	0.676
E12-18	47	457	38	0.745	0.843	0.855	0.583	0.927	0.787	1.006
E6-9	46	229	38	0.373	0.511	0.519	0.485	0.609	0.457	0.503
E18-9	46	229	38	0.373	0.511	0.519	0.485	0.609	0.584	0.504

*B-Black bars; E-Epoxy coated bars

Table 7.10–Comparison between the calculated crack spacing values using code formulae with the measured experimental values for test specimens by Hossin and Marzouk (2008)

Slab No.*	f_c' (MPa)	Bar spacing, mm	Concrete cover (mm) C_c	ACI w_k	CSA w_m	NS w_k	CEB-FIP w_k	EC2 w_k	Experiment w_k (mm)	Proposed Eq. w_k (mm)
NSC1	35	150	30	0.192	0.336	0.341	0.439	0.467	0.406	0.278
HSC1	69	150	50	0.192	0.409	0.419	0.350	0.536	0.772	0.638
HSC2	70	150	60	0.193	0.447	0.458	0.333	0.570	0.950	0.873
HSC3	67	200	30	0.256	0.403	0.412	0.428	0.544	0.486	0.404
HSC4	61	250	30	0.319	0.477	0.488	0.472	0.627	0.483	0.468
HSC5	70	100	30	0.129	0.200	0.204	0.137	0.263	0.327	0.286
HSC6	33	240	30	0.307	0.377	0.383	0.393	0.455	0.248	0.439
NSC2	34	240	40	0.307	0.333	0.338	0.207	0.348	------	0.438

*NSC-Normal strength slabs; HSC-High strength slabs

Table 7.11–Comparison between the calculated crack width values using code formulae with the measured experimental values

Series No	Slab No.*	Experiment w_k (mm)	Proposed Eq. w_k (mm)	ACI w_k (mm)	CSA w_m (mm)	NS w_k (mm)	CEB-FIP w_k (mm)	EC2 w_k (mm)
I	NS1	----	0.497	0.269	0.393	0.401	0.226	0.431
	NS2	----	0.496	0.307	0.403	0.411	0.307	0.470
	NS3	0.465	0.640	0.470	0.638	0.649	0.413	0.707
	HS1	0.402	0.722	0.470	0.634	0.649	0.294	0.707
	NS4	0.714	0.546	0.470	0.619	0.630	0.493	0.709
	HS2	0.596	0.609	0.470	0.615	0.630	0.415	0.709
	HS3	0.362	0.773	0.470	0.688	0.705	0.326	0.797
II	HS4	0.581	0.741	0.470	0.662	0.679	0.431	0.791
	HS5	0.876	0.486	0.278	0.445	0.456	0.265	0.562
	HS6	0.435	0.688	0.370	0.514	0.526	0.371	0.648
	NS5	0.439	0.541	0.278	0.471	0.480	0.366	0.628
	HS7	0.469	0.380	0.278	0.469	0.480	0.348	0.628

*NS-Normal strength slabs; HS-High strength slabs

7.10 Summary

- Most of the available expressions for estimating the crack spacing and width are based on test results for beams and one-way slabs. The behaviour of reinforced concrete plates and two-way slabs is different from the behaviour of beams.
- A new theoretical expression is recommended for plates and two-way slabs with longitudinal and transverse reinforcements. The proposed method takes into consideration, the effects of steel bond in the loading direction and the contribution of the splitting bond stresses for the transverse steel. The proposed equation gives a good estimate for crack spacing in plates and two-way slabs with concrete covers equal to ($C_c < 2.5\ d_b$). The proposed method can be used for thick concrete covers, ($C_c = 2.5 - 5.0\ d_b$) plates and two-way slabs after reducing one third of the tensile stress constant k_t. However, for two-way slabs with concrete covers larger than 5.0 d_b, it can be speculated that the crack spacing behaves randomly. This is due to the fact that such slabs act as cross sections that contain two separate materials.
- Crack control can be achieved by limiting bar spacing. The proposed model in Eq. (7.10) or (7.13) allows designers to specify bar spacing during the design process to control flexural crack width to an acceptable limit.
- For bar spacing greater than 300 mm, the entire existing models estimate average crack spacing higher than the one measured during testing. For bar spacing less than 250 mm, the CEB-FIP (1990) model code estimates average crack spacing smaller than the one measured during testing. The test results revealed that crack

spacing is increased as the bar spacing or the concrete cover is increased for the specimens with low reinforcement ratio that fail under flexure.

- The analytical investigation reveals that the crack widths calculated using CSA-S474-04 and NS 3473 E (1989) are relatively close.

Chapter 8

Minimum Shear Reinforcement for Thick Concrete Plates Based on a Strut-and-Tie Model

8.1 Introduction

Concrete slabs without shear reinforcement usually exhibit brittle shear failure under central force that is transferred between the column and slab. Shear reinforcement has been proven to be very effective in preventing such failures. Conventional design methods consider potential punching failures in the vicinity of concentrated loads. Nominal shear stresses at well-defined critical sections are limited to guard against such failure modes. With the extensive use of thick plates made of high strength concrete for offshore structures and nuclear containment structures, shear reinforcement must be provided by different codes of practice for such thick plates. The strut-and-tie method considers the flow of forces in a reinforced concrete element to consist of a series of compressive struts and tension ties joined at nodes. The strut-and-tie method is a rational approach to structural concrete design which results in a uniform and consistent design philosophy. A strut-and-tie model has been developed to model the punching shear behaviour of a concrete slab. This model provides a quick and simple approach to punching shear behaviour. It is applicable for both normal and high strength concrete slabs under symmetric loading; with and without shear reinforcement. The developed strut-and-tie model has been also used to evaluate the minimum shear reinforcement required to prevent brittle shear failure of two-way slabs in the vicinity of concentrated loads. The strut-and-tie model for symmetric punching consists of a "bottle-shaped" compressive zone in the upper section of the slab depth leading to a "rectangular-stress"

compressive zone in the lower section depth. Inclined shear cracking develops in the bottle-shaped zone prior to failure in the lower zone. Cracking in the bottle-shaped zone is related to the splitting tensile strength of the concrete. Ultimate punching failure occurs in the rectangular-stress zone by a high radial compressive stress failure. An equation based on failure criteria for the strut-and-tie method is used to model the behaviour in the lower compressive stress zone. The results of the strut-and-tie model for symmetric punching shear behaviour were compared to experimental test results performed and published by others. The results of the strut-and-tie model show excellent agreement with available test results.

8.2 Bottle-Shaped Strut

Bottle-shaped struts are assumed to exist at the slab-column connection based on the shape of punching shear cracks that develop in the vicinity of slab-column connection at a load level less than the ultimate punching shear load. The bottom node represents the bearing at the column head. The top node represents physical surface failure crack, also represents the stress concentration at the crack perimeter. Narrow plate-like rectangles represent stress field near the column.

A strut-and-tie model is a system of forces in equilibrium with a given set of loads. In a strut-and-tie model, the struts represent concrete compression stress fields with the prevailing compression in the direction of the strut. Struts are frequently idealized as prismatic or uniformly tapering members, but often vary in cross section along their length, as shown in Figure 8.1b, since the concrete is wider at mid-length of the strut than at the ends. Struts that vary in width are sometimes idealized as bottle-shaped as shown in Fig. 8.1b, or are idealized using local truss models as shown in Figure 8.1d. The spreading of

the compression forces gives rise to transverse tension as shown in Figure 8.1a that may cause the strut to crack longitudinally. If the strut has no transverse reinforcement, it may fail after cracking occurs. If adequate transverse reinforcement is provided, the strut will fail by crushing. In strut-and-tie models, the compression struts are shown by dashed lines along the axes of the struts.

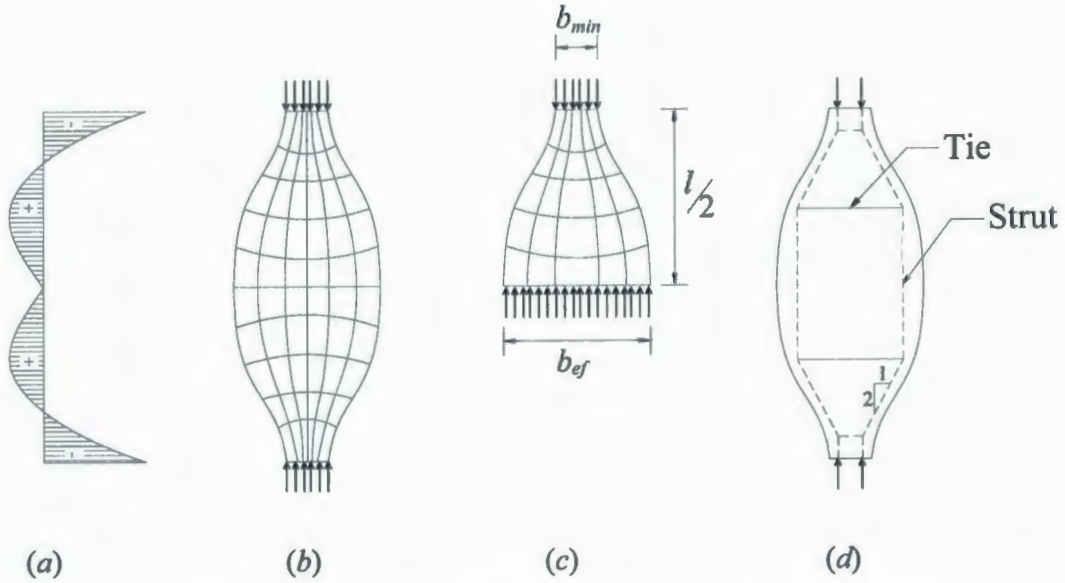

Figure 8.1: Strut-and-tie model for bottle-shaped strut; (*a*) Transverse stress distribution; (*b*) Compression isostatics; (*c*) Elastic distribution; (*d*) equivalent strut-and-tie model

8.2.1 Strut Failure by Longitudinal Cracking

Figure 8.1c shows one end of a bottle-shaped strut. The width of the bearing area is b_{min}, and the thickness of the strut is t. At mid-length, the strut has an effective width b_{ef}. Schlaich and Weischede (1982) assumed that a bottle-shaped region at one end of a strut extended approximately 1.5 b_{ef} from the end of the strut and proposed the value of $b_{ef} = l/3$ but not less than b_{min}, where l is the length of the strut from face-to-face of the nodes. For short

struts, the limit that b_{ef} is not be less than b_{min} often governs. Based on the assumption made by Rogowsky and Marti (1991), the longitudinal projection of the inclined struts is equal to $b_{ef}/2$. The transverse tension force T at one end of the strut could be calculated as follows:

$$T = \frac{C}{2}\left(\frac{b_{ef}/4 - b_{min}/4}{b_{ef}/2}\right) \tag{8.1}$$

$$T = \frac{C}{4}\left(1 - \frac{b_{min}}{b_{ef}}\right) \tag{8.2}$$

The force T causes transverse stresses in the concrete that may cause cracking along the axis of the strut. The transverse stresses are distributed as shown in Figure 8.1a by the curved line. Analyses by Adebar and Zhou (1993) suggested that the tensile stress distributions at the two ends of a strut are completely separate when l/b_{min} exceeds 3.5, and overlap completely when l/b_{min} is 1.5 to 2. The maximum load on an unreinforced conical-shape strut in a plate-like member is governed by longitudinal cracking of the concrete in the strut, and is given by equation (8.3), assuming a unit width for the 3D conical strut.

$$C = 0.57 b_{min} f_c' \tag{8.3}$$

Reinforcement crossing the strut will restrain the opening of the crack and hence increases the capacity of the strut. Brown and Oguzhan (2006) determined the necessary amount of minimum transverse reinforcement for a bottle-shaped strut to control cracking. A minimum equivalent reinforcement ratio of 0.003 was recommended to control crack width considering shear slip formulation along the splitting crack. This value is in agreement with requirements of ACI 318-08. The CSA-A23.3-04 standard requires the ratio to be only 0.2% in each direction. The researchers recommended that the use of

bottle-shaped strut without transverse reinforcement should not be permitted regardless of efficiency factor. A minimum amount of reinforcement should be used to compensate for effects of temperature, restrained shrinkage, and other effects that may not be explicitly taken into account.

8.3 Minimum Shear Reinforcement Based on Strut-and-Tie Model

In this model, the width of the bearing area b_{min} is assumed to be equal to 0.25 multiplied by the effective width of a bottle-shaped strut b_{ef}. The angle of the failure plane θ (the angle between the reinforcement and the axis of the strut) normally varies between 22° and 45°. The transverse stress distribution is assumed to be a second degree parabola, the maximum tensile stress value is assumed to be equal to the splitting tensile strength of concrete $f_{sp,t}$.

8.3.1 Evaluation of Transverse Tensile Forces acting on a Bottle-Shaped Strut

Based on the strut-and-tie model used to describe a bottle-shaped strut, the amount of transverse reinforcement (slab shear reinforcement) (Fig. 8.1d) can be calculated. The geometry of the assumed bottle-shaped strut is shown in two-dimensional (Figure 8.2) for simplicity; however, it is actually three-dimensional "cone-shaped" bottle-shaped strut located around the perimeter of the column. The compression forces are held together by perpendicular tensile forces in the concrete. Cracking occurs when the stress in these tensile zones equal to or exceed the splitting tensile strength of the concrete $f_{sp,t}$, which is defined as the mean value of splitting tensile strength determined according to ASTM C496-96. Given that, when the splitting crack occurs, a sudden rupture of the slab occurs with a total loss of strength, it is important that the slab contains a minimum shear reinforcement to prevent brittle failure. Considering the failure plane to be inclined at an

angle θ to the slab axis (Figure 8.3), from the equilibrium of forces in the vertical direction along a projected length of the failure plane (l cot θ), the minimum shear reinforcement is calculated as follows:

Assuming a slab unit width, the maximum tensile force resultant is equal to the area under the transverse tensile stress distribution curve (Figure 8.3) multiplied by the slab unit width:

$$T = 2\frac{2}{3} f_{sp,t} (0.35l) = 0.47 f_{sp,t} l \tag{8.4}$$

where $f_{sp,t}$ is the splitting tensile strength, given by CEB-FIP (1990) model code as follows:

$$f_{sp,t} = 1.11 f_{ctm} \tag{8.5}$$

where f_{ctm} is the mean tensile strength value of the concrete that is calculated according to the CEB-FIP (1990) model code and l is the length of the strut. Considering the failure plane to be inclined at an angle θ to the slab axis, from the equilibrium of forces in the vertical direction along a projected length of the failure plane (l *cot* θ), the minimum shear reinforcement could be calculated as follows:

$$A_{z,\min} f_y = T \cos\theta \tag{8.6}$$

the maximum tensile force resultant is evaluated as follows:

$$T = 0.47 f_{sp,t} l \tag{8.7}$$

For a slab unit width,

$$A_{z,\min} = \rho_{z,\min} \; l \cot\theta \tag{8.8}$$

$$\rho_{z,\min} = \frac{A_{z,\min}}{l \cot\theta} \tag{8.9}$$

Substituting the value for T calculated using equation (8.7) into equation (8.6), equation (8.9) could be written as follows:

$$\rho_{z,\min} = 0.47 \frac{f_{sp,t}}{f_y} \sin\theta = 0.52 \frac{f_{ctm}}{f_y} \sin\theta \tag{8.10}$$

Introducing the term $(l_{ch}/h)^{0.33}$ to account for the size effect, again equation (8.10) could be written as follows:

$$\rho_{z,\min} = 0.52 \frac{f_{ctm}}{f_y} \sin\theta \frac{1}{(l_{ch}/h)^{0.33}} \tag{8.11}$$

For θ=30°, $\rho_{z,\min} = 0.26 \frac{f_{ctm}}{f_y} \frac{1}{(l_{ch}/h)^{0.33}}$ (8.12)

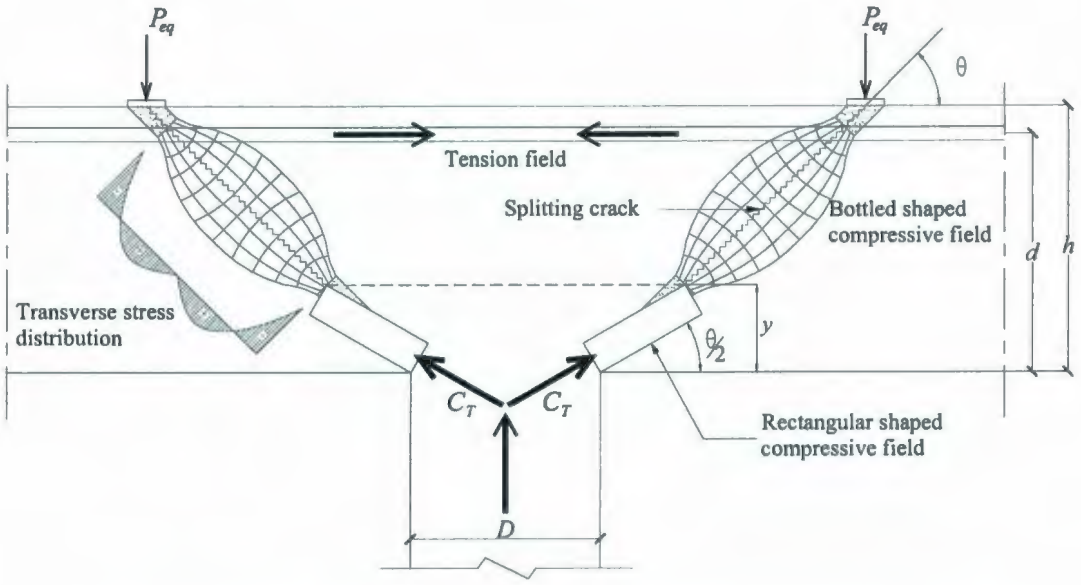

Figure 8.2: Stress fields generated in a slab column connections after cracking

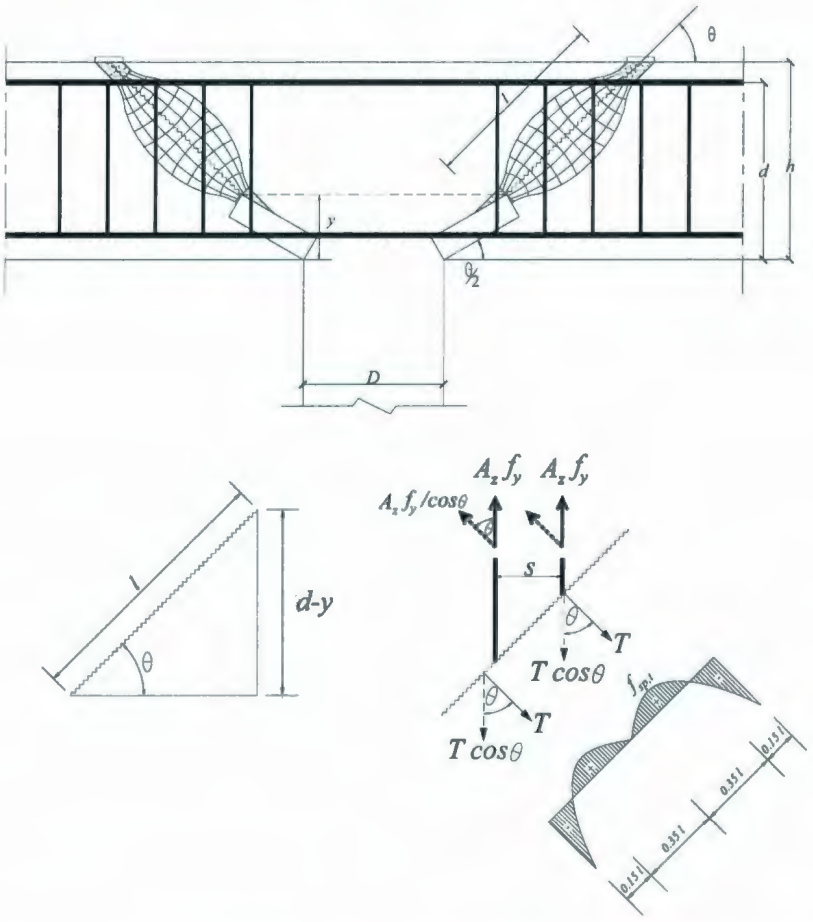

Figure 8.3: Strut and tie model for a slab column connection reinforced with minimum shear reinforcement

8.4 Proposed Strut-and-Tie Model for Punching Shear of Concrete Slabs

8.4.1 Symmetric Punching Shear of Concrete Slabs

Figure 8.5 shows the general punching shear behavior of a uniformly loaded slab supported by a circular column. The applied uniform load can be replaced by an equivalent point load. The inclined shear crack that develops from the top surface at an angle θ, and forming the critical section is shown. Punching of the slab occurs when the concrete in the ultimate failure zone fails by a high concrete compression stress. For

normal strength concrete, the angle of inclination θ has been experimentally determined to be between 26 and 30 degrees, whereas for high strength concrete the angle varies between 32 and 38 degrees as determined through experimental testing by Marzouk and Hussein (1991) at Memorial University of Newfoundland. Hegger et al. (2006) found that the observed angle of the failure cone was approximately 45° in all tested specimens. Hallgren et al. (1998) found that the shear crack propagated from the plane of the flexural reinforcement to the slab-column root was at an angle of about 50° to 60°, measured between the shear crack and the horizontal plane. This is a considerably steeper angle than the shear crack angles observed in punching shear tests of more slender slabs.

8.4.2 Stress Fields, Strut-and-Tie Model

Figure 8.2 shows the stress fields in the slab due to symmetric punching shear. The crack zone is made up of a bottle-shaped compression field in which the tensile strength of the concrete perpendicular to this field controls cracking. The ultimate failure zone is a rectangular-shaped compression field. From these stress fields, a refined strut-and-tie model is developed as indicated in Figure 8.4. The zones in these figures are shown in two-dimensional for simplicity; however, they are actually three-dimensional "cone-shaped" fields located around the perimeter of the column.

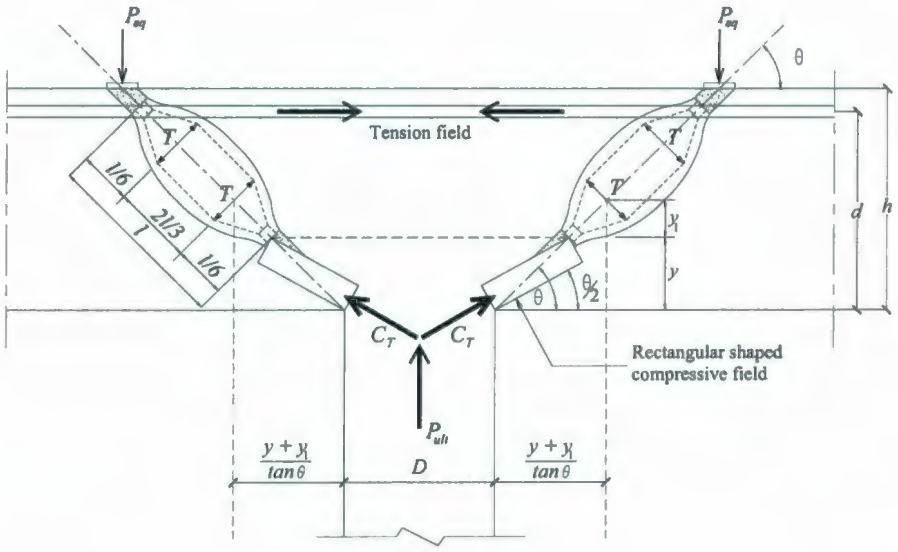

Figure 8.4: Refined strut and tie model for symmetric punching of concrete slab

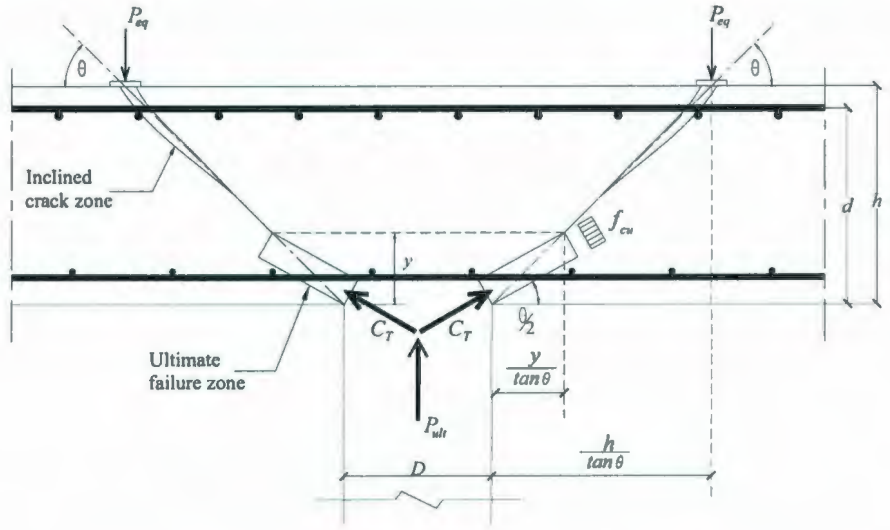

Figure 8.5: High radial compression stress failure mechanism

8.4.3 Shear Cracking, the Crack Zone

A refined strut-and-tie model can be developed in the upper zone of the proposed model (Figure 8.4). Two compression struts radiate at dispersion angles of approximately 2:1 (as proposed by Schlaich and Weischede 1982) from the angle of inclination, θ. The compression forces are held together by two perpendicular tensile forces in the concrete.

Cracking occurs when the stress in these tensile zones equals or exceeds the splitting tensile strength of the concrete. $f_{sp,t}$, given by CEB-FIP (1990) model code. The punching shear cracks that develop in the crack form at a load level less than the ultimate punching shear load. The punching shear crack load can be established by equating and solving the inclined truss shown in Figure 8.4 and comparing the tension force to $f_{sp,t}$ of the concrete. It is assumed that the inclined length of the crack zone is l as shown in Figure 8.4, and that cracking will occur first in the lower tension tie due to its lower perimeter relation with the column. Hence, shear reinforcement must be provided to resist shear cracking. The perimeter of the critical section with respect to the column is:

$$\pi\left(D+2\left(\frac{(y+y_1)}{\tan\theta}\right)\right) \tag{8.13}$$

The cracking load can then be calculated from geometry by the following equation:

$$T=0.235 f_{sp,t}\, l\, \pi\left(D+2\left(\frac{(y+y_1)}{\tan\theta}\right)\right) \tag{8.14}$$

where y is the depth of flexural compression zone in slab (depth of neutral plane); l is the inclined length of the crack zone (length of strut) calculated using equation (8.15); y_1 is the distance from the neutral axis to the center of the lower tensile force calculated using equation (8.16); and D is the diameter of column. (A square column can be replaced in the equation by an equivalent circular column with the same perimeter, i.e. $D=4C/\pi$)

$$l=\frac{d-y}{\sin\theta} \tag{8.15}$$

$$y_1=\frac{l\sin\theta}{6} \tag{8.16}$$

Although ultimate punching shear failure of the slab is not dependent on the crack zone, this zone is important in that presence of cracking in this zone around this periphery of the column may be a warning sign the applied loads are nearing the ultimate punching shear level. In many structures, such as offshore structures, crack control is an important serviceability limit state. The presence of punching shear cracks in these applications is to be avoided and knowledge of the cracking mechanism behavior is required.

8.4.4 Punching Failure Mechanism, Ultimate Failure Zone

Punching shear failure occurs when the concrete in compression in a rectangular stress field near the column fails by a high radial compressive stress. P_{ult} denotes the corresponding ultimate punching shear capacity of failure mechanism. The basis of this approach has been successfully implemented by the rational model developed by Kinnunen and Nylander (1960). This approach is used as the basis for the proposed strut-and-tie model to determine the ultimate punching capacity of a slab under symmetric loading.

8.4.5 High Radial Compression Stress Failure Mechanism

The rectangular stress compression zone in the vicinity of a circular column is shown in Figure 8.5. The column force P_{ult} is transferred to the slab via inclined radial forces that must pass under the root of the shear crack. The crack is assumed to have propagated down to the neutral axis at flexure in the radial direction. The radial compressed concrete strut is assumed to form an imaginary conical shell-strut with constant thickness, at an angle inclination that is $\theta/2$. Punching shear failure is assumed to occur when the stress in the conical shell-strut reaches the value of the crushing strength of cracked concrete, $f_{c2,\max}$, given by the following equation:

$$f_{c2,\max} = \frac{\lambda \phi_c f_c'}{0.8 + 170 \varepsilon_1} \leq \phi_c f_c' \tag{8.17}$$

The refined strut-and-tie model of Figure 8.4 shows the complete force fields developed due to symmetric punching. Equilibrium equations can be developed in the vertical direction, horizontal direction, and due to the moment developed due to the individual forces acting at their respective distances from the column face. The equation for equilibrium in the vertical direction determines P_{ult}, the ultimate punching shear load. The ultimate punching load, P_{ult}, can be determined from the maximum concrete stress, $f_{c2,\max}$ acting on the thickness of the conical shell-strut. This can be expressed as the total compression force, C_T, around the periphery of the circular column equal to the bearing area of the conical shell-strut periphery multiplied by the maximum concrete strength allowed in the strut.

C_T = Periphery of bearing area × concrete strength, or

C_T = (perimeter of cone × thickness of strut face) × concrete strength,

where

$$\text{Perimeter of cone} = \pi\left(D + \frac{2y}{\tan\theta}\right) \tag{8.18}$$

$$\text{Thickness of strut face} = \frac{y \sin\theta/2}{\sin\theta} \tag{8.19}$$

Concrete stress = $f_{c2,\max}$ as per equation (8.17).

$$C_T = \frac{P_{ult}}{\sin\theta/2} = \left[\pi\left(D + \frac{2y}{\tan\theta}\right)\frac{y\sin\theta/2}{\sin\theta}\right] f_{c2,\max} \tag{8.20}$$

Introducing the term $(l_{ch}/h)^{0.33}$ to account for the size effect, equation (8.20) could be written as follows:

$$C_T = \frac{P_{ult}}{\sin\theta/2} = \left[\pi\left(D + \frac{2y}{\tan\theta}\right)\frac{y\sin\theta/2}{\sin\theta}\right] f_{c2,\max}\,(l_{ch}/h)^{0.33} \tag{8.21}$$

Solving for P_{ult}

$$P_{ult} = \pi\left(D + \frac{2y}{\tan\theta}\right)\frac{y\sin\theta/2}{\sin\theta} f_{c2,\max}\,(l_{ch}/h)^{0.33}\sin\theta/2 \tag{8.22}$$

The height of the rectangular stress compression zone, y, is determined based on the position of the neutral axis in a reinforced concrete flexural member under elastic conditions. Based on a simplified equation proposed by Shehata (1990), the neutral axis depth for an ordinary reinforced slab in the elasto-plastic stage has been suggested to be calculated from:

$$y = 0.67(n\rho_e)^{1/2}\left(\frac{35}{f_c'}\right)^{1/2} d \tag{8.23}$$

where y is the neutral axis depth, f_c' is the cylinder strength in MPa and ρ_e is the ratio of reinforcement for a basic yield strength of 500 MPa. According to Shehata (1990) research, the effective reinforcement ratio for any other than 500 MPa yield strength steel, can be calculated as follows:

$$\rho_e = \rho\left(\frac{f_y}{500}\right) \tag{8.24}$$

8.5 Strut-and-Tie Model for Symmetric Loaded Concrete Slabs with Punching Shear Reinforcement

The proposed strut-and-tie model for a concrete slab with punching shear reinforcement consists of decentered fan shaped compression struts oriented at angles θ = 25° to 65° (Marzouk and Jiang 1996). Therefore, shear reinforcement is effective for a distance $2d$

from the face of the column. The shear reinforcement bars act as vertical tension ties in the model. The top tension tie (flexural reinforcing bars) effectively anchors the horizontal component of the fanned struts. Nodal zones are developed at the intersection of the struts and ties.

The strut-and-tie model is solved by calculating P_{ult}, the equivalent force resulting from the load on the slab. The true strut-and-tie model for this situation extends around the periphery of the column in a three-dimensional cone shape. However, it is proposed for simplicity to solve the strut-and-tie model in a two-dimensional manner, therefore, P_{ult} is based on a contributing effective width to each row of punching shear reinforcement.

The proposed strut-and-tie model is shown in Figure 8.6a. This is the sum of two models: one model uses a direct compression strut running from the load to the support. This conical shape strut carries a shear V_c. It should be noted that the actual profile of compression strut is not straight line but instead it tends to take a parabolic arch profile (Alexander and Simmonds 1992), for simplicity it will be assumed to take a straight pass; the other model uses the shear reinforcement as vertical tension members and has compression fans under the load and over the support. The vertical force in each shear reinforcement row is computed assuming that the shear reinforcement has yielded. The vertical force component in each of the small compression struts must be equal to the yield strength of its shear reinforcement for the joint to be in equilibrium.

The compression struts radiating from the load point intersect the shear reinforcement at the level of the centroid of the bottom steel, because a change in the force in the bottom steel is required to equilibrate the horizontal component of the force in the compression strut, the force in the bottom steel is increased at each vertical by the horizontal

component of the compression diagonal intersecting at that point. This is illustrated in Figure 8.6c, where the stepped line shows the resulting tensile force in the bottom steel. The ultimate punching load, P_{ult}, can be determined from the maximum concrete stress, $f_{c2,max}$ acting on the thickness of the conical shell-strut. This can be expressed as total compression force, V_c, around periphery of the circular column, equals the bearing area of the conical shell-strut periphery multiplied by the maximum concrete strength allowed in the strut plus the contribution of the yielded shear reinforcement, V_s.

$$P_{ult} = 0.75V_c + V_s \tag{8.25}$$

$$P_{ult} = 0.75\pi\left(D + \frac{2y}{\tan\theta}\right)\frac{y\sin(\theta/2)}{\sin\theta} f_{c2,max}\,(l_{ch}/h)^{0.33}\sin(\theta/2) + 0.9A_v f_{ywd,ef}\cos\theta \tag{8.26}$$

where $A_v f_{ywd,ef}\cos\theta$ is the total force in the transverse reinforcement inside an assumed failure plane. The constant (0.75) is a reduction factor to account for the reduced punching shear stress for slabs with shear reinforcement (Marzouk and Jiang 1996). The failure plane is assumed to be inclined at an angle θ to the slab axis (Figure 8.6). The effective design strength of the punching shear reinforcement $f_{ywd,ef}$, MPa, is calculated according to EC 2 (2004) provisions:

$$f_{ywd,ef} = 250 + 0.25d \le \frac{f_y}{1.15} \tag{8.27}$$

where d is the slab effective depth, mm, and f_y is steel reinforcement yield strength, MPa. Comparison of the ultimate punching shear capacity of a concrete slab to experimental test results is given in the following section.

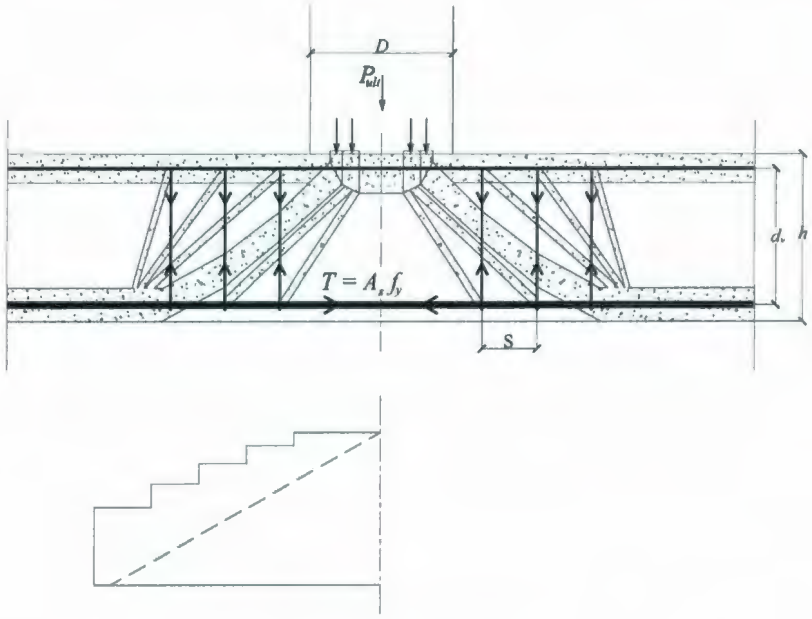

(*a*) Equivalent plastic truss

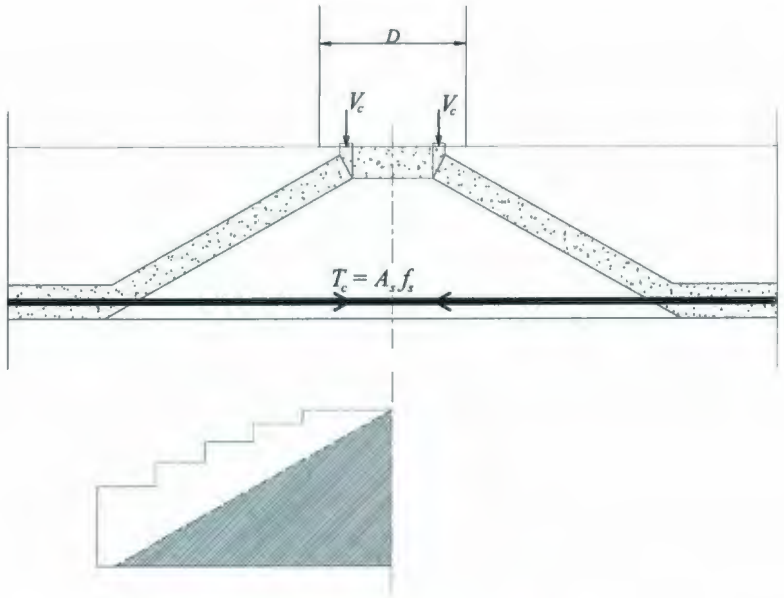

(*b*) Force carried by concrete

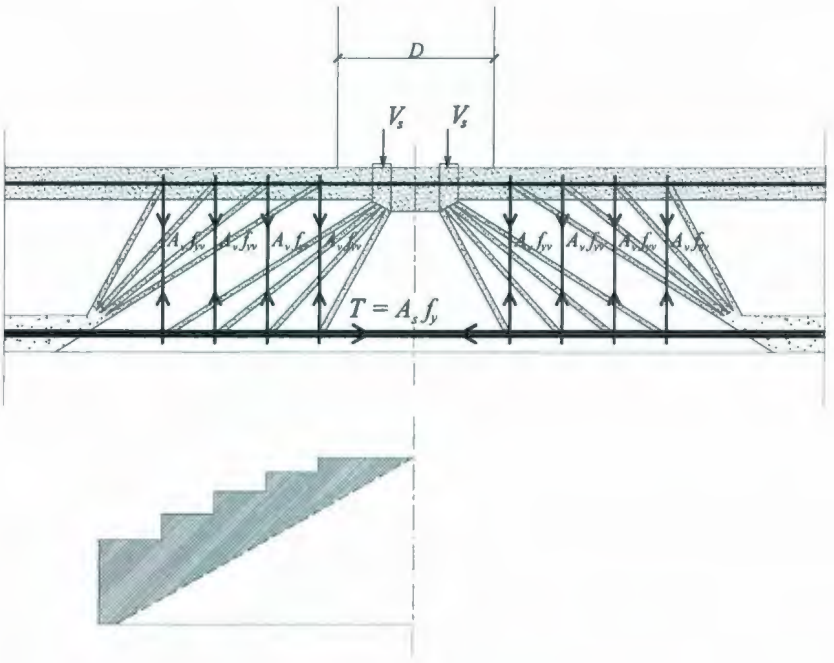

(*c*) Force carried by shear reinforcement

Figure 8.6: Strut-and-tie Model for a thick plate with shear reinforcement; (*a*) Equivalent plastic truss; (*b*) Force carried by concrete; (*c*) Force carried by shear reinforcement

8.6 Comparison of Available Test Results versus the Proposed STM Model

Tables 8.1 to 8.4 summarize the results of the strut-and-tie model for symmetric punching compared to published test results. The proposed model was applied to predict the ultimate strength of normal and light-weight concrete test slabs reported in the literature and failing in punching shear, where either the steel reinforcement ratio or the concrete strength was systematically varied. The results indicate that there exists a very good correlation between theoretical and observed strengths. In this research, the model has been applied to forty tests to predict the punching strength of normal and high strength concrete slabs mainly. The geometry of test slabs, analysis and results are shown in Tables 8.1-8.4, and include seventeen test results by Marzouk and Hussein (1991) with

concrete strength varying from 30 to 80 MPa, six test results by Osman et al. (2000) with concrete strength varying from 35 to 75 MPa mainly, eight test results by Marzouk and Hossin (2008) with concrete strength varying from 35 to 70 MPa, and nine test results by Birkle and Dilger (2008) with concrete strength equal to 35 MPa. For the proposed model, the overall average theory/test ratio is 1.09 with a S.D. of 0.14, giving strong support to the ability of the theory to explain the structural differences in slabs. It is therefore concluded that, the model appears to be equally valid for high strength concrete slabs as for normal strength concrete slabs. It is also worth emphasizing that the slabs analyzed and presented in Tables 8.1-8.4 cover many variables that influence shear behavior such as the type of concrete, concrete strength, tension steel ratio and shear reinforcement ratio. The theoretical model developed here is an excellent representation of the physical behavior of slab connections. Therefore, the strut-and-tie model would have applications in offshore platforms and nuclear containment structures where thick concrete plates, high strength concrete and high steel reinforcement ratios are quite common.

Table 8.1–Comparison between ultimate calculated loads with test results

Slab No.	Depth d, mm	D, mm	ρ %	f_y, MPa	f_c', MPa	y, mm	V_{test}, kN	P_{ult}, kN	P_{ult}/V_{test}
NS1	95	191	1.47	490	42	25.9	320	339	1.06
HS1	95	191	0.49	490	67	10.5	178	187	1.05
HS2	95	191	0.84	490	70	13.3	249	257	1.03
HS7	95	191	1.19	490	74	15.2	356	317	0.89
HS3	95	191	1.47	490	69	17.8	356	358	1.00
HS4	90	191	2.37	490	66	22.1	418	447	1.07
NS2	120	191	0.94	490	30	33.7	396	407	1.03
HS5	125	191	0.64	490	68	15.6	365	280	0.77
HS6	120	191	0.94	490	70	17.8	489	337	0.69
HS8	120	191	1.11	490	69	19.6	436	372	0.85
HS9	120	191	1.61	490	74	22.3	543	470	0.87
HS10	120	191	2.33	490	80	25.4	645	535	0.83
HS11	70	191	0.95	490	70	10.4	196	213	1.09
HS12	70	191	1.52	490	75	12.5	258	282	1.09
HS13	70	191	1.87	490	68	14.9	267	314	1.18
HS14	95	280	1.47	490	72	17.3	498	492	0.99
HS15	95	382	1.47	490	71	17.4	560	643	1.15

Slabs tested by Marzouk and Hussein (1991).

Table 8.2–Comparison between ultimate calculated loads with test results

Slab No.	Depth d, mm	D, mm	ρ %	f_y, MPa	f_c', MPa	y, mm	V_{test}, kN	P_{ult}, kN	P_{ult}/V_{test}
NS1	120	318	0.5	490	76	11.1	304	283	0.93
HS1	115	318	1.0	490	73	15.5	474	434	0.92
HS2	115	318	1.5	490	76	18.6	539	549	1.02
HS7	115	318	2.0	490	74	21.8	613	647	1.06
HS3	115	318	1.0	490	36	26.3	432	397	0.92
HS4	120	318	0.5	490	38	18.8	310	279	0.90

Slabs tested by Osman et al. (2000).

Table 8.3–Comparison between ultimate calculated loads with test results

Slab No.	Depth d, mm	D, mm	ρ %	f_y, MPa	f_c', MPa	y, mm	V_{test}, kN	P_{ult}, kN	P_{ult}/V_{test}
NSC1	157.5	318	2.17	400	35	49.2	678	773	1.14
HSC1	137.5	318	2.48	400	69	27.8	788	1077	1.37
HSC2	127.5	318	2.68	400	70	26.3	801	1033	1.29
HSC3	157.5	318	1.67	400	67	26.6	802	997	1.24
HSC4	157.5	318	1.13	400	61	23.4	811	782	0.96
HSC5	112.5	318	1.88	400	70	19.5	480	794	1.65
NSC2	162.5	318	0.52	400	33	26.0	479	381	0.80
NSC3	105.0	318	0.40	400	34	14.4	228	218	0.95

Slabs tested by Hossin and Marzouk (2008).

Table 8.4–Comparison between ultimate calculated loads with test results

Slab No.	Depth d, mm	D, mm	ρ %	f_y, MPa	f_c', MPa	y, mm	V_{test}, kN	P_{ult}, kN	P_{ult}/V_{test}
1	124	318	1.54	488	33	41.2	483	543	1.12
2	124	318	1.54	488	28	47.1	634	925	1.46
4	124	318	1.54	488	36	38.6	574	795	1.38
7	190	382	1.30	531	34	59.9	825	1077	1.31
8	190	382	1.30	531	35	58.0	1050	1058	1.01
9	190	382	1.30	531	36	56.6	1091	1058	0.97
10	260	446	1.10	524	31	79.4	1046	1580	1.51
11	260	446	1.10	524	30	81.4	1620	1625	1.00
12	260	446	1.10	524	34	74.4	1520	1409	0.93

Slabs tested by birkle and Dilger (2007).

8.7 Experimental Test Results versus Codes Predictions and STM Model

Modern European codes of practice treat punching in terms of shear stresses calculated for control perimeters at relatively large distances from columns or loaded areas. In the CEB-FIP (1990) model code the distance is 2.0 *d*. In BS 8110-97 it is 1.5 *d*, but the perimeter has square corners as compared to CEB-FIP (1990) model code rounded corners. In ACI 318-08, the control perimeter is only 0.5 *d* from the loaded area. The ACI code does not include the influence of either the flexural reinforcement or the size effect on the limiting shear stress.

The analysis of the present results is made in relation to ACI 318-08, CEB-FIP (1990) and BS 8110-97. ACI 318-08 requires that the ultimate shear resistance for slabs without prestress is given by equations (2.25), (2.26), and (2.27).

In CEB-FIP (1990) model code the punching shear resistance, V_{CEB} is expressed as proportional to $(f_{ck})^{1/3}$, where f_{ck} is the characteristic compressive strength of concrete. The highest concrete grade considered in CEB-FIP (1990) model code is C80, which corresponds to f_{ck} equal to 80 MPa. Influences of tension reinforcement and slab depth are also considered in this design code. The relevant punching resistance according to

CEB-FIP (1990) model code is given by equation (2.28), whereas the relevant punching resistance according to BS 8110-97 is given by equation (2.29).

The EC 2 (2004) code recommends that the punching shear resistance, $v_{Rd,c}$, is expressed as proportional to $(f_{ck})^{1/3}$, where f_{ck} is the characteristic compressive strength of concrete. Influences of reinforcement and slab depth are also considered in this design code. The punching shear stress resistance in accordance to the EC 2 (2004) code is calculated as:

$$v_{Rd,c} = C_{Rd,c}\, k \left(100 \rho f_{ck}\right)^{1/3} \frac{2d}{a_{crit}} \geq v_{\min} \frac{2d}{a_{crit}} \tag{8.28}$$

where $C_{Rd,c} = 0.18/\gamma_c$ is an empirical factor derived from a regression analysis, with γ_c being the material resistance factor for concrete (=1.5); d is the slab effective depth, mm; $k = 1 + \sqrt{200/d} \leq 2.0$ is the size factor of the effective depth; ρ is the flexural reinforcement ratio $\leq 2\%$; f_{ck} is the characteristic cylinder compressive concrete strength, MPa; a_{crit} is the distance from the column face to the control perimeter considered. The minimum shear capacity of the concrete, including the material resistance factor for concrete $\gamma_c = 1.5$ is given by:

$$v_{\min} = 0.035\, k^{3/2} \sqrt{f_{ck}} \tag{8.29}$$

The ultimate recorded test loads versus code predictions are given in Table 8.5, together with the details of the specimens and the results of comparisons with the values estimated by different codes. The limit of 40 MPa of the maximum useful cube strength has been ignored when applying BS 8110-97. ACI 318-08 was applied with the omission of the capacity reduction factor. It is clear from Table 8.5 that ACI 318-08 underestimates the punching shear capacity of thick specimens more than 250 mm thick; in one case, for Slab NS5, it underestimates the punching load by 38%. The best ultimate load predictions were given by

CEB-FIP (1990) model code equation. The proposed strut-and-tie model for punching shear compares quite well with experimental test results. It is clear that the strut-and-tie model overestimates the punching capacity for thick slabs more than 300 mm. For symmetric punching, the overall average theory/test ratio is 0.93 with a S.D. of 0.18, when compared to experimental test results, giving strong support to the ability of the theory to explain the structural differences in slabs. It is therefore concluded that the model appears to be equally valid for thick high strength concrete plates as for thick normal strength concrete plates.

Table 8.5–Comparison of code predictions with test results

Slab No.*	Compressive Strength f_c', MPa	Steel ratio, ρ%	Ultimate load P_u, kN	P_{code}/P_u				P_u/P_{flex}
				BS 8110 1997	CEB-FIP 1990	ACI-318 2008	STM model	
NS1	45	0.48	219	1.11	1.28	1.13	1.04	1.37
NS2	50	0.54	491	0.91	1.05	0.88	0.94	1.19
NS3	35	0.35	438	1.01	1.15	1.05	0.95	1.18
HS1	70	0.35	574	0.97	1.10	1.14	0.63	1.53
NS4	40	0.73	882	0.86	0.99	0.72	0.93	0.81
HS2	65	0.73	1023	0.87	1.00	0.79	0.72	0.93
HS3	75	0.43	886	0.90	1.03	1.00	0.64	1.31
HS1	76	0.56	1722	0.78	0.89	0.89	1.10	1.25
HS2	70	1.42	2172	0.84	1.06	0.77	1.12	1.00
HS3	65	1.42	2090	0.81	0.93	0.66	1.00	0.64
NS1	40	1.58	2234	0.85	0.98	0.62	1.10	0.46
HS4	60	1.58	2513	0.87	1.00	0.68	1.01	0.50
Average				0.90	1.04	0.86	0.93	
Stdev				0.09	0.10	0.18	0.17	
Cov				0.10	0.10	0.21	0.19	

*NS-Normal strength slabs; HS-High strength slabs

8.8 Outline of Design Procedure using STM Model

Determine the depth of flexural compression zone in slab (depth of neutral plane), y, using Eq. (8.23). The inclined length of the crack zone (length of strut), l, is calculated using Eq. (8.15); the distance from the neutral axis to the center of the lower tensile force, y_1, calculated using Eq. (8.16). The cracking load can then be calculated using Eq. (8.14), $f_{sp,t}$ is the splitting tensile strength, given by CEB-FIP (1990) model code given by Eq. (8.5). Finally the ultimate punching load, P_{ult}, for slabs without shear reinforcement can be determined from the maximum concrete stress, $f_{c2,max}$ acting on the thickness of the conical shell-strut using Eq. (8.22), while for slabs with shear reinforcement P_{ult}, can be determined using Eq. (8.26), the value of the crushing strength of cracked concrete, $f_{c2,max}$, given by Eq. (8.17). The characteristic length, l_{ch} could be assumed to have an average value of 500 and 250 mm for normal and high strength concrete, respectively. For thick slabs more than 250 mm thickness, the designer can chose one of proposed two models [Eq. (6.54), (6.63) or Eq. (8.12)] to calculate the required minimum shear reinforcement area. Two design examples are given in appendix A.

8.9 Summary

- Slabs without shear reinforcement usually exhibit brittle shear failure. Minimum shear reinforcement that is required for thick plates and two-way slabs should be provided by different codes. Design codes ignore thick slabs over 250 mm and do not account for the fact that the size effect can cause shear failure for thick concrete slabs. This means that by increasing the member size, the behavior of the member becomes more brittle, hence more shear reinforcement is required to enhance the behavior of thick members.

- Strut-and-tie models present a unified, consistent, rational, and simplified model for the behaviour of concrete elements. The phenomena of punching shear behaviour of concrete slabs of various compressive strengths can be adequately modeled using strut-and-tie models.
- For symmetric loading situations, the punching shear behaviour can be modeled using a strut-and-tie model. The strut-and-tie model consisting of fan-shaped compression struts held in place by tension ties can be used to describe the situation where punching shear reinforcement is present. The proposed strut-and-tie models for punching shear compare quite well with experimental test results. For symmetric punching; the overall average theory/test ratio is 0.93 with a S.D. of 0.18, when compared to four separate sets of experimental test results. This gives strong support to the ability of the theory to explain the structural behaviour of concrete slabs. Therefore, it can be concluded that the model appears to be equally valid for high strength concrete slabs and normal strength concrete slabs.

Chapter 9

Summary and Conclusions

9.1 Summary

An experimental and theoretical analysis on the structural behaviour of thick concrete plates is presented. The experimental work includes investigating design issues for thick concrete plates such as minimum flexural reinforcement, minimum shear reinforcement, crack spacing, crack width and punching shear. The experimental work also includes investigating the phenomena of size effect in thick concrete plates.

The theoretical work includes developing the required constitutive relationships to describe crack spacing, crack width, minimum flexural reinforcement, minimum shear reinforcement and ultimate punching capacity of thick plates. The experimental results were used to calibrate and modify the recommended formulae.

Twelve full-scale, normal and high-strength concrete slab-column connections with different thick concrete covers and different reinforcement ratios were tested under flexural loading. Eleven specimens had no shear reinforcement, whereas, the remaining one included T-headed shear reinforcement consisting of vertical bars mechanically anchored at top and bottom by welded anchor plates. All specimens were instrumented to enable their various behavioral aspects to be studied as each test was carried out. The main test variables included concrete compressive strength, reinforcement ratio, bar spacing and slab effective depth. A new test setup was built to handle thick specimens that failed under high punching loads.

9.2 Conclusions

9.2.1 Minimum Flexural Reinforcement for Thick HSC Plates

- The analytical study revealed that the torsional moment (M_{xy}) effect is an important factor in determining the minimum flexural reinforcement ratio for thick concrete plates and should be taken into account.
- A new equation is developed to calculate minimum flexure reinforcement for thick concrete plates. The main contribution of this equation is to account for the torsional moment and the size effect factor. The proposed equation [Eq. (6.28)] can be applied to calculate minimum flexural reinforcement in each of the two orthogonal directions on both faces for thick concrete plates or walls more than 200 mm thickness.
- The size effect factor for slabs over 250 mm cannot be taken as a constant number related to the member depth only but it must be related to the concrete strength as well. Test specimens NS3 and HS1 are identical with the exception of concrete strength and both specimens displayed flexure failure. However, the energy absorption capacity for slab HS1 is higher than that for slab NS3. This confirms the dependence of minimum flexure reinforcement ratio on the size effect.
- The ACI 318-08 and CSA-A23.3-04 design codes overestimate the minimum reinforcement ratio required for thick concrete slabs greater than 200 mm; this is due to the fact that none of these codes contain a size effect factor, and this can result in a lot of money savings.

- Using ACI 318-08 design guidelines for slabs more than 250 mm depth can result in a brittle response and hence no adequate warning of an impending failure at extreme overloads and this is due to neglecting size effect.
- The use of minimum flexure reinforcement for thick high strength concrete plates enhances the energy absorption capacity. The values of ductility and energy absorption capacity for slab HS3 are more than twice the same values for slab HS2. The flexural reinforcement ratio chosen for slab HS2 was designed using ACI 318-08 formula while the flexural reinforcement ratio chosen for slab HS3 was designed using the proposed minimum flexural reinforcement formula and the slab displayed very ductile and pleasant behaviour compared to the brittle behaviour that was displayed by the slab that was designed using ACI guidelines .
- Slab HS4 of 350 mm thickness was designed according to the developed model with minimum reinforcement ratio less than that required by the ACI 318-08 and CSA-A23.3-04 design codes and the slab structural ductility and energy absorption was greatly improved.
- A size effect factor is recommended based on the thickness of the slab and fracture mechanics material property represented by the brittleness factor known as the characteristic length, l_{ch}.

9.2.2 Minimum Shear Reinforcement for Thick HSC Plates

- Two new models are presented that can be used to calculate minimum shear reinforcement required to prevent brittle shear failure for thick concrete plates and walls in the vicinity of concentrated loads. The first model is based on the diagonal shear cracking load while the second model is based on the modified

compression field theory. Both models account for the slab size effect by using principles of fracture mechanics. In addition, a different model is also developed to calculate minimum shear reinforcement for thick concrete plates based on a simple strut-and-tie model.

- The minimum amount of shear reinforcement is recommended for slabs and walls thicker than 250 mm. This value is a reflection of the measured characteristic length for high strength concrete of 70 MPa. This recommendation is also based on and supported by previous research done at Memorial University. For slabs, the shear reinforcement is recommended in the vicinity of connections with columns. In walls, the shear reinforcement is recommended for the area that can be subjected to a significant concentrated transverse load.
- A proposed arrangement of shear studs in a cross pattern is recommended for slabs. The dimensions of the pattern have not been varied in the present research. The dimensions recommended here are in accordance with the arrangement for minimum headed shear studs in ACI 421.2R-08. The distance between the column faces and the inner-most peripheral line of studs should not exceed $0.5d$; the spacing between peripheral lines should not exceed $0.75d$; the distance between the column faces and the outer-most peripheral line should not be less than $3.5d$. Nonetheless, this preliminary guideline needs further research investigation for thick slabs.
- The enhanced structural behavior of slab HS5 (300 mm) with T-headed shear stud reinforcement verified the importance of providing minimum shear reinforcement

for thick plates and reflected the advantage of using headed shear reinforcement. The addition of shear reinforcement with reinforcement ratio of approximately 0.68% by volume changed the punching failure mode to a ductile flexure failure.

9.2.3 Crack Spacing and Crack Width for Thick Concrete Plates

- A new theoretical expression is recommended for plates and two-way slabs with longitudinal and transverse reinforcements. The proposed method takes into consideration, the effects of steel bond in the loading direction and the contribution of the splitting bond stresses for the transverse steel. The proposed equation gives a good estimate for crack spacing in plates and two-way slabs with concrete covers equal to ($C_c < 2.5\ d_b$). The proposed method can be used for thick concrete covers, ($C_c = 2.5 - 5.0\ d_b$) plates and two-way slabs after reducing one third of the tensile stress constant k_t. However, for two-way slabs with concrete covers larger than 5.0 d_b, it can be speculated that the crack spacing behaves randomly. This is due to the fact that such slabs act as cross sections that contain two separate materials.
- For bar spacing greater than 300 mm, the entire existing models estimate average crack spacing higher than the one measured during testing. For bar spacing less than 250 mm, the CEB-FIP (1990) model code estimates average crack spacing smaller than the one measured during testing. The test results reveals that crack spacing is increased as the bar spacing or the concrete cover is increased for the specimens with low reinforcement ratio that fail in flexure.
- The analytical investigation revealed that the crack widths calculated using CSA-S474-04 and NS 3473 E (1989) are relatively close.

- The test results showed that as the concrete cover increases, the maximum crack width increases. Test results showed that the maximum crack width can be influenced by as much as 28% when the concrete cover increases from 60 to 70 mm for the same bar spacing.
- The test results showed that the maximum crack width can be influenced by as much as 50% when the bar spacing increases from 217 mm to 368 mm, this means that for the same concrete cover increasing the bar spacing by about 70% results in increasing the crack width by about 50%.
- Test results revealed that crack control can still be achieved by limiting the spacing of the reinforcing steel despite using thick concrete covers.

9.2.4 Punching Shear of Thick Concrete Plates

- A model is developed to calculate punching shear capacity of thick concrete plates based on a simple and rational strut-and-tie model. The model is verified using forty test slabs tested and published by other researchers. For symmetric punching; the proposed strut-and-tie model has an average theory/test ratio of 0.93 with a S.D. of 0.18, when compared to four separate sets of experimental test results found in literature. Therefore, it can be concluded that the model appears to be equally valid for high strength as well as normal strength concrete slabs.
- The nominal shear stress at failure of slab HS7 (400 mm) is lower than the nominal shear stress at failure of slab NS5 (400 mm). Both slabs have the same thickness and the same reinforcement ratio and were designed to fail under punching shear. This confirms that the size effect factor cannot be taken as a

constant number related to the member depth but it must be also related to the mechanical properties of concrete.

References

ACI Committee 318, "Building code requirements for structural concrete (ACI 318-89) and Commentary (ACI 318R-89)," ACI 318-89, American Concrete Institute, Farmington Hills, Michigan, 1989.

ACI Committee 318, "Building code requirements for structural concrete (ACI 318-95) and Commentary (ACI 318M-95)," ACI 318-95, American Concrete Institute, Farmington Hills, Michigan, 1995.

ACI Committee 318, "Building code requirements for structural concrete (ACI 318-99) and Commentary (ACI 318M-99)," ACI 318-99, American Concrete Institute, Farmington Hills, Michigan, 1999.

ACI Committee 318, "Building code requirements for structural concrete (ACI 318-02) and Commentary (ACI 318M-05)," ACI 318-05, American Concrete Institute, Farmington Hills, Michigan, 2005.

ACI Committee 318, "Building code requirements for structural concrete (ACI 318-08) and Commentary (ACI 318M-08)," ACI 318-08, American Concrete Institute, Farmington Hills, Michigan, 2008.

Adebar, P., and Zhou, Z., "Bearing Strength of Compressive Struts Confined by Plain Concrete," ACI Structural Journal, Vol. 90, No. 5, 1993, pp. 534-541.

Alexander, S., and Simmonds, S., "Shear-Moment Transfer in Column-Slab Connections," Structural Engineering Report, No. 141, Department of Civil Engineering, University of Alberta, 1986, 95 pp.

Alexander, S., and Simmonds, S., "Tests of Column-Flat Plate Connections," ACI Structural Journal, Vol. 89, No. 5, 1992, pp. 495-502.

Andrä, H., "Zum Tragverhalten von Flachdecken mit Dübelleisten-Bewehrung im Auflagerbereich" Beton, Stalbeton, (Berlin), Vol. 76, No. 3, 1981, PP. 53-57.

Angelakos, D., Bentz, E., and Collins, M., "Effect of Concrete Strength and Minimum Stirrups on Shear Strength of Large Members," ACI Structural Journal, Vol. 98, No. 3, 2001, pp. 290-300.

Battista, D.D., "Minimum Reinforcement Requirements of Reinforced High-Strength Concrete Slabs," M. Sc. Thesis, Department of Civil Engineering, University of Toronto, Canada, 1992, 172 pp.

Bazant, Z., and Byung, H., "Deformation of Progressively Cracking Reinforced Concrete Beams," ACI Structural Journal, Vol. 81, No. 3, 1984, pp 268-278.

Beeby, A., "The Prediction of Crack Widths in Hardened Concrete," The Structural Engineer (UK), Vol. 57A, No. 1, January 1979, pp. 9-17.

Bergner, H., "Minimum Reinforcement of High-Strength Concrete Members under Centrical Restraint," Darmstadt Concrete Vol. 9, Technische Hochschule Darmstadt, Germany, 1994.

Birkle, G., and Dilger, W., "Influence of Slab Thickness on Punching Shear Strength," ACI Structural Journal, Vol. 105, No. 2, 2008, pp. 180-188.

Bosco, C., Carpinteri, A., "Fracture mechanics evaluation of minimum reinforcement in concrete structures," in Applications of Fracture Mechanics to Reinforced Concrete (Proceedings of an International Workshop, Torino, Italy, 1990), Ed. A. Carpinteri, Elsevier Applied Science, London, 1992, pp. 347-377.

Bosco, C., Carpinteri, A., and Debernardi, P. G., "Minimum Reinforcement in High-Strength Concrete," Journal of Structural Engineering, ASCE, Vol. 116, No. 2, 1990,

pp. 427 - 437.

British Standards Association, BS 8110-97, "Structural Use of Concrete," Use of Concrete, Part 1: Code of Practice for Design and Construction, BSI, Milton Keynes, 1997.

Broms, C., "Elimination of Flat Plate Punching Failure Mode," ACI Structural Journal, Vol. 97, No. 1, 2000, pp. 94-101.

Brown, M., and Bayrak, O., "Minimum Transverse Reinforcement for Bottle-Shaped Struts," ACI structural journal, Vol. 103, No. 6, 2006, pp. 813-821.

Byung, H., and Young, J., "New Formulae for Maximum Crack Width and Crack Spacing in Reinforced Concrete Flexural Members," ACI Structural Journal, Vol. 84, No. 10, 1986, pp 103-112.

Carpinteri A. "Stability of fracturing process in RC beams," ASCE Structural Journal, Vol. 110, No. 3, 1984, pp. 544-558.

Comité Euro–International Du Béton–Fédération de la Précontrainte (CEB–FIP), Model Code, Bulletin D'Information No. 203–305, Lausanne, Switzerland, 1990, 462 pp.

CSA, Canadian Standards Association, "Design of Concrete Structures for Buildings," CSA-A23.3-84, Rexdale, Ontario, Canada, 1984, 281 pp.

CSA, Canadian Standards Association, "Design of Concrete Structures for Buildings," CSA-A23.3-94, Rexdale, Ontario, Canada, 1994, 199 pp.

CSA, Canadian Standards Association, "Design of Concrete Structures for Buildings", CSA-A23.3-04, Rexdale, Ontario, Canada, 2004, 258 pp.

CSA, Canadian Standards Association, "Concrete Structures," CSA-S474-04, Mississauga, Ontario, Canada, 2004, 258 pp.

Desayi, P., and Kulkarni A., "Determination of maximum crack width in two-way reinforced concrete slabs," Department of Civil Engineering, Indian Institute of Science, Bangalore, ICE Proceedings, V. 61, No. 2, 1976, pp. 343-349.

Dilger, W., and Ghali, A., "Shear Reinforcement for concrete Slabs," Journal of the Structural Division, ASCE, Vol. 107, No. 12, 1981, PP. 2403-2420.

Elgabry, A., and Ghali, A., "Test on Concrete Slab-Column Connections with Stud-Shear Reinforcement Subjected to Shear-Moment Transfer," ACI Structural Journal, Vol. 84, No. 5, Sept.-Oct. 1987, pp. 433-442.

Elgabry, A., and Ghali, A., "Design of Stud-Shear Reinforcement for Slabs," ACI Structural Journal, Vol. 87, No. 3, 1990, pp. 350-361.

Eurocode 2, "Design of concrete structures-Part 1-1: General rules and rules for buildings", 1992-1-1, 1992.

Eurocode 2, "Design of concrete structures-Part 1-1: General rules and rules for buildings", 2004-1-1, 2004.

Frosch, R., "Another Look at Cracking and Crack Control in Reinforced Concrete," ACI Structural Journal, V. 96, No. 3, 1999, pp. 437-442.

Frosch, R., Blackman, D., and Radabaugh, R., "Investigation of Bridge Deck Cracking in Various Bridge Superstructure Systems," FHWA/IN/JTRP Report No. C-36-56YY, File No. 7-4-50, School of Civil Engineering, Purdue University, West Lafayette, Indiana, 2003, 286 pp.

Gardner N., "Relationship of the punching shear capacity of reinforced concrete slabs with concrete strength," ACI Structural Journal, Vol. 87, No. 1, 1990, pp. 66-71.

Gergely, P., and Lutz, L., "Maximum Crack Width in Reinforced Concrete Flexural

Members, Causes, Mechanism, and Control of Cracking Concrete," SP-20, American Concrete Institute, 1968, pp 87-117.

Ghali, A., Favre, R., and Elbadry, M., 1986, "Concrete Structures: Stresses and Deformations," J. W. Arrowsmith Ltd., Bristol, United Kingdom.

Gilbert, R., and Nejadi, S., "An Experimental Study of Flexural Cracking in Reinforced Concrete Members under Sustained Loads," UNICIV Report No. R-435, School of Civil and Environmental Engineering, University of New South Wales, Sydney, Australia, 2004, 59 pp.

Gilbert, R., "Control of Flexural Cracking in Reinforced Concrete," ACI Structural Journal, V. 105, No. 3, May 1, 2008, pp. 301-307.

Hallgren, M., "Punching Shear Capacity of Reinforced High Strength Concrete Slabs," Doctoral thesis, Department of Structural Engineering, Royal Institute of Technology, Stockholm, Sweden, 1996, 206 p.

Hallgren, M., Kinnunen, S., and Nylander, B., "Punching Shear Tests on Column Footings," Nordic Concrete Research, Publication No. 21, Oslo, 1998, pp 1-22.

Hegger, J., Sherif, A., and Ricker, M., "Experimental Investigations on Punching Behavior of Reinforced Concrete Footings," ACI Structural Journal, Vol. 104, No. 3, 2006, pp. 604-613.

Hillerborg, A., "Strip Method of Design," E. & F., N. Spon, London, 1975, 258 pp.

Hillerborg, A., "Fracture mechanics concepts applied to moment capacity and rotational capacity of reinforced concrete beams," Engineering Fracture Mechanics, Vol. 35, No.1, 2, 3, 1990, pp. 233-240.

Hossin, M., and Marzouk, H., "Crack spacing for offshore structures," Canadian Journal

of Civil Engineering, Vol. 35, 2008, pp. 1446-1454.

Jaeger, T., and Marti, P., "Reinforced Concrete Slab Shear Prediction Competition: Experiments," ACI Structural Journal, Vol. 106, No. 3, 2009, pp. 300-308.

Jiang, D., Shah, S., and Andonian, A., "Study of the Transfer of Tensile Forces by Bond, ACI Structural Journal, Vol. 81, No 3, 1984, pp. 251-259.

Joint ACI-ASCE Committee 421, 2008, Shear Reinforcement for Slabs (ACI 421.1R-08), American Concrete Institute, Farmington Hills, Mich., 15 pp.

Kaar, P., "High Strength Bars as Concrete Reinforcement, Part 8: Similitude in Flexural Cracking of T-Beam Flanges," Journal, PCA Research and Development Laboratories, Vol. 8, No. 2, May 1966, pp. 2-12.

Kankam, C., "Relationship of Bond Stress, Steel Stress, and Slip in Reinforced Concrete," Journal of Structural Engineering, American Society of Civil Engineers, Vol. 123, No. 1, 1997, pp. 79-85.

Kinnunen, S., and Nylander, H., "Punching of Concrete Slabs without Shear Reinforcement," Transactions No. 158, Royal Institute of Technology, Stockholm. Sweden, 1960.

Kordina, K., Meichsner, H., "Minimum Shear Reinforcement of R. C. Slabs," Leipzig Annual Civil Engineering report, Lacer No. 1, 1996, pp. 99-108

MacGregor, J., and Bartlett, F., "Reinforced Concrete: Mechanics and Design," First Canadian edition, Prentice Hall, Scarborough, Ontario, Canada, 2000.

Makhlouf, H., and Malhas, F., "The Effect of Thick Concrete Cover on the Maximum Flexural Crack Width under Service Load," ACI Structural Journal, Vol. 93, No. 3, 1996, pp 257-265.

Marti, p., "Design of Concrete Slabs for Transverse Shear," ACI Journal, Vol. 87, No. 2, 1990, pp. 180 - 190.

Marzouk, H., and Hussein, A., "Experimental Investigation on the Behavior of High-Strength Concrete Slabs," ACI Structural Journal, Vol. 88, No. 6, 1991, pp. 701-713.

Marzouk, H., and Chen, Z., "Finite Element Analysis of High-Strength Concrete Slabs," ACI Structural Journal, Vol. 90, No. 50, 1993, pp. 505-513.

Marzouk, H., and Chen, Z., "Fracture Energy and Tension Properties of High-Strength Concrete," ASCE Journal of Material in Civil Engineering, Vol. 7, No. 2, 1995, pp. 108 - 116.

Marzouk, H., and Jiang, D., "Finite Element Evaluation of Shear Enhancement for High Strength Concrete Plates," ACI Structural Journal, Vol. 93, No. 6, 1996, pp. 667-673.

Marzouk, H., and Jiang, D., "Experimental Investigation on Shear Enhancement Types for High-Strength Concrete Plates," ACI Structural Journal, Vol. 93, No. 1, 1997, PP. 49-58.

Marzouk, H., Emam, M., and Hilal, S., "Sensitivity of shear strength to fracture energy of high-strength concrete slabs," Canadian Journal of civil engineering, Vol. 25, No. 1, 1998, pp. 40-50.

Mokhtar, A., Ghali, A., and Dilger, W., "Stud shear reinforcement for flat concrete plates," ACI Structural Journal, Vol. 82, No., 5, 1985, PP. 676-683.

Nawy, E., and Blair, K., "Further Studies on Flexural Crack Control in Structural Slab Systems," Cracking, Deflection, and Ultimate Load of Concrete Slab Systems, SP-30, American Concrete Institute, Farmington Hills, Mich., 1971, pp. 1-41.

Norwegian Standard, NS 3473 E (English Translation), "Concrete Structures, Design

Rules," Norwegian Council for Building Standardization, Oslo, Norway, 1989, 79 pp.

Osman, M., Marzouk, H., and Helmy, S., "Behaviour of High-Strength lightweight Concrete Slabs under Punching Loads", ACI Structural Journal, Vol. 97, No. 3, 2000, pp. 492- 498.

Randal H., Wood, R., and Armer, G., "The Theory of the Strip Method for Design of Slabs," Institution of Civil Engineers, London, Vol. 41, 1968, pp. 285-313.

Regan, P., and Braestrup, M., "Punching Shear in Reinforced Concrete: A State of Art Report," Bulletin d'information No. 168, Comite Euro-International du Beton, Lausanne, 1985, 232 p.

Rizk, E., and Marzouk, H., "New Formula to Calculate Minimum Flexure Reinforcement for Thick High-Strength Concrete Plates," ACI Structural Journal, Vol. 106, No. 5, 2009, pp. 656-666.

Rizkalla, S., Hwang, L., and EL-Shahawi, M., "Transverse Reinforcement Effect on Cracking Behaviour of Reinforced Concrete members," Canadian Journal of Civil Engineering, V. 10, No. 4, May 1983, pp. 566-581.

Rogowsky, D., and Marti, P., "Detailing for Post-Tensioning," VSL report series No. 3, VSL International Ltd, Bern, 1991, 49 pp.

Schlaich, J., and Weischede, D., "Detailing of Concrete Structures," Bulletin d'Information 150, Comité Euro-International du Béton, Paris, 1982, 163 pp.

Shehata, I., "Simplified model for estimating the punching resistance of reinforced concrete slabs," Materials and Structures Journal, Vol. 23, 1990, pp. 364-371.

Staller, "Analytical studies and numerical analysis of punching shear failure in reinforced concrete slabs," FIP Bulletin on Punching of Structural Concrete Slabs dedicated to

Professor Sven Kinnunen, in International Workshop on punching shear capacity of reinforced concrete slabs, Proceedings, Edts., Silfwerbrand, J., Hassanzadeh, G., Kungl, Tekniska Högskolan Stockholm, Royal Institute of Technology, TRITA-BKN, Bulletin 57, 2000.

Tiller, R., "Strut-and-Tie Model for Punching Shear of Concrete Slabs," Master's thesis, Faculty of Engineering and Applied Science, Memorial University of Newfoundland, St. John's, Newfoundland and Labrador, Canada, 1995, 103 p.

Timoshenko, S., and Woinowsky-Krieger S., "Theory of Plates and Shells," New York: McGraw Hill, 1959, 580 pp.

Vaz, A., Gomes, R., and Shehata, L., "Study on Minimum Shear Reinforcement of Reinforced Concrete Flat Slabs," IBRACON Structures and Materials Journal, Vol. 2, No. 1, 2009, pp. 1-12.

Wood, R., and Armer, G., "The Theory of the Strip Method for Design of Slabs," Proceedings, Institution of Civil Engineers, London, Vol. 41, 1968, pp. 285-313.

Woodson, C., "Shear Reinforcement in Deep Slabs." US Army Corps of Engineers Technical report, 1994, 138 pp.

Appendix A. Design Examples

Design Example 1 (Thick-Slab):

The geometry and material properties of test specimen should be given first before starting the solution. Input the following slab information, HS6 (Group B), Chapter 5:

Slab height $h = 350$ mm

Square column dimension, $C = 400$ mm

Equivalent circular column diameter, $D \approx 509$ mm

Structural depth, $d = 262.5$ mm

$f_c^{'} = 65.4$ Mpa, $f_y = 400$ Mpa

$\rho = 1.44\%$, $\rho^{'} = 0.24\%$

$E_s = 210000$ Mpa, $E_c = 36391$ Mpa

Crack angle $\theta = 45$ degrees

Symmetric Punching

Neutral axis depth, $y = 0.67(n\rho_e)^{1/2}\left(\frac{35}{f_c^{'}}\right)^{1/2} d$

$$\rho_e = \rho\left(\frac{f_y}{500}\right) = 2 \times \frac{1.44}{100} \times \frac{400}{500} = 0.023$$

$$y = 0.67(n\rho_e)^{1/2}\left(\frac{35}{f_c^{'}}\right)^{1/2} d$$

$$= 0.67 \times (5.77 \times 0.023)^{0.5} \times \left(\frac{35}{65.4}\right)^{0.5} \times 262.5$$

$$= 46.9\,\text{mm}$$

Crack Zone of Strut-and-Tie Model

Crack zone length, $l = \frac{d-y}{\sin\theta} = \frac{262.5-46.9}{\sin 45} = 304.9\,\text{mm}$

$$y_1 = \frac{l\sin\theta}{6} = \frac{304.9\times\sin 45}{6} = 35.9\,\text{mm}$$

Estimated crack load,

$$T = 0.235 f_{sp,t}\, l\, \pi\left(D + 2\left(\frac{(y+y_1)}{\tan\theta}\right)\right)$$

$$= 0.235\times 5.38\times 304.9\times 3.14\times\left(509 + 2\left(\frac{(46.9+35.9)}{\tan 45}\right)\right)$$

$$= 816.6\,\text{kN}$$

where $f_{sp,t}$ is the splitting bond stress of concrete

$$f_{sp,t} = 1.11 f_{ctm} = 1.11\times 4.85 = 5.38\,\text{MPa}$$

Ultimate Failure Zone of Strut-and-Tie Model

Ultimate punching shear based on strut and tie model, P_{ult}:

$$f_{cu} = \frac{f_c'}{0.8+170\varepsilon_1} \le f_c'$$

$$= \frac{65.4}{0.8+170\times 0.001} = 67.4\,\text{MPa}$$

Take $f_{cu} = f_c' = 65.4\,\text{MPa}$

$$P_{ult} = \pi\left(D + \frac{2y}{\tan\theta}\right)\frac{y\sin\theta/2}{\sin\theta} f_{cu}\,(l_{ch}/h)^{0.33}\sin\theta/2$$

$$= 3.14\times\left(509 + \frac{2\times 46.9}{\tan 45}\right)\times\left(\frac{46.9\times\sin 22.5}{\sin 45}\right)\times 65.4\times\left(\frac{288}{350}\right)^{0.33}\times\sin 22.5$$

$$= 2082\,\text{kN}$$

Ultimate punching shear based on CSA-A23.3-04:

$$V_u = 0.38\lambda\phi_c\sqrt{f_c'}\, b_o d$$

$$b_o = 2(c_1 + c_2 + 2d)$$
$$= 2\times(400+400+2\times262.5)$$
$$= 2650\,\text{mm}$$

$$V_u = 0.38\times(65.4)^{0.5}\times2650\times262.5\times\left(\frac{1300}{1000+262.5}\right)$$
$$= 2201\,\text{kN}$$

$P_{test} = 2090$ kN

Required minimum shear reinforcement ratio according to strut-and-tie model:

$$\rho_{z,\min} = 0.26\frac{f_{ctm}}{f_y}\frac{1}{(l_{ch}/h)^{0.33}}$$

$$\rho_{z,\min} = 0.26\frac{4.85}{400}\frac{1}{(288/350)^{0.33}} = 0.34\%$$

The shear reinforcement area is given by the following equation, for a slab unit width:

$$A_{z,\min} = \rho_{z,\min}\, l\cot\theta$$

$$A_{z,\min} = \frac{0.34}{100}\times304.9\times400\times\cot45 = 414.8\,\text{mm}^2$$

Use 12 #15M studs per each peripheral line (**Fig. A1**).

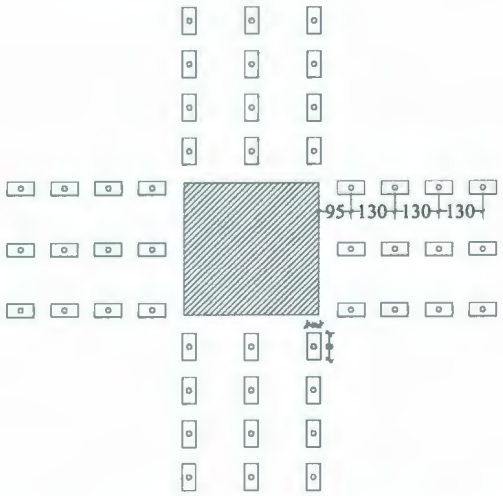

Figure A1: Arrangement of T-headed minimum shear reinforcement for slab HS6

Design Example 2 (Thin Slab):

Input the following slab information (Marzouk and Hussein (1991)), HS10:

Square column dimension, $C = 150$ mm

Equivalent circular column diameter, $D = 191$ mm

Structural depth, $d = 120$ mm

$f_c^{'} = 80$ Mpa, $f_y = 490$ Mpa

$\rho = 2.33\%$, $\rho^{'} = 0.33\%$

$E_s = 200000$ Mpa, $E_c = 40249$ Mpa

Crack angle $\theta = 35°$

Symmetric punching

Neutral axis depth, $y = 0.67(n\rho_e)^{1/2}\left(\frac{35}{f_c^{'}}\right)^{1/2} d$

$$\rho_e = \rho\left(\frac{f_y}{500}\right) = 2\times\frac{2.33}{100}\times\frac{490}{500} = 0.046$$

$$y = 0.67(n\rho_e)^{1/2}\left(\frac{35}{f_c^{'}}\right)^{1/2} d$$

$$= 0.67\times(4.96\times 0.046)^{0.5}\times\left(\frac{35}{80}\right)^{0.5}\times 120$$

$$= 25.4\,\text{mm}$$

Crack zone of strut and tie model

Crack zone length, $l = \frac{d-y}{\sin\theta} = \frac{120-25.4}{\sin 35} = 165\,\text{mm}$

$$y_1 = \frac{l\sin\theta}{6} = \frac{165\times\sin 35}{6} = 15.8\,\text{mm}$$

Estimated crack load,

$$T = 0.235 f_{sp,t} \, l \, \pi \left(D + 2\left(\frac{(y + y_1)}{\tan\theta} \right) \right)$$

$$= 0.235 \times 6.22 \times 165 \times 3.14 \times \left(191 + 2\left(\frac{(25.4 + 15.8)}{\tan 35} \right) \right)$$

$$= 207\,\text{kN}$$

where $f_{sp,t}$ is the splitting bond stress of concrete

$$f_{sp,t} = 1.11 f_{ctm} = 1.11 \times 5.6 = 6.22\,\text{MPa}$$

Ultimate failure zone of strut and tie model

Ultimate punching shear based on strut and tie model, P_{ult}:

$$f_{cu} = \frac{f_c^{'}}{0.8 + 170\varepsilon_1} \le f_c^{'}$$

$$= \frac{80}{0.8 + 170 \times 0.001} = 82.4\,\text{MPa}$$

Take $f_{cu} = f_c^{'} = 80\,\text{MPa}$

$$P_{ult} = \pi \left(D + \frac{2y}{\tan\theta} \right) \frac{y \sin\theta/2}{\sin\theta} f_{cu} \, (l_{ch}/h)^{0.33} \sin\theta/2$$

$$= 3.14 \times \left(191 + \frac{2 \times 25.4}{\tan 35} \right) \times \left(\frac{25.4 \times \sin 17.5}{\sin 35} \right) \times 80 \times \left(\frac{250}{150} \right)^{0.33} \times \sin 17.5$$

$$= 597\,\text{kN}$$

Ultimate punching shear based on CSA-A23.3-04:

$$V_u = 0.38 \lambda \phi_c \sqrt{f_c^{'}} \, b_o d$$

$$b_o = 2(c_1 + c_2 + 2d)$$

$$= 2 \times (150 + 150 + 2 \times 120)$$

$$= 1080\,\text{mm}$$

$$V_u = 0.38 \times (80)^{0.5} \times 1080 \times 120$$

$$= 440\,\text{kN}$$

$P_{test} = 645$ kN